AFFDL-TR-79-3036
Volume I

IMPROVED METHODS FOR PREDICTING SPECTRUM LOADING EFFECTS – PHASE I REPORT

Volume I – Results and Discussion

J. B. Chang
J. H. Stolpestad

Rockwell International Corporation
Los Angeles Division
P. O. Box 92098
Los Angeles, California   90009

M. Shinozuka
R. Vaicaitis

Modern Analysis, Inc.
Ridgewood, New Jersey   07450

Approved for public release; distribution unlimited.

Prepared for

AIR FORCE FLIGHT DYNAMICS LABORATORY
Air Force Wright Aeronautical Laboratories
Air Force Systems Command
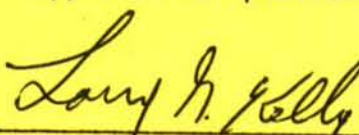Wright-Patterson Air Force Base, Ohio   45433

NOTICE

When Government drawings, specifications or other data are used for any purpose other than in connection with a definitely related Government procurement operation, the United States Government thereby incurs no responsibility nor any obligation whatsoever; and the fact that the government may have formulated, furnished, or in any way supplied the said drawings, specifications, or other data, is not to be regarded by implication or otherwise as in any manner licensing the holder or any other person or corporation, or conveying any rights or permission to manufacture, use, or sell any patented invention that may in any way be related thereto.

This report has been reviewed by the Information Office (OI) and is releasable to the National Technical Information Service (NTIS). At NTIS, it will be available to the general public, including foreign nations.

This technical report has been reviewed and is approved for publication.

ROBERT M. ENGLE, JR.
Project Engineer

LARRY G. KELLY, Chief
Structural Integrity Branch

FOR THE COMMANDER

RALPH L. KUSTER, JR., Col, USAF
Chief, Structures & Dynamics Division

REPORT DOCUMENTATION PAGE

READ INSTRUCTIONS
BEFORE COMPLETING FORM

1. REPORT NUMBER	2. GOVT ACCESSION NO.	3. RECIPIENT'S CATALOG NUMBER
AFFDL-TR-79-3036		NA-78-491-3, · Volume I

4. TITLE (and Subtitle)	5. TYPE OF REPORT & PERIOD COVERED
Improved Methods for Predicting Spectrum Loading Effects - Phase I Report Volume I - Results and Discussion	Interim Report 15 February 1978 to 15 January 1979
	6. PERFORMING ORG. REPORT NUMBER

7. AUTHOR(s) J. B. Chang, J. H. Stolpestad - Rockwell International, M. Shinozuka, R. Vaicaitis - Modern Analysis, Inc.	8. CONTRACT OR GRANT NUMBER(s) F33615-77-C-3121

9. PERFORMING ORGANIZATION NAME AND ADDRESS Los Angeles Division Rockwell International International Airport, Los Angeles, CA 90009	10. PROGRAM ELEMENT, PROJECT, TASK AREA & WORK UNIT NUMBERS

11. CONTROLLING OFFICE NAME AND ADDRESS Structural Integrity Branch (AFFDL/FBE) Air Force Flight Dynamics Laboratory Wright-Patternson Air Force Base, Ohio 45433	12. REPORT DATE 31 January 1979
	13. NUMBER OF PAGES 339

14. MONITORING AGENCY NAME & ADDRESS(if different from Controlling Office)	15. SECURITY CLASS. (of this report) Unclassified
	15a. DECLASSIFICATION. DOWNGRADING SCHEDULE

16. DISTRIBUTION STATEMENT (of this Report)

Approved for public release; distribution unlimited

17. DISTRIBUTION STATEMENT (of the abstract entered in Block 20, if different from Report)

18. SUPPLEMENTARY NOTES

19. KEY WORDS (Continue on reverse side if necessary and identify by block number)
fatigue crack growth, flight-by-flight loading, load interaction models, overload retardation, underload/acceleration, equivalent damage, fatigue crack growth rate equations, 2219-T851 Aluminum.

20. ABSTRACT (Continue on reverse side if necessary and identify by block number)
This report presents the interim status of a program which is aiming to upgrade the crack growth prediction technology required for the implementation of the damage-tolerance and durability control procedures throughout the life cycle of any weapon system. The controlling damage parameters in flight-by-flight loading for all classes of aircraft have been identified. Methodologies which characterize the flight spectra have been developed. Guidelines for development of three levels of crack growth analysis used for detail design, individual aircraft tracking, and preliminary design have been established.

FOREWORD

This report presents the results of phase I - Identification of Controlling Damage Parameters of a research program entitled "Improved Methods for Predicting Spectrum Loading Effects". This program is being administrated by the Air Force Flight Dynamics Laboratory, Air Force Systems Command, Wright-Patterson Air Force Base, Ohio, under contract F33615-77-C-3121. Mr. Robert M. Engle (AFFDL/FBE) is the Air Force project engineer.

The tasks covered in the phase I report were performed primarily by personnel from the Fatigue and Fracture Machanics Group, Dynamics Technology, and Structures Systems, supervised by George E. Fitch, Jr., Supervisor, Joseph S. Rosenthal, Manager, and Dr. George P. Haviland, Director. The program manager and principal investigator is James B. Chang. The deputy program manager is John A. Stolpestad. Principal contributors to this program include Martha Szamossi, Dr. John S. Cheng, and Ko-Wei Liu, Fatigue and Fracture Mechanics, Edward Klein, Internal Loads, Wally Ferentz, Structural Testing Laboratory, and Howard Ross, Manufacturing Engineering.

The analytical portion of task II, spectrum loading characterization, was undertaken by Modern Analysis Inc., headed by Dr. Masanobu Shinozuka. Major contributors were Drs. Rimas Vaicaitis, and Jan-Nan Yang.

A second volume, AFFDL-TR-79-3036 Volume II, contains tabulations of experimental data collected on this program and is available on request. Send requests to:

> AFFDL/FBE
> ATTN: R.M. Engle
> Wright-Patterson AFB, OH 45433

TABLE OF CONTENTS

LIST OF ILLUSTRATIONS

xvi

LIST OF TABLES

1.0 INTRODUCTION

The objective of this program is to upgrade the crack growth prediction methodology required for the implementation of the damage tolerance and durability control procedures throughout the life cycle of any weapon system. To accomplish this objective, a program consisting of the following three phases is being conducted.

Phase I   - Identification of controlling damage parameters

Phase II   - Development of predictive methodology

Phase III - Experimental verification

Phase I of this program has just been completed. In phase I, three interrelated tasks were performed. The first task was to conduct an evaluation of the state-of-the-art of currently used methods for analyzing fatigue crack growth behavior under flight-by-flight loading. The evaluation used experimental data generated from work sponsored by the U.S. Air Force since 1972, and other available test data as an experimental data base. The second task was the development of a general methodology for characterizing flight-by-flight loading such that the cycle-by-cycle crack growth analysis could be eliminated. To aid in the formulation of the methodology, an experimental testing program was conducted. The third task was to establish guidelines for development of three levels of crack growth analysis - detail design analysis, individual aircraft tracking, and preliminary design analysis.

Phase II will also contain three tasks. Task II-1 is the development of life prediction methodology for detailed crack growth analysis. The improved methodology will be capable of predicting spectrum loading effects commensurate with current cycle-by-cycle capability. A computer program which implements this technology will be developed. In task II-2, a methodology for parametric crack growth analysis, which is sensitive to change in usage of mission mix for use in an individual aircraft tracking program in the force management stage of a weapon system will be developed. A computer program which can be installed on a remote access or interactive terminal will be developed to implement the tracking technique. Task II-3 is to develop methodologies for incorporating the principle of damage tolerance requirements into the preliminary design. In this task, a crack growth calculation methodology will be developed and incorporated into the existing Air Force preliminary design program. STEP. In addition, "handbook" methods for evaluating spectrum variation effects in the preliminary design stage will be developed.

In phase III, baseline spectra for a fighter and a transport aircraft and variations of each spectrum will be generated. In addition, different mission mixes for each of the baseline flight-by-flight load histories will be developed. Crack growth behavior predictions for each case will be performed. An experimental program will then be conducted on cracked 2219-T851 aluminum panels using the developed load histories. Test results will be correlated to the analytical predictions.

2.0 STATE-OF-THE-ART METHODS

2.1 INTRODUCTION

The currently issued durability and damage-tolerance requirements[1 and 2][a] levied on the weapon systems that are presently in operation or under development have necessitated the advancement of analytical methods to predict growth behavior of cracks or crack-like flaws contained in structures under flight spectrum loading. A review and evaluation of presently used methods is deemed necessary in order to establish the most accurate crack growth analysis procedure that is within the state-of-the-art and yet is cost effective.

In the state-of-the-art methods evaluation task, efforts have been devoted to review and evaluate the primary elements for the performance of a fatigue crack growth analysis, using the deterministic approach, which include:

1. Crack growth rate relationships

2. Load interaction models

3. Damage accumulation techniques

4. Geometrical considerations

The criterion for evaluating each of the state-of-the-art methods classified as the deterministic approach, was the predictive accuracy of analysis in comparison with the test data. Experimental data generated from the work sponsored by the U.S. Air Force were used for the evaluation (3 through 6). The results of the reviews and evaluations are presented in this section.

Since fatigue crack growth predictions involve considerable statistical variability which is primarily attributed to (1) the statistical nature of service loads experienced by the aircraft structures, and (2) the inherent crack growth rate variability of materials, using a probabilistic approach to predict crack growth is a natural result. Various probabilistic approaches to fatigue crack growth predictions have been proposed in the literature (7,8, and 9.). A brief review of those approaches has been conducted.

2.2 CRACK GROWTH RATE RELATIONSHIPS

2.2.1 A BRIEF REVIEW

Historically, fatigue crack growth data generated in various test programs were often recorded in the form of crack growth measurements and the corresponding cycle counts. The relationship between the crack size a. and the

---

[a] Refer to Section 6.0.

number of applied cycles n. can then be represented as a crack growth curve drawn through the raw data points. Figure 1 shows a typical crack size versus number of cycle plot. However, this type of crack growth curve is not directly applicable for the crack growth behavior prediction, since it only represents the growth behavior of a specific crack configuration under a specific loading condition. To make use of these growth data, it is convenient to formulate a fatigue crack growth rate equation (sometimes incorrectly called a crack growth law).

Fatigue crack growth rate relationships given in the literatures take a variety of forms. In general, the instantaneous rate of change of crack length, or approximate to it, the slope of the growth curve; i.e.,

$$\frac{da}{dN} \doteq \frac{\Delta a}{\Delta N}$$

was chosen as the dependent variable in a crack growth rate equation.

The independent variable selected in most crack growth rate equations was intended to account for parameters which influence the fatigue crack growth behavior. These include the crack size, a; maximum stress, σ_{max}; stress ratio, $R = \sigma_{min}/\sigma_{max}$; and others such as environment, temperature, T, and frequency, f. In a general form, the fatigue crack growth rate equations are expressed as

$$\frac{da}{dN} = f(a, \sigma_{max}, R, Env., T, f, ...)$$

The following paragraphs briefly describe some of the rate equations developed to date. Several of them are not really considered to be the state-of-the-art. They are included here only for historical background.

The first crack growth law which drew wide attention was the one proposed by Head in 1953[10]. The mechanism proposed by Head considered a rigid-plastic work-hardening element at the crack tip and elastic elements over the remaining body. Head's law may be written as

$$\frac{da}{dN} = \frac{C_1 (\Delta\sigma)^3 \sqrt{a^3}}{(C_2 - \Delta\sigma) \sqrt{W_o}} \tag{1}$$

where C_1 is a constant which depends on the strain-hardening modulus, modulus of elasticity, yield stress and fracture stress of the material, $\Delta\sigma$ is the stress range, W_o is the size of the crack tip plastic zone, and C_2 is the yield strength of the material.

4

Numerous crack growth laws of this type have been proposed and published in the literature in the 1950's and early 1960's. These include the Frost's and Dugdale's law[11] and the Liu's law[12]. Frost's and Dugdale's law can be written as:

$$\frac{da}{dN} = \frac{\sigma^3 a}{C} \qquad (2)$$

where σ is the applied stress, a is the crack length, and C is an experiment constant.

Liu argued that the mean stress is of secondary influence and, using a model of crack extension employing an idealized elastic-plastic strain diagram and a concept of total energy absorption to failure, Liu's rate equation is:

$$\frac{da}{dN} = C\sigma^2 a \qquad (3)$$

Based on a method of analysis of static strength of plates with a crack, McEvily and Illg[13] proposed a crack growth theory as:

$$\frac{da}{dN} = F\left\{ K_N \sigma_{net} \right\}$$

where K_N is the stress concentration factor, and σ_{net} is the net area stress at the cracked section.

McEvily and Illg have empirically obtained the form of the function:

$$\log_{10}\left(\frac{da}{dN}\right) = 0.0051\, K_N \sigma_{net} - 5.472 - \frac{34}{K_N \sigma_{net} - 34} \qquad (4)$$

The first fatigue crack growth rate equation which is now widely used was developed by Paris.[14] Employing a linear eleastic fracture mechanics concept, Paris formulated a crack growth rate model in the late 1950's. The Paris model assumes that the intensity of the crack-tip stress field, as represented by K, should control the rate of crack extension; i.e.,

$$\frac{da}{dN} = f(K)$$

From the data of 7075-T6 and 2024-T3 aluminum alloy plates, Paris suggested the following equation as the crack propagation law:

$$\frac{da}{dN} = C(\Delta K)^4$$

where $\Delta K = K_{max} - K_{min}$ is the range of the stress intensity factor.

5

In general, the Paris power law has the following form:

$$\frac{da}{dN} = C(\Delta K)^n \tag{5}$$

The Paris crack growth rate model results in a straight-line presentation on a double-logarithm chart. The exponent n corresponds to the reciprocal slope of the straight line, and the constant C is a growth rate intercept corresponding to a unit value of ΔK.

It was observed that as the maximum cyclic stress intensity approaches some critical value, K_C, the growth rate increase beyond the linear behavior. To accommodate the K_C influenced crack growth rate, Forman, et al[15] expanded the simple Paris power law to:

$$\frac{da}{dN} = \frac{C(\Delta K)^n}{(1 - R)K_C - \Delta K} \tag{6}$$

The values of C and n are similar to those in the Paris equation but are not numerically equal.

As more and more test data generated under constant-amplitude loading at different stress ratios became available, fatigue crack growth rates seen to be obviously dependent on the stress ratio. To incorporate the effect of stress ratio such that all constant-amplitude data of various stress ratio may be represented by a single curve, Walker[16] introduced the idea of the effective stress, $\bar{\sigma}$, defined as:

$$\bar{\sigma} = (1 - R)^m \sigma_{max}$$

where m is an empirical constant that depends upon the material. In terms of the effective stress, the fatigue crack growth rate equation can be written as:

$$\frac{da}{dN} = f(\bar{\sigma}\sqrt{\pi c}) = f(\bar{\Delta} K)$$

Thus, if the Paris rate equation is used as a base, one has:

$$\frac{da}{dN} = C(\bar{\Delta} K)^n$$

$$= C\left[(1 - R)^m \sigma_{max}\sqrt{\pi c}\right]^n$$

$$= C\left[(1 - R)^m K_{max}\right]^n$$

6

To formulate da/dN in terms of ΔK, and adapt the threshold ΔK concept, the fatigue crack growth rate equation becomes:

$$\frac{da}{dN} = c \left[\frac{\Delta K}{(1 - \bar{R})^{1-m}} \right]^n, \quad \begin{array}{l} \Delta K > \Delta K_{th} \\ R \leq R_{cut}, \ \bar{R} = R \\ R > R_{cut}, \ \bar{R} = R_{cut} \end{array} \quad \text{and} \quad \frac{da}{dN} = 0, \quad \Delta K \leq \Delta K_{th} \tag{7}$$

Equation 7 is identified as the Rockwell equation in this report.

Crack growth data for many materials showed the characteristics of the sigmoidal curve when plotting da/dN vs ΔK on the log-log chart. Collipriest[17] formulated a rate equation as:

$$\frac{da}{dN} = \exp\left\{ n \left(\frac{\ln K_c - \ln \Delta K_{th}}{2} \right) \tanh^{-1} \left(\frac{\ln \Delta K - \frac{\ln[(1-R)K_c] + \ln \Delta K_{th}}{2}}{\frac{\ln[(1-R)K_c] - \ln \Delta K_{th}}{2}} \right) \right.$$

$$\left. + \ln \left[c \exp \left(\frac{\ln K_c + \ln \Delta K_{th}}{2} \ \text{x} \ n \right) \right] \right\} \tag{8}$$

where ΔK_{th} is the threshold stress intensity factor range.

To fit the crack growth rate data generated from an Air Force sponsored work, Hall, et al[3], developed a crack growth rate equation (identified as the Boeing equation) in the form:

$$\frac{da}{dN} = C(K_{max} - K_{th})^\alpha (\Delta K)^n \tag{9}$$

where K_{max} is the peak cyclic stress intensity factor, K_{th} is the peak cyclic threshold stress intensity factor, and c, α, and n are curve-fitted constants.

Bell, et al[4], proposed a crack growth rate equation (identified in this report as the Grumman equation) as follows:

$$\frac{da}{dN} = c \left[(1 + q\bar{R})\Delta K \right]^n, \quad \begin{array}{l} R \leq R_{cut}, \ \bar{R} = R \\ R > R_{cut}, \ \bar{R} = R_{cut} \end{array} \tag{10}$$

where q is an empirical constant.

This rate equation is a modified version of Elber's equation[18], which accounts for the overload retardation effect for a variable-amplitude loading.

For the analysis of elevated temperature fatigue crack growth data, especially for engine components, Annis, et al[19], developed an interpolative model which is based on a hyperbolic sine equation as

$$\log (da/dN) = C_1 \sinh (C_2(\log \Delta K + C_3)) + C_4 \tag{11}$$

where the coefficients are empirical functions of test frequency (f), stress ratio (R), and temperature (T):

C_1 = material constants

$C_2 = f_2(R,f,T)$

$C_3 = f_3(C_4,f,R)$

$C_4 = f_4(f,R,T)$

As the equation suggests, this model was aimed to be used to describe the effects of four fundamental parameters which influence the crack growth at elevated temperatures: frequency, temperature, stress ratio, and load excursion effects.

A three-component model based on adding the material's resistance to fatigue crack growth in the total region of log (da/dN) versus log (ΔK) was proposed by Hudak, et al[20]. The characteristic equation describing the crack growth rate is given by

$$\frac{1}{(da/dN)} = \frac{A_1}{(\Delta K)^{n_1}} + \frac{A_2}{(\Delta K)^{n_2}} - \frac{A_2}{[(1-R)K_c]^{n_2}} \tag{12}$$

where A_1, A_2, n_1, n_2, and K_c are constants that can be determined experimentally. The three terms in Equation 12 corresponding to the three regions of crack growth rates: region I, low-growth region; region II, intermediate-growth region; and region III, high-growth region. For materials that do not exhibit region III, or if growth rates are not characterized in that region, the last term in Equation 12 is set to zero. Notice that if A_1 is set equal to zero, Equation 12 reduces to Paris equation in region II.

2.2.2 CRACK GROWTH RATE DATA CORRELATIONS

To evaluate the state-of-the-art of fatigue crack growh rate relationships, baseline crack growth rate data generated from selected Air Force sponsored work were correlated. The correlation was performed by using a crack growth analysis computer program, EFFGRO, developed in-house at Rockwell. Appendix A of Reference 22 described the EFFGRO program in detail.

Fatigue crack growth rate equations, developed from two previously Air Force sponsored works, were used in the correlation study. They are the Boeing equation[3] and the Grumman equation (modified Elber equation).[4] The original EFFGRO program employed only the Rockwell equation. It has been modified to provide the option for selecting any of these three rate

8

equations in the analysis, such that a one-to-one comparison can be achieved in the evaluation. In order to present a broad cross-section view for this correlation study, two sets of 2219-T851 aluminum alloy baseline crack growth data generated separately by the Boeing Aerospace Company and Grumman Aerospace Corporation were correlated thoroughly. The Boeing baseline data were generated from part-through crack (PTC) specimens while the Grumman data were obtained from compact type (CT) or center cracked panel (CCP) specimens. In addition to aluminum alloy, baseline data of other two-material families were chosen for correlations. These were the Ti-6Al-4V titanium alloy and the 9Ni-4Co-0.2C steel alloy. The reason for choosing different material families in the correlation study was to investigate whether those crack growth rate equations are applicable for most of the commonly used airframe materials.

Crack growth rate constants of different materials corresponding to the three aforementioned growth rate equations used in the correlation study were those documented in the referenced reports. Table 1 summarizes the growth rate equations and the corresponding growth rate constants for all the materials correlated. The static and fracture properties of those materials were also summarized and are presented in Table 2. Detailed descriptions of each of the baseline crack growth rate data generation programs are summarized in Appendix A for references.

Analytical predictions obtained from the EFFGRO program were plotted against the growth data in "crack size" versus "number of cycles" format for each of the test cases in the first and second quarterly reports of this program.[22 and 24] Typical examples of such plots are presented here for illustration purposes. Figures 2 through 4 and 6 through 8 are the plots for 2219-T851 aluminum alloy baseline crack growth data generated from Boeing test program and Grumman test program, respectively. Similar plots for Ti-6Al-4V titanium alloys, either beta annealed or mill annealed, as well as the 9Ni-4Co-0.2C steel alloy are shown in Figures 10 and 11, 13 and 14, and 16 and 17, respectively. From those figures, it can be seen that in general, the analytical predictions correlate with the test data rather well.

For the purpose of evaluation, a predictability index $(\mathscr{R})$, which is defined as the ratio of the predicted life (N_{pred}) to the tested life (N_{test}) for each of the correlated cases, has been calculated. Tables 3 through 7 provide the summary of $\mathscr{R}$ values for all the baseline crack growth rate data correlated. Results shown in these summary tables indicate that each of the growth rate equations and the corresponding rate constants developed from the referenced test programs can be truly used to characterize the crack growth behavior under the constant amplitude loading for the batch of materials tested. It also demonstrates that the stress intensity factor solutions and the numerical integration technique employed in the EFFGRO program are very reliable since the original development work conducted in those referenced research programs did not use EFFGRO in the calculations.

For further illustration, histograms of the number of correlations versus the predictability index $\mathscr{R} = N_{pred}/N_{Test}$ for each of the groups correlated were constructed. They are as shown in Figures 5, 9, 12, 15, and 18 for Boeing 2219-T851 aluminum, Grumman 2219-T851 aluminum, Boeing 6Al-4V beta annealed titanium, Grumman 6Al-4V mill annealed titanium, and Boeing 9Ni-4Co-0.2C steel, respectively.

2.2.3 CROSS-CORRELATIONS OF BASELINE CRACK GROWTH DATA

Baseline fatigue crack growth data of 2219-T851 aluminum alloy generated by the Boeing Aerospace Company[3] and Grumman Aerospace Corporation [4] (Appendix B) were cross-correlated. The objective of the cross-correlation is to assess the predictive accuracies when different fatigue crack growth rate equations and the corresponding growth rate constants were employed in the analytical predictions for one batch of material. Again, the EFFGRO program was used in the performance of analytical predictions. Three different fatigue crack growth rate equations (Boeing, Grumman, and Rockwell equations) were selected for the cross-correlations. These three equations and the corresponding growth rate constants used in the analytical predictions are shown in Table 1. The corresponding static and fracture properties are listed in Table 2.

Figures 19 and 20 show typical results of the cross-correlations on Boeing 2219-T851 aluminum alloy baseline crack growth data. The crack growth behaviors predicted by using different rate equations were plotted against the test data. Since there is essentially no difference between the results predicted by the Rockwell and Grumman equations, only the results predicted by using the Boeing and Rockwell equations are presented. The summary of cross-correlation results is shown in Table 8. Statistics on the accuracy of the life predictions using three different fatigue crack growth rate equations and their corresponding crack growth rate constants are obtained and are presented in Table 9.

As can be seen from the table, all the statistical data show that the fatigue life predictions obtained by using the Rockwell equation and Rockwell growth constants are practically no different when they are compared to those obtained by using the Grumman equation and Grumman constants. There are only slight differences when they are compared to those obtained by using the Boeing equation and Boeing constants. For further illustration, histograms of the number of correlations against the ratio of the predicted life to the test life are plotted as shown in Figure 21.

The result of the cross-correlations conducted on the Grumman 2219-T851 aluminum alloy baseline crack growth data is summarized as shown in Table 10. The same statistics on the predictive accuracy using the Boeing, Rockwell, and Grumman equations and the corresponding growth rate constants as done previously on the Boeing baseline data are presented in Table 11. Again, it

can be seen that there are essentially no differences between the results predicted by the Grumman equation and by the Rockwell equation. Using the Grumman equation and the corresponding rate constants fitted by Grumman[4] to predict back Grumman crack growth data, 76 percent of the predictions are accurate within ±30 percent, yet when the Rockwell equation and the corresponding rate constants are used, a comparable 73 percent of the predicted cases are accurate within ±30 percent. Judging by the fact that Rockwell rate constants were developed from Rockwell's own fatigue crack growth data generation program, which was originally aimed in support of the application of fracture mechanics design requirements to the B-1 strategic bomber[25], the accuracy of the prediction is considered to be very good. Similar comments can be applied to the predicted results by using the Boeing equation and the rate constants derived by Boeing[3]. Figure 22 shows the accuracy of fatigue crack growth prediction with the three different rate equations.

2.2.4 AUTOMATED GRAPHIC PLOTTING PROCEDURE IN DETERMINING FATIGUE CRACK GROWTH RATE RELATIONSHIPS

Fatigue crack growth rate relationships given in the literatures take a variety of forms. In general, the instantaneous rate of change of crack length, or approximate to it, the slope of the crack growth curve (i.e., $\frac{da}{dN} \doteq \frac{\Delta a}{\Delta N}$) was chosen as the dependent variable in a crack growth rate model. The independent variable selected in most crack growth rate equations was intended to account for parameters which influence the fatigue crack growth behavior, including the crack size, a; applied maximum stress, σ_{max}; stress ratio, R; and others. A brief review of several commonly used crack growth rate equations, including those employed in the baseline crack growth rate data correlation and cross-correlation studies, is presented in the preceding sections.

A computer graphic plotting routine, PLOTRATE, which automatically plots the dependent variable, da/dN, against the independent variables in several forms and determines the corresponding constants for various crack growth rate equations, has been developed. Based on the linear elastic fracture mechanics concept which assumes that the crack-tip stress intensity factor, K, should control the rate of fatigue crack extension, a general fatigue crack growth rate model was built into the PLOTRATE program in the following form:

$$\frac{da}{dN} = c \ [f(K,R)]^n \tag{13}$$

where c and n are experimental deterministic constants for a given material.

PLOTRATE plots the dependent variable, da/dn versus the independent variable $f(K,R)$ on a double-logarithm chart. The independent variable $f(K,R)$ takes various forms in PLOTRATE. For the crack growth rate equations used in performing baseline crack growth data correlations and cross-correlations, $f(K,R)$ takes the following forms [24].

Boeing equation:

$$f(K,R) = (1-R) (K_{max} - K_{th})^{\beta} K_{max} \tag{14}$$

Grumman equation:

$$f(K,R) = (1-\overline{R}) (1 + q\overline{R}) K_{max}, \qquad \begin{array}{l} R \leq R_{co}, \overline{R} = R \\ R > R_{co}, \overline{R} = R_{co} \end{array} \tag{15}$$

Rockwell equation:

$$f(K,R) = (1-\overline{R})^{m} K_{max}, \qquad \begin{array}{l} R \leq R_{cut}, \overline{R} = R \\ R > R_{cut}, \overline{R} = R_{cut} \end{array} \tag{16}$$

Notice that in Equation (16), $f(K,R) = (1-R) K_{max} = \Delta K$ for $m = 1$. Thus, the original Paris rate equation is resumed.

Since the crack growth rate relationship built-in in PLOTRATE is in the form of Equation 13, it actually represents a straight line on the double-logarithm chart; i.e.,

$$\ln (\frac{da}{dN}) = c + n \ln [f(K,R)]$$

The exponent n corresponds to the reciprocal slope of the straight line, and the coefficient c is a growth rate intercept corresponding to a unit value of $f(K,R)$.

For a given set of crack growth rate data, once the independent variable $f(K,R)$, is chosen, PLOTRATE will plot the whole set of data in the da/dN versus $f(K,R)$ format on the double-logarithm chart, and the corresponding values of c and n will be determined automatically through a least-square fitting sub-routine built-in in PLOTRATE. Take the baseline fatigue crack growth rate data of 2219-T851 aluminum alloy generated by the Boeing Aerospace Company for example; the original crack growth rate data were plotted in the da/dN versus K_{max} format [3]. It was replotted as shown in Figure 23 by PLOTRATE. From the plot, it can be seen that $f(K,R) = K_{max}$ is obviously not an appropriate independent variable to be chosen to characterize the crack growth rates.

Plots of da/dN versus different independent variables derived from the Boeing, Grumman, and Rockwell equations, as formulated in Equations 14 through 16, are given in Figures 24, 25, and 26, respectively. From these figures, a tentative conclusion can be made; i.e., if the independent variable $f(K,R)$ together with its empirical parameter, such as "β" in the Boeing equation, "q" in the Grumman equation, and "m" in the Rockwell equation, are properly chosen, the data points fall nicely as a straight line on the log-log chart. Hence, it is appropriate to assume that the fatigue crack growth rate relationship for this material can be represented by equation 13. Employing a least-square fitting subroutine, a straight line can be drawn, and the corresponding values of c and n can be thus determined by PLOTRATE as shown in Figures 24 throug 26.

An interesting point is worth mentioning here. Examining Figures 25 and 26 closely, one will notice that these two sets of da/dn versus $f(K,R)$ plots are almost identical. Consequently, the values of c and n corresponding to Equations 15 and 16, determined by PLOTRATE, are very close (8.541×10^{-10} compared to 7.697×10^{-10} in "c", 3.68 compared to 3.72 in "n"). It explains why the results of the cross-correlation on the Boeing 2219-T851 aluminum baseline crack growth rate data using the Grumman and Rockwell equations (refer to Paragraph 2.2.3) are so close. The analytical predictions on Grumman 2219-T851 aluminum baseline crack growth rate data as summarized in Table 10 shows the same results. Again, it can be seen from Figures 27 and 28 that the plots of da/dN versus $f(K,R)$ of the Grumman equation deviate very little from that of da/dN versus $f(K,R)$ of the Rockwell equation. Consequently, the analytical predictions using these two equations are almost identical.

2.3 LOAD INTERACTION MODELS

2.3.1 A BRIEF REVIEW

The flight spectrum loadings of aircraft are variable amplitude in nature. A typical flight spectrum is shown in Figure 29. It is a typical stress spectrum of the lower wing skin of the B-1 strategic bomber. Various load interaction effects on the crack growth behavior under such variable amplitude loadings have been observed and investigated. The general effects can be summarized as follows:

1. Overloads introduce significant retardation of the crack growth. Some data indicate that if the overload is sufficiently high with respect to the following load, the crack may stop growing.

2. Compressive loads tend to negate the retardation effects caused by overloads.

3. Compression loads in tension-compression cycles tend to accelerate the crack growth.

4. Underloads in a low-high sequence of loading tend to accelerate the crack growth rate immediately following the low-high transition.

The need to have a methodology which is able to account for the load interaction effects on the crack growth under variable amplitude loading is obvious. To neglect the crack growth retardation caused by the overloads can lead to weight and cost penalties when designing the aircraft to fulfill damage tolerance and durability requirements. On the other hand, an unsafe design will result if acceleration effects introduced through the compressive loads or underloads are not accounted for.

Numerous fatigue crack growth models have been proposed to predict the load interaction effects, as previously mentioned, since Wheeler developed the first retardation model in the early 1970's[25]. These include the Willenborg model [26], Vroman/Chang model[27 and 28], Elber's Closure Model[18], Contact Stress Model [29], etc. They are mostly based on the linear elastic fracture mechanics (LEFM) concept; i.e., the fatigue crack growth behavior can be characterized by the crack tip stress field or displacement field. The following paragraphs contain brief summaries of these models.

2.3.1.1 Wheeler Model

The crack growth rate model proposed by Wheeler[25] which accounts for the overload retardation effect can be expressed in the following form:

$$\left(\frac{da}{dN}\right)_R = \left(\frac{R_y}{a_p - a}\right)^m \left(\frac{da}{dN}\right)_{uR} \quad ; \quad a + R_y < a_p \tag{17}$$

where $(da/dn)_{uR}$ is the corresponding steady-state (constant-amplitude) crack growth rate, R_y is the extent of the plastic zone formed by current loading, $(a_p - a)$ is the distance from the crack tip to the elastic-plastic interface formed by the overload, and m is the shaping exponent.

As shown in Figure 30, the dotted line represents the extent of the plastic zone due to some prior high-load application, and the solid line represents the current plastic zone. Thus, $(R_y/(a_p - a))$ is always bounded between 0 and 1 until the current plastic zone moves out of the previously yielded area. After that, the ratio is set equal to 1. The exponent, m, provides the flexibility to shape this scaling parameter to correlate with test data. Hence, the retardation parameter, $C_p = (R_y/(a_p - a))^m$ is made to depend on the current load application, through R_y, and on prior load history,

through the location of the plastic front, a_p, and the crack tip, a. The plastic zone size can be calculated from the following formula:

$$R_y = \frac{1}{4\sqrt{2\pi}} \left(\frac{K_I}{\sigma_{ys}}\right)^2 \tag{18}$$

where K_I is the stress intensity factor, σ_{ys} is the yield strength of the material.

The Wheeler retardation model has been modified by Gray and Gallagher[30] such that the retardation model is allowed to be used without reliance on data fitting and, therefore, without the restriction of using it on a specific material or a specific set of loading parameters. The modified Wheeler model uses a load interaction zone (LIZ) concept. A schematic showing the relationship between load and its corresponding LIZ is shown in Figure 31. Load p_1 applied at crack length a_1, develops a zone Z, which extends to some future crack length a_3. Load p_2 develops an LIZ which is represented by a_2 a_4.

Based on Wheeler's assumption, if p_2 develops an LIZ which extends out to or past the furthest extent of a previously developed LIZ; i.e., $a_2 + Z_2 \geq a_1 + Z_1$, the growth increment associated with the p_2 loading is calculated using the unretarded rate equation. Conversely, a crack growth rate deceleration is assumed if $a_2 + Z_2 < a_1 + Z_1$.

Wheeler's original assumption was that the load interaction zone, Z, equals the plastic zone size created under plane strain condition; i.e.,

$$Z = R_y = \frac{1}{4\sqrt{2\pi}} \left(\frac{K}{\sigma_{ys}}\right)^2$$

If the plane stress plastic zone size is used, the load interaction zone becomes

$$Z = \frac{1}{2\pi} \left(\frac{K}{\sigma_{ys}}\right)^2$$

Written in the general form, the load interaction zone is

$$Z = \alpha \left[\frac{K}{\sigma_{ys}} \right]^2$$

A quantity Z^*, which is equivalent to $a_p - a$ in Equation 17, is the difference between the load interaction zone due to a previous overload; Z_{oL}, and the current crack growth increment since the application of that overload, i.e.,

$$Z^* = Z_{oL} - \Delta a \tag{19}$$

As shown in Figure 32, Z^* is also the LIZ that would be necessary in order to have no retardation; that is, after the crack has grown some increment, Δa, away from the crack position immediately after the overload, a_{oL}, the quantity Z^* is the LIZ required to be coincident with the LIZ due to the overload. As the crack grows away from the overload position, a_{oL} (that is, as Δa increases) Z^* decreases. For the case of coincident LIZ boundaries, a K^*_{max} always exists such that Equation 18 is satisfied. Substituting Equation 18 into Equation 19 and rearranging the results, it yields

$$K^*_{max} = K^{oL}_{max} \left[1 - \frac{\Delta a}{Z_{oL}} \right]^{1/2} \tag{20}$$

The LOCUS of $\dot{K}^*_{max}$ values is identified in Figure 32. For a chosen unretarded crack growth rate equation, the general form can be expressed as

$$\left(\frac{da}{dN} \right)_{uR} = C \left[f(K,R) \right]^n$$

where C and n are constants for a given material and $f(K, R)$ is the function of controlling parameters, K and R, which drive the fatigue cracking process.

16

Hence, the generalized Wheeler model can be written in the following form:

$$
\left(\frac{da}{dN}\right)_R = \begin{cases} C\left(\left(\frac{K_{max}}{K_{max}^*}\right)^{\frac{2m}{n}} \times [f(K,R)]\right)^n, & K_{max} < K_{max}^* \\[3em] C[f(K,R)]^n, & K_{max} \geq K_{max}^* \end{cases}
$$

(21)

Equation 21 is the Wheeler model in the stress intensity format.

If the concept of the effective stress intensity factor range, ΔK_{eff} is employed, the fatigue crack growth rate equation for a spectrum loading becomes

$$
\left(\frac{da}{dN}\right)_{sp} = C\left[\Delta K_{eff}\right]^n
$$

(22)

where

$$
\Delta K_{eff} = \begin{cases} \left[\frac{K_{max}}{K_{max}^*}\right]^{\frac{2m}{n}} \times f(K,R), & K_{max} < K_{max}^* \\[3em] f(K,R), & K_{max} \geq K_{max}^* \end{cases}
$$

(23)

Experimental evidence indicates that there is a particular value, S, of K_{max}^{OL}/K_{max} such that when $K_{max}^{OL}/K_{max} \geq S$, crack arrest occurs. The limiting condition for crack arrest is $K_{max}^{OL}/K_{max} = S$. Thus,

$$
\Delta K_{eff} \text{ (at arrest)} = \left(\frac{1}{S}\right)^{\frac{2m}{n}} f(K,R) = \Delta K_{th}
$$

where ΔK_{th} is the threshold stress intensity factor range below which no measurable fatigue crack growth occurs. The Wheeler exponent, m, can be determined as follows:

$$m = \frac{n}{2} \left(\frac{\log \left[\frac{f\ (K,R)}{\Delta K_{th}} \right]}{\log S} \right) \tag{24}$$

It implies that m is not a constant but depends on the specific material being used and the loading subsequent to the overload.

2.3.1.2 Willenborg Model

The Willenborg retardation model[26] uses an "effective stress" concept to reduce the applied stresses and, hence, the crack tip stress intensity factor in the crack growth analysis. The effective values of the maximum and minimum applied stresses are calculated as follows.

$$\left(\sigma_{max} \right)_{eff} = \sigma_{max} - \sigma_{Red}$$

$$\left(\sigma_{min} \right)_{eff} = \sigma_{min} - \sigma_{Red} \tag{25}$$

where σ_{Red} is the reduced stress.

The effective values of the stress ratios, R, and the stress intensity factor range, ΔK, are calculated using $(\sigma_{max})_{eff}$ and $(\sigma_{min})_{eff}$. The crack growth law is then applied directly, using the effective R and K to obtain the growth during the interval in the following general form:

$$\frac{da}{dN} = C \left[f\ (K_{eff},\ R_{eff}) \right]^n$$

To determine the reduced stress, σ_{Red}, for a simple spectrum as shown in Figure 33, the following step-by-step procedure can be followed.

18

1. Apply load step 1. The plastic zone radius is calculated and saved for reference

$$a_p = \frac{K_1^2}{2\pi\sigma_{ys}^2} + a_1 \qquad (26)$$

2. Apply the first cycle in load step 2. Compare σ_2 to σ_1. Since $\sigma_2 < \sigma_1$, the retardation model is used.

3. Determine the applied stress, σ_{app} required to extend the crack length a_c at the beginning of the load cycle or load step to a_p. The yield zone radius for σ_{app} is given by

$$R_y = a_p - a_c = \frac{K_{app}^2}{2\pi\sigma_{ys}^2} = \frac{\left(M\,\sigma_{app}\,\sqrt{\pi a_c}\right)^2}{2\pi\sigma_{ys}^2} \qquad (27)$$

where M is the geometrical correction factor and σ_{ys} is the yield strength of a specific material.

For the first cycle of load step 2, σ_{app} can be obtained from

$$\sigma_{app} = \frac{\sigma_{ys}}{M} \sqrt{\frac{2(a_p - a_1)}{a_1}}$$

4. Obtain the reduction in the applied stress, σ_{Red} due to the progress through the plastic yield zone for a given load step, as follows:

$$\sigma_{Red} = \sigma_{app} - \sigma_{max}$$

For load step 2, the reduced stress is

$$\sigma_{Red} = \sigma_{app} - \sigma_2$$

If the crack has propagated through the plastic zone, σ_{Red} is set equal to zero.

Gallagher[31] reformulated the Willenborg model by using a residual stress intensity factor concept which suggests that the effective stress intensity factor, K_{eff}, be calculated from the equation

$$K_{eff} = K_\infty - K_R$$

Where K_∞ is the stress intensity factor corresponding to the remotely applied load and K_R is the residual stress intensity factor.

The equivalent residual stress intensity factor for Willenborg model is

$$K_R^W = K_{max}^{oL} \left(1 - \frac{\Delta a}{Z_{oL}}\right)^{1/2} - (K_\infty)_{max} \tag{28}$$

Where Z_{oL} is the overload created load interaction zone, which is approximately equal to the overload yield zone radius, and Δa is the increment of crack growth into the overload load interaction zone since the application of overload. Following an overload, Δa is approximately zero and the residual stress intensity factor is maximum.

Gallagher and Hughes[32] suggested that the actual residual stress intensity factor K_R may be proportional to K_R^W; i.e., $K_R = \phi K_R^W$. Thus, the effective maximum and minimum stress intensity factor can be written as

$$\left(K_{max}\right)_{eff} = K_\infty{}_{max} - \phi \left[K_{max}^{oL} \left(1 - \frac{\Delta a}{Z_{oL}}\right)^{1/2} - K_\infty{}_{max}\right] \tag{29}$$

and

$$\left(K_{min}\right)_{eff} = K_\infty{}_{min} - \phi \left[K_{max}^{oL} \left(1 - \frac{\Delta a}{Z_{oL}}\right)^{1/2} - K_\infty{}_{max}\right] \tag{30}$$

20

or

$$\left(K_{min}\right)_{eff} = \left(K_{min}\right)_{eff_{cut}} \quad \text{whichever is greater}$$

where $(K)_{eff_{cut}}$ is the cutoff value of the effective stress intensity factor which is set equal to zero normally.

The effective maximum and minimum stress intensity factors and the corresponding value of $R_{eff} = (K_{min})_{eff}/(K_{max})_{eff}$ calculated from the preceding equations can be then used in the crack growth analysis, assuming the following form of fatigue crack growth rate equation:

$$\frac{da}{dN} = C \left[f(K_{eff}, R_{eff}) \right]^n$$

The proportional constant, ϕ, in the previous equation can be obtained from

$$\phi = \frac{K^{\infty}_{max} - (K_{max})_{TH}}{K^{OL}_{max} - K^{\infty}_{max}} \tag{31}$$

Where $(K_{max})_{TH}$ is the maximum threshold stress intensity factor.

2.3.1.3 Closure Model

The closure model is based on the fact observed by Elber that the surface of the fatigue crack closed during fatigue crack propagation tests under cyclic loading with tension-tension load cycles. He postulated that the crack closure phenomenon, associated with a growing crack under cyclic loading, was caused by residual plastic deformation left in the wake of the propagating crack tip. These deformations effectively decrease the amount of crack opening displacement. On unloading, this can cause crack closure above zero load. Therefore, in attempting to predict crack growth

analytically, the crack opening stress level should be used as a reference stress level from which an effective stress range can be obtained. Elber defined the effective stress range as follows[18]:

$$\Delta\sigma_{eff} = \sigma_{max} - \sigma_{op}$$

where σ_{op} is the crack opening stress.

An effective stress range ratio is then defined as

$$U = \frac{\sigma_{max} - \sigma_{op}}{\sigma_{max} - \sigma_{min}} = \frac{\Delta\sigma_{eff}}{\Delta\sigma} \tag{32}$$

The Elber model is expressed in terms of the effective stress range ratio as

$$\frac{da}{dN} = C\ (U\Delta K)^n = C\ (\Delta K_{eff})^n \tag{33}$$

where ΔK is the stress intensity factor range.

The relationship between U and three important variables which have a significant effect on U can be established from constant-amplitude loading tests. These three variables are stress intensity range, ΔK, the size of the crack, a, and the stress ratio, R. From the experimental results obtained from the fatigue cyclic testing on sheets of 2024-T3 aluminum alloy, Elber concluded that only the stress ratio R is a significant variable for 2024-T3 aluminum alloy, Elber proposed that the relation between U and R is linear and can be expressed as

$$U = 0.5 + 0.4R \quad \text{where} \quad -0.1 < R < 0.7$$

Hence, for this material, the crack growth equation becomes

$$\frac{da}{dN} = C\ [(0.5 + 0.4R)\ \Delta K]^n \tag{34}$$

22

Elber extended the effect of crack-closure phenomenon to the crack growth from the constant-amplitude case to the variable-amplitude situation. He indicated that fatigue crack closure may be a significant factor in causing the load interaction effects on crack growth rates (retardation or acceleration). The following example illustrates his viewpoint.

Assume a crack in 2024-T3 aluminum alloy is propagating under the conditions R=o and K_{max} = 20 ksi $\sqrt{in}$. Under these conditions, the crack opening level is at K_{op} = 10 ksi $\sqrt{in}$. If the maximum stress intensity factor reduces to half of its original value, the new conditions are K_{max} = 10 ksi $\sqrt{in}$. and R = o. The crack opening level, however, is still K_{op} = 10 ksi $\sqrt{in}$., equal to the new peak stress intensity, so the crack does not open. Therefore, the crack does not propagate until the crack opening level changes.

Employing the Elber crack-closure concept and assuming that the crack closure stress is not different from the crack opening stress, Bell, et al[4], proposed a modified closure model for a through crack in an infinite-wide sheet as follows:

$$\frac{da}{dN} = C \left[\frac{\sigma_{max} - \sigma_c}{(1 - C_{fo})} \sqrt{\pi a} \right]^n \tag{35}$$

Where C_{fo} is defined as the closure factor at R = o, which is related to the closure stress σ_c as

$$C_f = \frac{\sigma_c}{\sigma_{max}}$$

If σ_c is defined as a function of stress ratio, then the previously stated rate equation will predict the effect of the stress ratio on fatigue crack growth. If it is defined as a function of the previous load history, then the equation will predict crack growth interaction effects. Hence, the modified closure model will properly predict crack growth for any condition once σ_c is defined as a function for that specific condition. The following are several functions defined for σ_c in several specific conditions:

1. Constant-amplitude loading:

$$\sigma_c = \left[C_{f_{-1}} + \left(C_{f_o} - C_{f_{-1}} \right) (1 + R)^P \right] \sigma_{max} \tag{36}$$

23

where C_{f-1} and C_{f_O} are the values of the closure factor C_f for $R = -1$ and 0, respectively, and P is an empirical constant. For 2219-T851 aluminum, $C_{f-1} = 0.347$, $C_{f_O} = 0.4$, and $p = 3.93$.

2. High-low loading sequence having constant minimum:

$$\sigma_c = \sigma_{c_1} - \left(\sigma_{c_1} - \sigma_{c_2}\right)\left(\frac{\Delta a}{\rho}\right)^B, \quad 0 \leq \Delta a \leq \rho \tag{37}$$

where σ_{c1} and σ_{c2} are the constant-amplitude closure stresses of high-stress cycles, σ_1, and lower stress cycles, σ_2, respectively, Δa is the crack growth since the stress change, ρ is the load interaction zone caused by σ_1, and B is an empirical constant. For 2219-T851 aluminum, Bell, et al, determined the values of the parameters as $\rho \cong 1/2\pi \ (K_I/\sigma_{ys})^2$, $B \cong 1$.

3. Variable-amplitude loading contains a number of overload cycles:

$$\sigma_c = \left[\gamma_1 + (1 - \gamma_1)\left(\frac{N_{oL} - 1}{N_{sat} - 1}\right)\right]\sigma_{c_1} \tag{38}$$

where N_{oL} is the number of overload cycles, N_{sat} is the number of overload cycles required to achieve saturation, and γ_1 is the ratio of the closure stress after one cycle of overload to the stabilized overload closure stress. σ_{c1} is the closure stress at constant stress σ_1.

2.3.1.4 Contact Stress Model

Another load interaction model based on the closure phenomenon is the contact stress model developed by Dill et al[29]. This method of crack growth analysis is based on evaluation of stress intensity caused by crack surface contact. An analysis of crack surface displacement during loading and unloading is used to determine the permanent plastic deformation left in the wake of the growing crack. Contact stresses caused by interference of these permanent deformations at maximum and minimum loads are determined by treating the interference as a wedge between the crack surfaces and performing an elastic-plastic analysis of stresses caused by the wedge. The effective stress intensity range used in the crack growth prediction is determined by subtracting the stress intensity factor caused by these contact stresses from the applied stress intensity factor range.

24

To determine displacements along the crack surface caused by loading and unloading, Dugdale's strip model[33] was employed by Dill et al. Dugdale's model treats the plastic zone as an extension of the elastic crack surface over which a strip of constant-yield stress acts. The plastic zone size is determined to be that length of constant-yield stress such that the stress intensity caused by the yield stress equals the applied stress intensity; hence, there is no singularity at the extended tip. The crack surface displacement at K_{max} is determined from the superposition of the displacement under remote loading and the displacement due to the constant-yield stress of the plastic zone. Figures 34 and 35 show the crack surface displacements at maximum load and during unloading, respectively. The elastic displacements near the crack tip for both loading situations are shown schematically in the upper portion of the figures. The constant-yield stress of the plastic zone tends to reduce the elastic displacements under remote loading by the amount shown in the middle portion of the figures. During unloading, the reversed plastic zone stress is increased to twice the yield stress used during loading, accounting for an elastic stress range equal to the difference of tensile and compressive yield stresses. The crack surface displacement at the minimum applied load are determined by subtracting the displacements occuring during unloading from those at maximum load; i.e.,

$$\delta_{K_{min}} = \delta_{K_{max}} - \delta_{\Delta K}$$

Figure 36 shows the elastic crack surface displacements at minimum load schematically.

The potential interference is the difference between the permanent plastic deformation and the minimum displacement of the elastic surface, as shown in Figure 36. The permanent plastic deformation at the crack tip at minimum load is considered to be equal to the crack opening displacement (COD) at that load. As obtained from Rice[34], the crack opening displacement is approximated as

$$COD_{K_{min}} = \alpha \left(K_{max}^2 - \frac{1}{2} \Delta K^2 \right) / 2E\sigma_{ys}$$

where $\alpha = 1$ for plane stress condition, $\alpha = (1-\nu^2)/2$ for plane strain condition.

The potential interference acts as a wedge behind the crack tip, creating a stress intensity factor at the crack tip. Dill, et al, used 25 constant-stress elements to idealize the wedge in order to determine the contact stresses. Bueckner's weight function approach[35] was employed to develop an influence coefficient matrix for the displacement-stress relationship between elements.

Once the contact stresses are determined, the contact stress intensity factor occurring at the minimum load, the effective stress intensity factor, and the effective stress intensity range can be computed. Thus, if the Forman crack growth rate equation for constant-amplitude loading situation is adopted, the following rate model can be used to account for the overload interaction effect:

$$\frac{da}{dN} = \frac{da}{dN}\bigg|_{\Delta K_{eff}} \left\{ \frac{K_c}{K_c - K_{max}} \right\} \tag{39}$$

The contact stress model has been extended to account for the compressive load acceleration effect by Dill, et al[36]. For tension-tension (including tension-zero) cycles, the computation of displacements and contact stresses is made with the origin of reference for the contact stress model placed at the physical tip. In the analysis of $COD_{K_{min}}$ for compression loads, the reference origin of the contact stress model is changed to the end of the forward plastic zone. As shown in Figure 37, the wedge is composed of the sum of the residual displacements in the forward plastic zone caused by loading and the elastic displacements due to applying compressive load. This wedge is represented schematically in the lower portion of Figure 37, and the resulting displacement and stress distribution is shown in the bottom of the figure.

2.3.1.5 Vroman/Chang Load Interaction Model

The original Vroman retardation model which was developed to account for the overload retardation effects on the crack growth for a cracked body subjected to variable-amplitude loading is somewhat similar to the Willenborg model. In fact, these two models were independently developed during the same time period (1970-71). In the mathematical form, Vroman model was expressed as follows[27]:

$$\frac{da}{dN} = c[f(\Delta K_{eff})]^n, \qquad R \geq 0$$

$$\Delta K_{eff} = \frac{4}{3}\left[K_{max} - \frac{3}{4}\left(K_{min} + \frac{1}{3} K_{max_{ol}} \sqrt{\frac{a_{ol} + R_{y_{ol}} - a}{R_{y_{ol}}}}\right)\right] \qquad (40)$$

where K_{max}, K_{min} are the maximum and minimum values of the stress intensity factors corresponding to the currently applied load cycle, a_{ol} and $K_{max_{ol}}$ are the values corresponding to the previously applied overload cycle, and $R_{y_{ol}}$ is the plastic zone radius corresponding to the maximum overload.

In plane strain condition, the plastic zone radius R_y is

$$R_y = \frac{1}{6\pi}\left(\frac{K_{max}}{\sigma_{y_s}}\right)^2$$

where σ_{y_s} is the yield strength of the material.

The effective stress intensity factor range, ΔK_{eff}, in the Vroman model (Equation 40), can be reformulated as

$$\Delta K_{eff} = \left(K_{max} - K_{min}\right) - 0.333\left[\left(\sqrt{\frac{a_{ol} + R_{y_{ol}} - a}{R_{y_{ol}}}}\right)K_{max_{ol}} - K_{max}\right] \qquad (41)$$

It can be seen very easily from the preceding equation the numerical value of ΔK_{eff} is always less than $\Delta K = K_{max} - K_{min}$ when the overload is existing; hence, the corresponding value of the fatigue crack growth rate, da/dn, is smaller than its constant-amplitude loading counterpart, resulting in crack growth retardation.

Chang, et al[37], modified the Vroman model slightly in their study of bomber spectrum variation effects on the behavior of crack growth. The

modification was made by changing the numerical constant 0.33 in the ΔK_{eff} equation to 0.067. Chang[38] later proposed to form the effective stress intensity factor range as

$$\Delta K_{eff} = \Delta K - A\left[\left(\sqrt{\frac{a_{ol} + R_{y_{ol}} - a}{R_{y_{ol}}}}\right)K_{max_{ol}} - K_{max}\right]$$

(42)

where A is a constant determined by variable-amplitude loading tests.

To account for the underload (small tension-tension cyclic loading) acceleration (crack sharpening) effects, Chang, et al[28], proposed an underload acceleration model arranged in the same format as the Vroman over-load retardation model. In its preliminary form, it is as follows:

$$\frac{da}{dN} = c[f(\Delta K_{eff})]^n \quad , \qquad R \geq 0$$

$$\Delta K_{eff} = \left(K_{max} - K_{min}\right) + B\left(1 - e^{-N_{ul}}\right)R_{ul}\left(\sigma_{max} - \sigma_{max_{ul}}\right)\sqrt{\left(K_{max}^2 - K_{max_{ul}}^2\right)}$$

(43)

where R_{ul}, $\sigma_{max_{ul}}$, and $K_{max_{ul}}$ are the stress ratio, maximum cyclic stress, and maximum stress intensity factor values corresponding to the previously applied underload cycles. N_{ul} is the number of the underload cycles.

The constant B in the equation is a combination of some material constants together with an empirical constant α as:

$$B = \alpha\sqrt{\frac{2(1 - \nu)}{\pi G \sigma_{y_s}}}$$

where ν is the Poisson's ratio, G is the shear modulus, and σ_{y_s} is the yield strength of the material.

The compressive load acceleration effects in a spectrum containing tension-compression cycles have been studied by a number of investigators in the last few years[39, 40, 41]. To account for the acceleration effect, Chang[38] proposed to employ the crack growth rate equation which takes the similar form as Walker's rate equation; i.e.,

$$\frac{da}{dN} = c\left[\left(1 - R\right)^{q(R)} K_{max}\right]^n \quad , \quad R < 0 \tag{44}$$

where $q(R)$ is the acceleration index which is determined by tension-compression cyclic test for a specific value of negative stress ratio, R.

The combined Vroman/Chang load interaction model can be written as:

$$\frac{da}{dN} = c[f(\Delta K_{eff})]^n \quad , \quad R \geq 0$$

where

$$\Delta K_{eff} = \Delta K - Af_1(K,Ry) + Bf_2(k,\sigma)$$

and

$$\frac{da}{dN} = c\left[\left(1 - R\right)^{q(R)} K_{max}\right]^n \quad , \quad R < 0 \tag{45}$$

2.3.2 VARIABLE-AMPLITUDE LOADING CRACK GROWTH DATA CORRELATIONS

Variable-amplitude load fatigue crack growth data of 2219-T851 aluminum alloy generated from the Crack Growth Analysis for Arbitrary Spectrum Loading program conducted by Grumman[4] were selected as the primary data base for the evaluation of two load interaction models - the modified closure model and the Vroman/Chang model. Results of the fatigue crack growth behavior prediction by Vroman/Chang model were obtained using Rockwell's computer program (EFFGRO). The closure model predictions were those documented in the original Grumman report. Fatigue crack growth data of two other family materials, 6Al-4V titanium and HP 9Ni-4Co-0.2C steel, were also correlated to the

29

Vroman/Chang model predictions in order to verify if this load interaction model is applicable to most of the aircraft materials. Appendix B presents the detailed description of the variable amplitude loading tests correlated in this work. The crack growth equations and the corresponding rate constants and other material properties used in the analytical predictions are shown in Tables 1 and 2.

Typical results of the correlation of analytical predictions to the Grumman 2219-T851 aluminum alloy test data are shown in Figures 38 through 42. It can be seen that for periodically applied overload cases, both the closure model and the Vroman/Chang model predictions correlate with test data satisfactorily. Yet, for block loading cases, closure model provides better prediction than that of the Vroman/Chang model. This is primarily because the present Vroman/Chang model cannot account for the effect of a large number of overload cycles, which tend to retard the crack growth more than a single overload cycle.

Samples of correlation results of Grumman Ti-6A1-4V mill-annealed titanium alloy variable-amplitude loading crack growth data are shown in Figures 43 and 44. In general, the analytical predictions obtained by both the Vroman/Chang model and the closure model provide satisfactory results for most of the cases correlated.

Typical correlations of Rockwell HP 9-4-20 steel alloy flight-by-flight spectrum loading crack growth data are shown in Figures 45 and 46. Results of correlations demonstrate the capability of the Vroman/Chang model in predicting the flight spectrum contains compressive cycles situation.

2.4 GEOMETRICAL CONSIDERATIONS

The prediction of the fatigue crack growth behavior for a crack growing in a complex stress field caused by geometrical variations of the cracked body such as a plate containing an open hole, a cold-worked fastener hole, a row of fastener holes, or a hole with interference-fit fastener is a complex problem with many aspects. First of all, even in the absence of a crack, the determination of the stress field of such a geometry involves the rigorous elastic or elastic-plastic stress analysis. A precise determination of the stress intensity factor for such geometries containing cracks is very difficult, if not impossible, to obtain. Secondly, most of the currently developed techniques used on the prediction of the crack growth behavior for those cases involving large-scale yielding such as cracks emanating from cold-worked fastener holes or hole-contained interferenced fastener systems are based on the linear elastic fracture mechanics concept. The question has often arisen whether the stress intensity factor K is a proper fracture parameter in the presence of the large plastic strains[42]. Other fracture

parameter such as the J-integral have been suggested to be employed in dealing with the fatigue crack growing under elastic-plastic conditions[43 and 44]. Although the application of the J-integral approach is considered to be beyond the state-of-the-art for predicting crack growth behavior, the fact that a number of investigators are working in this area reflects the potential use of this approach.

Currently, for analyzing problems of practical significance in aircraft industry applications, there exist a good many engineering solution techniques in the determination of the stress intensity factor K. These include the weight function approach introduced by Bueckner[35], the alternating technique employed by Kobayashi, et al[45], the reciprocal theorem proposed by Rice[46], the finite-element method [47 and 48], the boundary-integral-equation approach[49], Green's function technique[50], as well as experimental approaches such as the combination of stress-freezing photoelasticity and a numerical technique used by McGowen and Smith[51], the fatigue crack growth calibrating method employed by Snow[52], etc. Several documnets have excellent collections of the stress intensity factor solutions[53 through 55]. A brief summary of some of these techniques is presented here. Engineering approximation solution methods, including the "compounding from known solutions" approach and the "effective stress field" method, are also briefly summarized and presented.

2.4.1 THE FINITE-ELEMENT METHOD (FEM)

Among several approximate methods such as boundary collocation, conformal mapping, asymptotic approximation, etc, developed over the past years to analyze realistic crack problems, FEM has the advantage of being able to solve problems with complex geometries, anisotropic materials, nonhomogenious properties, or complex problems of combined mechanical and thermal loadings. During the past years, FEM has been successfully applied to elastic crack analysis to determine stress intensity factors. The application seems to have evolved in three stages. Initially, Kobayashi, et al[47], applied to existing conventional finite elements to the solution of fracture mechanics. This approach requires very-fine-grid work in the crack tip region as well as fitting the known near-field stress or displacement solutions such as the crack opening displacement (COD) to the approximate numerical solutions. During the second stage, Byskov[56], in 1970, introduced a cracked finite element in conjunction with conventional elements. This approach violates the compatibility condition between the cracked element and the conventional element. During the third stage of development, Tong[57], in 1970, and Pian, et al[58], in 1971, developed the hybrid displacement model and the hybrid stress model, respectively, where they used a special crack tip singular element in which the correct singular distribution of stress and strain was embedded in the shape functions, and the singularity coefficient, stress

intensity factor are solved directly as unknowns in the final matrix equations along with nodal displacements. This approach does not require very-fine-grid work, and the compatibility condition is also maintained through the Lagrange multiplier technique. Since the convergence rate of FEM applied to crack analysis is dominated by the singular nature of solution near crack tip, the proper incorporation of singularity in the hybrid model greatly improves the accuracy and efficiency of the stress intensity factor solution.

Figure 47 shows a typical finite-element model for two through-cracks emanating from two adjacent fastener holes contained in a rectangular plate subjected to tensile load solved by Rockwell's in-house hybrid displacment finite-element program (HYCRAK)[59]. HYCRAK is a two-dimensional program which calculates mode I, mode II, and mixed mode stress intensity factor for a single crack as well as multiple cracks.

Recently, Atluri, et al[60], extended the hybrid displacement finite-element method to the solution of mode I, II, and III stress intensity factor for an arbitrary curved three-dimensional (3-D) crack front in a structural component. Pian, et al[61], also developed a special crack element for 3-D fracture analysis using a hybrid stress finite-element method. However, the huge computer cost still remains as an obstacle in using the 3-D finite-element method in real engineering situations.

2.4.2 GREEN'S FUNCTION METHOD

Many stress intensity factor solutions can be constructed by using the results of the concentrated force problem such as Green's function. For a concentrated normal force P and tangential force Q applied to the crack surface in Figure 48, the stress intensity factors are known to be[54]

$$K = K_I - iK_{II} = \frac{Q + iP}{2\pi\sqrt{a}} \left[\frac{\kappa - 1}{\kappa + 1} + \sqrt{\frac{b + a}{b - a}} \right] \quad b < a \qquad (46)$$

where K_I and K_{II} are the mode I and II stress intensity factor, respectively, $\kappa = 3 - 4\nu$ for plane strain, and $\kappa = (3 - \nu)/(1 + \nu)$ for generalized plane stress.

Equation 46 may be used as the fundamental Green's function for generating solutions to crack problems involving arbitrary distributed surface tractions such as σ_{yy} and σ_{xy}.

For a through-crack emanating from an open hole with arbitrary distributed stress σ along crack length such as in Figure 49, the stress intensity factor solution is

$$K(a) = \int_0^a k(x, a) \, \sigma(x) \, dx \tag{47}$$

where $k(x, a)$ is the normalized stress intensity factor due to the arbitrary distributed stress σ.

By defining $G = K(\sqrt{a/\pi})$ and normalize x and σ through $\xi = x/a$, Equation 47 becomes

$$K(a) = \sigma_0 \sqrt{\pi a} \, \beta$$

where

$$\beta = \int_0^1 \bar{\sigma}(\xi) \, G(\xi, a) \, d\xi \,,$$

σ_0 is the uniform far-field stress and $\bar{\sigma} = \sigma/\sigma_0$ is the normalized unflawed stress distribution on the propective crack surface.

Hsu, et al[50], have generated Green's function to compute the mode I stress intensity factor for cracks emanating from many types of fastener hole, including interference-fit fastener holes and cold-worked holes with the consideration of the effects of elastic-plastic stress distribution around the fastener holes. The method is briefly described in the following paragraphs.

Figure 50 shows a double-radial crack emanating from a fastener hole. From the principle of the linear superposition, the stress intensity factor of problem A is equivalent to the sum of those of problems B and C. Since problem B is crack-free, the stress intensity factor of problem A is equivalent to that of problem C with the K solution expressed in Equation 47.

With a knowledge of Green's function, G, and the stress distribution, $\bar{\sigma}$, on the prospective crack surface with the crack absent, the stress intensity factor $K(a)$ can be obtained from Equation 47.

For the generation of Green's function of complex geometry, such as in problem A, Hsu, et al, proposed to use a high-order singularity finite-element program to compute the mode I stress intensity factor, K_I, for a double-radial crack emanting from an open hole and subjected to concentrated loads on and perpendicular to the crack surface. The computed K_I can be then used to develop Green's function.

The unflawed stress field $\bar{\sigma}$ can be computed from various finite-element programs with or without the consideration of the effects of nonlinear plastic behavior according to the degree of approximation to the real engineering situation.

The following summarized the correction factor β for several types of fastener holes obtained by Hsu et al.

1. Open hole

$$K = \sigma_o \sqrt{\pi a} \; \beta_{op}$$

$$\beta_{op} = \int_0^1 f_{op} \, (\xi) \; g \, (\xi, \, a) \; d\xi$$

where f_{op} is the normalized unflawed stress distribution on prospective crack surface.

The factor β which is equivalent to the Bowie factor[62] in the purely elastic case, accounts for the hole effect when the local yielding occurs.

2. Interference-fit fastener hole

$$K = \sigma_{ys} \sqrt{\pi a} \; \beta_{IF}$$

$$\beta_{IF} = \int_0^1 f_{IF} \, (\xi) \; G \, (\xi, \, a) \; d\xi$$

where σ_{ys} is the yield strength of the material, and f_{IF} is the unflawed elastic-plastic stress on the prospective crack surface normalized by the material yield strength. β_{IF} is a function of the crack length, far-field load, and the amount of fastener hole interference.

3. Cold-worked hole

$$K = \sigma_{ys} \sqrt{\pi a} \, \beta_{cw}$$

$$\beta_{cw} = \int_{0}^{1} f_{cw} (\xi) \, G (\xi, a) \, d\xi$$

where f_{cw} is the normalized unflawed elastic-plastic stress on the prospective crack surface, β_{cw} is a function of crack length, far-field applied load, and level of cold working.

2.4.3 "COMPOUNDING FROM KNOWN SOLUTION" APPROACH

Estimates of the stress intensity factor for complex geometries can be obtained by an appropriate set of available simple solutions. This method is labeled as "Compounding from Known Solutions[55]. In this method, each K expression is constructed using a "fundamental" solution multiplied by an appropriate set of correction functions which is dimensionless. In a recently published report, Brussat, et al[63], have developed a series of stress intensity factor solutions for cracks growing in complex structures, primarily in multiple-element, mechanically fastened metallic structures based on three fundamental stress intensity factor solutions. The first is the well-known case of a uniform tension applied to a through-thickness crack at a circular hole (as shown in Figure 51). Bowie originally derived the so-called Bowie function in the 1950's[62]. Tweed and Rooke[64] improved the accuracy of Bowie's original solution to:

$$K_I^{(1)} = F \left(\frac{C}{C + R} \right) \sigma \sqrt{\pi C} \tag{48}$$

where

$$F \left(\frac{C}{C + R} \right) = \exp \left[1.2133 - 2.205 \left(\frac{C}{C + R} \right) + 0.6451 \left(\frac{C}{C + R} \right)^2 \right]$$

The second "fundamental" solution used by Brussat, et al, is the line crack problem, as shown in Figure 52. This is the case when the crack is very long and the crack tip is very far away from the hole. The stress intensity factor is thus approximated by[65]

$$K_I^{(2)} = \sigma \sqrt{\pi C_e}$$

where C_e is the equivalent half-crack length.

For the case that the crack is very short and the crack tip is very close to the edge of the hole, a third fundamental solution is[63]

$$K_I^{(3)} = \frac{k_t}{3} F \left(\frac{C}{C + R} \right) \sigma \sqrt{\pi C} \tag{49}$$

where k_t is the stress concentration factor.

A set of multiplicative correction functions account for the deviations from the fundamental cases were developed by Brusset, et al. The following paragraphs cover some of the cases for the purpose of illustrating the compounding from the known solutions approach.

2.4.3.1 Crack Approaching a Hole

For the case such as the chordwise splice structure, a crack is expected to grow from one fastener hole to another fastener hole, as shown in Figure 53. The stress intensity factor for this configuration can be approximated as

$$K_I = \beta_{AH} K_I^{(2)} = \beta_{AH} \sigma \sqrt{\pi C_e} \tag{50}$$

where

$$\beta_{AH} = \left(\frac{\ell - C_e}{R + \ell - C_e} + \frac{0.1 C_e}{R + C_e} \right)^{-0.3} \quad \text{was derived from Isida's solution}[66].$$

2.4.3.2 Eccentrically Cracked Strip in Uniform Tension

The stress intensity factor solutions for a crack eccentrically located in a finite-width strip under uniform tension load (as shown in Figure 54) can be formulated as follows:

$$K_I^{(R)} = \beta_{FW}^{(R)} K_I^{(2)} = \beta_{FW}^{(R)} \sigma \sqrt{\pi C} \tag{51}$$

$$K_I^{(L)} = \beta_{FW}^{(L)} K_I^{(2)} = \beta_{FW}^{(L)} \sigma \sqrt{\pi C}$$

where

$$\beta_{FW}^{(R)} = \sqrt{\sec\left(\frac{\pi C}{2b^{(R)}}\right)},$$

$$\beta_{FW}^{(L)} = \sqrt{\sec\left[\frac{\pi}{6}\left(\frac{2C}{b^{(R)}} + \frac{C}{b^{(L)}}\right)\right]},$$

2.4.3.3 Corner Crack at a Hole

The stress intensity factor for a nearly quarter-circular corner crack at an open hole contained in a plate subjected to uniform tension load is

$$K_I = 0.7114 \, K_I^{(1)} = 0.7114\left\{ F\left(\frac{C}{C+R}\right) \sigma \sqrt{\pi C} \right\} \tag{52}$$

During the transition from a corner crack to a through thickness crack, the stress intensity factor at the crack tip is

$$K_I^{TR} = \beta_{TR} \, K_I^{(1)} = \left[1 - \frac{0.2886}{1 + 2\,(a/t)^2}\right] F\left(\frac{C}{C+R}\right) \sigma \sqrt{\pi C} \tag{53}$$

where t is the thickness of the plate, a is the depth of the crack.

2.4.3.4 Inside and Outside Cracks in a Tee Stringer

Stress intensity factors for the inside and outside cracks existing in a tee stringer (as shown in Figure 55) can be approximated by the following equations:

$$K_I^{(is)} = \beta_{TR} \, \beta_{FW} \, \beta_{SF} \, K_I^{(1)} \tag{54}$$

and

$$K_I^{(os)} = \beta_{TR} \, \beta_{RE} \, \beta_{NE} \, K_I^{(1)}$$

where β_{TR}, β_{FW}, β_{SF}, β_{RE}, and β_{NE} are the transition correction factor, finite-width correction factor, stiffener-flange effect correction factor, fastener load effect correction factor, and near-edge correction factor, respectively. Numerical values of these correction factors are available in reference 63.

2.4.4 EFFECTIVE STRESS FIELD METHOD

The effective stress field method was originally proposed by Chang[67] in his work on prediction of fatigue crack growth behavior at fastener holes. Chang observed that the stress intensity factor solution for a semi-infinite plate containing a single through-the-thickness edge crack is

$$K = 1.12 \ \sigma_\infty \ \sqrt{\pi a}$$

where σ_∞ is the remotely applied tensile stress, a is the crack length. In the uncracked state, the stress immediately adjacent to the hole contained in an infinite plate is three times the stress at infinity. Thus, for an existing crack which is small compared to the hole radius, the crack may be considered as an edge crack embedded in an effective stress field of $\bar{\sigma} = 3 \ \sigma_\infty$. The estimated K is then

$$K = 1.12 \ \bar{\sigma} \ \sqrt{\pi a}$$

or

$$K = 3.36 \ \sigma_\infty \ \sqrt{\pi a}$$

For a very small crack (i.e., a <<R), the stress intensity factor obtained by Bowie is[62]

$$K = 3.39 \ \sigma_\infty \ \sqrt{\pi a},$$

The error is only 1 percent.

In general, for cracks emanating from a hole contained in a plate with finite width b, the single-edge crack correction factor f (a/b), instead of the value 1.12, should be used to account for the disturbance of the stress field due to the existence of the crack, i.e.,

$$K = f \left(\frac{a}{b}\right) \ \bar{\sigma} \ \sqrt{\pi a} \tag{55}$$

38

At some distance x from the edge of the hole, the elastic stress distribution is

$$\bar{\sigma}(x) = \frac{\sigma_\infty}{2}\left[2 + \frac{\gamma^2}{x^2}\left(1 + 3\frac{\gamma^2}{x^2}\right)\right]$$

where

γ is the radius of the hole,

σ_∞ is the remotely applied tensile stress.

For through-cracks emanating from the hole with the crack tip located at x, the local stress field $\bar{\sigma}(x)$ can be considered as the effective stress in the stress intensity factor equation, i.e.,

$$K(x) = f\left(\frac{a}{b}\right)\bar{\sigma}(x)\ \sqrt{\pi a} \tag{56}$$

In terms of the elastic stress concentration factor k_t, the preceding equation becomes

$$K(x) = f\left(\frac{a}{b}\right)k_t(x)\ \sigma_\infty\ \sqrt{\pi a}$$

Thus, if the elastic stress concentration factor k_t for an unflawed hole is known, the corresponding stress intensity factor, K, for the cracked hole can be estimated by the preceding equation.

Figure 56 shows a comparison of the effective stress field solution to the known Bowie solution. It is shown that when the crack is small, the discrepancy is less than 10 percent.

The effective stress field method was employed by Chang in his study of fatigue crack growth at cold-worked fastener holes.[68] The effective stress intensity factor $\bar{K}$ was formulated in terms of the effective stress $\bar{\sigma}$, which is defined as

$$\bar{\sigma} = \left(F_c\ \sigma_\infty + \sigma_{Res}\right)$$

where σ_∞ is the remotely applied tensile stress, σ_{Res} is the residual stress introduced by the cold-working process. F_c is the correction factor for the influence of the hole to the local stress field.

In the general form, the effective stress intensity factor can be written as

$$\overline{K} = \beta \left(F_c\, \sigma_\infty + \sigma_{Res} \right) \sqrt{\frac{\pi a}{Q}} \qquad (57)$$

where β is the geometrical correction factor, a is the crack depth and Q is the shape factor.

2.5 DAMAGE ACCUMULATION TECHNIQUES

The state-of-the-art fatigue crack growth analytical prediction methods are primarily based on a damage accumulation scheme which interrelates the following elements:

1. Fatigue crack growth rate relationship and the corresponding rate constants, fatigue fracture properties, as well as other related material properties.

2. Loading spectra descriptions and other information, such as residual stresses etc

3. Initial flaw (crack) configurations, sizes, locations, and geometries of the cracked body.

4. Crack tip stress intensity factor solution

5. Integration procedures

As discussed in previous sections, the growth rate of a crack subjected to cyclic loadings can be expressed in general as

$$\frac{da}{dN} = F\left(a, \sigma_{max}, R, \beta(a) \ldots\right)$$

where a is the crack size, σ_{max} is the maximum applied cyclic stress, $\beta(a)$ is a geometrical function, and R is the cyclic stress ratio. The preceding equation is a first-order differential equation. Numerous methods can be used to solve this equation depending on the specific application. In general, two categories

40

of analytical predictions are commonly required. Category I is the estimation of the elapsed time (number of cycles) which is required to grow a crack from an initial size a_0, to the final size, a_f, subjected to cyclic-loading conditions. Category II is the prediction of the incremental growth of a known crack within a period of time (cycles). In mathematical forms, one has

category I:

$$N = \sum_{i=1}^{N-1} \Delta N_i = \sum_{i=1}^{N-1} \left[\frac{a_{i+1} - a_i}{F\left(a, \sigma_{max}, R, \beta(a)\right)_i} \right] \tag{58}$$

category II:

$$\Delta a = a_f - a_o = \sum_{i=1}^{N} \left. \frac{da}{dN} \right|_i \tag{59}$$

In category I, for a simple case such as a center crack contained in a wide plate subjected to constant amplitude cyclic loading, equation 58 can be directly integrated as follows:

$$\Delta N = \int_{a_o}^{a_f} \frac{da}{f\left(a, \sigma_{max}, \ldots\right)} = \int_{a_o}^{a_f} \frac{da}{C\left[(1-R)^m K_{max}\right]^n}$$

$$= \frac{2}{C(2-n)(1-R)^{mn}\left(\sigma_{max}\sqrt{\pi}\right)^n} \left(a_f^{\frac{2-n}{2}} - a_o^{\frac{2-n}{2}} \right) \tag{60}$$

Equation 60 resulted by employing the following fatigue crack growth rate equation and the crack tip stress intensity factor solution:

$$\frac{da}{dN} = c\left[(1-R)^m K_{max}\right]^n$$

$$K_{max} = \sigma_{max}\sqrt{\pi a}$$

41

where c, m, and n are the crack growth rate constants, R is the stress ratio, and σ_{max} is the maximum cyclic stress.

If both the initial and final crack sizes are known, the elapsed time (number of cycles) which is required to grow the crack can be obtained directly from the closed form solution as represented by Equation 60.

In most cases, closed form solutions are not always feasible. This is due to the complexity of crack growth rate expressions when overload and under-load cycles are existing and rapid changes in the geometrical correction function of the stress intensity factors. A crack emanating from a fastener hole contained in an airframe structure subjected to flight-by-flight spectrum loading is a typical example. In such case, a load interaction crack growth model in conjunction with a complex stress intensity factor solution for cracked fastener holes as presented in preceding paragraphs shall be used. Numerical integration of Equation 58 is thus necessary.

To calculate the increase in crack size resulting from a known period of time (load cycles), ΔN can be evaluated by solving Equation 59. Several integration techniques are available to provide the solution of Equation 59. These include the Runge-Kutta, Taylor series approximation, and linear approximation methods.

2.5.1 RUNGE-KUTTA INTEGRATION TECHNIQUE

The Runge-Kutta integration technique[69] requires the knowledge of the current crack size a_n as follows:

$$\Delta a = a_{N+1} - a_N = \frac{1}{6}(k_0 + 2k_1 + 2k_2 + k_3) \tag{61}$$

where the Runge coefficients are defined as

$$k_0 = \Delta N \cdot \left.\frac{da}{dN}\right|_{a_N}$$

$$k_1 = \Delta N \cdot \left.\frac{da}{dN}\right|_{a_N + k_0/2}$$

$$k_2 = \Delta N \cdot \left.\frac{da}{dN}\right|_{a_N + k_1/2}$$

$$K_3 = \Delta N \cdot \left.\frac{da}{dN}\right|_{a_N + k_2}$$

42

Figure 57 illustrates the geometrical interpretation of the values k_0 through k_3. All four k-values represent the slopes at various points; value k_0 is the slope at the starting point, k_3 is the slope at the right-hand point whose ordinate is $a_N + k_2 \Delta N$; k_2 is one of the two slopes considered at the midpoint with the ordinate $a_0 + 1/2\ k\ \Delta N$; and finally, k, is the second slope at the midpoint whose ordinate is $a_0 + 1/2\ k_1\ \Delta N$.

The Runge-Kutta integration method is currently used in the CRACKS program developed by Engle[70]. This method is very accurate, yet it consumes a substantial amount of computer time, since the Runge-Kutta integration technique involves calculating da/dN a minimum of four times for each load cycle.

2.5.2 TAYLOR SERIES APPROXIMATION METHOD

The Taylor series approximation method is employed by the CGR program developed by Johnson[71]. The following paragraphs briefly describe how it works.

Applying the Forman equation for example, and separating terms a and N yields

$$C\Delta N = \int_{a_i}^{a_f} \frac{(1 - R)K_c - \Delta K(a)}{\left[\Delta K(a)\right]^n}\ da \tag{62}$$

Define

$$\mu = \int_{a_i}^{a_f} G(a)\ da \tag{63}$$

where $\mu = C\Delta N$ and $G(a) = \dfrac{(1 - R)K_c - \Delta K(a)}{\left[\Delta K(a)\right]^n}$

Since μ is generally smaller than $G(a)$, Equation 63 can be approximated with

$$\mu \simeq G(a_i) \int_{a_i}^{a_f} da = G(a_i)\ (a_f - a_i) \tag{64}$$

43

Expanding $G(a)$ into the Taylor series about $a = a_i$ whereupon the resulting series is integrated yields

$$\mu = \sum_{m=0,1,2} P_m (\Delta a)^{m+1} \tag{65}$$

where

$$P_m = \frac{a_i^{m+1}}{(m+1)!} \left. \frac{d^m G(a)}{da^m} \right|_{a = a_i}$$

and

$$\Delta a = \frac{a_f}{a_i} - 1$$

In his original work, Johnson[71] assumed that Δa is expressed into a power series expansion:

$$\Delta a = \sum_{P = 1,2,\ldots} \mu^P a_p \tag{66}$$

Upon substituting Equation 66 into Equation 65 and equating to zero the coefficients of every integral power of μ, a sequence of equations can be obtained as follows:

$$P_o a_1 = 1$$

$$P_o a_2 + P_1 a_1^2 = 0$$

$$P_o a_3 + 2P_1 a_1 a_2 + P_2 a_1^3 = 0$$

$$\cdot$$
$$\cdot$$
$$\cdot$$

44

Solutions of a_1, a_2, a_3, etc. can then be determined from the following relationships:

$$a_1 = \frac{1}{P_0}$$

$$a_2 = -\frac{P_1}{P_0^3}$$

$$a_3 = \left(\frac{-P_0 P_2 + 2P_1^2}{P_0^5} \right)$$

The final crack size a_f can be calculated by using Equation 66, or

$$a_f = a_i (1 + \Delta a) = a_i \left(1 + \sum_{P=1,2,3,\ldots} \mu^P a_P \right) \tag{67}$$

2.5.3 LINEAR APPROXIMATION METHOD

The linear approximation method assumes that the growth rate is constant throughout a load step in the spectrum so that the crack size is in a linear relationship with the number of load cycles. This damage accumulation technique was proposed by Vroman, which was first employed in the Rockwell in-house developed computer routine program, EFFGRO,[72] and is currently widely adopted throughout the industry. The following paragraphs describe this accumulation procedure used in EFFGRO.

The load spectrum in the actual integration portion of the EFFGRO program is:

Step	Max stress	Min stress	No. of cyc/ block (flight)
1	σ_{max_1}	σ_{min_1}	N_1
2	σ_{max_2}	σ_{min_2}	N_2
3	σ_{max_3}	σ_{min_3}	N_3
$\vdots$	$\vdots$	$\vdots$	$\vdots$
i	σ_{max_i}	σ_{min_i}	N_i

The damage accumulation scheme proceeds by considering a load step (i) and using σ_{max_i} and σ_{min_i} to calculate K_{max}, K_{min}, R, and da/dN.

The value of (0.01a)/(da/dN) is then compared to N_i, where "a" is the crack size. If (0.01a)/da/dN) is greater than N_i, then the crack growth for that particular load step is $\Delta a = N_i$ x (da/dN); "a" is increased by Δa, and the program proceeds to the next load step.

If (0.01a)/da/dN) is less than or equal to N_i, then the number of cycles to grow (0.01a) is (0.01a)/(da/dN). This value is subtracted from N_i, the crack size "a," is increased by (0.01a), and the load step is reconsidered. This process continues with (0.01a)/(da/dN) being compared to the remaining cycles in the step. When all load steps in the block (or flight) are exhausted, the program proceeds to the first step of the next block (or flight). The calculation ends when K_{lim} computed with the limit load or the maximum spectrum load, whichever is greater, exceeds the input critical stress intensity factor value.

2.6 PROBABILISTIC APPROACHES

The prediction of fatigue crack growth in service is one of the most important problems in the fatigue analysis and design of aircraft structures. Unfortunately, crack growth in service involves considerable statistical variability which is attributed to, among others, (1) the inherent crack growth variability of materials, and (2) the statistical nature of service loads experienced by the aircraft structures. Even under laboratory-controlled conditions, test results indicate statistical scatter in crack growth rate when the specimen is subjected to constant-amplitude fatigue loading.

It is well known that gust turbulences to aircraft structures are statistical in nature. While the maneuver loads are controlled, they do exhibit significant statistical variability. As a result, various probabilistic approaches to fatigue crack growth have been attempted in the literature. Probabilistic approaches to deal with the crack growth variability due to material and that due to service loads are discussed in the following paragraphs.

2.6.1 FATIGUE CRACK GROWTH UNDER CONSTANT-AMPLITUDE LOADING

Under laboratory test conditions, the crack growth rate, da/dN, is related to the stress intensity range, ΔK, through the following equation[73,74,75]

$$\frac{da}{dN} = C(\Delta K)^b \tag{68}$$

in which C and b are experimental constants which depend on such factors as the mean cyclic stress, the test environment, and the cyclic frequency.[75-84] Both C and b are subjected to some statistical variability and

$$\Delta K = \beta \Delta S \sqrt{a} \tag{69}$$

in which ΔS is the stress range, and β is the geometric term for structural configuration which may be a function of the crack size.

While both C and b are treated as random variables, it is assumed in References 7 and 85 that only one of them is an independent random variable. It has been observed that the variability of the slope, b, of the crack growth rate (in log scale) is relatively small and, hence, it can be neglected.[84,86] Consequently, the statistical variability of the crack growth rate can reasonably be reflected by that of C.

Taking the log on both sides of equation 68, one obtains

$$\log \frac{da}{dN} = \log C + b \log \Delta K \tag{70}$$

Let

$$Y = \log \frac{da}{dN} ; \quad X = \log \Delta K \tag{71}$$

$$\alpha = \log C ; \quad \gamma = b$$

Then equation 70 can be written as

$$Y = \gamma X + \alpha \tag{72}$$

Using techniques of standard linear regression analysis, one can find the estimates of α and γ, denoted by $\hat{\alpha}$ and $\hat{\gamma}$. If α is assumed to be a normal random variable with the mean $\hat{\alpha}$, then the standard deviation of α can be estimated from a given set of test data. Thus, it follows from equation 72 that the statistical distribution of the crack growth rate, da/dn, is lognormal. The mean and the coefficient of variation of da/dN can then be obtained from the mean and the coefficient of variation of α.

Let a_{cr} be the critical crack size associated with the design load P_{xx}. Then, the number of cycles, N_F, to fatigue fracture (i.e., the number of cycles to propagate a crack from its initial crack size, a(0), to the critical crack size, a_{cr}) can be obtained by integrating equation 68, as follows:

$$N_F = \int_{a(0)}^{a_{cr}} \frac{da}{C(\Delta K)^b} \tag{73}$$

Because of the scatter exhibited by both the initial crack size and the crack growth rate, N_F is clearly a random variable. For a special case where ΔS and b are both constants during the entire crack growth process, equation 73 can be integrated in a closed form yielding the following relationship:

$$a_{cr} = [a^{-m}(0) - mC(\beta\Delta S)^b N_F]^{-1/m} \tag{74}$$

in which

$$m = \frac{b}{2} - 1 \tag{75}$$

If the critical crack size, a_{cr}, is much larger than the initial crack size, $a(0)$ (i.e., $a_{cr}/a(0) >> 1$), then equation 74 can be approximated by:

$$N_F (\Delta S)^b = 1/m \; a^m(0)C\beta^b \tag{76}$$

Equation 76 can be written in the form of the classical S-N curve, as follows:

$$\bar{K}(\Delta S)^b N_F = 1 \tag{77}$$

in which

$$\bar{K} = ma^m(0)C\beta^b \tag{78}$$

It can be observed from equation 78 that $\bar{K}$ is a statistical variable and that the statistical dispersions of both the initial crack size, $a(0)$, and the crack growth rate, C, are reflected by that of K. The statistical approach, using the S-N curve of equation 77 along with the Miner's damage rule, considering $\bar{K}$ as a statistical variable, has been used in the literature.[87-88]

From various published reports, the scatter of the crack growth inherent in materials, as represented by the coefficient of variation of C, is approximately 15 to 20 percent. Such a statistical scatter is clearly much smaller than that of the fatigue life, which involves also the crack initiation. Thus, the statistical dispersion of the fatigue life is essentially contributed by that of the time to crack initiation. Recent investigations[89] indicate that the statistical dispersion of the time to fatigue crack initiation can be derived from that of the equivalent initial crack size. As a result, the statistical variability of the fatigue life under constant-amplitude loading is essentially due to the statistical variability of the equivalent initial flaw size, which depends on the materials, manufacturing, and assembling processes.

2.6.2 FATIGUE CRACK GROWTH UNDER VARIABLE-AMPLITUDE LOADING

For simplicity, service loadings to aircraft structures are usually simplified by repetitive spectrum loadings with variable amplitudes. Under variable-amplitude loading, the retardation effect due to high tensile loads and the acceleration effect due to compressive loads are of particular importance. The crack propagation equations for variable-amplitude loading proposed to-date take the following form:

$$\frac{da}{dN} = f(\overline{K}_{max}, \overline{R})$$

(79)

where $\overline{K}$ and $\overline{R}$ are the effective stress intensity factor and effective stress ratio, respectively.

Integration of either equation 68 or 79 from the initial crack size $a(0)$ to any intermediate crack size $a(N) < a_{cr}$ yields

$$a(N) = a(0) + \sum_{j=1}^{N} \Delta a(j)$$

(80)

in which $a(N)$ is the crack size at N cycles.

Various models and approaches have been proposed to account for the load interaction effect in a deterministic manner in which the cycle-by-cycle integration is used in equation 80, as summarized in Paragraph 2.3 and in References 90 through 95.

2.6.3 FATIGUE CRACK GROWTH UNDER STATIONARY GAUSSIAN RANDOM LOADING

Service loads to aircraft structures are random in nature.[97-102] Hence, crack propagation under stationary Gaussian random loading has attracted considerable attention. The following power law for crack propagation has been observed experimentally and used in the literature:[94,103,109]

$$\frac{da}{dN} = C \overline{\Delta K^b}$$

(81)

in which C and b are material and geometrical constants, and $\overline{\Delta K^b}$ is the average value of the bth power of the range, ΔK, of the stress intensity factor. For a through-thickness crack, one has

$$\overline{\Delta K^b} = \overline{S^b} a^{b/2}$$

(82)

49

where $\overline{S^b}$ is the average value of the bth power of rises and falls of the Gaussian random stress history X(t). (See Figure 58.)

A stationary Gaussian random stress history X(t) is defined by its one-sided power spectral density $G(\omega)$.[99-102] It can be observed from equation 82 that in order to predict the crack growth rate da/dn for a given power spectral density $G(\omega)$ of X(t), the average value of the bth power of rises and falls, $\overline{S^b}$, has to be estimated. The mathematical approach to estimate $\overline{S^b}$ is proposed in References 104 and 105, in which cumbersome multiple numerical integrations have to be performed.

A simpler approximation to compute $\overline{S^b}$ is suggested in Reference 109 using the statistics of envelope. For instance, for b=4,

$$\overline{S^4}(\sigma_i) = \overline{S^4} = A_4 \sigma_i^4 \tag{83}$$

$$A_4 = 16 + 12\pi {}_2F_1 \left(-\frac{1}{2}, -\frac{3}{2}; 1; k_0^2\right) + 24 {}_2F_1 \left(-1, -1; 1, k_0^2\right)$$

in which $\overline{S^4}(\sigma_i)$ is equal to $\overline{S^4}$ when the root mean square of the applied stress S(t) is σ_i, ${}_2F_1$ is the hypergeometric function, and k_0^2 is the sum of the squares of the sine Fourier transform and the cosine Fourier transform of the normalized power spectral density, $G(\omega)/\sigma_i^2$.

Analytical expressions of $\overline{S^b}$ for other values of b are given in Reference 109. It is proposed in Reference 110 to obtain the statistics, $\overline{S^b}$, by use of the Monte Carlo simulation.

2.6.4 FATIGUE CRACK GROWTH UNDER GUST LOADS

The atmospheric turbulences and, hence, the gust loads to aircraft have been modeled as a stationary composite Gaussian random process[97-102] which differ from a single stationary random process described in the preceding. The gust loading S(t) consists of a series of turbulence patches modeled as stationary Gaussian random processes $S(t,\sigma_i)$, i=1,2,..., where σ_i is the root mean square of each turbulence patch. The power spectral densities $G_i(\omega)$ for $S(t,\sigma_i)$, i=1,2,..., are identical when normalized with respect to σ_i^2; i.e., $G_i(\omega)/\sigma_i^2$ is invariant for all i=1,2,....

Under the gust loads thus defined,[97-102] it is shown in References 9 and 111 that the average value, $\overline{S^b}$, of the bth power of rises and falls of the applied stress, S(t), for b=4 is

$$\overline{S^4} = 3A_4 (P_1 \sigma_{c1}^4 + P_2 \sigma_{c2}^4) \tag{84}$$

50

in which P_1 and P_2 represent the fractions of nonstorm turbulence (clear air) and the thunderstorm turbulence, respectively, with associated intensities σ_{c1} and σ_{c2}, where $P_1+P_2=1$. Parameters P_1, P_2, σ_{c1}, and σ_{c2} are referred to as turbulence field parameters and they are specified in Reference 112 for various altitudes.

Thus, equation 81 can be used for predicting the crack growth under gust turbulences where S^4 is given by equation 84. Such an approach is used in References 110, 9, and 111.

2.6.5 FATIGUE CRACK GROWTH UNDER SPECTRUM LOADING

Service loads to aircraft structures can be very complex, including gust turbulences, ground-air-ground loads, ground loads, maneuver loads (air-to-ground combat, air-to-air combat, training, etc). In addition, aircraft is also intended for multiple missions or usages, thus complicating the service loads. As a result, the fatigue crack growth analysis using cycle-by-cycle integration is very cumbersome. From the standpoint of numerical analysis and laboratory testing, it is extremely desirable if a highly complex spectrum loading can be converted into equivalent constant- or variable-amplitude loading that will produce the same crack growth. Then, the crack growth damage prediction can be made by performing the flight-by-flight integration, thus reducing the significant amount of computer time.

The search of an equivalent constant-amplitude test to replace the random load test was made by Barsom.[94] He showed that for some random loads the rate of crack growth was approximately equivalent to the rate of crack growth under constant-amplitude test with the same minimum load and an amplitude representing the root-mean-square amplitude of the random test (equation 80).

2.6.5.1 Elber's Approach

Elber[18,91] proposed an equivalent constant-amplitude concept which was developed based on the crack-closure phenomenon. Test results[18] indicate that the crack opening load remains fairly constant, while cracks propagate under repeated random load sequence containing several thousands of load peaks. When the crack opening load is essentially constant and known, the equivalent constant-amplitude concept, in effect, replaces the random loads with constant-amplitude loads in the crack growth calculation.

The crack propagation law proposed by Elber[18] states that the crack growth rate is a power function of the effective stress intensity factor range only; i.e.,

$$\frac{da}{dN} = C(\Delta K_{eff})^{\lambda} \tag{85}$$

where the effective stress intensity range, ΔK_{eff}, is measured relative to the load at which the crack fully opens.

Therefore, the entire approach hinges on the determination of the crack opening load. An empirical or analytical method for predicting the crack opening for a particular load spectrum is needed in order to apply the concept to fatigue design and analysis. A numerical analysis to calculate the crack opening load was proposed by Newman.[93] An equation of crack growth equivalence was developed by Elber[91] to obtain equivalent failure crack lengths or equivalent crack growth modes. Elber's method has been applied to crack growth of Ti-8Al-1Mo-1V with real time and accelerated flight-by-flight loading by Imig.[92]

2.6.5.2 Gallagher's Approach

Perhaps the most significant contribution in converting the complex flight spectra into equivalent constant-amplitude loading that will produce the same crack growth lives is made by Gallagher,[75-77] called miniblock approach. Gallagher's approach uses a crack-incrementation scheme to analytically generate "miniblock" crack growth rate behavior prior to predicting life. The miniblock approach, in effect, combines such features of methods as (1) cycle-by-cycle integration,[78-83,90-96] (2) statistically based stress-parameter characterization,[94,103-109] and (3) crack growth data generated by tests.[95,113,114]

Service stress spectra normally have a few identifiable stress events which repeat themself with a period ΔT. Within each period, the stress histories or events can only be described statistically. The repeatable stress events in the service spectrum can then be used to separate the spectrum into a series of consecutive stress miniblock. One distinctive repeated miniblock of aircraft spectra is the "flight," which consists of takeoff, landing, and all stress events in between. The stress characteristics of the miniblock (or flight) depend on the mission of the aircraft. Military aircraft are usually multimission vehicles, so that each miniblock will not contain identical stress histories. However, in order to develop a tractable approach for fatigue crack growth behavior induced by complicated spectra, the variation of the stress events between each repeatable miniblock should be averaged out statistically.

The aforementioned approach is also motivated by the observation of the flight-by-flight crack growth rate behavior, da/dF, induced by two multi-mission military-transport-wing stress spectra (A and B) as a function of the

52

root-mean-square stress intensity factor parameter $\overline{K}_{max}$, as shown in Figure 59. The average crack growth rate per flight shown in Figure 59 can be written as

$$\frac{da}{dF} = C(\overline{K}_{max})^\lambda \tag{86}$$

in which

$$\overline{K}_{max} = \overline{(\sigma_{max}^2)}^{1/2} \psi(a) \tag{87}$$

where $\overline{\sigma_{max}^2}$ is the root-mean-square of the stress histories, and $\psi(a)$ can be expressed in terms of the stress intensity factor coefficient, $\beta(a)$, as

$$\psi(a) = \beta(a)\sqrt{\pi a} \tag{88}$$

While equation 86 is statistically similar to equation 81, it applies to the miniblock in which gust loading is only a stress event. Service spectrum having a stress event periodically described in the preceding is referred to as the steady-state spectrum by Gallagher.

When the experimental data, such as those shown in Figure 59, are available, a least-square-curve fitting can be used to estimate C and λ appearing in equation 86. Then, the miniblock damage-integration equation equivalent to equation 80 is

$$a(N) = a(0) + \sum_{j=1}^{N_F} \Delta a(j) \tag{89}$$

in which N_F represents the number of miniblocks corresponding to the crack length a(N), and $\Delta a(j)$ as computed using equation 86, where C and λ have been experimentally determined.

The miniblock growth rate can also be determined analytically in the following manner. [77] The periodicity of the spectrum is established by isolating the group of statistically repeating miniblocks. Let N_G be the number of miniblocks in a statistically repetitive group, and let N_H be the total number of miniblocks in a spectrum. Then, the efficiency of the miniblock damage integration equation given by equation 89 can be combined with the accuracy of cycle-by-cycle damage integration given by equation 80, as follows:

$$\Delta a = a(N) - a(0) = \sum_{j=1}^{N_G} \sum_{i=1}^{N_j} \Delta a(i) \tag{90}$$

53

in which Δa is the crack-length increments for any group of N_G miniblocks, and N_j is the total number of stress cycles in the jth miniblock.

Two methods have been proposed by Gallagher[75-77] to obtain the analytical equivalent of equation 86 by coupling a crack-incrementation scheme to the application of equation 90. These two methods are referred to as the simple crack incrementation-miniblock approach and the statistical crack-incrementation miniblock approach, respectively. It was shown that the crack growth behavior and the life prediction based on the miniblock approach had good correlation with experimental test results.

2.6.6 STATISTICAL DISTRIBUTION OF CRACK DAMAGE

Current Air Force durability requirement states that the economic life of aircraft structures should be in excess of the design life. The prediction of the economic life of aircraft structures is based on the statistical distribution of the intermediate crack size $a(N)$. Since the intermediate crack size $a(N)$ is related to the initial crack size $a(0)$ through equation 80 or 89, the statistical distribution of $a(N)$ can be obtained from that of $a(0)$.

Test results of the initial crack size $a(0)$ are available, and they have been characterized by the Johnson distribution.[73] Recently, a new distribution has been proposed for $a(0)$ based on additional test results.[115] With a given distribution function of $a(0)$, the numerical integration schemes proposed in Reference 73 (equation 80) and Reference 18 (equation 89) can be used to obtain the statistical distribution of $a(N)$ by selecting a number of sample values of $a(0)$ to determine the corresponding sample values of $a(N)$. The approach, referred to as the Monte Carlo simulation, is schematically shown in Figure 60. In fact, the statistical variability of the crack growth rate inherent in materials can also be taken into account in this approach. The method is straightforward and accurate, although it may be tedious numerically and expensive in computational cost.

For a given distribution function of $a(0)$, for instance the Johnson distribution, the distribution of $a(N)$ has been obtained analytically using the flight-by-flight crack growth rate equation similar to equation 86, where $\beta(a)$ appearing in equation 88 is expressed as a power function of the crack size a.[116] With a general crack growth equation, such as equation 80, the statistical distribution of $a(N)$ has recently been obtained analytically.[115]

It has been observed that the statistical variability of the crack growth rate parameters c, b, and λ in Equations 68, 81, 85, and 86 are much smaller than that of the initial crack size a(0). Hence, the statistical dispersion of the intermediate crack size a(n) is essentially contributed by that of the initial crack size a(0). Consequently, the statistical variability of the crack growth rate parameters c, b, and λ can reasonably be neglected in the durability analysis.

For the damage-tolerance analysis, on the other hand, the initial crack size a(0) is specified in order to simulate possible existence of material and manufacturing defects. Moreover, the maximum design load P_{xx} is also specified so that the critical crack size a_{cr} is a deterministic value. Thus, the statistical variability of the fatigue life is essentially attributed to that of the crack growth rate parameters, c, b, and λ. Consequently, for the damage-tolerance design, the statistical variability of the crack growth rate parameters should be taken into account to reflect the variability of fatigue life.

3.0 METHODOLOGY DEVELOPMENT TESTING

3.1 METHODOLOGY DEVELOPMENT TEST PROGRAM

3.1.1 INTRODUCTION

Task I of Phase I called for an evaluation of the state-of-the-art of present methods for predicting fatigue crack growth under flight-by-flight loading. Following the completion of this study, it was planned that a general methodology would be developed for characterizing flight-by-flight loading, eliminating the necessity for a cycle-by-cycle analysis while predicting equivalent crack growth behavior. To aid in the formulation of this methodology, an experimental program was planned to study the significant stress parameters which control the rate of damage on a flight-by-flight basis, and the load interaction effects such as tension overload retardation, compressive load acceleration, tension-tension underload acceleration, high-low, low-high block loading sequence, etc.

3.1.2 TEST DESCRIPTION

The methodology development test program consisted of a series of eight baseline tests to develop basic fatigue crack growth rate properties plus five groups of methodology development test specimens varying in complexity from simple constant-amplitude tests to complex random cycle-by-cycle spectrum tests. The baseline tests applied a common maximum stress of 20 ksi with variations in the R-factor ranging from +0.70 to -0.30. One special static test was conducted on a precracked specimen to verify the fracture toughness of the material. The methodology development tests consisted of the following five groups:

Group I   - Constant-amplitude loads - 10 tests

Group II   - Single or periodical overload/underload - 20 tests

Group III- Multiple overload/underload - 30 tests

Group IV   - Simplified flight spectrum - 25 tests

Group V   - Random cycle-by-cycle spectrum - 13 tests

Details of the loading conditions for each test are shown in Appendix C. The magnitudes of the maximum stresses, the stress ratios, and the number of cycles selected for each test were aimed to study the parameters which control the damage on a flight-by-flight basis. The random cycle-by-cycle spectra were selected based on the load data furnished by the Air Force,[117, 118] where the simplified flight spectra were generated by the equivalent damage criteria developed in this program. (Refer to Section 4.0 for details.)

3.1.3 MATERIAL AND SPECIMENS

All experimental evaluations were performed on plates from a single heat of 2219-T851 aluminum alloy procured to specification QQ-A-250/30. The plates were 48 by 144 inches and had a nominal thickness of one-fourth inch. The plate material was purchased from Ti-Con Industries, Huntington Beach, Calif. A description of the material, including the chemical and physical properties, follows:

2219-T851 aluminum QQ-A-250/30,
1/4 x 48 x 144 inches

Mill source: Reynolds

Chemical properties									
Heat no.	Al	Mg	Mn	Zn	Zr	Si	Fe	Cu	Ni
7430252D		0.02	0.20 0.40	0.02 0.10		0.05 0.15	0.10 0.25	5.8 6.8	
	Cr	Ti	Th	Ca	c	S	P	Others	
	0.10	0.20 0.30						Each 0.05 max Total 0.15 max	

Physical properties			
Heat no.	Yield strength	Tensile strength	% Elong
7430252D	46,000 min (psi)	62,000 min (psi)	8 min

The test specimen blanks were machined from three plates. Each blank was uniquely serialized to identify the plate from which it came and it location within that plate. The blanks were then finish-machined to the configuration shown in Figure 61. All test section thicknesses were 0.250 inch and the longitudinal grain was oriented parallel to the loading direction. The center notches were installed by EDM Laboratories, Garden Grove, Calif., employing the wire electrical discharge machining process. The center-notch configuration was selected in order to minimize the geometric considerations in the calculation of the stress intensity factor.

3.1.4 TESTING PROCEDURES

All tests were conducted in Rockwell LAD's Structure Test Laboratory, employing the 500 and 1,500K MTS Fatigue Testing Systems. An MTS load tower (Figure 62) consists of a rigid load frame and incorporates a dual bridge load cell and hydraulic actuator. Applied loads are controlled through a closed-loop servo system and load programmer test system, with load cells and servo valves optimized for controllability and cyclic load rate. The MTS system uses a Digital PDP 8E digital computer for program control. All tests except the randomized cycle-by-cycle spectrum tests were controlled by the MTS system. The randomized tests were controlled by the Datum Servo System 70, a computer-controlled fatigue test system selected for this application because of its capability to handle much longer waveforms than is possible with the integral MTS computer equipment. As used on the random spectrum tests, the Datum system acts as a waveform generator and provides a command signal output to the MTS servo controller. The MTS system returns a load cell feedback signal to the Datum system which was used for "desired versus actual load" error checking. The only other interfaces between the two systems are discrete signals providing test control, including hold, run, and ramp on servo controller error detection. A schematic of the interrelationship of the MTS and Datum 70 systems is shown in Figure 63. Loads were transmitted from the test machine heads to the specimens through hydraulically actuated friction grips.

The EDM crack starter slot in each specimen was precracked to produce an initial crack length, 2a, of 0.30 inch, approximately. Precracking was performed under constant amplitude cycling at an R-factor of zero and with maximum cyclic stresses of 8 ski or 10 ski, but in no case exceeding the maximum stress applied in the subsequent test. All tests were run in ambient laboratory air at room temperature. The cyclic rate for constant amplitude testing was approximately 6 Hz and for spectrum testing between 4 and 6 Hz depending on such factors as load level, load range, and the presence of compression loads. Crack growth was measured by visual optics reading from precision scales attached to each side of the specimen adjacent to the EDM slot. Measurements were made and recorded after approximately each 0.05-inch increment of growth. The long edges of the specimens were restrained against lateral motion when subjected to compression loads.

All raw test data tabulations and plots are contained in Volume II of this report. The data as measured in the laboratory is listed in columns of measured crack length and cumulative cycles. Additionally, a curve of half-crack length, a, versus cycles, N, is plotted for each test through use of the PLOTRATE program.

3.2 RESULTS AND DISCUSSION OF TEST DATA

3.2.1 BASELINE TEST RESULTS

The baseline tests were used to develop the crack growth rate constants employed in the selected growth-rate equations. To obtain these constants, the raw data, which were collected and tabulated by the laboratory in the form of crack length vs cycles, were processed through the PLOTRATE program. PLOTRATE is an automated fatigue crack-growth-rate data processing program which calculates and plots the cyclic crack growth rate, da/dN, versus various functions of K and R, such as ΔK, $(1-R)^m K_{max}$, etc, on a double logarithmic scale. The cyclic growth rate da/dN is calculated by the seven-point incremental polynominal method.

PLOTRATE determines the crack growth rate constants C and n by least square fitting of the test data. An alternate form of raw test data presentation by PLOTRATE is a linear scale plot of crack length versus test cycles. In either form of plotting, data from several tests can be plotted on a single graph to compare crack growth characteristics and/or to obtain a set of growth-rate constants for a specific test parameter.

For the baseline tests, the desired output from PLOTRATE was a graph of crack growth rate, da/dN, versus the selected form of f (K, R). An example of the PLOTRATE output for four tests run at an R-factor of zero is shown in Figure 64. The constants C, m, and n listed in the figure were used in the crack-growth-rate equations for all subsequent predictions of the methodology development tests.

3.2.2. CRACK GROWTH PREDICTION METHODOLOGY TESTING RESULTS

The crack-growth prediction methodology tests consisted of specimen groups I, II, and III as described in Section 3.1.2, a total of 60 tests identified as M-1 through M-60. These tests were confined to relatively simple cyclic load sequences including constant amplitude tests at different R-factor and maximum stresses (M-1 through M-10), single or periodical overload/underload tests (M-11 through M-30), and multiple overload/underload tests (M-31 through M-60). The measured crack growth data were processed through the PLOTRATE program resulting in a tabular listing and a linear scale plot of crack size versus test cycles. (Refer to Volume II). Typical plots of crack size versus test cycles are shown in Figures 65 through 68. The effects of stress ratio, overload, underload, and compressive load to the crack growth are clearly shown.

3.2.2.1 Crack-Growth-Rate Equation and Load Interaction Models

Data from test groups I, II, and III were correlated with analytical predictions made by Rockwell's EFFGRO program using the Vroman/Chang model and also by the Air Force CRACKS program with the Willenborg model.

The EFFGRO prediction employed the following formulations for growth rate and load interaction; all compressive stresses were retained in the predictions by EFFGRO.

- $$\frac{da}{dN} = c \left[\frac{\Delta K_{eff}}{(1 - \bar{R})^{1-m}} \right]^n \quad , \qquad \begin{array}{l} 0 \leq R \leq R_{cut}, \ \bar{R} = R \\[6pt] 0 \leq R \geq R_{cut}, \ \bar{R} = R_{cut} \end{array}$$

$$\Delta K_{eff} = (K_{max} - K_{min}) - 0.33 \left[\left(\sqrt{\frac{a_{o\ell} + R_{y_{o\ell}} - a}{R_{y_{o\ell}}}} \right) K_{max_{o\ell}} - K_{max} \right]$$

- $$\frac{da}{dN} = c \left[(1 - R)^q K_{max} \right]^n \quad , \quad R < 0$$

- $$\frac{da}{dN} = 0 \quad , \quad \Delta K_{eff} \leq \Delta K_{th}$$

where

$C = 8.367 \times 10^{-10}$ 　　　　$n = 3.64$ 　　　　$m = 0.6$

$q = 0.3$ 　　　　$R_{+cut} = 0.75$ 　　　　$\Delta K_{th} = 1.5 \ KSI\sqrt{in.}$

These growth-rate constants were established by the PLOTRATE program using crack growth data generated from the baseline test group as described in Section 3.2.1.

The CRACKS predictions employed the following formulations for growth rate and load interaction; all compressive stresses were truncated to zero in the predictions by CRACKS.

- $$\frac{da}{dN} = C \left[(1-R_{eff})^m \, K_{max_{eff}} \right]^n \quad , \quad R \geq 0$$

where

$$c = 8.367 \times 10^{-10} \qquad m = 0.6, \quad n = 3.64$$

- $$\frac{da}{dN} = 0 \quad , \quad \Delta K = \Delta K_{th}$$

where

$$\Delta K_{th} = \Delta K_0 \, (1 - AR) \qquad \Delta K_0 = 1.5 \, KSI\sqrt{in.}, \qquad A = 0$$

3.2.2.2 Correlation Results

The predictions from EFFGRO and CRACKS were correlated to the experimental data in order to identify the required areas of refinement to the existing load interaction models. Figures 69 through 72 are plots of the measured crack growth data for typical tests of groups II and III together with analytical predictions by the Vroman/Chang and Willenborg models. These four tests represent a cross section of the single, periodic, and multiple overload sequences that were applied in these test groups.

Table 12 summarizes the crack-growth-data correlations for tests M-1 through M-60, including the test life predictions by Vroman/Chang and Willenborg, and the ratios of these predictions to the test lives. It can be seen that both the Vroman/Chang model and the Willenborg model predicted rather well for the periodic overload cases but not for those cases containing block of overloads such as M-43, -44, -45, and -46. Refinements of the load interaction models to accomodate the effect of the number of overload cycles are necessary. For loading cycles containing compressive stresses, the Vroman/Chang model provided apparently better predictions.

3.2.3 Spectrum Characterization Test Results and Data Correlations

The spectrum characterization tests consisted of specimen groups IV and V, a total of 38 tests identified by test numbers between M-61 and M-94. Group V consisted of 13 tests to random cycle-cy-cycle spectrum of four typical fighter missions generated by using data furnished by the

Air Force where the maximum spectrum stresses related to limit stresses of 20, 30, and 40 ksi, and two random cycle-by-cycle transport spectrum with maximum spectrum stresses of 14 and 19.6 ksi. Group IV consisted of 25 tests to simplified flight spectra with maximum stress levels related to limit stress conditions in both fighters and transports. There was a one-for-one correspondence between each of the random spectra and one or more of the simplified spectra which were generated by using the equivalent damage criterion developed in this program (refer to Appendix for detail). As were done previously, the crack growth test data were processed through the PLOTRATE program. The raw data tabulations and plots are contained in volume II of this report.

Comparisons were made on the crack-growth behavior among the random cycle-by-cycle spectra and their corresponding simplified versions. Satisfactory results were shown. For an air-to-air fighter spectrum, 30 ksi limit stress case, the crack-growth data generated under the random cycle-by-cycle loading (M-82) are shown in Figure 73 by cross symbols, where the growth data generated from their simplified versions (one-step flight segment, M-61A; two-step flight segments, M-69A; and two-step ground flight segments M-77A) are shown. It can be seen that the error of the equivalency in crack growth in M-61A, M-69A, and M-77A as compared to random loading (M-82) is about 30 percent. Similar plots for other cases are shown in Figures 74 through 79. A detailed discussion of the significance of the test results is in Section 4.0.

Analytical predictions obtained from EFFGRO were again correlated to the test data. All crack growth rate constants used in the predictions were identical to those which were employed in the correlation study presented previously. The random spectra were range-pair counted before the performance of the crack growth calculations. All correlations (M-61 to M-94) were summarized and are presented in Table 13. It can be seen that the Vroman/ Chang model predictions correlate satisfactorily with test data in this test series.

4.0 CHARACTERIZATION OF THE FLIGHT-BY-FLIGHT LOADING

4.1 INTRODUCTION

One of the primary objectives of Phase I of the present program is to identify the significant parameters which control damage on a flight-by-flight basis, and to develop methodology for characterizing flight loading which would eliminate the necessity for cycle-by-cycle analysis while producing equivalent crack growth behavior. To achieve this objective, major emphasis is placed on the parametric and statistical characterization of fighter and transport aircraft load spectra. The parametric characterization implies reduction of the flight-by-flight spectra to some combination of stress parameters within the flight. Statistical characterization implies replacement of the actual stress history with a simplified history which produces equivalent crack growth behavior.

With respect to the parametric characterization, the following four types of missions are considered for fighters: air-to-air (A-A), air-to-ground (A-G), instrumentation-navigation (I-N), and composite. Transport aircraft utilizations are defined by three flight profiles: assault, logistics, and training. The load spectra of these missions are generated with the aid of the random process theory, satisfying exceedance and spectral density requirements characteristic to their respective missions.

The crack growth rate per flight, dc/dF, is evaluated for each of these missions, taking the effect of compression stresses into account, as a function of $\overline{K} = (\overline{\Delta\sigma^b})^{1/b} \psi(c)$, where $\overline{\Delta\sigma^b}$ represents the average of the b-th power of the stress rise $\Delta\sigma$ in the stress history, and $\psi(c)$ indicates a function of crack length c whose analytical form depends on the crack shape. The unitblock approach has primarily been used for this evaluation with the aid of a Fortran code called CYCGRO. The CYCGRO program is developed on the basis of the EFFGRO program and has a capability of integrating crack growth equations cycle-by-cycle under arbitrary random flight-by-flight load spectra.

The relationship between dc/dF and $\overline{K}$ thus evaluated is, in general, a nearly perfect straight line when plotted on the log-log scale. The two parameters C and λ therefore completely describe the relationship $dc/dF = C(\overline{K})^\lambda$. The crack length c under various missions is then evaluated as a function of the number of flights by integrating such a relationship. The integration is analytically carried out by expanding $\psi^{-\lambda}(c)$ into a power series for the through-the-thickness crack. The CYCGRO program has been used to check the validity of this approach.

A study is then made to implement Method I, where an equivalent relationship for crack growth behavior under different load spectra is established and used to develop equivalent load spectra in terms of constant-amplitude stress histories (either one cycle per flight or multiple cycles per flight), or in terms of simplified (but not so simple as constant amplitude) load spectra. It is found that the simplified load spectra could provide more realistic simplifications for the real-life random flight-by-flight load spectra than constant-amplitude spectra. Furthermore, information on the crack growth behavior under simplified load spectra has provided guidelines for the experimental methodology development performed in this program. A study is also made on the implementation of Method II. In this method, each random mission segment is replaced by a constant-amplitude spectrum, and a flight is assumed to consist of such constant-amplitude mission spectra, mission transitions, and a ground-air-ground cycle. To establish in Method II the relationship among the stress parameters that will produce equivalent crack growth behaviors (under random flight-by-flight loading and under the simplified load spectra proposed in Method II), it is necessary to first establish the equivalent relationship for each individual mission segment and then the entire load spectra. For this purpose, random load spectra corresponding to three typical mission segments and flight spectra consisting of these three are generated, and the notion of equivalent average stress ratio is introduced and used for crack growth calculations. The results are then compared with those obtained by means of cycle-by-cycle integration and Method I.

An experimental testing program on crack growth for 2219-T851 aluminum specimens contained through-the-thickness cracks has been conducted as described in Section 3.0. These tests were performed under constant-amplitude loading, simplified load spectra, and random load spectra. The constant-amplitude and simplified load spectra used in the experiments were developed, satisfying the condition that an equivalent crack growth is produced under these spectra and the complex random load spectra. A comparison is then given between the experimental results and the theoretical predictions under constant-amplitude, simplified, and random load spectra.

4.2 RANDOM STRESS SPECTRA

4.2.1 FIGHTER AIRCRAFT

With the aid of computer program SPECGN1, developed for random stress process simulations in Reference 117, sufficiently long cycle-by-cycle random stress histories (in terms of peaks and valleys) based on the baseline load spectra for the F-15 aircraft are generated for A-A, A-G, I-N, and composite maneuvers. The generated peaks and valleys are in the form of percentage of design limit stress. The baseline spectral densities corresponding to A-A,

A-G, and I-N maneuvers (furnished by the Air Force) are shown in Figures 80, 81, and 82, respectively. A portion of the simulated sequence of peaks and valleys of each of these maneuvers is given respectively in Figures 83, 84, and 85.

Using these simulated stress histories, a unitblock was constructed where a unitblock implies a block of flights most representative of the missions throughout the lifetime of the aircraft. Each flight in the block contains ground-air-ground (G-A-G) cycles and all the stress events in between. To be more specific, a unitblock was constructed by selecting 50 stress history segments, each corresponding to a duration of one flight and each beginning with a valley stress and ending with a peak stress. The G-A-G cycles were inserted at the beginning and end of each flight in such a way that in each flight the first valley was replaced by and the last peak was followed by the ground load. The exception is that for the first flight in the unitblock, the first simulated stress rise was replaced by a stress rise consisting of the ground load and 70 percent of σ_{LIM}. Hence, the magnitude of the G-A-G cycles varies with each flight in the unitblock. The maneuver durations per flight were measured in terms of the number of peaks and valleys in the following fashion: A-A (52 peaks and valleys), A-G (38 peaks and valleys), and I-N (12 peaks and valleys). These selections were based on the observed peak exceedances of those type of maneuvers per flight [117, 118]. The ground loads are taken to be -5 percent of σ_{LIM} for A-A and I-N maneuvers, and -10 percent of σ_{LIM} for A-G maneuvers. The composite unitblock is constructed in the following form:

<div align="center">

11 A-A
11 A-G
 3 I-N
11 A-A
11 A-G
 3 I-N
_____

50 flights

</div>

4.2.2 TRANSPORT AIRCRAFT

A typical transport aircraft utilization was defined by three mission profiles (flights): assault, logistics, and training. Each mission was composed of four mission segments: climb, cruise, gust, and descent. Ground loads were inserted at the beginning and end of each mission. The aircraft usage mix are taken to be 57-percent assault, 5-percent logistics, and 38-percent training. The number of load cycles, the ground loads and the 1 g stresses for each mission segment are given in Table 14.

The stress histories for each mission segment were obtained from

$$S(t) = (1 + n(t)) \beta \tag{91}$$

where $n(t)$ is the incremental normal load factor and β is the conversion factor given in Table 14. The random time histories $n(t)$ (in terms of peaks and valleys)were generated again with the aid of the computer program SPECGN1 and the aid of peak exceedance diagrams given in References 119 and 120. Three levels of loading intensity are considered by multiplying the peak and valley values of stress histories constructed on the basis of peak exceedance diagrams selected from References 119 and 120 by a factor $\eta = 1.0$, 1.2 and 1.4

The necessary input to SPECGN1 in this case, is the spectral density $S_n(\omega)$, the mean value M to be used in transforming Gaussian histories into real histories, and the power exponent R* to be used in the same transformation procedure. The explicit form of spectral density $S_n(\omega)$ for a transport-type aircraft was not furnished in the present study. For simplicity, a rectangular form corresponding to a bandwidth limited white noise is assumed:

$$S_n(\omega) = S_0, \quad \beta_c \omega_c \leq \omega \leq \omega_c \tag{92}$$

$$= 0, \text{ otherwise}$$

The frequency cutoffs, $\beta_c \omega_c$, and ω_c, on the spectral density are determined by the total number of zero crossings per unit time with positive slope

$$N_0 = \left[\int_{\beta_c \omega_c}^{\omega_c} \omega^2 S_0 d\omega \Bigg/ \int_{\beta_c \omega_c}^{\omega_c} S_0 d\omega \right]^{1/2} \Bigg/ (2\pi) \tag{93}$$

68

and by the irregularity ratio $R_r = N_0/N_p$ where N_p is the number of peaks per unit time given by

$$N_p = \left[\int_{\beta_c \omega_c}^{\omega_c} \omega^4 S_0 d\omega \bigg/ \int_{\beta_c \omega_c}^{\omega_c} \omega^2 S_0 d\omega \right]^{1/2} \bigg/ (2\pi) \tag{94}$$

For the spectral shape used in equation 92, the irregularity ratio is

$$R_r = \sqrt{5/3} \left[1 - \beta_c^3 \right] \bigg/ \sqrt{(1 - \beta_c)(1 - \beta_c^5)} \tag{95}$$

Assuming the same value of parameter β_c for all mission segments, R_r is constant for all mission segments. Then, the same spectral density function can be used for all segments and only N_0 needs to be specified so that the frequency cutoffs on the spectral density function can be defined. From equation 93,

$$\omega_c = 2\pi\sqrt{3} \, N_0 \left[(1 - \beta_c) \bigg/ \left(1 - \beta_c^3 \right) \right]^{1/2} \tag{96}$$

The variance of the process n(t) can be obtained from

$$\sigma^2 = S_0 \omega_c (1 - \beta_c) \tag{97}$$

When $\beta_c = 0.5$, from equations 95, 96, and 97, $R_r = 0.937$, $\omega_c = 8.23 \, N_0$, and $\sigma^2 = 4.12 \, S_0 N_0$, where N_0 is measured in cycles/sec.

For the case of a narrow-band random process (i.e., $R_r \doteq 1$), the cumulative peak exceedances of the process x(t) can be determined from

$$N_x = N_0 e^{-x^2/2\sigma^2} \tag{98}$$

69

Equation 98 is the exceedance curve for a narrow-band Gaussian random process. The actual exceedance curves for a transport aircraft exhibit non-Gaussian characteristics.[119,120] However, in approximation, these exceedances can be taken to be symmetric with mean equal to 1 g loading. To match the actual exceedance curves, Gaussian random histories $x(t)$ are adjusted through the following transformation:

$$n = x^{R*} \tag{99}$$

Substituting equation 99 into equation 98, the exceedance curves for the actual process are obtained as

$$N_n = N_0 e^{-n^{2/R*} / 2\sigma^2} \tag{100}$$

The values of $R*$ and σ^2 are unknown and are determined by selecting two points on the actual exceedance curve. Selecting n_1 and n_2 as two points on the exceedance curve and N_1 and N_2 as the corresponding peak exceedances, we obtain from equation 100.

$$R* = 2\ell n(n_2/n_1) \Big/ \Big[\ell n\{\ell n(N_0/N_2)/\ell n(N_0/N_1)\} \Big] \tag{101}$$

$$\sigma^2 = (n_1)^{2/R*} \Big/ \Big[2\ell n(N_0/N_1) \Big] \tag{102}$$

The values of $R*$, σ^2, and N_0 for the missions selected in this study are given in Table 15. These results are based on $n_1 = 0.1$ and $n_2 = 0.5$. Peak exceedances obtained from equation 100 and from Refererences[117] and 118 are plotted in Figures 86 through 95. For comparison, simulation results obtained from SPECGN1 are also included in these plots. We observe from these results that the simulated real-time histories fit closely to the actual exceedances for low values of incremental normal load factor n. The number of exceedances at high values of n are rare events, and the simulation would not predict these values without an excessive amount of computation effort.

70

For the purpose of crack growth evaluation, a composite unitblock consisting of 21 flights is constructed in the following form:

3 Assault
2 Training
3 Assault
2 Training
3 Assault
2 Training
3 Assault
2 Training
1 Logistics
_____
21 Flights

The number of cycles for each mission segment is given in Table 14. The average number of cycles per flight for the composite unitblock is taken to be equal to 133. Peaks and valleys for each mission segment are generated using SPECGN1 and data given in Table 15.

4.3 CRACK GROWTH ESTIMATION BY METHOD I

Simplification of the flight-by-flight stress histories generated in Paragraph 4.2 begins with the introduction of the notion of crack growth rate per flight, dc/dF, and requires the following steps to be taken.

1. A particular combination of stress parameters defined in Paragraph 4.2 (such as spectral density function, exceedance curve, irregularity ratio, ground stress level, etc) is selected.

2. Sample stress histories are generated as described previously for all missions and mission segments considered in this combination. Repeating the same procedure N_A times to produce N_A consecutive sample flight spectra, a block of flights called a unitblock is constructed.

3. A computer code for the cycle-by-cycle crack growth estimation (CYCGRO) is used to evaluate the crack growth Δc due to the unitblock flight spectra under a prescribed number of different values of initial crack size c_0. Then, dc/dF can be evaluated as $\Delta c/N_A$.

4. Establish the following relationship on the basis of the foregoing numerical results

$$dc/dF = C(\overline{K})^{\lambda}$$

(103)

71

where $\bar{K}$ is a measure of the stress intensity factor representing the overall effect of the unitblock on the crack propagation. For $dc/dF = \Delta c/N_A$ to be plotted against $\bar{K}$, $\bar{K}$ needs to be estimated at a number of different values of crack size c. The crack size at the end of each unitblock is calculated from

$$c_j = c_{0j} + (\Delta c)_j \qquad (104)$$

in which c_{0j} are the selected values of the initial crack size c_0 and $(\Delta c)_j$ is the incremental change in the crack size under a unitblock loading. The values for the initial crack size c_{0j} are selected in such a way that they cover the full range of crack size from that corresponding to the initial flaw to that expected at the failure. The average stress intensity factor $\bar{K}$ is written as

$$\bar{K} = \left(\overline{\Delta\sigma^b}\right)^{1/b} \psi(c)$$

where $\overline{\Delta\sigma^b}$ represent the statistical average of the b-th power of the stress rise $\Delta\sigma$ in the stress history, and $\psi(c)$ is a function of crack size c whose analytical form depends on the crack shape. For example, for a centered through-the-thickness crack

$$\psi(c) = \sqrt{\pi c} \sqrt{\sec(\pi c/w)} \qquad (105)$$

where w is the width of the plate.

5. Each of these generated flight spectra (Figure 96a) representing a particular combination of the stress parameters, with the rate of crack growth evaluated in the form of equation 103, is then replaced by a constant-amplitude stress spectrum (Figure 96b) with the equivalent rate of crack growth. Details of such an equivalence relationship are described in Paragraphs 4.5 and 4.6. In an equivalent constant-amplitude stress spectru, one flight may be represented by one stress cycle or a number of stress cycles. The same procedures are then repeated for other combinations of stress parameters, resulting

72

in corresponding values of C, λ, and $\overline{(\Delta\sigma^b)}^{1/b}$ and also in corresponding equivalent constant-amplitude stress spectra. Thus, we now have a number of sets of parameters

$$\left[C_1, \lambda_1, \overline{\left(\Delta\sigma^b\right)}_1^{1/b} \right] , \left[C_2, \lambda_2, \overline{\left(\Delta\sigma^b\right)}_2^{1/b} \right] , \dots,$$

and a number of crack growth laws applicable to each of the stress parameter combinations:

$$dc/dF_1 = C_1 (\overline{K}_1)^{\lambda_1}$$

$$dc/dF_2 = C_2 (\overline{K}_2)^{\lambda_2}$$

$$\cdot$$
$$\cdot$$
$$\cdot$$

$$dc/dF_N = C_N (\overline{K}_N)^{\lambda_N}$$

(106)

where N is the total number of stress parameter combinations to be considered. Hence, the problem of mission mix can also be solved by using equation 106, choosing only those equations pertinent to the missions in the mix and applying them in the sequence corresponding to the mix.

6. The crack growth per flight is estimated by solving equation 103 (or 106). Such a solution can be obtained by numerical integration of

$$\int_{c_0}^{c} \psi(\xi)^{-\lambda} d\xi = C\left(\overline{\Delta\sigma^b}\right)^{\lambda/b} (F)$$

(107)

However, this way of obtaining the solution is inefficient if the required number of numerical integrations is large. By expanding the function $[\psi(c)]^{-\lambda}$ into a polynomial

$$[\psi(c)]^{-\lambda} = c^{-\lambda/2} \sum_{i=1}^{n} A_{i-1} \; c^{i-1} \qquad (108)$$

and estimating the coefficients A_{i-1} by fitting the polynomial to $[\psi(c)]^{-\lambda}$, a closed form solution for c can be obtained:

$$\sum_{i=1}^{n} \left[(2A_{i-1})/(2i-\lambda) \right] \; (c^{2i-\lambda/2} - c_0^{2i-\lambda/2}) = C \left(\overline{\Delta\sigma^b} \right)^{\lambda/b} (F) \qquad (109)$$

If one of the terms in the left side of equation 109 satisfies $\lambda = 2i$, then that term should be replaced by

$$A_{i-1} \; \ln(c/c_0) \qquad (110)$$

The polynomial fit is performed for the through-the-thickness-type cracks for which the function $\psi(c)$ is given in equation 105. In Figure 97, the relative error in fitting the curve $[\psi(c)]^{-\lambda}$ to the polynomial with a different number of terms is plotted as a function of the ratio c/w. As can be observed from these results, a polynomial consisting of 10 terms gives a good fit for $c/w \leq 0.46$ which covers the practical range for the crack growth. From equation 109, the solution corresponding to $\psi(c)$ given in equation 105 is

$$\sum_{i=1}^{n} \left[(2A_{i-1})/(2i-\lambda)w^{\lambda/2} \right] \left[(c/w)^{2i-\lambda/2} - (c_0/w)^{2i-\lambda/2} \right] = C \left(\overline{\Delta\sigma^b} \right)^{\lambda/b} (F)$$

$$(111)$$

In Figure 98, the crack length c is plotted as a function of the number of flights using the solution given in equation 111 for $\lambda = 3.4$, $C = 1.83 \times 10^{-6}$, $w = 6$ in, and $N = 10$. For comparison, the solution for c obtained by cycle-by-cycle integration of equation 103 (CYCGRO) is included in this plot. It can be observed from these results that the agreement between these two solutions is excellent.

4.4 CRACK GROWTH UNDER RANDOM LOADING

The methodology described in Paragraph 4.3 is now applied to establish the equivalent crack growth under random loading and simplifed loading for fighter and transport aircraft. The generation of random flight-by-flight load spectra for these aircraft is performed by the method described in Paragraph 4.2.

4.4.1 FIGHTER SPECTRA

The parameters λ, C, $(\overline{\Delta\sigma^b})^{1/b}$, and the product $C(\overline{\Delta\sigma^b})^{\lambda/b}$ are calculated for a through-the-thickness crack using the unitblock approach under A-A, A-G, I-N, and composite maneuvers for F-15 aircraft. One unitblock here contains 50 flights. In this procedure, several values of initial crack size c_0 are selected and the crack growth is estimated in each case for one unitblock. The sensitivity of the parameters λ and C to the number of initial crack sizes to be considered has been investigated, and it has been observed that seven to 20 initial crack sizes are adequate to evaluate λ and C for the crack growth estimation. The results are obtained with and without the effect of compressive stresses. The compressive stresses result from the ground loads and manuever excursions into negative stress regions as shown in Figures 83, 84, and 85.

The crack growth rate per flight with and without compression stresses taken into consideration is shown in Figures 99 and 100, respectively. The resulting values of λ, C, $(\overline{\Delta\sigma^b})^{1/b}$, and the product $C(\overline{\Delta\sigma^b})^{\lambda/b}$ with $b = 2$ are obtained from Figures 99 and 100 and shown in Tables 16 and 17 for three different ranges of $\overline{K}$:

$$\overline{K} \leq K_{TH}$$

$$K_{TH} < \overline{K} < K_{IC}$$

$$\overline{K} < K_{IC}$$

where K_{TH} = threshold stress intensity factor and K_{IC} = critical stress intensity factor. For the present study, $K_{TH} = 2.5$ ksi$\sqrt{\text{in.}}$, $K_{IC} = 33$ ksi$\sqrt{\text{in.}}$ (plane strain), and $K_C = 66$ ksi$\sqrt{\text{in.}}$ (plane stress).

Similar results are presented in Tables 18 and 19 for σ_{LIM} = 30 ksi, and σ_{LIM} = 40 ksi, respectively. From direct comparison of the results shown in Tables 16 and 17, it can be observed that the effect of compressive stresses is to increase the value of parameter C, while the parameter λ changes only slightly. The value of C also increases with increasing value of design limit stress σ_{LIM}. The parameter λ decreases slightly with increasing σ_{LIM}. Using the results given in these tables and the closed-form solution of the steady-state equation 111, the crack growth behavior is evaluated as a function of the number of flights. In Figures 101, 102, and 103, the crack length c is plotted as a function of the number of flights for initial crack size c_0 = 0.02 in., c_0 = 0.25 in., and c_0 = 0.5 in., respectively. These results are obtained for σ_{LIM} = 20 ksi with and without considering the effect of the compressive stresses. From these results it can be observed that with the compressive stresses considered, the number of flights to reach critical crack size decreases by about 40 percent. The sensitivity of crack growth to different design limit stress values is demonstrated in Figures 104 and 105 for the case where c_0 = 0.25 in. These results are summarized in Figure 106 for a composite maneuver load spectra input.

The numerical results presented in Figures 99 through 106 and Tables 16 and 19 are calculated using C_w = 1.7203 x 10^{-9}, n = λ_w = 3.415, m = 0.30143, and K_{TH} = 2.5 ksi$\sqrt{in.}$ where C_w and λ_w are the proportionality constant and power exponent in the Walker crack growth rate model and m is a shape factor which accounts for the effect of the stress ratio R = $\sigma_{min}/\sigma_{max}$.

Recently, new parameter values have been estimated using the fatigue crack growth data generated from the baseline testing as described in Paragraph 3.2.2.1. These new parameter values are C_w = 8.367 x 10^{-10}, n = λ_w = 3.640, m = 0.6, and K_{TH} = 1.5 ksi$\sqrt{in.}$ The crack growth rate per flight, the parameter values of λ, C, $\left(\overline{\Delta\sigma^b}\right)^{1/b}$ (b = 2), and the product $C\left(\overline{\Delta\sigma^b}\right)^{\lambda/b}$ are obtained using these values for A-A, A-G, I-N, and composite random load spectra. The crack growth rates per flight corresponding to σ_{LIM} = 20, 30 and 40 ksi are shown in Figures 107, 108, and 109, respectively. The resulting values of λ, C, $\left(\overline{\Delta\sigma^b}\right)^{1/b}$, and the product $C\left(\overline{\Delta\sigma^b}\right)^{\lambda/b}$ evaluated by the unitblock method are given in Tables 20, 21, and 22. Using these results, the crack growth behavior is evaluated as a function of the number of flights and is plotted in Figures 110 through 113. All results presented with the new material parameter values include the effect of compressive stresses.

4.4.2 TRANSPORT SPECTRA

The cycle-by-cycle random stress histories are generated in terms of peaks and valleys following the procedure described in Paragraph 4.2.2. As mentioned also in Paragraph 4.2.2, three levels of loading intensity represented by η = 1.0, 1.2, and 1.4 are considered.

Parameters λ and C per flight and per cycle are estimated using the unitblock approach. The resulting values of λ, C, $\left(\overline{\Delta\sigma^b}\right)^{1/b}$, and the product $C\left(\overline{\Delta\sigma^b}\right)^{\lambda/b}$ with b = 2 are shown in Table 23. The crack growth rate per cycle corresponding to random loading of a transport aircraft is plotted in Figure 114 against the average stress intensity factor $\overline{K}$. The corresponding crack growth is plotted as a function of the number of flights in Figure 115.

4.5 CRACK GROWTH ESTIMATION PER FLIGHT UNDER CONSTANT-AMPLITUDE LOAD SPECTRA

One of the major tasks of the current program is the development of the methods that characterize the complex real-life flight-by-flight load spectra and replace them by simplified equivalent load spectra, equivalent in the sense that they produce the same crack growth behavior. The simplest of these equivalent load spectra is obviously the constant-amplitude spectra. While a little more complex and much more realistic spectra can be construc- ted to replace the real-life spectra, as is considered later, the analysis herein is performed for the crack growth estimation under the constant- amplitude load spectra with maximum stress σ_{max} and the minimum stress σ_{min} to establish the conditions of analytical equivalence between the real-life flight-by-flight and constant-amplitude load spectra. Figure 116 illustrates such a constant-amplitude load spectrum where one flight may be represented by n constant-amplitude cycles.

The analysis reported herein uses, under the assumption that one flight con- sists of one cycle (n = 1), the CYCGRO program in conjunction with the unit- block approach, resulting, for example, in the estimated values of λ, C, $\left(\overline{\Delta\sigma^b}\right)^{1/b}$, and $C\left(\overline{\Delta\sigma^b}\right)^{\lambda/b}$. In Tables 24, 25, and 26, respectively for σ_{LIM} = 20, 30, and 40 ksi, these values are listed for 60 different combinations of σ_{max}, σ_{min}, and R values (σ_{max} = 30, 40, ..., 120 percent of σ_{LIM}, and R = -0.1, 0, 0.1, ..., 0.4). Since each flight is considered here to consist of one cycle of the stress rise and fall and one unitblock contains 50 flights as usual, one unitblock is made up of 50 such cycles. It is noted that, under the constant-amplitude load spectra, $\left(\overline{\Delta\sigma^b}\right)^{1/b} = \Delta\sigma = \sigma_{max} - \sigma_{min}$ = stress rise by definition. In Tables 24, 25, and 26, the maximum stress is expressed in terms of the percentage of the design-limit stress σ_{LIM}, which is assumed to be 20, 30, and 40 ksi for the numerical analysis. For the purpose of com- parison, the values of λ, C, $\left(\overline{\Delta\sigma^b}\right)^{1/b}$, and $C\left(\overline{\Delta\sigma^b}\right)^{\lambda/b}$ corresponding to A-A, A-G, I-N, and composite maneuvers derived from F-15 baseline spectra are also included in these tables.

These results indicate that the parameter λ varies very little as different load spectra are considered, provided that we deal with the same material and the same crack geometry. This fact suggests that an equivalent

crack growth behavior is expected in approximation under those load spectra which produce nearly identical values of the product $C\left(\overline{\Delta\sigma^b}\right)^{\lambda/b}$

In view of such significance, this product is plotted for the case of constant-amplitude load spectra as a function of the maximum stress σ_{max} in Figures 117 and 118, respectively, for R = 0 and R = 0.1. In both diagrams, the curves associated with n = 1 are constructed directly from Table 24, while those associated with n = 2, 5, and 10 are constructed from the curves with n = 1. To be specific, the curve with n = k (k = 2, 5, 10) is obtained by shifting the curve with n = 1 in the same diagram upward so that it will have the value of $C\left(\overline{\Delta\sigma^b}\right)^{\lambda/b}$ equal to k times for n = 1 at each value of σ_{max}. This method of constructing the relationship between $C\left(\overline{\Delta\sigma^b}\right)^{\lambda/b}$ and σ_{max} (with R as a parameter) is acceptable for the following reasons. Since, whether or not one flight consists of multiple cycles, the relationship between dc/dN and the total number N of constant-amplitude stress cycles is unique, an approximation dc/dF $\doteq$ k dc/dN is valid and, hence, C for n = k is approximately equal to C for n = 1 so long as k is not very large. The product $C\left(\overline{\Delta\sigma^b}\right)^{\lambda/b}$ is further plotted on the log-log scale for the case of constant-amplitude load spectra as a function of the maximum stress σ_{max} in Figures 119, 120, and 121 for σ_{LIM} = 20 ksi, σ_{LIM} = 30 ksi, and σ_{LIM} = 40 ksi, respectively, and for the stress ratio R ranging from R = -0.1 to R = 0.4

In Figures 117 and 118, the values of the product $C\left(\overline{\Delta\sigma^b}\right)^{\lambda/b}$ for the load spectra corresponding to composite maneuvers are indicated by dashed lines for both cases with and without the effect of the compression stress taken into consideration. An equivalence of the crack growth behavior then exists, for example, between the composite spectrum and the constant-amplitude load spectrum with σ_{max} = 100 percent in approximation and σ_{min} = 0 as indicated in Figure 117. Thus, this constant-amplitude spectrum is an "equivalent constant-amplitude load spectrum" to the composite spectrum when one flight consists of one stress cycle (n = 1).

The crack growth rates per flight under constant-amplitude load spectra are plotted against the stress intensity factor $\overline{K}$ in Figures 122, 123, and 124 for σ_{LIM} = 20 ksi, σ_{LIM} = 30 ksi, and σ_{LIM} = 40 ksi, respectively. These results are obtained for σ_{max} = 120 percent of σ_{LIM} and six values of the stress ratio R. The 14 crack growth rates dc/dF estimated by means of the unitblock approach are shown by solid circles only for the case of σ_{max} = 120 percent, R = 0.4, and σ_{LIM} = 20 ksi (Figure 122) to illustrate how well a straight line can be interpolated (with the aid of the least-square method) through these solid circles and how little they scatter around the straight line. The trend is the same for all other cases for which only the interpolated straight lines are shown. The crack growth behaviors corresponding to R = 0.4 and -0.1 are shown in Figures 125, 126, and 127, where the crack length c is plotted as a

function of the number of flights for initial crack size c_0 = 0.25 in. For the purpose of comparison, crack growth behaviors under A-A, A-G, and composite maneuver spectra are also shown in these figures.

As mentioned earlier, under constant-amplitude load spectra, dc/dF can be calculated in approximation as n dc/dN when one flight consists of n cycles. In estimating the parameters λ and C under these circumstances, however, the unitblock approach is taken with each unitblock consisting of 50,000 cycles, and the number of cycles involved in the unitblock depends on the value of n. The values of λ and C then reflect this fact to the extent that the crack length, when plotted as a function of the total number N of the cycles applied, is not quite identical, depending on the value of n. Figure 128 illustrates such a discrepancy, which, however, is not very large. The computation based on the single-cycle-per-flight approximation can therefore be used with reasonable accuracy to predict the crack growth behavior under multiple-cycles-per-flight conditions.

The maximum and minimum stresses for the constant-amplitude n-cycles-per-flight spectra can be selected from Figures 117 and 118. For example, to simulate the crack growth corresponding to composite load spectra with compressive stress effect considered, we select one of the following σ_{max} for R = 0:

σ_{max} = 100 percent (20 ksi), n = 1

σ_{max} = 84 percent (16.8 ksi), n = 2

σ_{max} = 62 percent (12.8 ksi), n = 5

σ_{max} = 55 percent (10.7 ksi), n = 10

The crack growth corresponding to A-A, A-G, and I-N maneuver spectra can be simulated by constant-amplitude loading in a similar fashion for which the maximum and minimum stress amplitudes are selected again from Figures 117 and 118. Similar procedures can be implemented for different stress ratios R and different values of limit design stress σ_{LIM} using the results given in Figures 119, 120, and 121.

4.6 CRACK GROWTH ESTIMATION PER FLIGHT UNDER SIMPLIFIED LOAD SPECTRA

The same equivalence relationship introduced in the preceding section is used in the crack growth estimation under simplified load spectra of increasing complexity, as shown in Figures 129, 130, and 131. Each of these load spectra is assumed to represent one flight. At the present time, the analysis is

limited to the values of the stress ratio $R = \sigma_{min}/\sigma_{max}$ between -0.15 and 0.45. The proposed simplified load spectra are characterized by:

1. Stress levels σ_{max}, σ_{min}, σ'_{min}, and the number of stress cycles n (Figure 129)

2. Stress levels σ_{max}, σ_{min}, σ'_{min}, σ''_{min}, and the number of two-step stress cycles n_1 and n_2 (Figure 130)

3. Stress levels σ_{max}, σ_{min}, σ'_{max}, σ'_{min}, σ''_{min}, σ'''_{min}, the number of two-step ground cycles n_1 and n_2, and the number of two-step flight stress cycles n_3 and n_4 (Figure 131)

These load spectra provide a large number of possible parameter variations. To achieve the equivalent crack growth behavior under this type of loading, a trial-and-error procedure needs to be implemented until the desired value of the product $C\left(\overline{\Delta\sigma^b}\right)^{\lambda/b}$ is reached. To save computation time, only a limited number of parameter variations is considered. This is achieved by preselecting constant values for σ_{min} for the load spectra shown in Figures 129 and 130, and σ_{min}, σ'_{min}, σ'_{max}, n_1, and n_2 for load spectra given in Figure 131. The selected stress levels, the number of cycles, the stress variations, and the corresponding missions, for which the equivalent simplified load spectra are prepared, are given in Tables 27, 28, and 29. The designated test cases performed in the phase I methodology development test program are indicated in these tables. The estimated values of λ, C, $\left(\overline{\Delta\sigma^b}\right)^{1/b}$, and $C\left(\overline{\Delta\sigma^b}\right)^{\lambda/b}$ corresponding to load spectra in Tables 27, 28, and 29 are given in Tables 30, 31, and 32. For the purpose of comparison, the values for λ, C, $\left(\overline{\Delta\sigma^b}\right)^{1/b}$, and $C\left(\overline{\Delta\sigma^b}\right)^{\lambda/b}$ corresponding to A-A, A-G, I-N, and composite maneuvers derived from F-15 baseline spectra are also included in these tables. All values of λ, C, etc, are determined from the dc/dF - $\overline{K}$ relationship (Figures 132 through 136) constructed with the aid of the unitblock approach, with one unitblock consisting of 50 flights. The smallest initial crack considered in the approach is $c_0 = 0.02$ in. Figures 132 through 136 indicate that the values of dc/dF under the simplified load spectra jump upward, as $\overline{K}$ increases, by a significant amount at around $\overline{K} = K_{TH}$. This jump results from the fact that, depending on the shape of the simplified load spectra and on the value of initial crack size c_0, in some cases only the G-A-G cycles contribute to crack growth at the beginning, while, as the crack grows, its size eventually reaches a value for which $\overline{K} > K_{TH}$ for every stress cycle, thus producing a rather sharp increase in dc/dF. At any rate, because of this, the values of λ, C, etc, are listed for different ranges of $\overline{K}$ in Tables 30, 31, and 32. The values listed for the range "(1)" are evaluated by the least-square method using only those points, if any, that fall in the range $\overline{K} \leq K_{TH}$ (= 2.5 ksi$\sqrt{in.}$) in the log-log plot, while the values listed for

80

the range "(2)" are obtained from the points falling in the range $K_{TH} < \bar{K} < K_{IC}$. The values under the category "(3)" are estimated by using all these points combined. For comparison of equivalent crack growth behavior, however, it appears reasonable to use the values of the product $C\left(\overline{\Delta\sigma^b}\right)^{\lambda/b}$ corresponding to the range (2). Then, for example, the composite maneuver load spectra can be approximated by M-64 (case II), M-72 (case IV), or M-78 (case IV).

In Figures 137 through 141, the values of the product $C\left(\overline{\Delta\sigma^b}\right)^{\lambda/b}$ are plotted as functions of rms stress values for the simplified load spectra shown in Figures 129, 130, and 131. For example, three circles in Figure 137 typically indicate such a plot for the spectrum M-61, with a dashed curve representing an interpolation. The values of the same product and corresponding rms stress values for A-A, A-G, I-N, and composite maneuvers are also indicated in Figures 137 through 141. For example, a cross mark in Figure 137 indicates the value of the product and the corresponding rms stress value associated with the A-A maneuver. Figure 137 further indicates that the cases III and IV, respectively, of M-61 and M-69 spectra are the simplified spectra providing the crack growth behaviors closest (among those tried) to that under the A-A maneuver. Indeed, this is the reason why the dc/dF - $\bar{K}$ relationships of these two cases are compared with that of the A-A maneuver in Figure 132. Similarly, Figures 133 through 136 plot the dc/dF - $\bar{K}$ relationships for those cases that produce the crack growth behaviors closest to those under A-G, I-N, composite, and A-A maneuvers, respectively.

The results given in Figures 132 through 141 and Tables 30 through 32 are obtained using C_w = 1.7203 x 10^{-9}, n = λ_w = 3.415, m = 0.30143, and K_{TH} = 2.5 ksi$\sqrt{in}$. The same analysis is repeated with new parameter values: C_w = 8.367 x 10^{-10}, n = λ_w = 3.640, m = 0.6, and K_{TH} = 1.5 ksi$\sqrt{in}$. The estimated values of λ, C, $\left(\overline{\Delta\sigma^b}\right)^{1/b}$, and $C\left(\overline{\Delta\sigma^b}\right)^{\lambda/b}$ corresponding to the load spectra given in Table 33 are shown in Table 34. Using these results, the crack growth is estimated as a function of the number of flights and is plotted in Figures 142 through 149.

The equivalence condition between random flight-by-flight and simplified load spectra has thus been established for a fighter aircraft. A similar equivalence relationship can be established for a transport aircraft. Again, a trial-and-error procedure is implemented until the desired value of the product $C\left(\overline{\Delta\sigma^b}\right)^{\lambda/b}$ is reached. The selected stress levels, the number of stress cycles, the stress variations, and the corresponding missions for which the equivalent simplified load spectra are prepared are given in Table 35. The estimated values of λ, C, $\left(\overline{\Delta\sigma^b}\right)^{1/b}$, and $C\left(\overline{\Delta\sigma^b}\right)^{\lambda/b}$ corresponding to load spectra in Table 35 are given in Table 36 From the results given in Tables 23 and 36, the equivalence between random flight-by-flight and simplified load spectra can be established. The equivalent simplified load spectra are given in Table 37. The results given for transport aircraft are obtained using only the new material parameter values discussed earlier.

4.7 CRACK GROWTH ESTIMATION BY METHOD II

Method I may not be appropriate for tracking and preliminary design purposes because it requires repeated use of a sophisticated computer code over a block of well-established flight spectra, while the spectra are usually not well defined in tracking situations or at the preliminary design stage. Method II, presented herein, is a potential alternative under the circumstances and also can be used to cover those combinations of the stress parameters that are not considered in Method I for reasons of economics as well as of importance. The method consists of the following steps:

1. Choose particular combinations of the stress parameters to be considered.

2. Identify all mission segments involved in these combinations. A mission segment is identified by its mean or reference value, duration, exceedance curve, and underlying spectral density function.

3. Generate sample stress histories for all these mission segments with aid of SPECGN1 program, described earlier. For each mission segment, a sample function of the random process representing this mission segment is generated. The duration, however, must be long enough to eliminate the possible large fluctuation in the statistical property of such a sample function of finite length that will be particularly pronounced for a sample function of a narrow-band process of short duration.

4. Use cycle-by-cycle integration with aid of CYCGRO program or unit-block approach to establish a curve relating crack size, c, to number of (rise and fall) cycles, n, using generated sample stress histories.

5. Establish the following relationship for each mission segment:

$$(dc/dN)_i = C_w \left[\Delta\sigma_i \psi(c)/(1 - \bar{R}_{eq})^{1-m} \right]^{\lambda_w} \tag{112}$$

where $\Delta\sigma_i = \left(\overline{\Delta\sigma^b} \right)_i^{1/b}$ is b-th root of average of b-th power of rise of stress history of i-th mission segment, C_w, λ_w, and m are material constants, and $\bar{R}_{eq}$ is average equivalent stress ratio selected in such a way that an equivalent crack growth can be obtained between random

82

flight-by-flight and constant-amplitude load spectra (discussed in later paragraphs in more detail).

6. Use equation 112 for each mission segment to evaluate crack growth during that mission segment. Note that each mission segment has now been reduced to equivalent stress cycles around its mean stress with a constant amplitude equal to $\left(\overline{\Delta\sigma^b}\right)^{1/b}$, as schematically shown in Figure 150. Unlike Method I, however, Method II requires the evaluation of the effect of mission segment transitions on the crack growth. The mission segment transitions in the present idealization of the spectrum (Figure 150) essentially produce acceleration and retardation effects. To calculate crack growth for the rise transition with intensity $\Delta\sigma_i = \sigma_{max} - \sigma_{min}$ and $R = \sigma_{min}/\sigma_{max}$, we use

$$(dc/dN)_i = C_w \left[\Delta\sigma_i \psi(c)/(1 - R)^{1-m} \right]^{\lambda_w} \tag{113}$$

The crack growth for the cycle (or cycles) immediately following the transition cycle is determined from

$$(dc/dN)_i = C_w \alpha \left[\Delta\sigma_i \psi(c)/(1 - \bar{R}_{eq})^{1-m} \right]^{\lambda_w} \tag{114}$$

where the parameter α needs to be determined experimentally. A computer code (METHODII) has been developed to integrate equations 112, 113, and 114 for the simplified load spectra shown in Figure 150.

4.7.1 ESTIMATION OF AVERAGE EQUIVALENT STRESS RATIO $\bar{R}_{eq}$ AND CRACK GROWTH PREDICTION FOR DIFFERENT MISSION SEGMENTS

The equivalent stress ratio $\bar{R}_{eq}$ plays a major role in implementing Method II. To demonstrate this, first a random flight-by-flight load spectrum consisting of three distinct mission segments is generated using the SPECGN1 program with the following input data:

	S(f)	M	R*
Case I	F-15 baseline for I-N maneuvers	6% of design limit stress	1.7
Case II	F-15 baseline for A-G maneuvers	6.5% of design limit stress	1.6
Case III	Gaussian white noise $S = 2000$ for $0 \leq f \leq 0.1$; otherwise, $S = 0$	40% of design limit stress	0.8

where S(f) = spectral density function in (% of design limit stress)^2/Hz, f = frequency in Hz, M = mean value to be used in mapping procedure to transform Gaussian histories into real-time histories, and R* = power exponent to be used in the same mapping procedure. In addition, one composite flight is constructed (case IV) by taking 50 cycles per flight, the first 20 cycles of which are taken from case I, the second 20 cycles are from Case II, and the last 10 cycles from Case III, and by adding ground loads of -10% of σ_{LIM} at the beginning and the end.

Using the unitblock approach, the parameters λ and C are estimated per cycle for all four cases and also per flight for case IV where one flight is well defined. Several values of initial crack size c_0 are selected, with the smallest being $c_0 = 0.02$ in. The crack growth for one unitblock is estimated for each of these initial crack values and divided by the number of cycles in a unitblock (500, 1,000, and 1,000, respectively, for cases I, II, and III) to obtain the crack growth rate per cycle dc/dn and by the number of flights in a unitblock (25) to obtain the crack growth rate per flight dc/dF (for case IV). The crack growth rate per cycle dc/dn is plotted as a function of $\bar{K}$ in a log-log diagram, as shown in Figure 151. The stress intensity factor $\bar{K}$ is evaluated from

$$\bar{K} = \left(\overline{\Delta\sigma^b}\right)^{1/b} \psi(c) \Big/ (1 - \bar{R})^{1-m} \tag{115}$$

where $\left(\overline{\Delta\sigma^b}\right)^{1/b}$ = root mean square stress with b = 2, $\overline{R}$ = average stress ratio (defined in the following), m = material constant, and $\psi(c) = \sqrt{\pi c}\ \sqrt{\sec(\pi c/w)}$ for the through-the-thickness crack with w = plate width. The results shown in Figure 151 are obtained by using the stress intensity factor $\overline{K}$ in equation 115 with $\overline{R}$ = 0. From these results, values of λ and C are estimated on a per cycle basis and are listed in Table 38. We observe from Table 38 that the value of the proportionality constant C changes significantly from mission segment to mission segment, while the value of the power exponent λ varies only slightly. Such a strong dependence of C on the type of mission segment is somewhat expected, however, since these parameters λ and C are estimated using the stress intensity factor $\overline{K}$ (in equation 115) and assuming $\overline{R}$ = 0 therein, thus disregarding the effect of stress ratios. Then, it could be argued that if a proper value of the average stress ratio $\overline{R}$ is used in equation 115 for $\overline{K}$, the estimated values of λ and C would be mission-independent. Indeed, such is the case for crack growth under constant-amplitude load spectra where the crack growth per cycle is estimated from

$$dc/dN = C_w(\Delta\sigma)^{\lambda_w}\psi^{\lambda_w}(c)\Big/\left[(1-R)^{1-m}\right]^{\lambda_w} \tag{116}$$

in which $R = \sigma_{min}/\sigma_{max}$, $\Delta\sigma = \sigma_{max} - \sigma_{min}$, and C_w, λ_w and m are constants. In this constant-amplitude situation, all straight lines indicating the relationship between log (dc/dN) and log $\overline{K}$ ($\overline{K}$ specified in equation 115 with $\overline{R}$ = R, $(\overline{\Delta\sigma^2})^{1/2} = \Delta\sigma$) collapse into one for any value of stress ratio R.

Unfortunately, no such unique representation seems to be possible for the case of random loading where stress ratio R varies randomly from cycle to cycle. In fact, it is the purpose of introducing the average stress ratio $\overline{R}$ in equation 115 to account for the effect of the variability in R. In Figures 152, 153, and 154, the crack growth rate per cycle dc/dN is plotted respectively for cases I through III against the average stress intensity factor $\overline{K}$ under several different definitions of average stress ratios $\overline{R}$. Similar results are shown in Figure 155 for composite flight spectra (case IV) where crack growth rate per flight dc/dF is plotted against the average stress intensity factor $\overline{K}$, again under different definitions of $\overline{R}$. The following five definitions of the average stress ratio are used in this study:

1. $\overline{R}_0 = 0$ (by assumption) $\tag{117}$

2. $\overline{R}_1 = \sum_{j=1}^{n} R_j/N$ $\tag{118}$

where

$$R_j = \left(\sigma_{min}/\sigma_{max}\right)_j$$

3. $\quad \overline{R}_2 = \sum_{j=1}^{n} R_j/N$ \hfill (119)

where

$$R_j = R_{cut}^{+} \quad \text{if } R_j > R_{cut}^{+}$$

$$R_j = R_{cut}^{-} \quad \text{if } R_j < R_{cut}^{-}$$

with

$$R_{cut}^{+} = 0.45 \text{ and } R_{cut}^{-} = -0.15$$

4. $\quad \overline{R}_3 = \left[\mu - \left(\overline{\Delta\sigma^2}\right)^{1/2}\Big/2 \right] \Big/ \left[\mu + \left(\overline{\Delta\sigma^2}\right)^{1/2}\Big/2 \right]$ \hfill (120)

where μ = mean value of random stress loading and $\left(\overline{\Delta\sigma^2}\right)^{1/2}$ = root-mean-square value of random stress loading.

5. $\quad \overline{R}_4 = \sum_{r=1}^{k} R_{4r}/k$ \hfill (121)

with

$$R_{4r} = \sum_{j=1}^{N_{THr}} R_j/N_{THr}$$ \hfill (122)

86

and

$$R_j = R^+_{cut} \quad \text{if } R_j > R^+_{cut}$$

$$R_j = R^-_{cut} \quad \text{if } R_j < R^-_{cut}$$

where k = number of values of initial crack size c_{0r} (r = 1,2, ..., k) selected to estimate parameters λ and C using the unitblock approach, and N_{THr} = number of cycles contributing to crack growth for each r. In equation 122, only those stress cycles satisfying the condition that $\Delta K_{eff} \geqq K_{TH}$ are considered. The quantity ΔK_{eff} is given by

$$\Delta K_{eff} = 4/3 \left[K_{max} - 3/4 \left(K_{min} + 1/3\sqrt{(c_p - c)/R_{yol}} \right) \right] \tag{123}$$

in which K_{max} and K_{min} are the maximum and minimum values of the stress intensity factor corresponding to the currently applied load cycle, and c_p and R_{yol} are the values corresponding to the previously applied overload. The stress ratios R_{4r} and $\bar{R}_4$ as well as the number of cycles N_{THr} contributing to crack growth are given in Table 39 for each r for the three mission segments considered in this study. The values of μ, $\left(\overline{\Delta\sigma^b}\right)^{1/b}$ (b = 2), λ, C, and $C\left(\overline{\Delta\sigma^b}\right)^{\lambda/b}$ per cycle are estimated using average stress ratios $\bar{R}_i$ (i = 0,1,2,3,4) and are given in Table 40. These results indicate that the estimated values of λ and C are sensitive to the average stress ratio $\bar{R}$ used, but no particular definition of $\bar{R}$ can produce the values of λ and C, which are mission-independent under random load spectra. It is noted that the value of C and, therefore, of $C\left(\overline{\Delta\sigma^b}\right)^{\lambda/b}$ per flight for case IV can be obtained by multiplying the corresponding values per cycle listed in Tables 38 and 40 by 50.

In the proposed Method II, each mission segment is completely characterized by a constant-amplitude load spectrum with the stress range $\Delta\sigma$, the stress ratio R, and the number of cycles n. For the equivalent crack growth to be established between random flight-by-flight spectra and the constant-amplitude spectra for each mission segment, these parameters must satisfy certain conditions. In the present approach, we select $\Delta\sigma$ to be equal to $\left(\overline{\Delta\sigma^2}\right)^{1/2}$ and the number of cycles in a random load spectrum to be equal to

the number of cycles in the constant-amplitude spectrum. Further, we select for the stress ratio R the equivalent average stress ratio $\bar{R}_{eq}$ determined from the condition that

$$(dc/dN)_{\substack{random \\ loading}} = (dc/dN)_{\substack{constant- \\ amplitude \\ loading}} \tag{124}$$

where

$$(dc/dN)_{\substack{random \\ loading}} = C\left[\left(\overline{\Delta\sigma^b}\right)^{1/b} \psi(c)\right]^{\lambda} \tag{125}$$

$$(dc/dN)_{\substack{constant- \\ amplitude \\ loading}} = C_w\left[\Delta\sigma\psi(c)\bigg/\left(1 - \bar{R}_{eq}\right)^{1-m}\right]^{\lambda_w} \tag{126}$$

Equations 124, 125, and 126 can be solved for R_{eq} in terms of the parameters λ_w, C_w, m, λ, and C:

$$\bar{R}_{eq}(c) = 1 - (C_w/C)^{1/\lambda_w(1-m)} \times \left[\left(\overline{\Delta\sigma^b}\right)^{1/b} \psi(c)\right]^{[(\lambda_w-\lambda)/\lambda_w(1-m)]} \tag{127}$$

If $\lambda_w = \lambda$, the stress ratio $\bar{R}_{eq}$ is independent of crack size c, and in this case it is a relatively simple function of C/C_w, as shown in Figure 156. In Figure 157, the same equivalent stress ratio $\bar{R}_{eq}(c)$ is plotted (without assuming that $\lambda = \lambda_w$) against crack size c for three mission segments considered in this study. The values λ and C used for constructing Figure 157 are taken from Table 40 ($\bar{R}_0 = 0$).

In Figures 158, 159, and 160, the crack length is plotted as a function of the number of cycles for the three mission segments. The curves indicated by "Random Loading" are determined from equation 125, with parameters λ and C given in Table 40 ($\bar{R}_0 = 0$); hence, these represent essentially the result of applying Method I to the load spectra for the three mission segments. The crack growth behaviors under the constant-amplitude load spectra with $\Delta\sigma = \left(\overline{\Delta\sigma^b}\right)^{1/b}$ (b = 2) are obtained by solving equation 126 with $\bar{R}_{eq}(c)$ calculated from equation 127. Two cases are considered. In the first case, we set $\lambda = \lambda_w$ and determine $\bar{R}_{eq} = \bar{R}_{eq}^{(1)}$ from Figure 156. In the second case, $R_{eq} = R_{eq}^{(2)}$ is

88

obtained from Figure 157 at $c = w/4$ where the plate width $w = 6$ in. Figures 158, 159, and 160 indicate that the use of $\bar{R}_{eq}$ produces reasonable approximations in evaluating the crack growth behavior as long as $\lambda \doteq \lambda_w$, and that the use of $\bar{R}_{eq}^{(2)}$ results in more conservative approximations than the use of $\bar{R}_{eq}^{(1)}$.

The preceding numerical results presented are calculated using $C_W = 1.7203 \times 10^{-9}$, $n = \lambda_w = 3.415$, $m = 0.30143$, and $K_{TH} = 2.5$ ksi$\sqrt{in}$. The same analysis is repeated for new material parameter values; $C_W = 8.367 \times 10^{-10}$, $n = \lambda_w = 3.640$, $m = 0.6$, and $K_{TH} = 1.5$ ksi$\sqrt{in}$. The results are shown in Tables 44, 42, and 43 and Figures 161 through 165.

The present study has demonstrated that when λ is equal to λ_w, the crack growth behaviors estimated from equations 125 and 126 are identical if the equivalent stress ratio $\bar{R}_{eq}$ as defined in equation 127 is used in equation 126. It has further been demonstrated that reasonable approximations can be established when λ is approximately equal to λ_w, as shown in Figures 158 through 160, and 163 through 165. The equivalent stress ratio $\bar{R}_{eq}$ thus plays a major role in implementing Method II and can be evaluated if parameters λ_w, C_W, λ, and C are known. The parameters λ_w and C_W are usually known from constant-amplitude tests, while λ and C are to be evaluated by the unitblock approach for each significant mission segment.

The crack growth behavior under the composite (case IV) load spectra is estimated by several different methods, and the result is shown in terms of the crack length as a function of the number of flights in Figure 166. The dashed curve is obtained with the aid of the CYCGRO program using the random input and cycle-by-cycle integration procedure, while the curve denoted by "Random Loading (Method I)" is obtained by solving equation 125, for which constants C and λ are given in Table 43 (case IV, $\bar{R}_0 = 0$). The results indicated by $\bar{R}_{eq}^{(1)}$ and $\bar{R}_{eq}^{(2)}$ are obtained by solving equation 126 with $\Delta\sigma = \left(\overline{\Delta\sigma^b}\right)^{1/b}$ ($b = 2$). As in cases I, II, and III, the values for $R_{eq}^{(1)}$ and $\bar{R}_{eq}^{(2)}$ are estimated from Figures 161 and 162 respectively. These results indicate that the use of equation 125 with $\bar{R}_{eq} = \bar{R}_{eq}^{(2)}$ gives a conservative approximation in evaluating the crack growth behavior.

4.7.2 APPLICATION OF METHOD II

The crack length c estimated by Method II for the load spectra shown in Figure 167 is plotted as a function of the number of flights for initial crack size $c_0 = 0.25$ in. The results indicated by $\bar{R}_{eq}^{(1)}$ and $\bar{R}_{eq}^{(2)}$ are obtained by integrating equations 112, 113 and 114 cycle by cycle with the equivalent stress ratio $\bar{R}_{eq}$ determined respectively from Figures 161 and 162. For the purpose of comparison, crack growth estimated by cycle-by-cycle integration under random load spectra (case IV) is also shown in this figure. The crack growth for the

cycle (or cycles) immediately following the transition cycle is determined from equation 114 where $\alpha \doteq 1.2$ for a transition involving a stress rise and $\alpha \doteq 0.8$ for a transition involving a stress fall.

These results indicate that Method II produces less conservative crack growth behavior than cycle-by-cycle integration under random loading. However, the use of $\bar{R}_{eq}^{(2)}$ results in better approximation than the use of $\bar{R}_{eq}^{(1)}$. The main discrepancy in evaluating crack growth by Method II can be attributed to the accuracy of parameter α and the number of cycles n' needed to account for the transition effect. Furthermore, the values of parameters λ and C are estimated for each mission segment without taking into account the effect of compressive cycles due to ground loads. Since compressive loads followed by tension loads tend to accelerate crack growth much faster, a different, perhaps much larger, value of the constant α needs to be assigned for the transition cycle involving negative stresses due to ground loads than for other transition cycles. In fact, a preliminary sensitivity study to determine the effect of α and n' on the crack growth has been performed.

The parameters λ, C, and the product $C\left(\overline{\Delta\sigma^b}\right)^{\lambda/b}$ (b = 2) are evaluated per flight for several values of α and n'. (Refer to Table 44.) These parameters are estimated using the unitblock approach, with each unitblock consisting of 50 flights. The crack growth behavior is plotted as a function of number of flights in Figures 168, 169, and 170 for the same values of α and n' given in Table 44. For comparison, the crack growth behavior under the random flight-by-flight spectra is evaluated by cycle-by-cycle integration and indicated by dashed curves in these figures. These results tend to indicate that using larger values of α and n' improve predictions considerably.

4.8 VERIFICATION OF THEORY VERSUS EXPERIMENT

An experimental test program on the crack growth in the through-the-thickness precracked 2219-T851 aluminum specimens has been conducted. Details of the test program are presented in a preceding section. The tests were conducted under constant-amplitude, simplified, and random flight-by-flight load spectra. The random load spectra were generated in terms of peaks and valleys using the SPECGN1 program, for A-A, A-G, I-N, and composite maneuvers for fighter aircraft, and composite load spectra for transport aircraft. The constant-amplitude and simplified load spectra are constructed so that the equivalent crack growth is produced between these spectra and the random flight-by-flight load spectra. As discussed earlier, a trial-and-error procedure is needed to establish these equivalent load spectra. Since, however, such a trial-and-error approach is usually time-consuming, the equivalence conditions are enforced only in approximation in the present study.

90

4.8.1 CONSTANT-AMPLITUDE SPECTRA

The selected stress levels and the designated test cases are given in Table 45. These are the cases where the conditions of equivalence to the random flight-by-flight spectra are reasonably well satisfied, as is shown later. Corresponding to these stress levels, values of parameters λ, C, and the product $C\left(\overline{\Delta\sigma^b}\right)^{\lambda/b}$ with $b = 2$ are estimated by the unitblock approach and are shown in Table 46 for $\sigma_{LIM} = 40$ ksi. Using these results, the crack growth is evaluated as a function of the number of flights (1 flight = 1 cycle), and the results are shown in Figures 171 through 174. For comparison, experimental data are also included with these plots. The ratio N_{thr}/N_{exp}, where N_{exp} is the number of cycles required to reach the largest crack in the experiment and N_{thr} is the corresponding theoretical value, is given in Table 47. The results given in Figures 171 through 174 are determined using the initial crack size measured experimentally. The sensitivity of the crack growth behavior to the initial crack size c_0 is illustrated in Figure 175 for the M-8 case. The results given in Tables 46 and 47 and Figures 171 through 175 were obtained using the unitblock approach. A comparison of the crack growth estimated by this method and by the cycle-by-cycle integration for the M-8 case is shown in Figure 176. We observe from these results that the unitblock approach overestimates the crack growth by about 15 to 20 percent for the constant-amplitude spectra considered here.

4.8.2 RANDOM LOAD SPECTRA

The crack growth rate per flight, the parameter values of λ, C, $\left(\overline{\Delta\sigma^b}\right)^{1/b}$ ($b = 2$), and the product $C\left(\overline{\Delta\sigma^b}\right)^{\lambda/b}$ are obtained using the new values of material parameters (determined from constant-amplitude tests) for A-A, A-G, I-N, and composite random load spectra with the aid of the unitblock method and are given in Tables 20, 21, and 22. Using these results, the crack growth is evaluated as a function of the number of flights and plotted in Figures 110 through 113. The ratios of the number of flights to failure predicted by the theory and the experiment are given in Table 48. As these results indicate, the agreement between the theory and the experiment is fairly good in most cases.

4.8.3 SIMPLIFIED LOAD SPECTRA

The crack growth behavior investigated under simplified load spectra of increasing complexity is given in Table 33. The estimated values of λ, C, $\left(\overline{\Delta\sigma^b}\right)^{1/b}$, and the product $C\left(\overline{\Delta\sigma^b}\right)^{\lambda/b}$ corresponding to these load spectra are shown in Table 34. Using these results, the crack growth is estimated as a function of the number of flights and are plotted in Figures 142 through 149. The ratios of the number of flights to failure predicted by the theory and the experiment are given in Table 49.

91

4.8.4 DISCUSSION

The experimental and theoretical results on the crack life prediction described in the preceding sections are summarized in Table 50. Since the equivalence conditions are not exactly satisfied for the constant-amplitude and simplified spectra with respect to the target random flight-by-flight load spectra, the ratio

$$r = \left[C\left(\overline{\Delta\sigma^b}\right)^{\lambda/b}\right] \text{random loading} \bigg/ \left[C\left(\overline{\Delta\sigma^b}\right)^{\lambda/b}\right] \text{constant-amplitude or simplified loading} \tag{128}$$

is equal to unity only in approximation. This ratio can be estimated using the results of the product $C(\overline{\Delta\sigma^b})^{\lambda/b}$ given in Tables 20, 21, 22, and 46. Then by dividing by these ratios, the numbers of flights to failure under constant-amplitude, and simplified load spectra given in Table 50, we obtain revised numbers of flights that would correspond to the load spectra more equivalent to the target random flight-by-flight spectra. These revised flight numbers are given in parentheses in Table 50. We can observe that after this revision, the number of flights to failure estimated analytically is about the same for constant-amplitude, simplified, and random flight-by-flight load spectra. Such results are expected since for a constant value of power exponent λ, the crack growth estimated by Method I is controlled by the product $C\left(\overline{\Delta\sigma^b}\right)^{\lambda/b}$.

The equivalent input load spectra for experimental testing are determined analytically. However, as discussed previously, the equivalence condition is established only in approximation. The experimental results shown in parentheses are the expected number of flights to failure if the input load spectra would correspond to more equivalent random flight-by-flight loading. These results are obtained by dividing the experimental number of flights to failure by ratio r.

The test cases denoted by a star in Table 50 are obtained under simplified load spectra selected for the purpose of a preliminary study with no equivalence condition imposed. The stress levels and the number of cycles are therefore approximately representative of the target random flight-by-flight load spectra. However, the results indicate that these simplified load spectra are too conservative to replace any of the random flight-by-flight load spectra. If the number of flights to failure observed in the experiment are adjusted by the ratio r, however, the results seem to improve as compared with the results obtained under the target random flight-by-flight load spectra.

5.0 GUIDELINES FOR THREE LEVELS OF CRACK-GROWTH
ANALYSES DEVELOPMENT

5.1 INTRODUCTION

Since the first imposition of damage tolerance requirements on the B-1 Strategic Bomber, the Air Force specifications for incorporating structural integrity into aircraft systems have been upgraded substantially into a coherent and comprehensive set, MIL-STD-1530A,[121] MIL-A-834444A, and MIL-A-8866B.

The far-reaching impact of the new philosophy approach contained in those documents is such that crack-growth behavior must be evaluated in all phases of any weapon system; i.e., preliminary design, detail (final) design, and force management (individual aircraft tracking and life extension program), each of which requires appropriately developed crack-growth-prediction techniques. Current practice in the industry for predicting crack-growth behavior under flight spectrum loading relies on processing the load history on a stress-level-by-stress-level basis. For complex random flight-by-flight load histories, the processing of spectrum data and the computation cost become excessive. Usually, there are different requirements on the predictive accuracy in the performance of crack-growth analysis in each phase. For instance, it is not cost effective to perform a very detail analysis when only an order-of-magnitude-type comparison between spectra is needed in the preliminary design phase. Trade-offs shall be made between the accuracy of prediction and the sophistication of models used in the prediction. Hence, the need for the development of different levels of crack-growth analyses is obvious.

Three levels of analysis will be developed in phase II of this program for assessing the impact of durability and damage tolerance requirements from the preliminary design stage through detailed stress analysis stage to individual aircraft tracking and life extension in-force management stage for any weapon system development and production.

The following are the minimum goals for each level of crack-growth analyses:

1. Preliminary design analysis which will provide rapid comparative analyses and realistically account for the load interaction effect

2. Detailed design analysis which will be capable of predicting effects commensurate with existing cycle-by-cycle techniques

3. Individual aircraft tracking analysis which is sensitive to aircraft usage or mission mix

Based on the past experience gained from the B-1 development program, other durability and damage tolerance analysis related projects, and results of tasks conducted in phase I of this program, guidelines for the development of the three levels of crack-growth analyses have been established. The following paragraphs summarize the guidelines for each level in detail.

5.2 GUIDELINES FOR DEVELOPMENT OF DETAILED DESIGN LEVEL CRACK-GROWTH ANALYSIS

Currently, most of the fatigue crack-growth-analysis methods used for life prediction throughout the aerospace industry are based on the cycle-by-cycle analysis techniques but differ in various ways on the accumulation scheme employed in the computation procedure. A brief summary of the accumulation schemes commonly used in the crack-growth-analysis computer programs (i.e., Air Force CRACKS IV and Rockwell EFFGRO) was presented in the preceding sections. The fact that cycle-by-cycle analysis techniques provide the most accurate predictions within the state-of-the-art limitations will most likely not be challenged.

For the performance of damage tolerance and durability analyses in the detailed design stage as specified in the military standard (MIL-STD-1530A), a reliable and accurate analytical prediction tool is needed to substantiate the ability of structural components to meet the requirements of MIL-A-83444 and MIL-A-8866B. Hence, it is necessary to emphasize that the detailed design level crack-growth-analysis method should adopt an existing cycle-by-cycle technique. Based on this premise, the following guidelines for the development of a detailed design level crack analysis have been established:

1. The crack-growth-analysis procedure shall be constructed based on the principles of linear elastic fracture mechanics (LEFM). In the concept of LEFM, the primary cause of fatigue crack growth is the cyclic variation in the local stress field adjacent to the crack tip. This variation is characterized by stress intensity factor K and stress ratio R. A mathematical model with crack-growth per cycle, da/dN as the dependent variable and some kind of function $F(K,R)$ as the independent variable, shall be chosen to represent the crack-growth relationship. Since in analyzing airframe structures, especially in performing damage tolerance analyses on primary structures, the range of crack-growth rates covered is normally between 1×10^{-6} in./cycle and 1×10^{-3} in./cycle, a relatively simple fatigue crack-growth-rate equation ($da/dN = c[F(K,R)]^n$) can be adopted. Several such growth-rate equations commonly used throughout the aircraft industry are the Walker (Paris equation

is a special case), Boeing, Grumman, and Forman equations. A brief review and evaluation on those equations has been conducted and is summarized in the preceding sections. Based on the results, a tentative conclusion has been drawn - any of these rate models is adequate to represent the fatigue-crack-growth rate relationship in the rate range normally of interest to aircraft design analysts.

2. A load interaction model shall be selected for the detail design level analysis. The first criterion is that the load interaction model chosen shall be capable to account for effects of interactions of loads including the overload retardation, compressive load acceleration, tension-tension underload acceleration, and coupling effects such as reducing retardation by compressive load cycle immediately following the overload cycles. The second criterion for choosing an appropriate load interaction model is that the model shall be formulated based on the stress intensity factor variations. Another criterion is that there will be no excessive data or lengthy computation needed in application of the selected model. Existing load interaction models which can be modified to fulfill the aforementioned criteria are the Willengborg, Vroman/Chang, modified closure, and contact stress models. Basic assumptions and formulations of each model have been summarized and are presented in the preceding sections.

3. The service loads spectra for detailed design level crack-growth analysis shall be assembled on a flight-by-flight basis. Each flight consists of a series of cycles that combine take-off, maneuver, and landings describing the type of mission. Gusts and other periodically occurring loads shall be incorporated in the development of the service-load spectra. The service-load spectra shall be transformed into stress spectra for each critical area on the airframe where the crack-growth analysis is to be performed. Internal load solutions obtained by reliable stress analysis techniques, such as the finite element method, shall be used to formulate the stress-load transfer function.

4. The integration scheme used in the detailed design level crack-growth analysis shall be efficient. The linear approximation method adopted in the existing crack-growth computation routines such as EFFGRO and CRACKS is an appropriate choice. The accumulation interval shall be made flexible depending on the range of the crack-growth-rate or stress intensity factor gradient $(\frac{dK}{da})$. For crack configurations other than through-the-thickness crack, the change of aspect ratio should be accounted for.

5.3 GUIDELINES FOR DEVELOPMENT OF PRELIMINARY DESIGN LEVEL CRACK-GROWTH ANALYSIS

Current MIL-STD-1530A specifies the need to perform damage tolerance and durability design concepts/material/weight/performance/cost trade studies during the early design phase in order to obtain a low-weight, cost-effective design which complies with the damage-tolerance and durability requirements. To meet these design criteria, the structure must be sized to provide a sufficient slow (subcritical) crack-growth period and residual strength so that cracks can be detected before catastrophical failure occurs.

A proper approach to incorporate crack-growth requirements in the preliminary design stage is to pre-establish the crack-growth allowable stresses for a specific material and a specific cracked geometry configuration. A schematic plot of determining the crack-growth allowable stresses is shown in Figure 177. For performing material selection or spectra comparison, a family of such curves can be constructed. Those curves were based on the "a" versus "N" curves obtained from crack-growth analyses. Figure 178 shows a typical plot.

To perform such crack-growth analyses, one can certainly employ a damage accumulation package such as CRACKS or EFFGRO. Yet economically, it is not cost-effective to use those programs to conduct such cycle-by-cycle analyses when only order-of-magnitude comparisons are needed. Hence, a more efficient means to predict the crack-growth behavior is necessary.

One method which can be used is the choice of a larger scale time base in the crack-growth-rate law such as crack-growth per period, da/dp. The essence of this method is to generate a set of point values of crack-growth per period Y_i at distinct crack length a_i to approximate the periodic rate functional values of $f_p(a_i)$. This set of $f_p(a_i)$ is then used to construct an interpolation polynomial $P_p(a)$ such that $da/dp = P_p(a)$. Fatigue crack growth will then be determined by integrating $P_p(a)$ instead of a cycle-by-cycle summation. Brussat (122) was the first one to use this concept. Presently this crack-growth-analysis methodology has been incorporated into a Rockwell in-house developed computer program, PRDGRO.[28] It has been demonstrated that an order-of-magnitude saving on the computation time can be achieved.

Another alternative is to employ the spectrum characterization methodology (designated as Method II) developed in phase I of this program such that the input loading spectrum is much simpler than its random cycle-by-cycle counterpart. A detail procedure of Method II, for obtaining corresponding simplified spectra which produce the equivalent damage, has been presented in the preceding section. In the proposed Method II, each mission segment of a spectrum loading is completely characterized by a constant amplitude load spectrum with the stress range $\Delta\sigma$, stress ratio R, and number of cycles n. It has been demonstrated that if one selects Δa to be equal to $(\overline{\Delta\sigma^2})^{\frac{1}{2}}$

and the number of the constant amplitude cycles n to be equal to the number of cycles in a random spectrum, then an equivalent stress ratio $\bar{R}_{eq}$ can be determined such that the equivalent spectrum can be constructed. Any damage accumulation package such as CRACKS and EFFGRO can be used for performing the analysis. An average factor of five can be saved on computer time as comparing with growing crack in random cycle-by-cycle spectrum loading format.

5.4 GUIDELINES FOR DEVELOPMENT OF CRACK-GROWTH-ANALYSIS METHOD FOR INDIVIDUAL AIRCRAFT TRACKING (IAT)

Based on current U.S. Air Force Aircraft Structural Integrity Program Requirements, (121) the following major force management activities designed to focus attention on each potential crack problem shall be included: the Force Structural Maintenance (FSM) plan and IAT. In addition, force management activities also include loads/environmental spectral survey (L/ESS), updating the design analysis developing inspection and repair criteria, and forming a structural strength survey. The crack-growth-analysis method development guidelines presented here are to be employed only in the IAT program.

The phase I report of a research program which is being conducted by the University of Dayton/Lockheed/Vought team (123) contains a comprehensive review of all current IAT methods. A brief summary of those methods are presented here for references. For transport/bomber aircraft, the following general methods have been widely used or considered:

Method 1 - Flight hours/landing

Method 2 - Pilot log + time by data block + parametric fatigue damage tables

Method 3 - Pilot log + equivalent mission type + mission fatigue damage tables

Method 4 - Pilot log + time by data block + parametric crack-growth tables

Method 5 - Pilot log + equivalent mission type + mission crack-growth tables

Method 6 - Pilot log + calculated stress occurrence + cycle-by-cycle crack growth

Among these methods, only 4, 5, and 6 are based on the crack-growth concept. In method 4, stress exceedance are derived for each data block and a sequence of stress cycles is generated in random fashion. Crack-growth rates per block da/db, as a function of crack length for each data block, are generated by any crack-growth program. These rates become the parametric crack-growth tables. During the operational part of this method, the pilot log data

is converted to time spent in each data block. The crack growth for each data block is then a product of time and crack-growth rate.

Method 5 is similar to method 4 except that the crack-growth tables are in crack-growth per flight (da/dF) for selected mission categories which include breakdown by mission parameters such as takeoff weight, takeoff fuel weight, percentage of time in low level, etc. The advantage of treating crack growth for an entire flight is that the sequence effects within can be accounted for more rigorouly for standard missions.

In method 6, stress exceedance curves are generated for each data block (or mission segment) and stored in parametric stress occurrence tables. During IAT operation, the pilot log data is converted to time in each data block. The stress occurrence tables for each data block are adjusted for the time spent and a sequence of stress cycles is generated for the flight by summing the data block. The crack growth is then computated by a cycle-by-cycle growth computer program.

For attack/fighter/trainer aircraft, the following five general tracking methods have been either adopted or proposed:

Method 7 - AFM 65-110 data + time by mission + mission fatigue damage tables

Method 8 - Forms + time by mission + mission fatigue tables

Method 9 - Forms/counting accelerometer + N_Z counts by mission + parametric fatigue damage tables

Method 10 - Counting accelerometer + N_Z counts by month + normalized crack-growth curves

Method 11 - MSR + stress exceedances by 50 hours + normalized crack-growth curves

Among the above mentioned five methods, only Methods 10 and 11 use the crack-growth technology. Method 10 is used on the F-4 and A-7 IAT program. The data collected are the monthly reported aircraft flying hours and the reported exceedance of the vertical normal load factor. This method is based upon the ability to experimentally and analytically grow cracks in a structure with a given known stress spectra. For convenience, both F-4 and A-7 aircraft use a Σ n/N approach to the accumulation of damage index, and the damage index allowable limits are based on corresponding crack length limits.

Tracking method 11, which is identified as the normalized stress exceedance crack-growth method, represents the current F-16 approach. At this stage in the F-16 IAT program, the proposed method is to calculate the crack-growth curves for every critical location in the airframe for each of five usage

spectra. These five usage spectra are chosen to cover the range from the least severe to the most severe expected usage of F-16. The crack curves are computed using both analytical model and coupon test results. Corresponding to each of the five usage spectra, there is a strain spectrum at the monitored station which is expressed as normalized exceedance of a derived strain function mechanical strain recorder (MSR) data gathered on a particular airplane for a period of time are then expressed in the normalized exceedance manner. Aircraft usage spectra can be then related back to an interpolated crack-growth curve for each critical point through the use of interpolation method. Given the crack size a_o at the beginning of time period Δt, the interpolated crack-growth curve, and the normalized time period ΔtN, a crack increment Δa can be computed for the period representd by MSR data. To give the current crack length at each critical point, Δa is added to a_o.

Four of the previously mentioned methods have been recommended for incorporation in the force'management handbook. They are Methods 4, 5, 10, and 11. These four methods relate to some kind of crack-growth analysis method. From an economical point of view, it is definitely not cost effective to employ the cycle-by-cycle calculation technique as recommended for the detail design level analysis for obtaining the growth information of a given crack in the force management stage. Instead, the spectrum characterization methodology developed in this program is considered to be more practical.

Method II of the spectrum characterization methodology described in Section 4 can be used as a tool for streamlining crack-growth calculation. Recall that in the proposed method II, each mission segment is completely characterized by a constant amplitude load spectrum with the stress range $\Delta\sigma$, the stress ratio R, and the number of cycles n, and a flight is assumed to consist of constant amplitude mission spectra, mission transitions, and a ground-air-ground cycle. Hence, except the mission transition and the ground-air-ground cycle, the crack growth can be determined very rapidly as in any constant amplitude case. The mission segment transitions can be treated as a step increasing in crack-growth rate for the situation of underload acceleration (including compressive load cycle) or a step decreasing in crack-growth rate for overload retardation situations. This is because in IAT, the result of crack-growth prediction does not have to be highly accurate. Consequently, the crack-growth analysis program can be performed on computing machines with a much smaller capacity than is needed on a big computer such as IBM 370 system or CDC CYBER 175. The final goal is that crack-growth analyses can eventually be done by the onboard computer.

6.0 REFERENCES

1. Anon, "Military Specification, Airplane Strength and Rigidity Reliability Requirements, Repeated Loads and Fatigue," MIL-A-8866B, 22 August 1975

2. Anon, "Military Specification, Airplane Damage Tolerance Requirements," MIL-A-83444, 2 July 1974

3. Hall, L. R., Shah, R. C., and Engstrom, W. L., "Fracture and Fatigue Crack Growth Behavior of Surface Flaws and Flaws Originating at Fastener Holes," AFFDL-TR-74-47, Air Force Flight Dynamics Laboratory, WPAFB, Ohio, 1974

4. Bell, P. D., and Creager, M., "Crack Growth Analyses for Arbitrary Spectrum Loading," AFFDL-TR-74-129, Air Force Flight Dynamics Laboratory, WPAFB, Ohio, 1974

5. Stolpestad, J., "Summary Report of the B-1 Fracture Mechanics Analysis Verification Test Program," NA-75-675, Rockwell International, Los Angeles Division, 2 December 1975

6. Ferguson, R. R., and Berryman, R. C., "Fracture Mechanics Evaluation of B-1 Materials," AFML-TR-76-137, Air Force Materials Laboratory, WPAFB, Ohio, 1976

7. Whittaker, I. C., and Saunders, S. C., "Exploratory Development for Application of Reliability Analysis of Aircraft Structures Considering Interaction of Cumulative Fatigue Damage and Ultimate Strength," AFML-TR-72-283, Air Force Material Laboratory, WPAFB, Ohio, 1973

8. Wirsching, P. H., Stahl, B., and Nolte, K. G., "Probability Based Fatigue Design Algorithm for Offshore Structures," ASCE Spring Convention, April 1977, Dallas, Texas

9. Yang, J. N., and Trapp, J. W., "Reliability Analysis of Fatigue-Critical Aircraft Structure Under Random Loading and Periodic Inspections," AFML-TR-75-29, Air Force Material Laboratory, WPAFB, Ohio, 1975

10. Head, A. K., "The Growth of Fatigue Cracks," The Philosophical Magazine, Vol 44, Series 7, 1953

11. Frost, N. E., and Dugdale, D. S., "The Propagation of Fatigue Cracks in Sheet Specimens," Journal of the Mechanics and Physics of Solids, Vol 6, No. 2, 1958

12. Liu, H. W., "Crack Propagation in Thin Metal Sheets Under Repeated Loading," The Journal of Basic Engineering, Trans of ASME, Series D, Vol 83, 1961

13. McEvily, E. J., and Illg, W., "The Rate of Crack Propagation in Two Aluminum Alloys," NACA-TN-4396, 1958

14. Paris, P. C., Gomez, M. P., and Anderson, W. E., "A Rational Analytic Theory of Fatigue," The Trend in Engineering, Vol 13, No. 1, 1961

15. Forman, R. G., Kearney, V. E., and Engle, R. M., "Numerical Analysis of Crack Propagation in Cyclic-Loaded Structures," Journal of Basic Engineering, Trans of ASME, Vol 89, 1967

16. Walker, K., "The Effect of Stress Ratio During Crack Propagation and Fatigue for 2024-T3 and 7-75-T6 Aluminum," ASTM STP 462, American Society for Testing and Materials, 1970

17. Collipriest, J. E., Jr., and Ehret, R. M., "Computer Modeling of Part-Through-Crack Growth," SD72-CE-15, Rockwell International, Space Division, 1972

18. Elber, W., "The Significance of Fatigue Crack Closure," ASTM STP 486, Damage Tolerance in Aircraft Structures, American Society for Testing and Materials, pp 230-242, 1971

19. Annis, C. G. Jr., Wallace, R. M., and Suns, D. L., "An Interpolative Model for Elevated Temperature Fatigue Crack Propagation," AFML-TR-76-176, Air Force Materials Laboratory, Ohio, 1976

20. Hudak, S. J., Jr., Saxener, A., Bucci, R. J., and Malcolm, R. C., "Development of Standard Methods of Testing and Analyzing Fatigue Crack Growth Rate Data," AFML-TR-78-40, Air Force Materials Laboratory, WPAFB, Ohio, 1978

21. Chang, J. B., "Assessment of the Sensitivity of Crack Growth Rate Constants to Predictive Accuracy on Part-Through Crack Fatigue Life Predictions," Presented at ASTM Symposium on Part-Through Crack Life Prediction, San Diego, October 1977

22. Chang, J. B., "Improved Methods for Predicting Spectrum Loading Effects, First Quarterly Technical Report," NA-78-491, Rockwell International, Los Angeles Division, 31 May 1978

23. Anon, "B-1 Fracture Mechanics Memorandum of Agreement," NA-71-958, Rockwell International, Los Angeles Division, 1971

24. Chang, J. B., and Shinozuka, M., "Improved Methods for Predicting Spectrum Loading Effects, Second Quarterly Technical Report," NA-78-491-1, Rockwell International, Los Angeles Division, 30 August 1978

25. Wheeler, O. E., "Spectrum Loading and Crack Growth," Transaction of the ASME, Journal of Basic Engineering, pp 181-186, March 1972

26. Willenborg, J., Engle, R. M., and Wood, H. A., "A Crack Growth Retardation Model Using an Effective Stress Concept," AFFDL-TR-71-1, January 1971

27. Vroman, G. A., "Analytical Prediction of Crack Growth Retardation Using a Residual Stress Concept," Briefing Charts, Rockwell International, Los Angeles Division, May 1971

28. Chang, J. B., and Cheng, J. S., "Cost-Effective Fatigue Crack Growth Analysis for Flight Spectrum Loading," NA-78-629, Rockwell International, Los Angeles Division, 1978

29. Dill, H. D., and Saff, C. R., "Spectrum Crack Growth Prediction Method Based on Crack Surface Displacement and Contact Stress," ASTM STP 595, Fatigue Crack Growth, American Society for Testing and Materials, May 1976

30. Gray, T. D., and Gallagher, J. P., "Predicting Fatigue Crack Retardation Following a Single Overload Using a Modified Wheeler Model," ASTM STP 590, Mechanics of Crack Growth, American Society for Testing and Materials, 1976

31. Gallagher, J. P., "A Generalized Development of Yield Zone Models," AFFDL-TM-74-28, January 1974

32. Gallagher, J. P., and Hughes, T. F., "Influence of Yield Strength on Over-Load Affected Fatigue Crack Growth Behavior in 4340 Steel," AFFDL-TR-74-27, Air Force Flight Dynamic Laboratory, Ohio, July 1974

33. Dugdale, D. S., Journal of Mechanics and Physics of Solids, Vol 8, July 1960

34. Rice, J. R., International Journal of Solids and Structures, Vol 8, 1972

35. Bueckner, H. F., "A Novel Principle for the Computation of Stress Intensity Factors," Z. Angew, Math. Mech., Vol 50, 1970

36. Dill, H. D., and Saff, C. R., "Analysis of Crack Growth Following Compression High Load Based on Crack Surface Displacement and Contact Analysis," ASTM STP 637, <u>Cyclic Stress-Strain and Plastic Deformation Aspects of Fatigue Crack Growth</u>, American Society for Testing and Materials, 1977

37. Chang, J. B., Streitmatter, S. P., and Tung, P. P., "Effect of B-1 Bomber Spectra Variation on Crack Growth," NA-75-881, Rockwell International Corporation, Los Angeles Division, 26 March 1976

38. Anon, "Technical Proposal for Improved Methods for Predicting Spectrum Loading Effects," NA-77-648, Rockwell International, Los Angeles Division, 1977

39. Hudson, C. M., and Hardrath, H. F., "Investigation of the Effects of Variable Amplitude on Fatigue Crack Propagation Patterns," NASA TND-1803, August 1963

40. Hsu, T. M., and Lassiter, L. W., "Effect of Compressive Overload on Fatigue Crack Growth," AIAA paper 74-365, April 1974

41. Stevens, R. I., Chen, D. K., and Nom, B. W., "Fatigue Crack Growth with Negative Stress Ratio Following Single Overloads in 2024-T3 and 7075-T6 Aluminum Alloy," ASTM, STP 595, <u>Fatigue Crack Growth Under Spectrum Loads</u>, American Society for Testing and Materials, 1976

42. Begley, J. A., and Landes, J. D., "A Comparison of the J-Integral Fracture Criterion With the Equivalent Energy Concept," <u>Progress in Flaw Growth and Fracture Toughness Testing</u>, ASTM, STP 536, July 1973

43. Begley, J. A., and Landes, J. D., "The J-Integral as a Fracture Criterion," <u>Fracture Toughness</u>, ASTM, STP 514, 1972

44. Begley, J. A., Landes, J. D., and Wilson, W. K., "An Estimation Model for the Application of the J-Integral," <u>Fracture Analysis</u>, ASTM, STP 560, 1974

45. Kobayashi, A. S., and Enetanya, A. N., "Stress Intensity Factor of a Corner Crack," <u>Mechanics of Crack Growth</u>, ASTM STP 590, 1976

46. Rice, J. R., "Some Remarks on Elastic Crack-Tip Stress Fields," <u>International Journal of Solids and Structures</u>, Vol 8, pp 751-758, 1972

47. Kobayashi, A. S., Maiden, D. E., Simon, B. J., and Iida, S., "Application of the Method of Finite Element Analysis to Two-Dimensional Problems in Fracture Mechanics," ASME paper 69-WA/PVP-12, 1969

48. Wilson, W. K., "Some Crack Tip Finite Elements for Plane Elasticity," <u>Stress Analysis and Growth of Cracks</u>, ASTM, STP 513, 1972

49. Cruse, T. A., and Meyers, G. J., "Three-Dimensional Fracture Mechanics Analysis," Journal of the Structural Division, Transactions of ASCE, 1977

50. Hsu, T. M., McGee, W. M., and Aberson, J. A., "Extended Study of Flaw Growth at Fastener Holes," AFFDL-TR-77-83, Vol 1, Air Force Flight Dynamics Laboratory, WPAFB, Ohio, 1978

51. McGorwan, J. J., and Smith, C. W., "Stress Intensity Factors for Deep Cracks Emanating From the Corner Formed by a Hole Intersecting a Plate Surface," Mechanics of Crack Growth, ASTM STP 590, 1976

52. Snow, J. R., "A Stress Intensity Factor Calibration for Corner Flaws at an Open Hole," AFML-TR-74-282, Air Force Materials Laboratory, WPAFB, Ohio, 1975

53. Tada, H., Paris, P. C., and Irwin, G. R., The Stress Analysis of Cracks Handbook, Del Research Corp, Hellertown, Pennsylvania, 1973

54. Sih, G. C., Handbook of Stress-Intensity Factors for Researchers and Engineers, Institute of Fracture and Solid Mechanics, Lehigh University, Bethlehem, Pennsylvania, 1973

55. Rooke, D. P., and Cartwright, D. J., Compendium of Stress Intensity Factors, Her Majesty's Stationery Office, London, 1976

56. Byskov, E., "The Calculation of Stress Intensity Factors Using the Finite Element Method With Cracked Elements," International Journal of Fracture Mechanics, Vol 6, No. 2, pp 159-167, 1970

57. Tong, P., "New Displacement Hybrid Finite Element Models for Solid Continua," International Journal for Numerical Methods in Engineering, Vol 2, 1970

58. Pian, T. H. H., Tong, P., and Luk, C. H., "Elastic Crack Analysis by a Finite Element Hybrid Method," Proceedings of the Third International Conference on Matrix Methods in Structural Mechanics, WPAFB, Ohio, 1971

59. Cheng, J. S., "Stress Intensity Factor Solutions by Assumed Displacement Hybrid Finite Element Program, HYCRAK, User's Manual," NA-76-763, Rockwell International, Los Angeles Division, 1977

60. Atluri, S. N., and Kathiresan, K., "Stress Analysis of Typical Flaws in Aerospace Structural Components Using 3-D Hybrid Displacement Finite Element Method," AIAA/ASME 19th Structures, Structural Dynamics, and Materials Conference, Bethesda, Maryland, 1978

61. Pian, T. H. H., and Moriga, K., "Three-Dimensional Fracture Analysis by Assumed Stress Hybrid Element," International Conference on Numerical Methods in Fracture Mechanics, England, 1978

62. Bowie, O. L., "Analysis of an Infinite Plate Containing Radial Cracks Originating From the Boundary of an Internal Circular Hole," Journal of Mathematics and Physics, Vol 35, pp 60-71, 1956

63. Brussat, T. R., Chiu, S. T., and Creager, M., "Flaw Growth in Complex Structure, Vol I — Technical Discussion," AFFDL-TR-77-79, Air Force Flight Dynamics Laboratory, WPAFB, Ohio, 1977

64. Tweed, J., and Rooke, D. P., "The Distribution of Stress Near the Tip of a Radial Crack at the Edge of a Circular Hole," International Journal of Engineering Science, Vol 11, pp 1185-1195, 1974

65. Paris, P. C., and Sih, G. C., "Stress Analysis of Cracks," Fracture Toughness Testing, ASTM STP 381, 1965

66. Isida, M., "Stress Intensity Factors for the Tension of an Eccentrically Cracked Strip," ASME Transaction, Journal of Applied Mechanics, Vol 33, pp 674-675, 1966

67. Chang, J. B., "Development of Finite Element Techniques for Fatigue Crack Growth Prediction at Fastener Holes," NA-75-822, Rockwell International, Los Angeles, 1975

68. Chang, J. B., "Prediction of Fatigue Crack Growth at Cold-Worked Fastener Holes," Journal of Aircraft, Vol 14, No. 9, pp 903-908, 1977

69. Shan, S. K., Numerical Methods and Computers, Addison-Wesley Publishing Company, Inc., 1965

70. Engle, R. M., "CRACKS, A Fortran IV Digital Computer Program for Crack Propagation Analysis," AFFDL-TR-70-107, Air Force Flight Dynamics Laboratory, WPAFB, Ohio, 1970

71. Johnson, W. S., "CGR, An Improved Computerized Model to Predict Fatigue Crack Growth Under Spectrum Loading," NSRDC, Report 4577, 1975

72. Szamossi, M., "Crack Propagation Analysis by Vroman's Model, Program EFFGRO," NA-72-94, Rockwell International, Los Angeles, 1972

73. Wood, H. A., Engle, R. M., Gallagher, J., and Potter, J. M., "Current Practice on Estimating Crack Growth Damage Accumulation With Specific Application to Structural Safety, Durability and Reliability," U.S. Air Force Flight Dynamic Lab, AFFDL-TR-75-32, WPAFB, 1976

74. Wood, H. A., "The Use of Fracture Mechanics Principles in the Design and Analysis of Damage Tolerant Aircraft Structures," Fatigue Life Prediction for Aircraft Structures and Materials, AGARD-LS-62, pp 4.1-4.3, 1973

75. Gallagher, J. P., and Stanaker, H. D., "Predicting Flight-by-Flight Fatigue Crack Growth Rates," Journal of Aircraft, AIAA, Vol 12, pp 699-705, 1975

76. Gallagher, J. P., and Stalnaker, H. D., "Methods for Analyzing Fatigue Crack Growth Rate Behavior Associated With Flight-by-Flight Loading," AIAA paper 74-367, presented at AIAA/ASME 15th Structures, Structural Dynamics and Materials Conference, Las Vegas, Nevada, 17-19 April 1974

77. Gallagher, J. P., "Estimating Fatigue Crack Lives for Aircraft: Techniques," Experimental Mechanics, Vol 16, No. 11, pp 425-433, November 1976

78. Gallagher, J. P., "What the Designer Must Know About Fracture Mechanics Fundamentals," SAE Paper 710151, Society of Automotive Engineers, 1971

79. Gallagher, J. P., "Fatigue Crack Growth Laws," presentation of Task Force report E24.04.04-1 to ASTM Subcritical Crack Growth Subcommittee E24.04, Philadelphia, Pennsylvania, 9 October 1974

80. Gallagher, J. P., "A Generalized Development of Yield Zone Models," AFFDL-TM-FBR-74-27, Air Force Flight Dynamics Laboratory, Wright-Patterson AFB, January 1974

81. Gallagher, J. P., and Hughes, T. F., "Influence of Yield Strength on Overload Affected Fatigue Crack Growth Behavior in 4340 Steel," AFFDL-TR-74-28, Air Force Flight Dynamics Laboratory, Wright-Patterson AFB, May 1974 (AD 787655)

82. Petrak, G. J., and Gallagher, J. P., "Predictions of the Effect of Yield Strength on Fatigue Crack Growth Retardation in HP-9Ni-4Co-30C Steel," ASME paper 75-Mat-N, to appear in ASME Trans, Journal of Engineering Materials and Technology

83. Brussat, T. R., "An Approach to Predicting the Growth to Failure of Fatigue Cracks Subjected to Arbitrary Uniaxial Cyclic Loading," Damage Tolerance in Aircraft Structures, ASTM STP 486, American Society for Testing and Materials, pp 122-143, 1971

84. Damage Tolerant Design Handbook, MCIC-HB-01, Air Force Materials Laboratory, Air Force Flight Dynamic Laboratory, WPAFB, December 1972

85. Varanasi, S. R., and Whittaker, I. C., "Structural Reliability Prediction Method Considering Crack Growth and Residual Strength," Fatigue Crack Growth Under Spectrum Loads, ASTM STP 595, pp 292-305, 1976

86. Johnson, W. S., Heller, R. A., and Yang, J. N., "Flight Inspection Data, Crack Initiation Times, and Initial Crack Size," Proc 1977 Annual Reliability and Maintainability Symposium, January 1977

87. Yao, J. T. P., "Fatigue Reliability and Design," Journal of Structural Division, ASCE, Vol 100, No. ST9, 1974

88. Wirsching, P. H., and Ellingwood, B., "Criteria for Assurance of Reliability Against Fatigue/Fracture," Committee Report Chapter 2, Fatigue and Fracture Reliability, ASCE, 1979

89. Yang, J. N., "Statistical Relationship Between Equivalent Initial Flaw Size and Time to Crack Initiation," Interim Technical Quarterly Report, F33615-77-C-3123, General Dynamics, Sep 15 to Dec 15, 1978

90. Porter, T. R., "Method of Analysis and Prediction of Variable Amplitude Fatigue Crack Growth," Engineering Fracture Mechanics, Vol 4, 1972

91. Elber, W., "Equivalent Constant-Amplitude Concept for Crack Growth Under Spectrum Loading," Fatigue Crack Growth Under Spectrum Loads, ASTM STP 595, pp 236-250, 1976

92. Imig, L. A., "Crack Growth in Ti-8Al-1Mo-1V With Real-Time and Accelerated Flight-by-Flight Loading," Fatigue Crack Growth Under Spectrum Loads, ASTM STP 595, pp 251-264, 1976

93. Newman, J. C., "A Finite-Element Analysis of Fatigue Crack Closure," NASA TM X-72005, 1975

94. Barsom, J. M., "Fatigue-Crack Growth Under Variable Amplitude Loading in ASTM A 514B Steel," Progress in Flaw Growth and Fracture Toughness Testing, ASTM STP 536, American Society for Testing and Materials, pp 147-167, 1973

95. Smith, S. H., Porter, T. R., and Engstrom, W. L., "Fatigue Crack Propagation Behavior and Residual Strength of Bonded Strap Reinforced, Lamellated, and Sandwich Panels," Proc Air Force Conf on Fatigue and Fracture of Aircraft Structures and Materials, AFFDL TR 70-144, Air Force Flight Dynamics Laboratory, Wright-Patterson AFB, pp 611-634, 1970

96. Forman, R. G., Kearney, V. E., and Engle, R. M., "Numerical Analysis of Crack Propagation in Cycle-Loaded Structures," Journal of Basic Engineering, ASME, Vol 89, No. 3, pp 495-521, 1967

97. Houbolt, J. C., "Design Manual for Vertical Gust Based on Power Spectral Techniques," AFFDL-TR-70-106, WPAFB, 1970

98. Neulieb, R. L., et al, "Atmospheric Turbulence Field Parameters Determination," AFFDL-TR-72-51, WPAFB, 1972

99. Houbolt, J. C., et al, "Dynamic Response of Airplanes to Atmospheric Turbulence Including Flight Data on Input and Response, " Report R-199, NASA, 1964

100. Press, H., Meadows, M. T., and Hadlock, I., "A Reevaluation of Data on Atmospheric Turbulence and Airplane Gust Loads for Application in Spectral Calculation," Report 1272, NASA, 1956

101. Lin, Y. K., Probabilistic Theory of Structural Dynamics, McGraw-Hill, New York, 1967

102. Lin, Y. K., and Howell, L. J., "Response of Flight Vehicles to Nonstationary Turbulence," AIAA Journal, Vol 9, pp 2201-2207, 1971

103. Paris, P. C., "The Fracture Mechanics Approach to Fatigue," Proc of the 8th Sagamore Army Materials Research Conf, Syracuse University Press, pp 107-127, 1964

104. Rice, J. R., and Beer, F. P., "On the Distribution of Rises and Falls in a Continuous Random Process," Journal of Basic Engineering, ASME, pp 398-404, 1965

105. Rice, J. R., etaal, "On the Prediction of Some Random Loading Characteristics Relevant to Fatigue," Proc of the Second Inter Conf on Acou Fatigue in Aero Structures, Syracuse Univ Press, pp 121-143, 1965

106. Smith, S. H., "Fatigue Crack Growth Under Axial Narrow and Broad Band Random Loading," Acoustical Fatigue in Aero Structures, Syracuse Univ Press, 1965

107. Smith, S. H., "Random Loading Fatigue Crack Growth Behavior of Some Aluminum and Titanium Alloys," Structural Fatigue in Aircraft, ASTM-STP 404, 1966

108. Swanson, S. R., Cicci, F., and Hoppe, W., "Crack Propagation in Clad 7079-T6 Aluminum Alloy Sheet Under Constant and Random Amplitude Fatigue Loading," Fatigue Crack Propagation, ASTM STP 415, American Society for Testing and Materials, pp 312-362, 1967

109. Yang, J. N., "Statistics of Random Loading Relevant to Fatigue," Journal Engr Mech Div, ASCE, Vol 100, No. EM3, pp 469-475, 1974

110. Shinozuka, M., "Development of Reliability-Based Aircraft Safety Criteria: An Impact Analysis," AFFDL-TR-76-29, WPAFB, 1975

111. Yang, J. N., and Trapp, W. J., "Reliability Analysis of Aircraft Structures Under Random Loading and Periodic Inspection," AIAA Journal, Vol 12, No. 12, pp 1623-1630, 1974

112. Anon, "Airplane Strength and Rigidity, Flight Loads, "Military Specification MIL-A-008861A, U.S. Air Force, Washington, D.C., March 1971

113. Graziano, W. D., and Fitch, G. E., Jr., "Initiation and Growth of Fatigue Cracks in and Residual Strength of the F-100 Wing," Damage Tolerance in Aircraft Structures, ASTM STP 486, American Society for Testing and Materials, pp 144-163, 1971

114. Swift, T., and Wang, D. Y., "Damage Tolerant Design-Analysis Methods and Test Verification of Fuselage Structure," Proc Air Force Conf on Fatigue and Fracture of Aircraft Structures and Materials, AFFDL TR 70-144, Air Force Flight Dynamics Laboratory, Wright-Patterson AFB, pp 653-697, 1970

115. Yang, J. N., "Statistical Estimation of Economic Life for Aircraft Structures," to appear in Proceedings of the AIAA/ASME/ASCE/AHS 20th Structures, Structural Dynamics and Materials Conference, April 1979, St. Louis

116. Yang, J. N., "Statistical Estimation of Service Cracks and Maintenance Cost for Aircraft Structures," Journal of Aircraft, AIAA, Vol 13, No. 12, pp 929-937, December 1976

117. Dill, H. D., and Young, M. T., "Stress History Simulation," Volume I, A User's Manual for a Computer Program to Generate Stress History Simulation, AFFDL-TR-76-113, Air Force Flight Dynamics Laboratory, Wright-Patterson Air Force Base, Ohio, March 1977

118. Young, M. T., Foster, F. R., and Dill, H. D., "Stress History Simulation," Volume II, A User's Manual for a Computer Program to Modify Stress History Simulations, AFFDL-TR-76-113, Volume II, Air Force Flight Dynamics Laboratory, Wright-Patterson Air Force Base, Ohio, March 1977

119. USAF Contract F33615-76-C-3116, "Effects of Transport/Bomber Spectrum on Crack Growth"

120. Durkee, E. D., "Flight Loads Data from Cargo Aircraft," AFFDL Technical Memorandum 75-26-FBE, Air Force Flight Dynamics Laboratory, Wright-Patterson Air Force Base, Ohio, 1975

121. Anon, "Military Standard, Aircraft Structural Integrity Program, Airplane Requirements," MIL-STD-1530A, December 1975

122. Brusset, T. R., "Rapid Calculation of Fatigue Crack by Integration" Fracture Toughness and Slow-Stable Cracking, ASTM STP559, 1974

123. Clay, L. E., Sandlin, N. H., Marcock, D. S., Brown, K. E., Johnson, R. L., and David, J. C., "Force Management Method, Task I Report, Current Methods," AFFDL-TR-78-183, Air Force Flight Dynamics Laboratory, WPAFB, Ohio, 1978
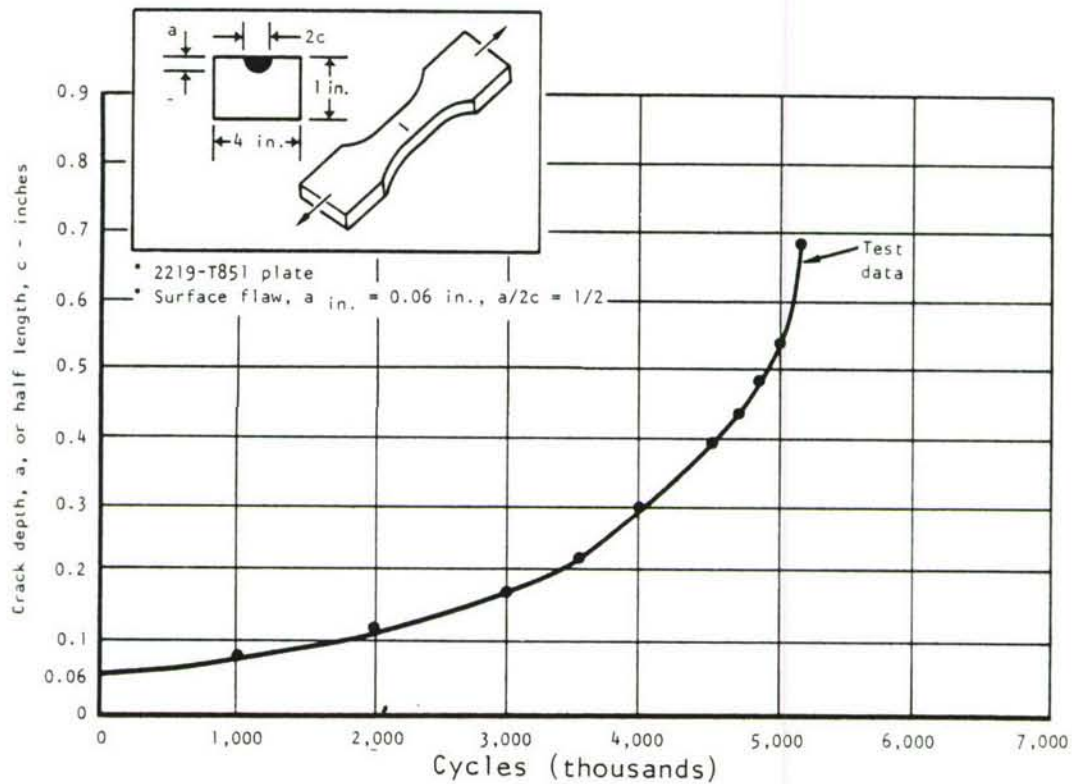
Figure 1. Crack growth curve, a 2219-T851 aluminum plate containing a surface crack subjected to spectrum loading.
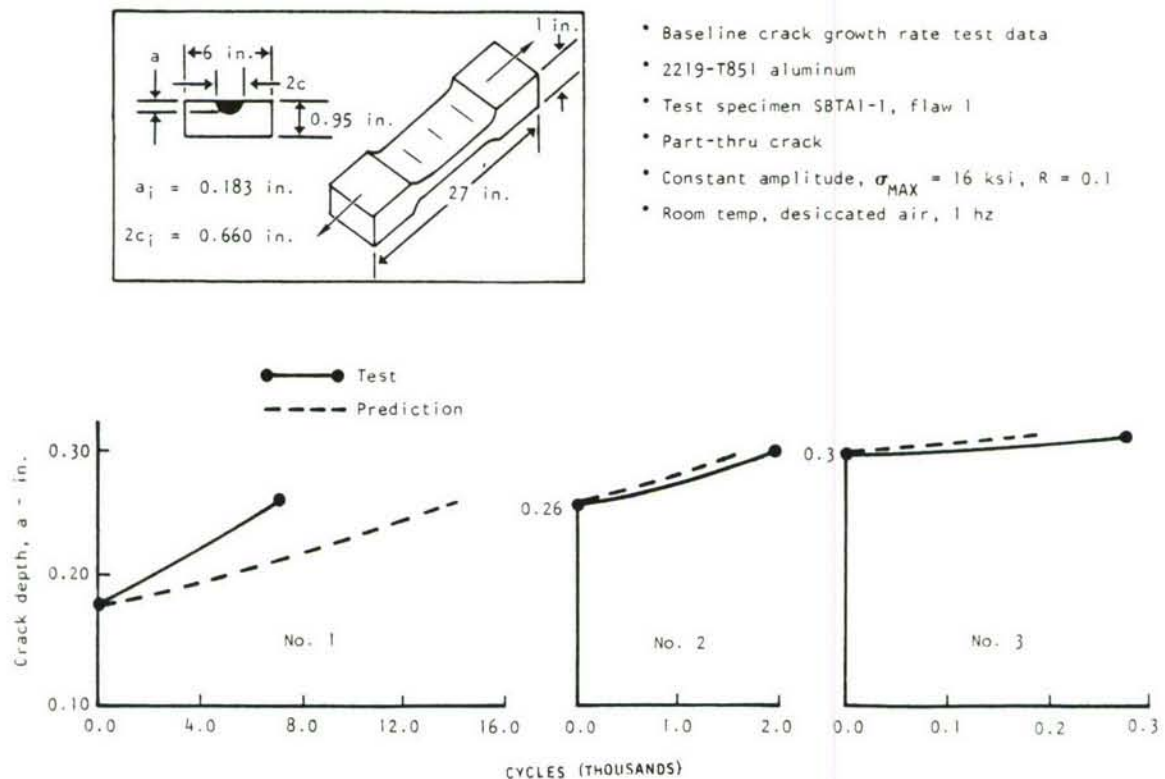
Figure 2. Boeing 2219-T851 aluminum baseline crack growth rate data correlation - specimen SBTA 1-1, flaw 1.

111
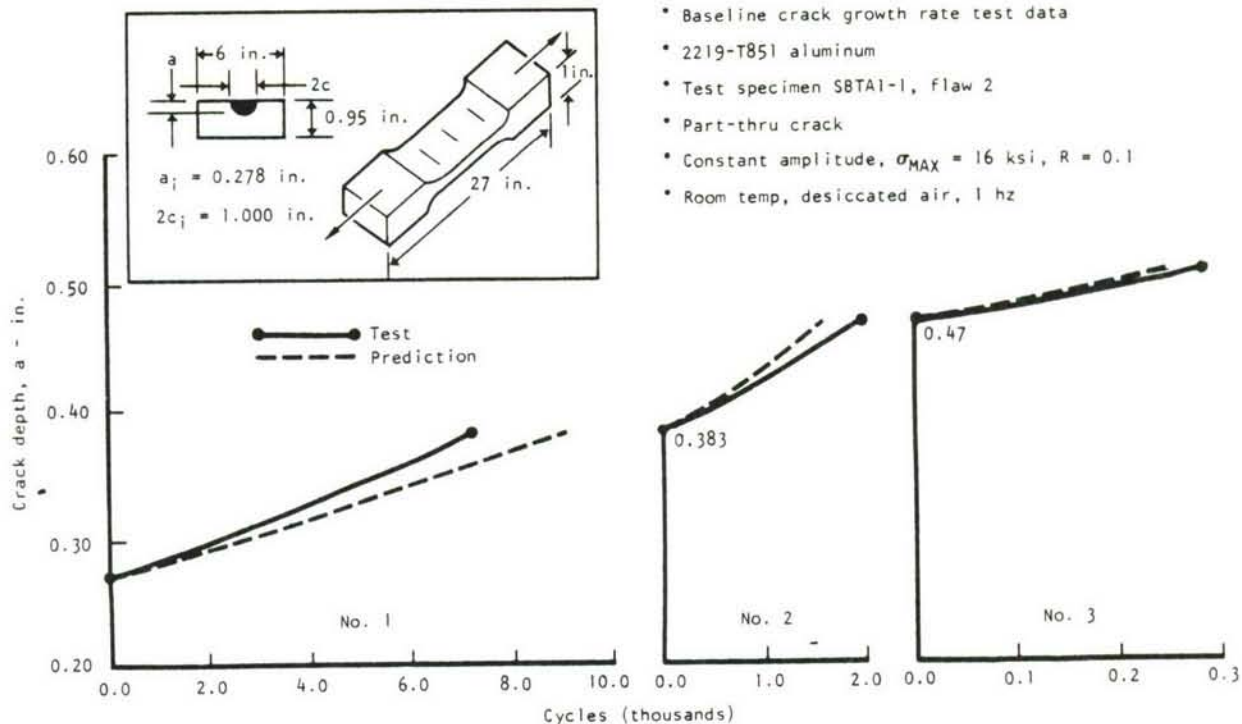
Figure 3. Boeing 2219-T851 aluminum baseline crack growth rate data
correlation - specimen SBTA 1-1, flaw 2.
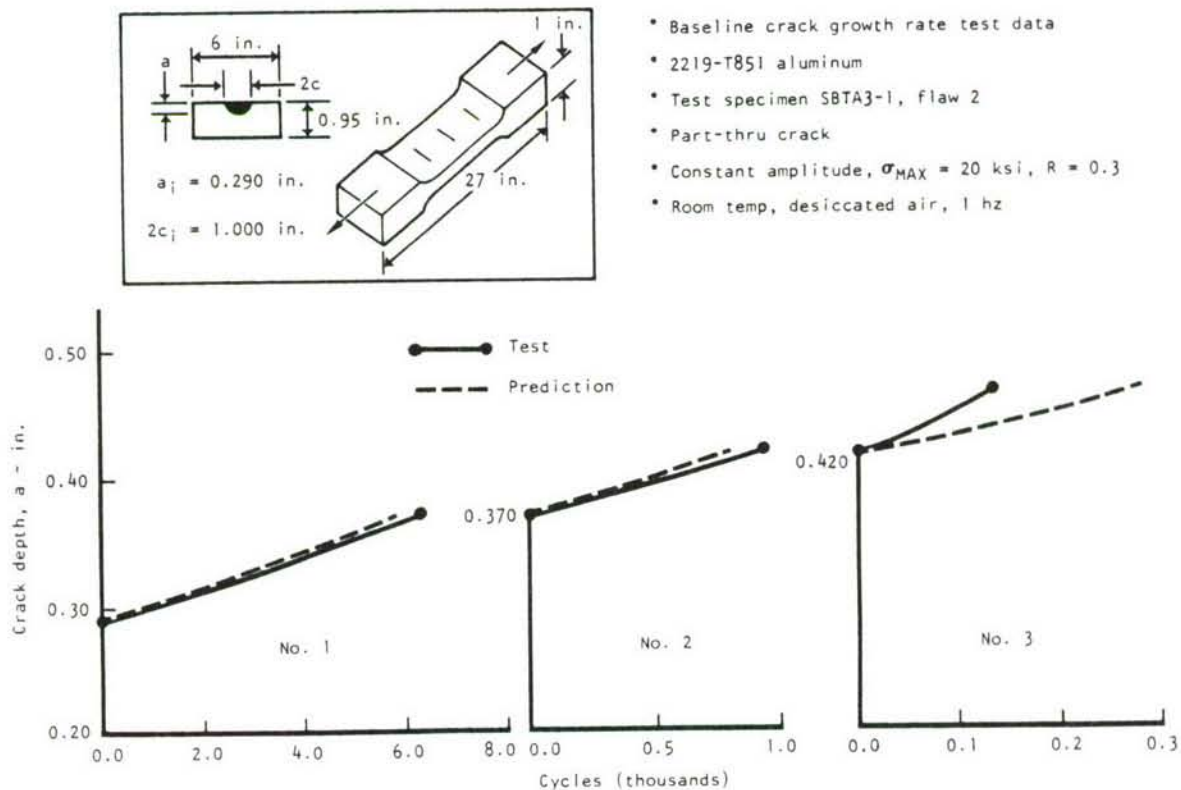
Figure 4. Boeing 2219-T851 aluminum baseline crack growth rate data
correlation - specimen SBTA 3-1, flaw 2.

112

- Boeing baseline crack growth rate data correlation
- 2219-T851 aluminum
- Constant amplitude loading
- Predicted by EFFGRO using Boeing rate equation & constants

Mean R = 1.14

R = Life (analysis)/life (test)
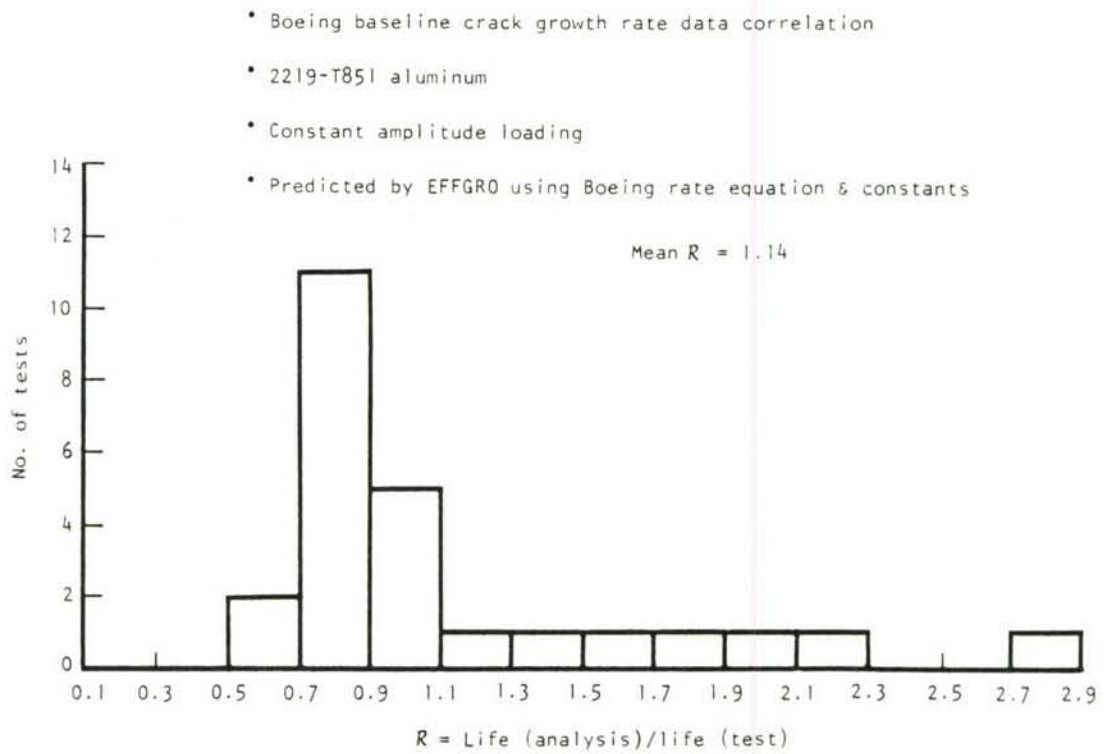
Figure 5. Histogram, crack growth correlation on Boeing 2219-T851 aluminum baseline data.

W = 2.5 in.
H/W = 0.6
d/W = 0.25
t = 0.25 in.

- Baseline crack growth test data
- 2219-T851 aluminum, compact-type specimen
- Test specimen AD-25-6CA
- Constant amplitude
- Room temp, lab air

Test
Prediction

No. 12 No. 13 No. 14 No. 15

1.489 1.534 1.58

Cycles (thousands)
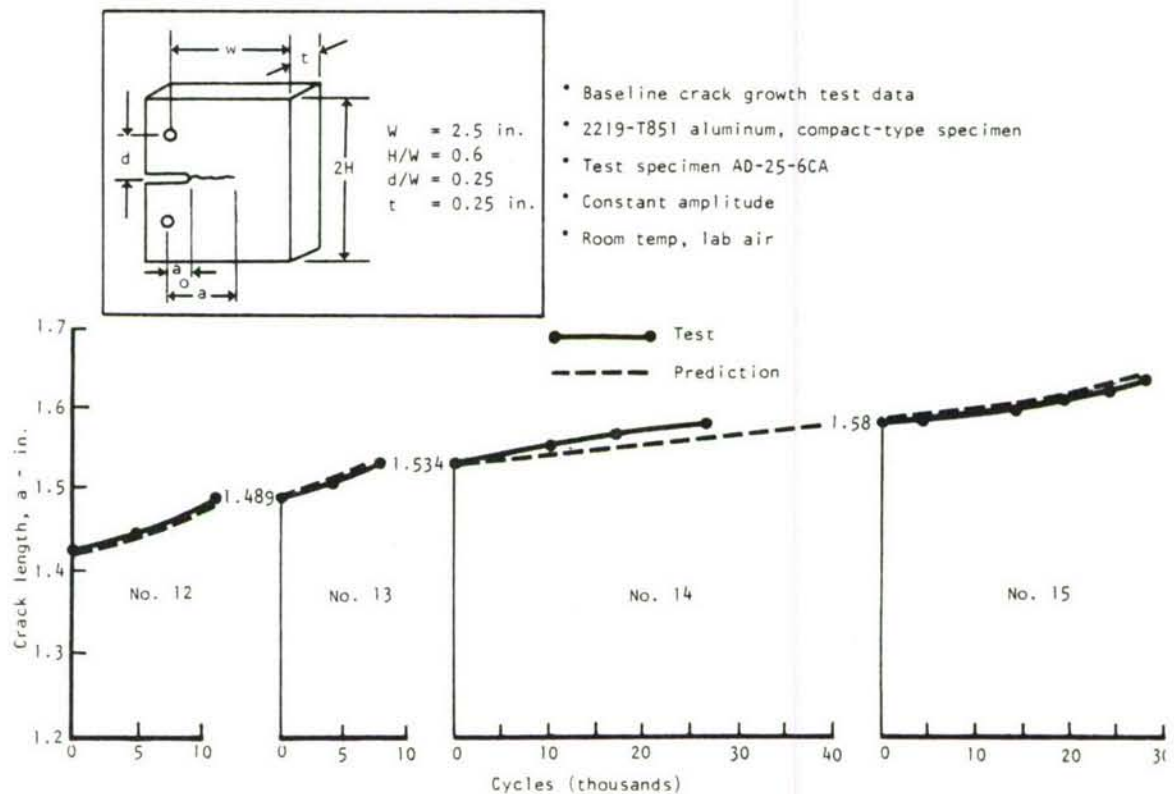
Figure 6. Grumman 2219-T851 aluminum baseline crack growth rate test data correlation - specimen AD-25-6CA.

113
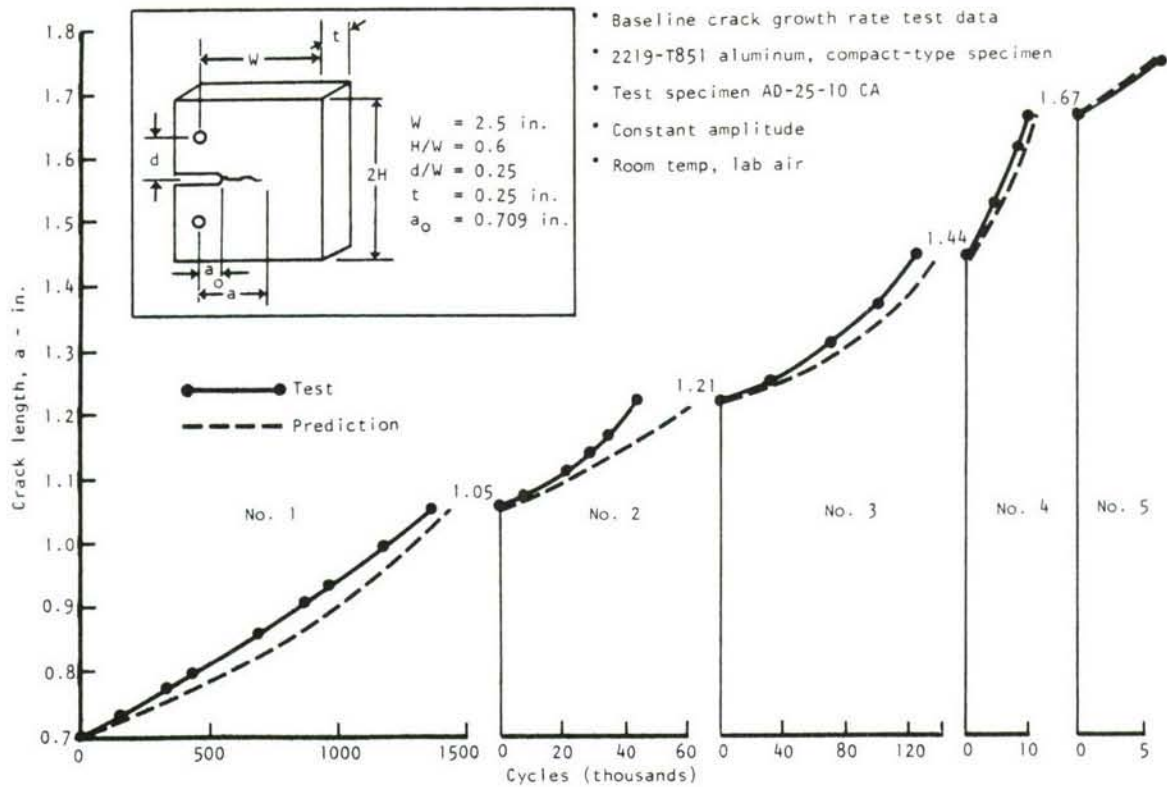
Figure 7. Grumman 2219-T851 aluminum baseline crack growth rate test data correlation - specimen AD-25-10CA.
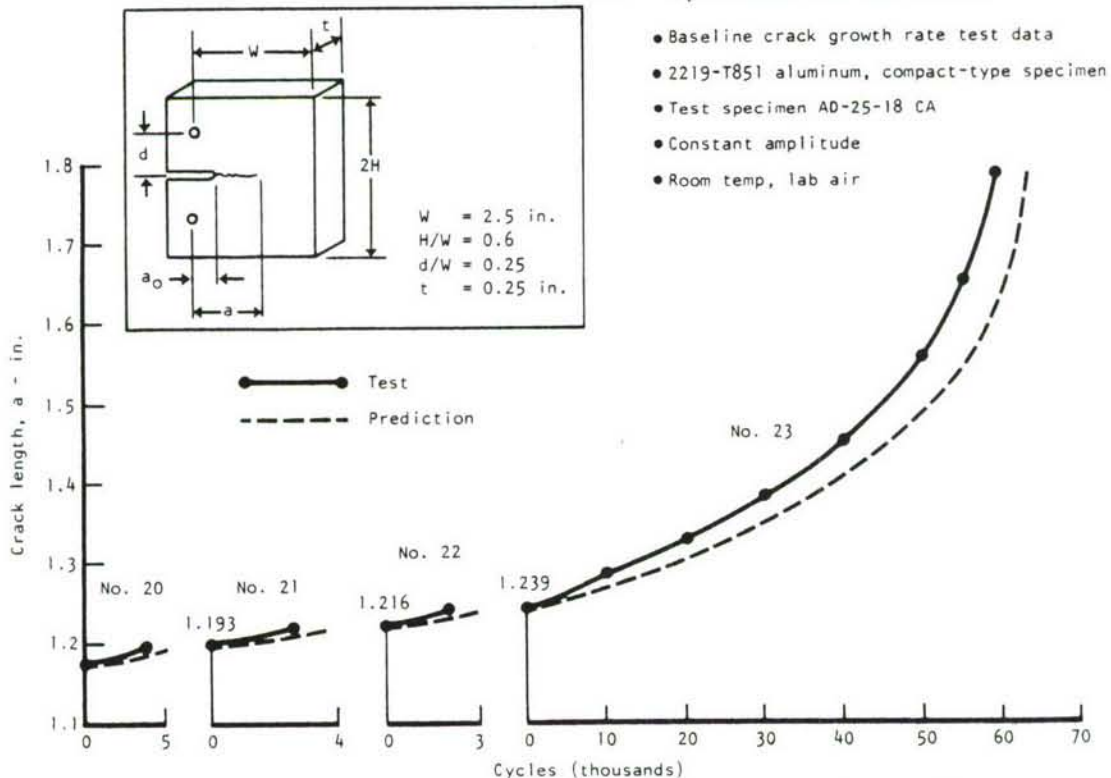
Figure 8. Grumman 2219-T851 aluminum baseline crack growth rate test data correlation - specimen AD-25-18CA.

114
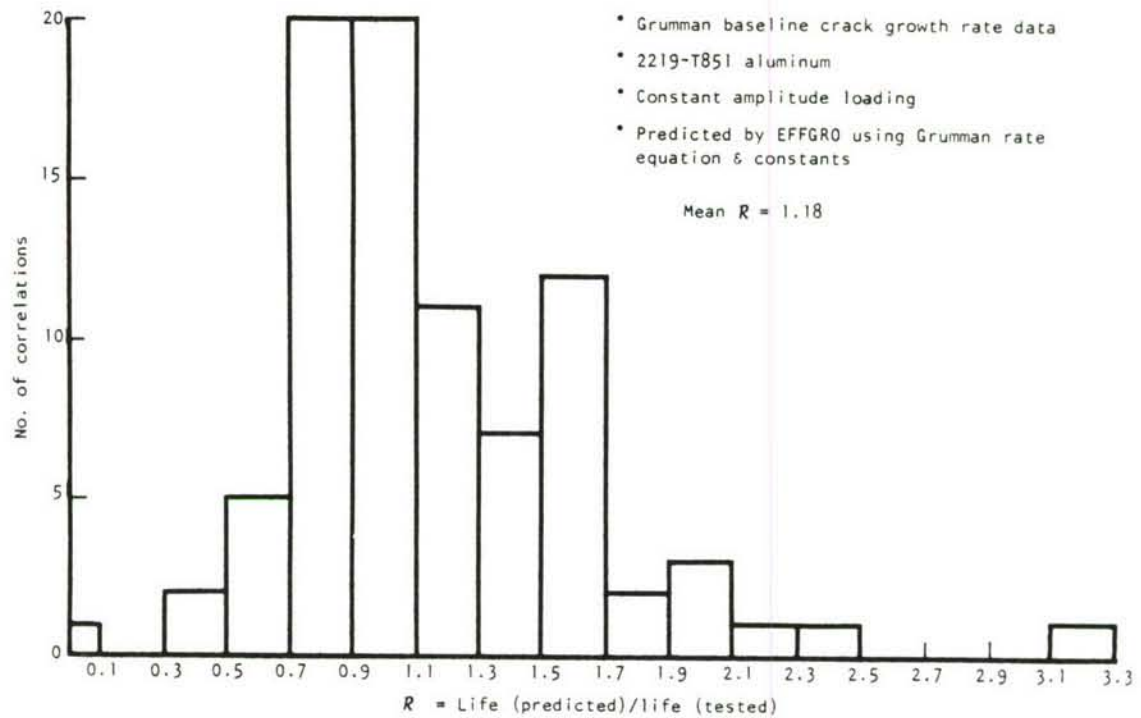
Figure 9.   Histogram, crack growth correlation on Grumman
2219-T851 aluminum baseline data.
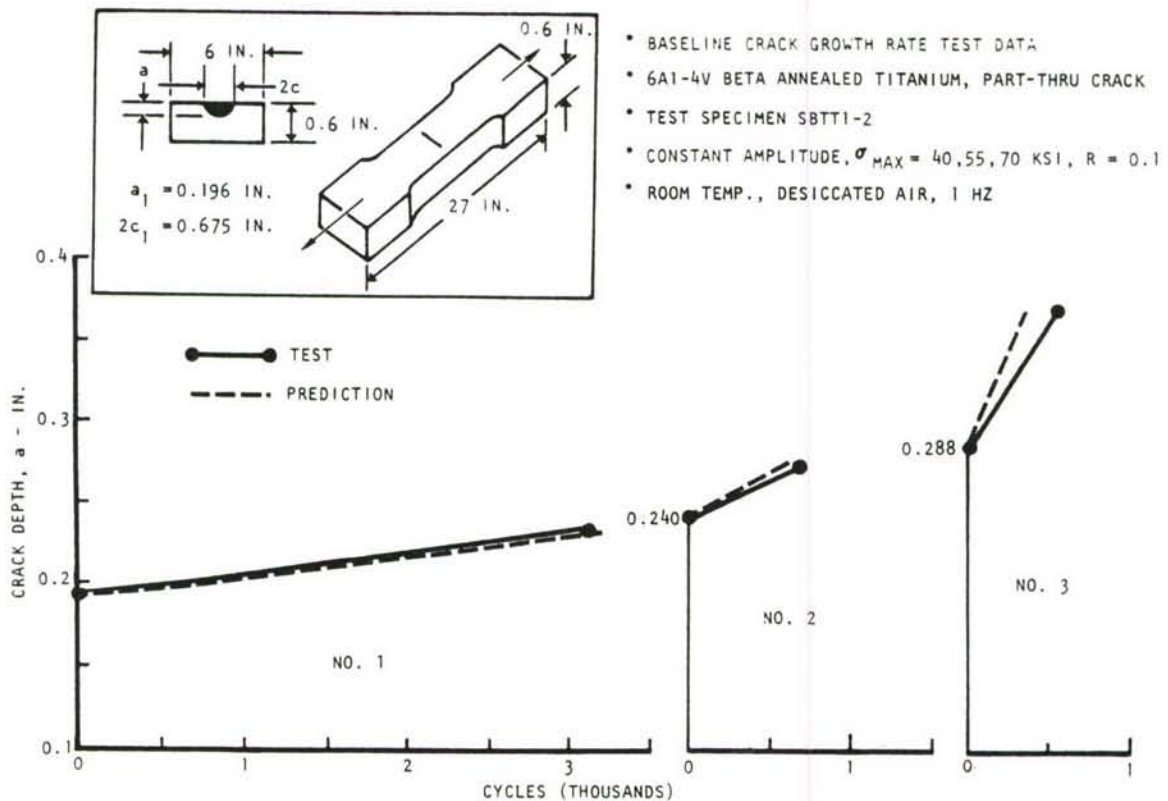
Figure 10.   Boeing Ti-6Al-4V β-annealed baseline crack growth rate data
correlation, specimen SBTT1-2.

115
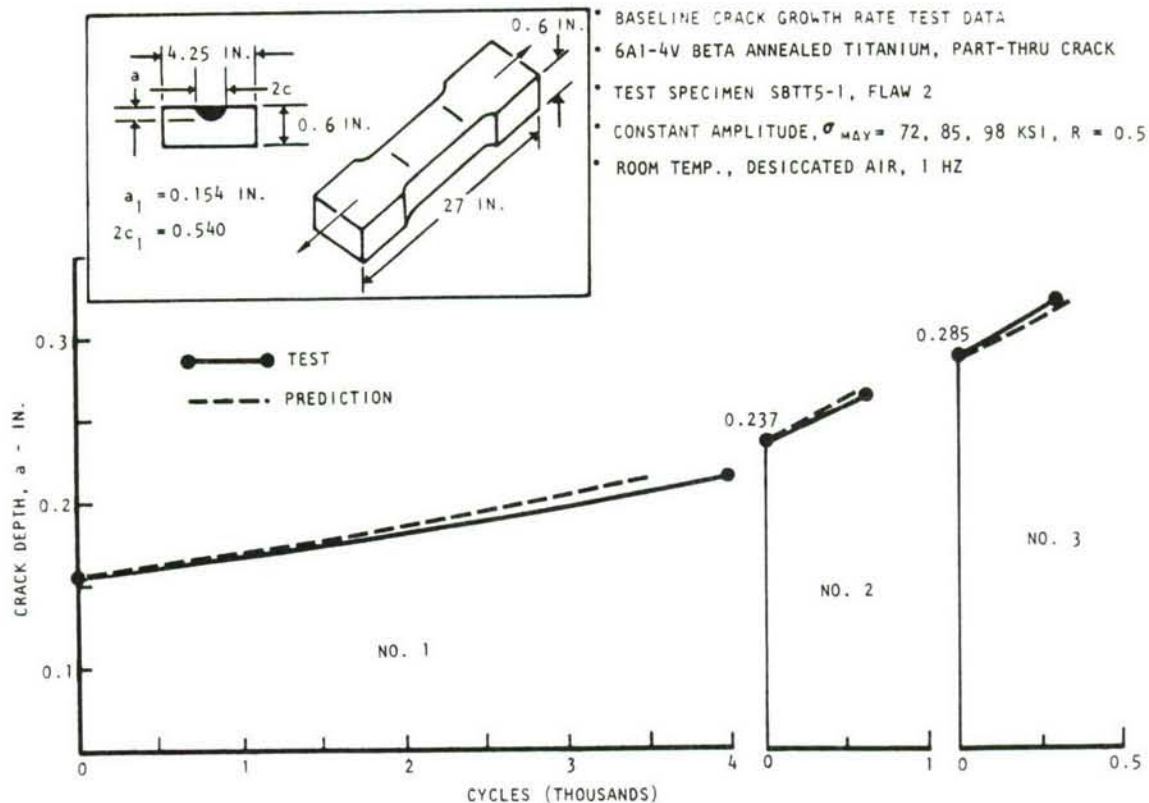
Figure 11. Boeing Ti-6Al-4V β-annealed baseline crack growth rate data correlation, specimen SBTT5-1, flaw 2.

- BOEING BASELINE CRACK GROWTH RATE DATA CORRELATION

- 6Al-4V BETA-ANNEALED TITANIUM

- CONSTANT AMPLITUDE LOADING

- PREDICTED BY EFFGRO USING BOEING RATE EQUATION & CONSTANTS
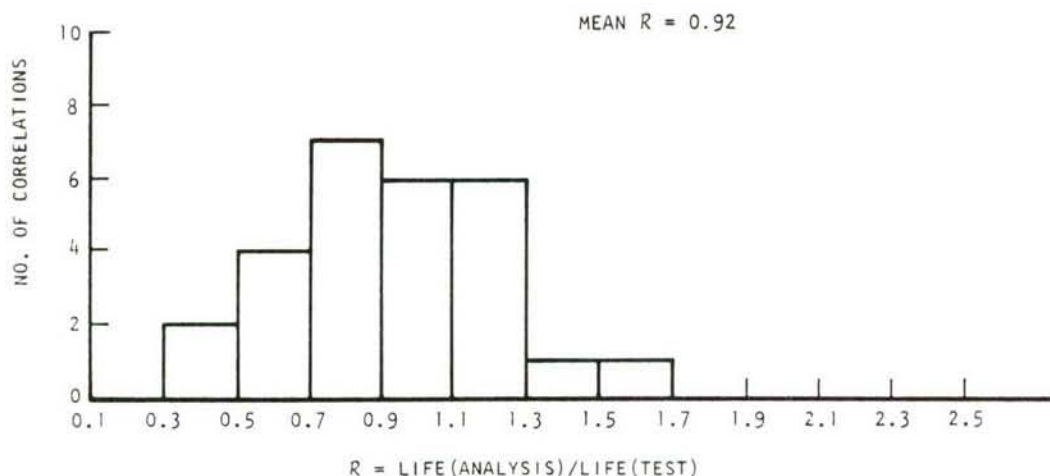
Figure 12. Histogram, crack growth correlation on Boeing Ti-6Al-4V beta-annealed baseline data.

116
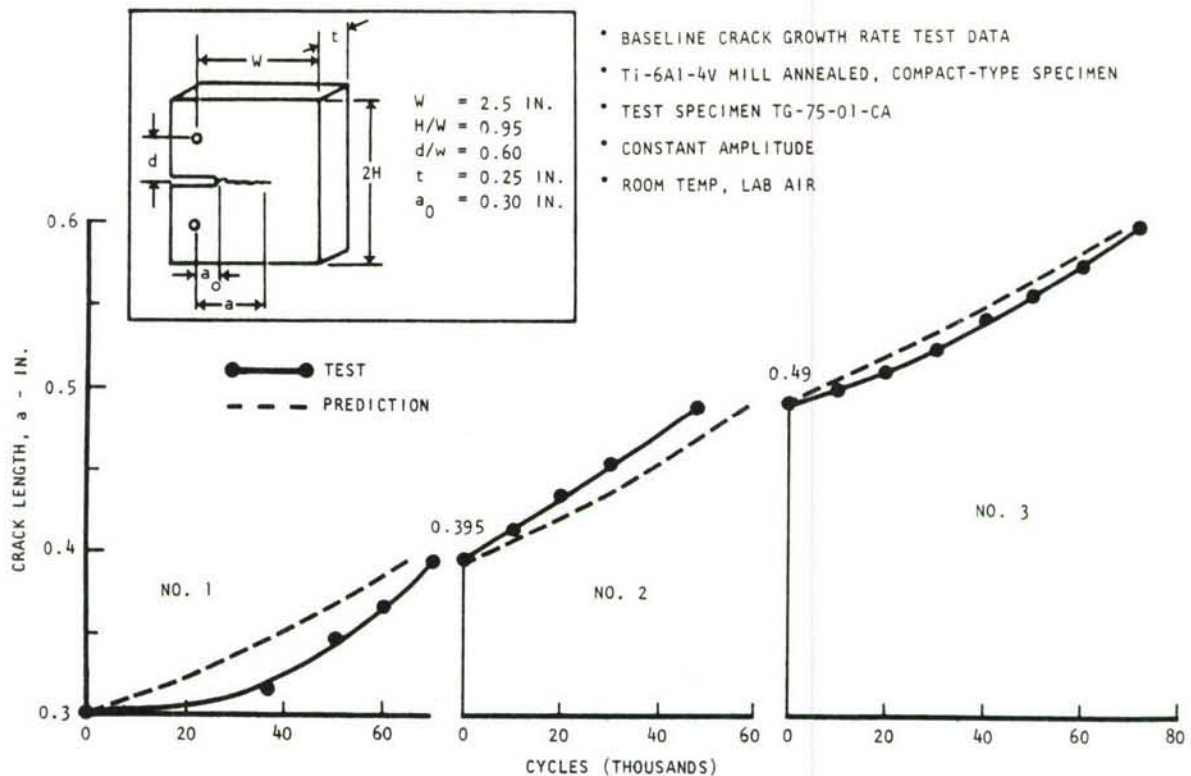
Figure 13.   Grumman Ti-6Al-4V mill-annealed baseline crack growth rate test
data correlation, specimen TG-75-01.
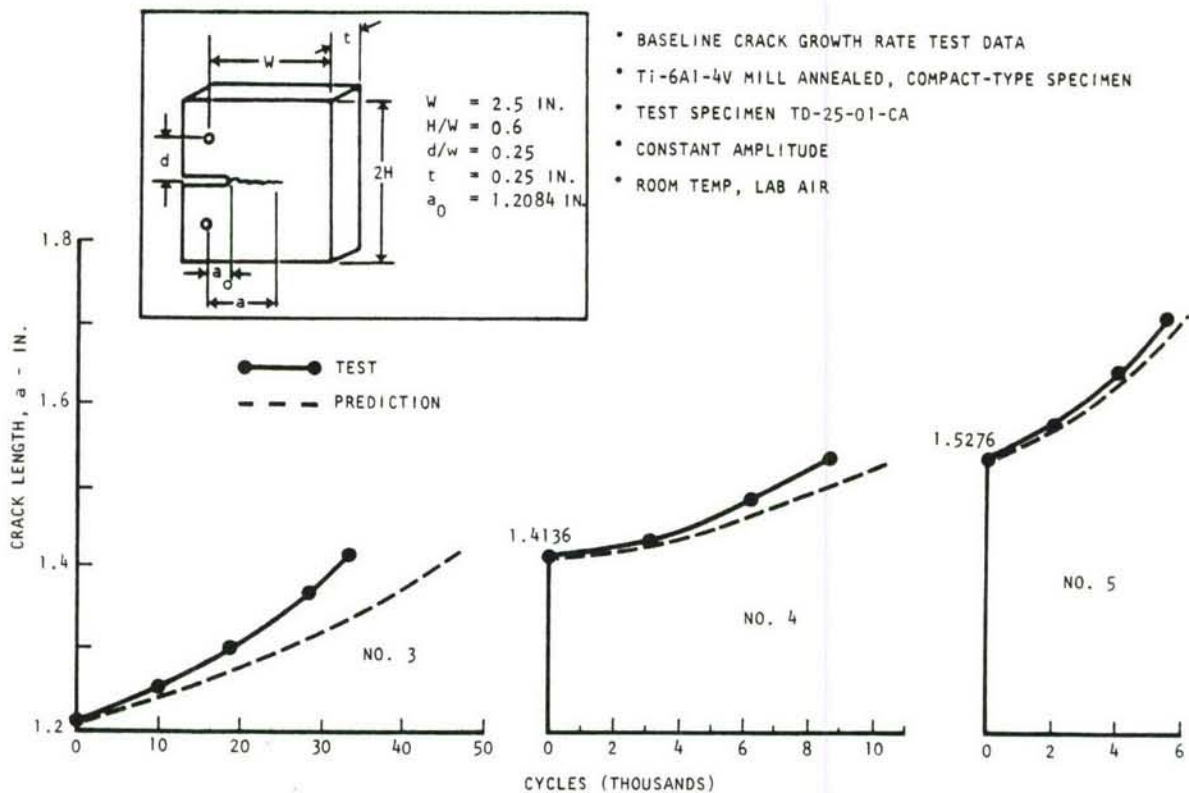
Figure 14.   Grumman Ti-6Al-4V mill-annealed baseline crack growth rate test
data correlation, specimen TD-25-01.

117
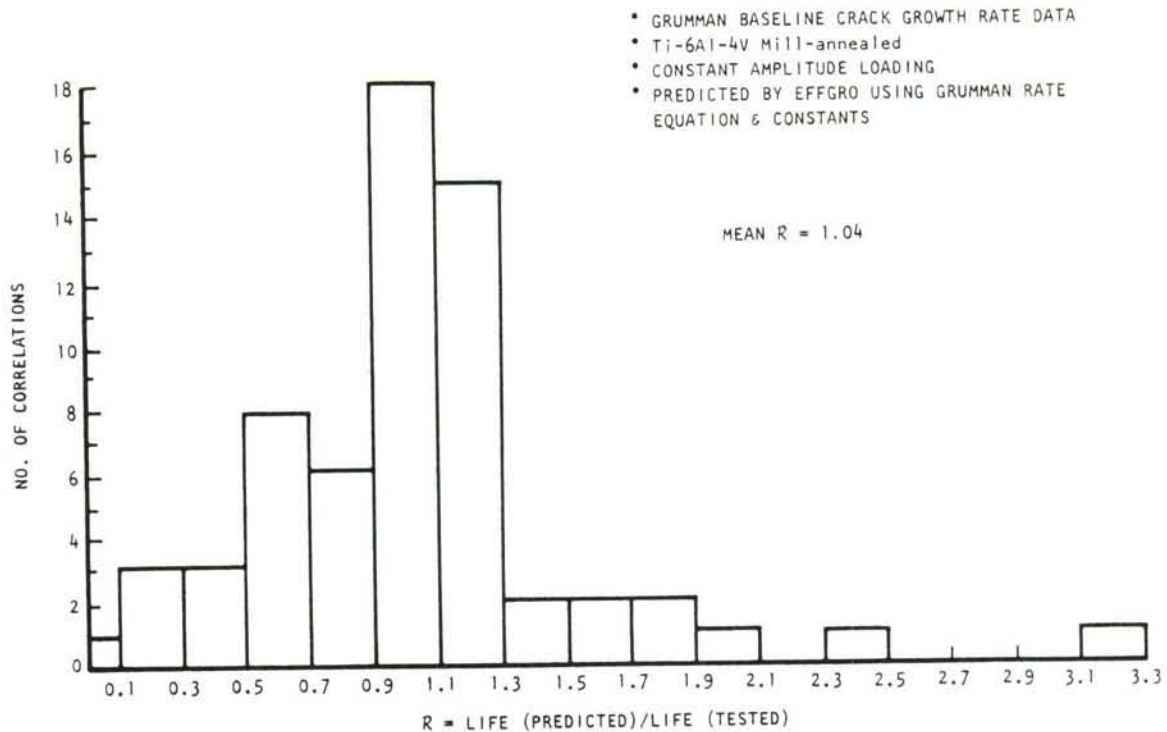
Figure 15. Histogram, crack-growth correlation on Grumman Ti-6Al-4V mill-annealed baseline data.
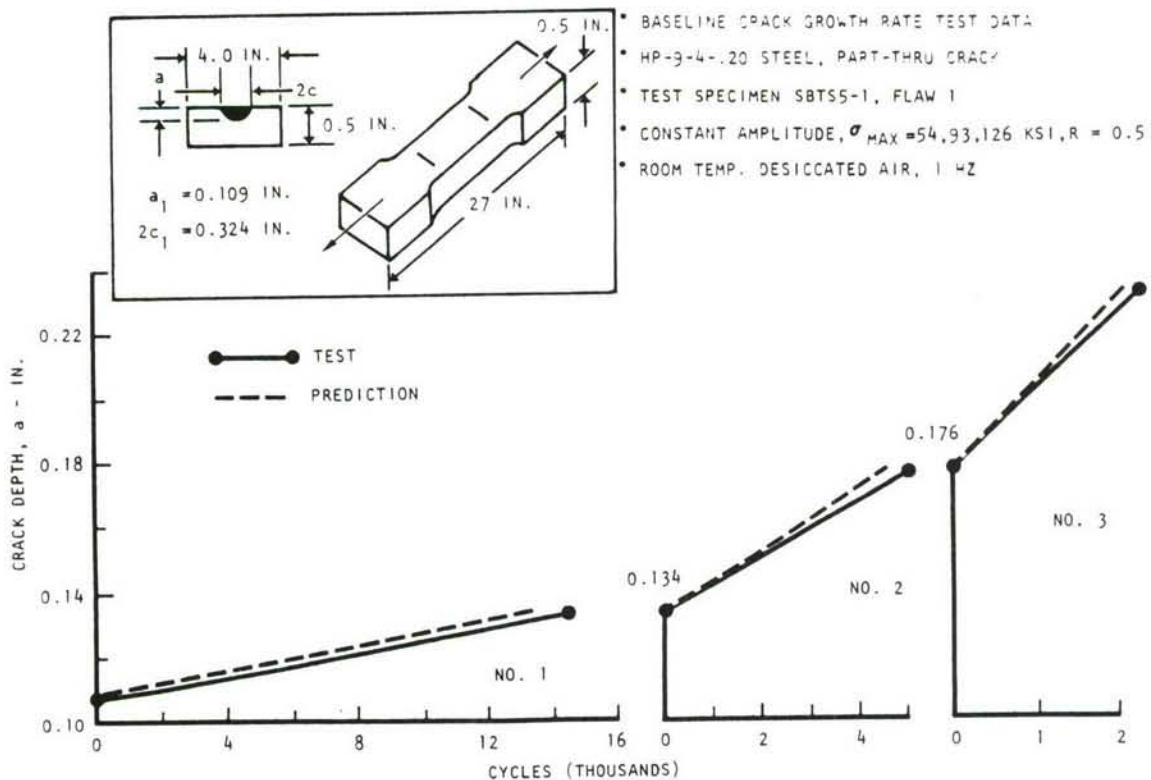
Figure 16. Boeing HP-9-4-.20 steel baseline crack growth rate data correlation, specimen SBTS5-1, flaw 1.

118
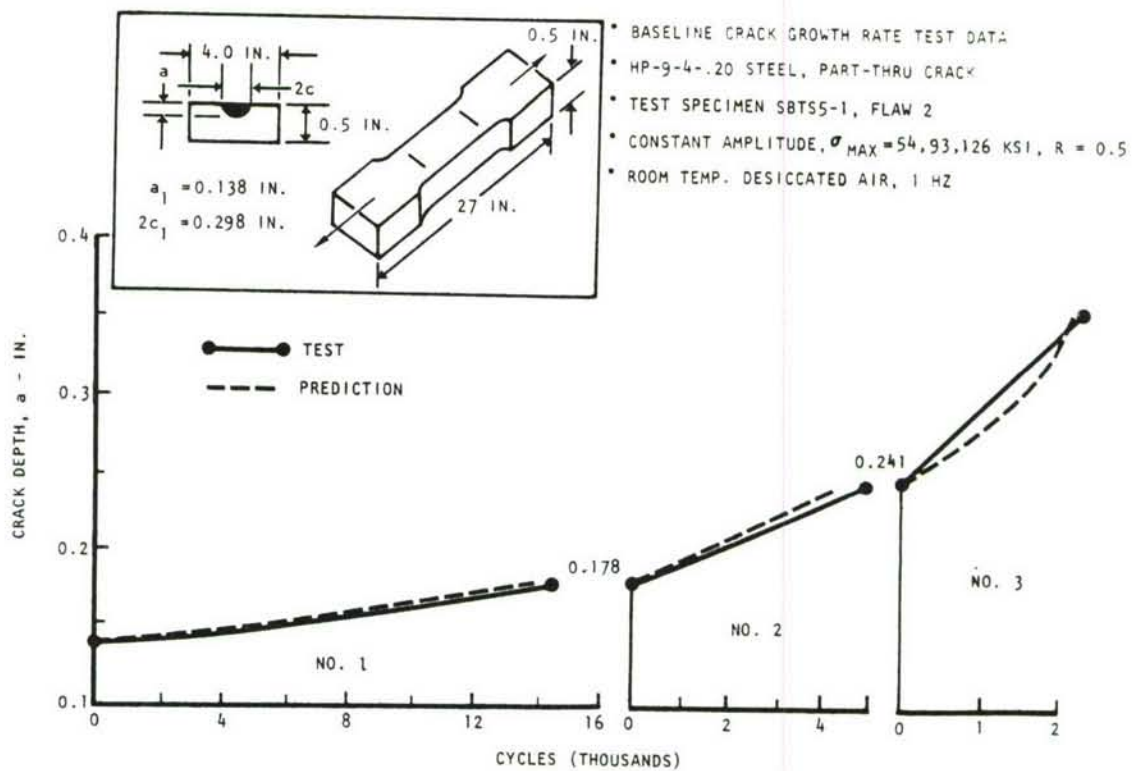
Figure 17. Boeing HP-9-4-.20 steel baseline crack growth rate data correlation, specimen SBTS5-1, flaw 2.
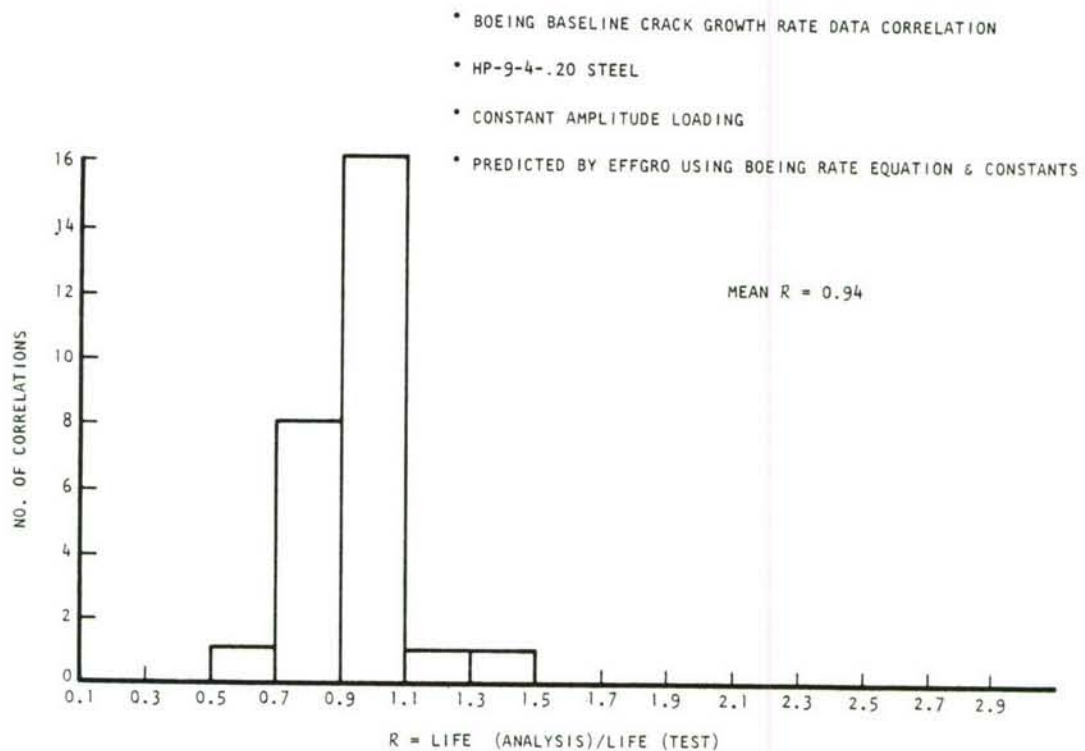
Figure 18. Histogram, crack-growth correlation on Boeing HP-9-4-.20 steel baseline data.

119
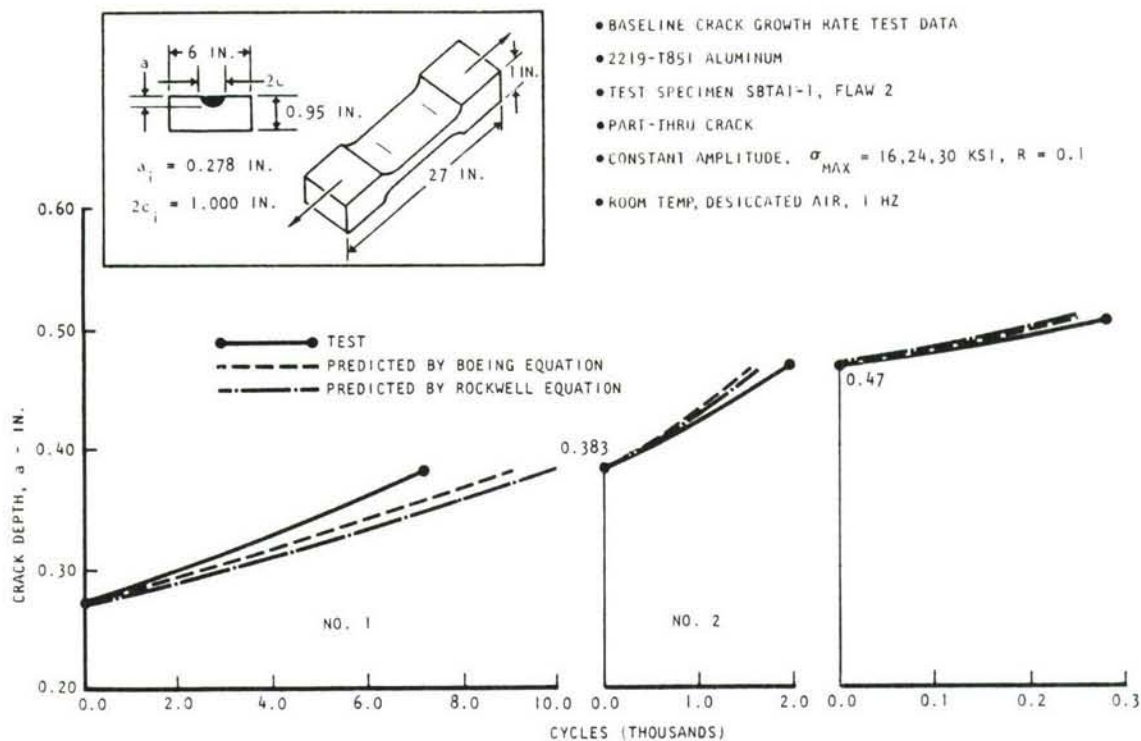
Figure 19. Boeing 2219-T851 aluminum baseline crack growth rate data
cross-correlation, specimen SBTA1-1, flaw 2.
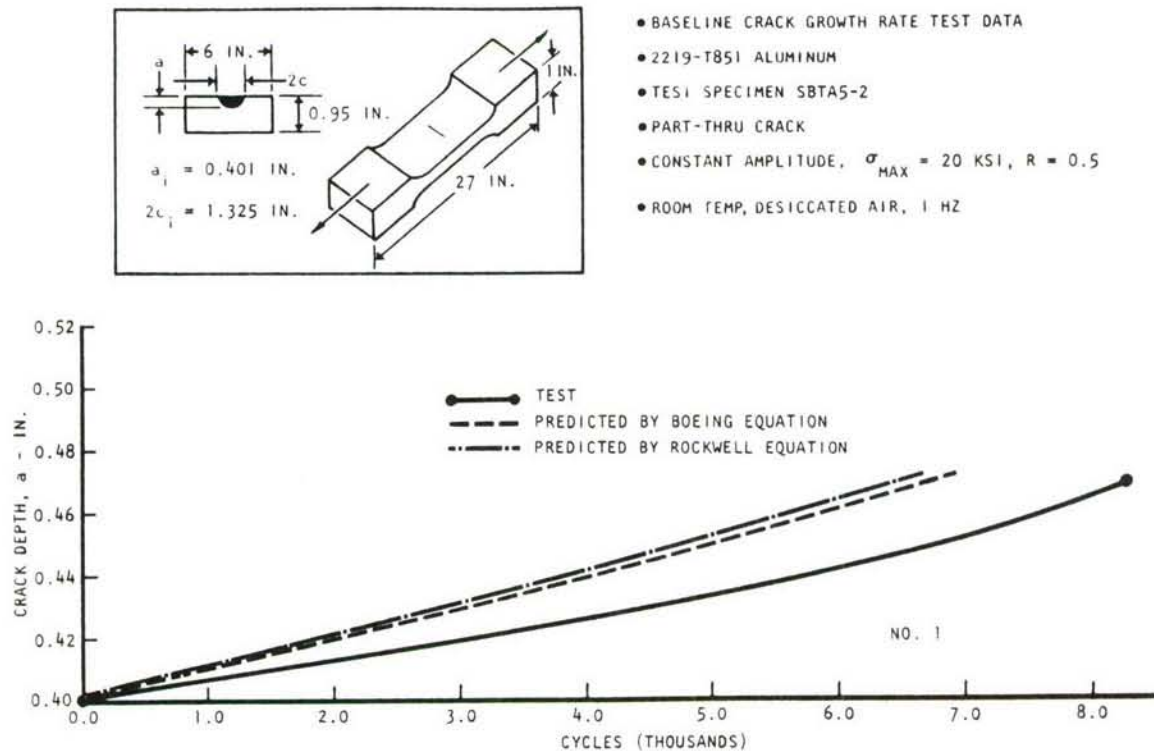
Figure 20. Boeing 2219-T851 aluminum baseline crack growth rate data
cross-correlation, specimen SBTA5-2.

* Boeing baseline crack growth rate data
* 2219-T851 aluminum
* Constant-amplitude loading
* Predicted by EFFGRO using rate equation & constants
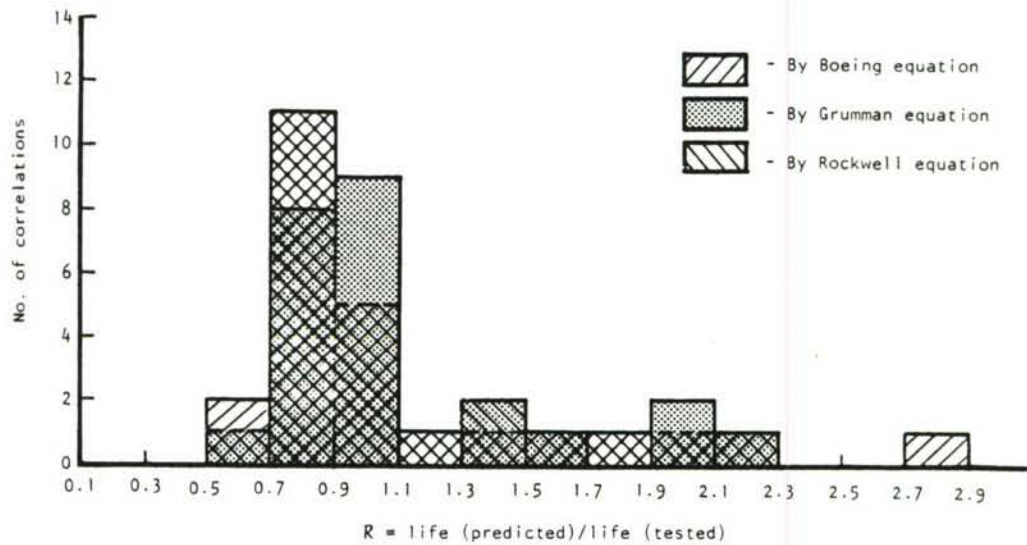
Figure 21.   Histogram, cross-correlation on Boeing 2219-T851 aluminum baseline crack growth rate data.
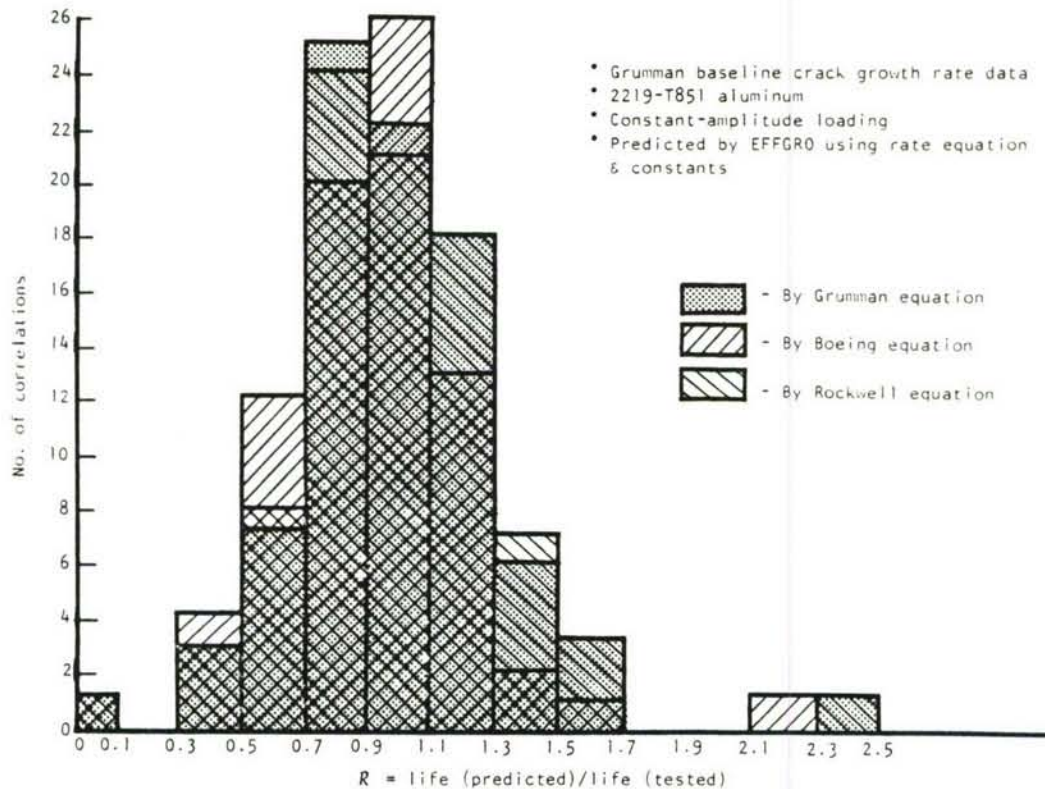
Figure 22.   Histogram, cross-correlation on Grumman 2219-T851 aluminum baseline crack growth rate data.

121
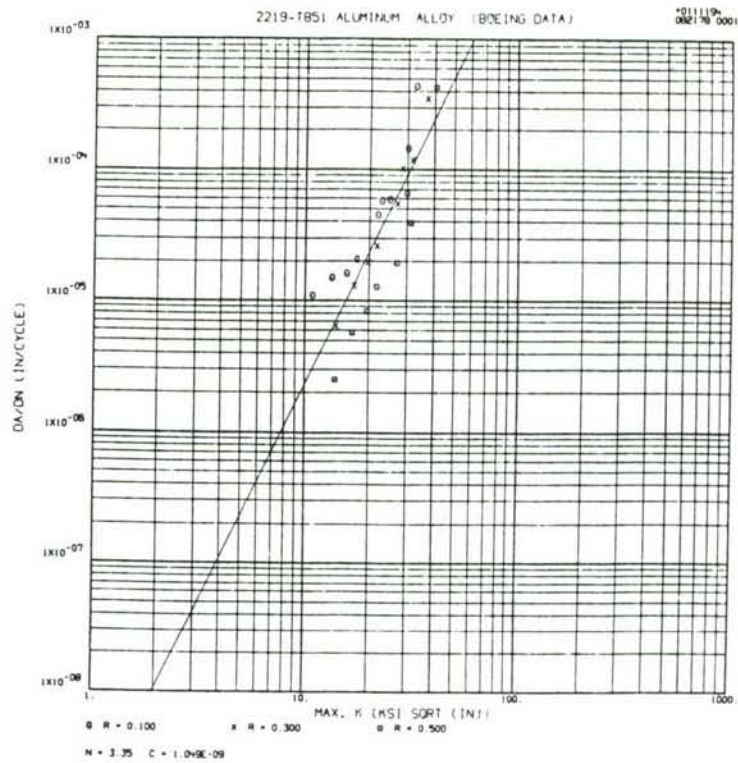
Figure 23. Original Boeing 2219-T851 aluminum baseline
crack growth rate data.
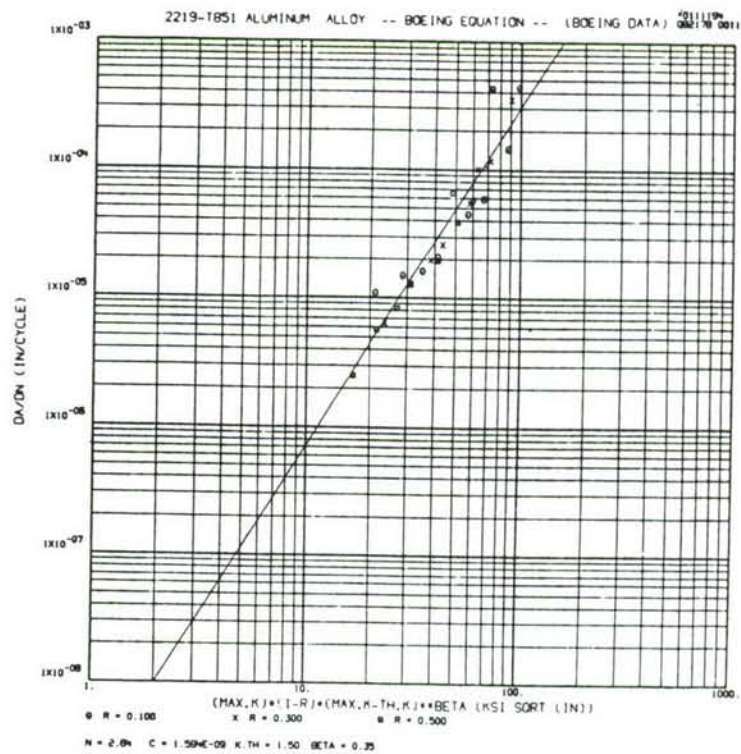
Figure 24. Boeing 2219-T851 aluminum baseline crack growth rate
data plotted in da/dN versus $(1-R)$ $(K_{max}-K_{th})^{\beta} K_{max}$ format.

122
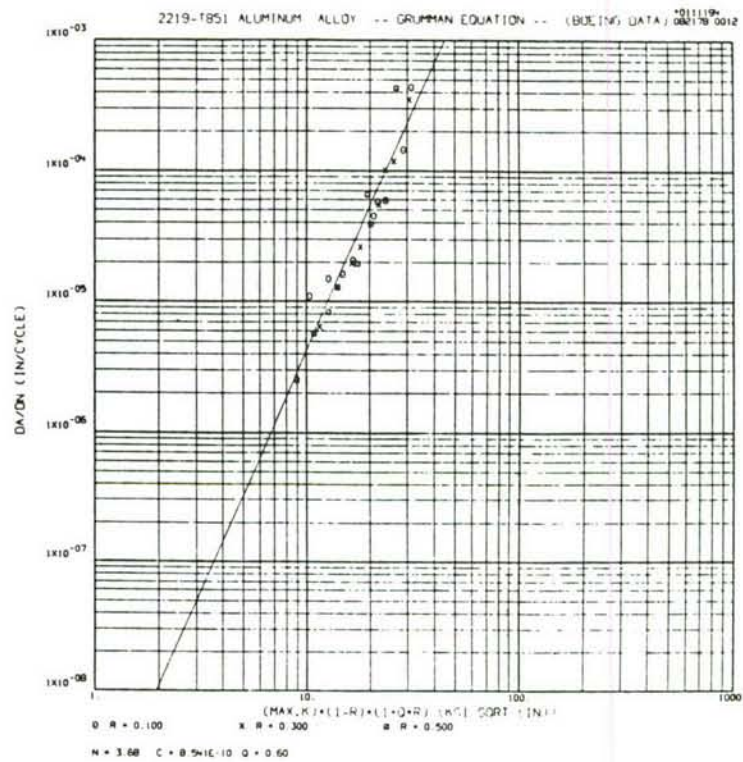
Figure 25. Boeing 2219-T851 aluminum baseline crack growth rate data plotted in da/dN versus $(1-R) (1+qR) K_{max}$ format.
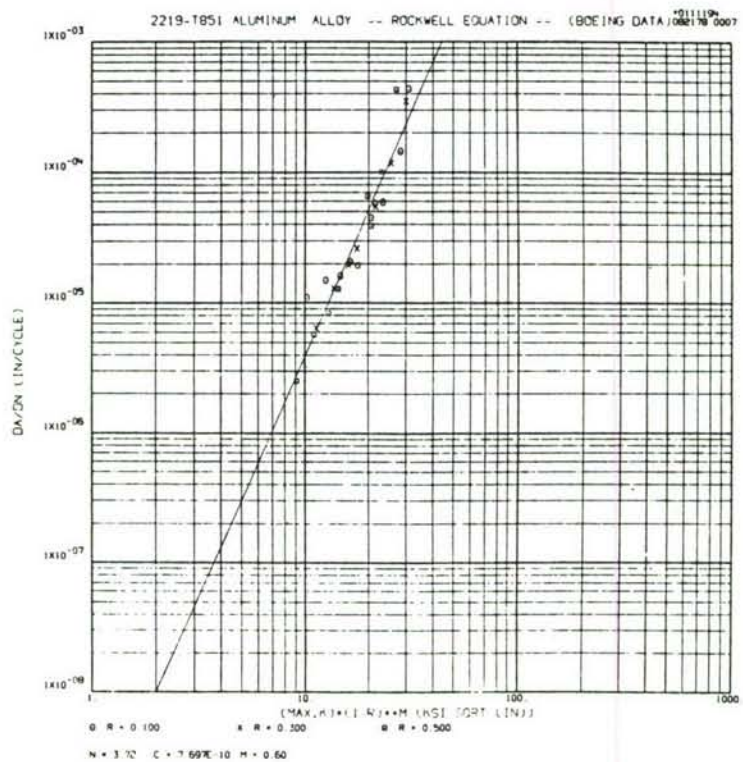
Figure 26. Boeing 2219-T851 aluminum baseline crack growth rate data plotted in da/dN versus $(1-R)^m K_{max}$ format.
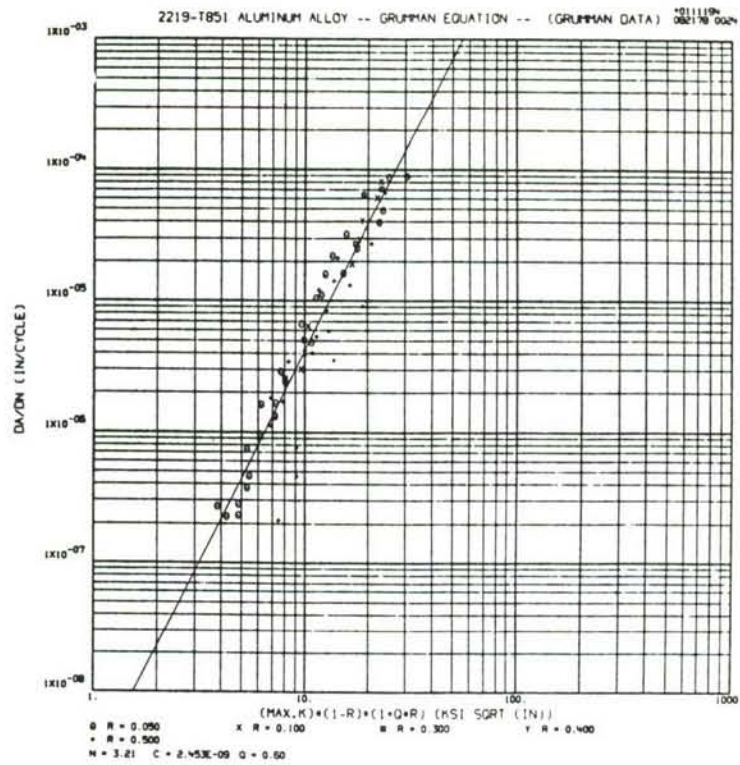
Figure 27. Grumman 2219-T851 aluminum baseline crack growth rate data plotted in da/dN versus $(1-R)$ $(1+qR)$ K_{max} format.
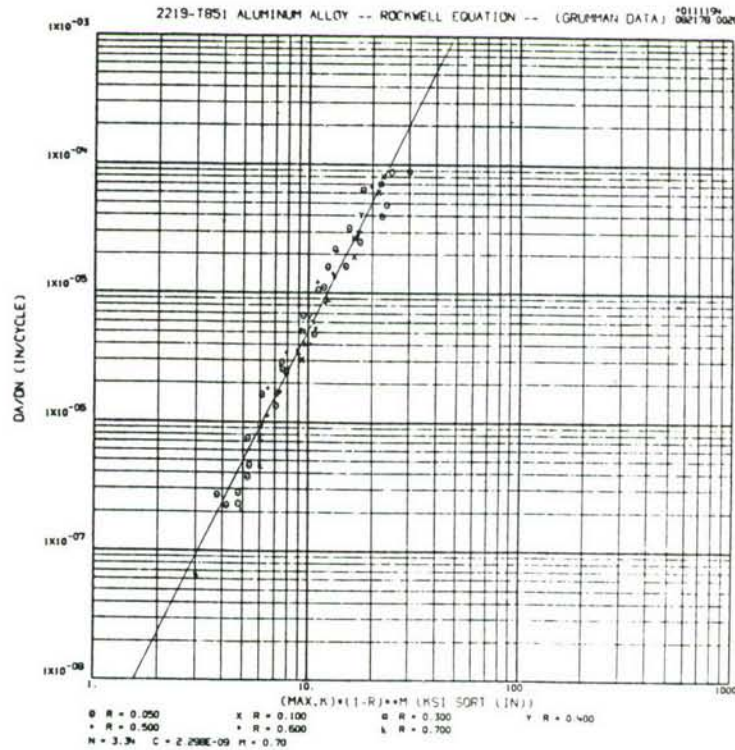
Figure 28. Grumman 2219-T851 aluminum baseline crack growth rate data plotted in da/dN versus $(1-R)^m$ K_{max} format.
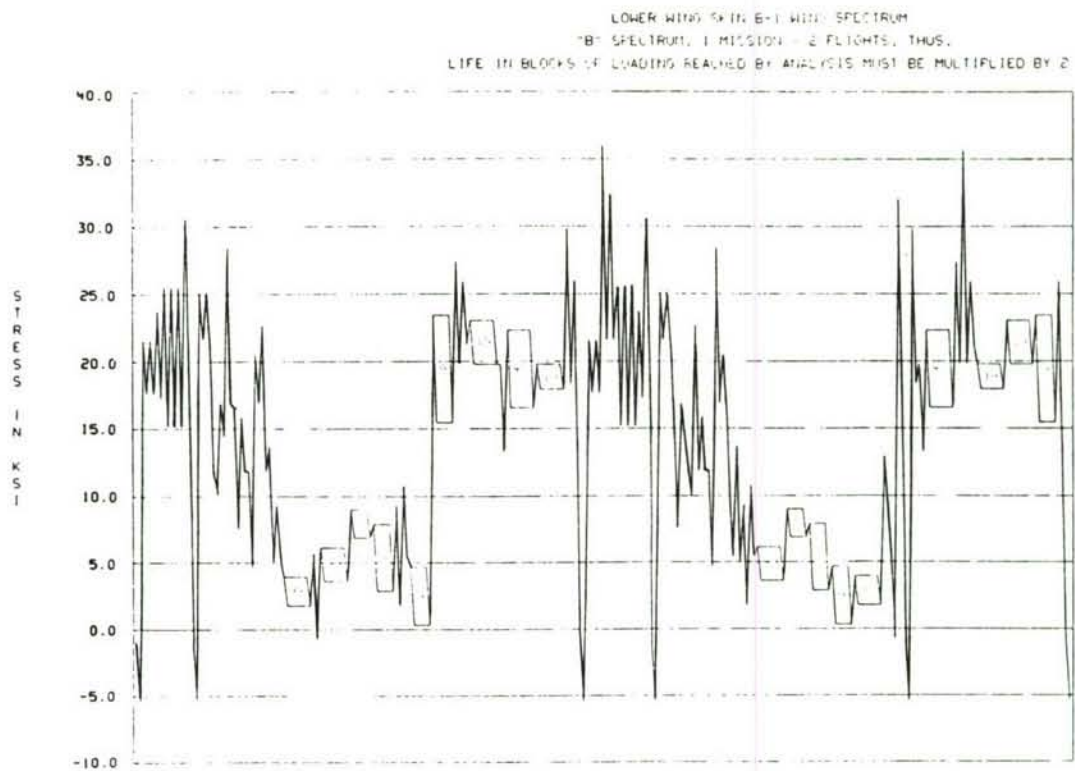
Figure 29.   Flight-by-flight B-1 wing "B" spectrum.
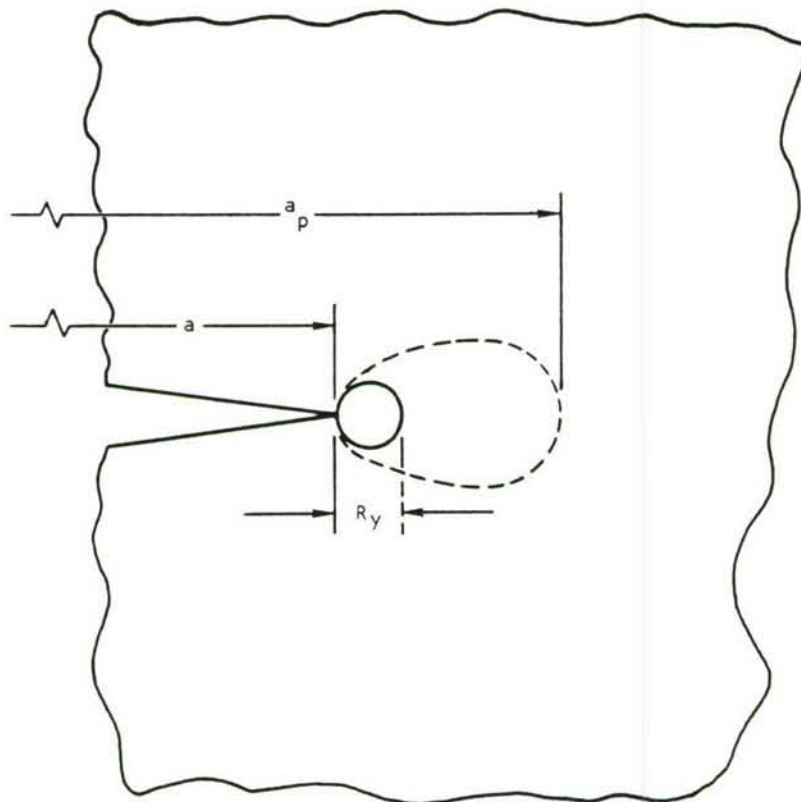
Figure 30.   Wheeler retardation model.
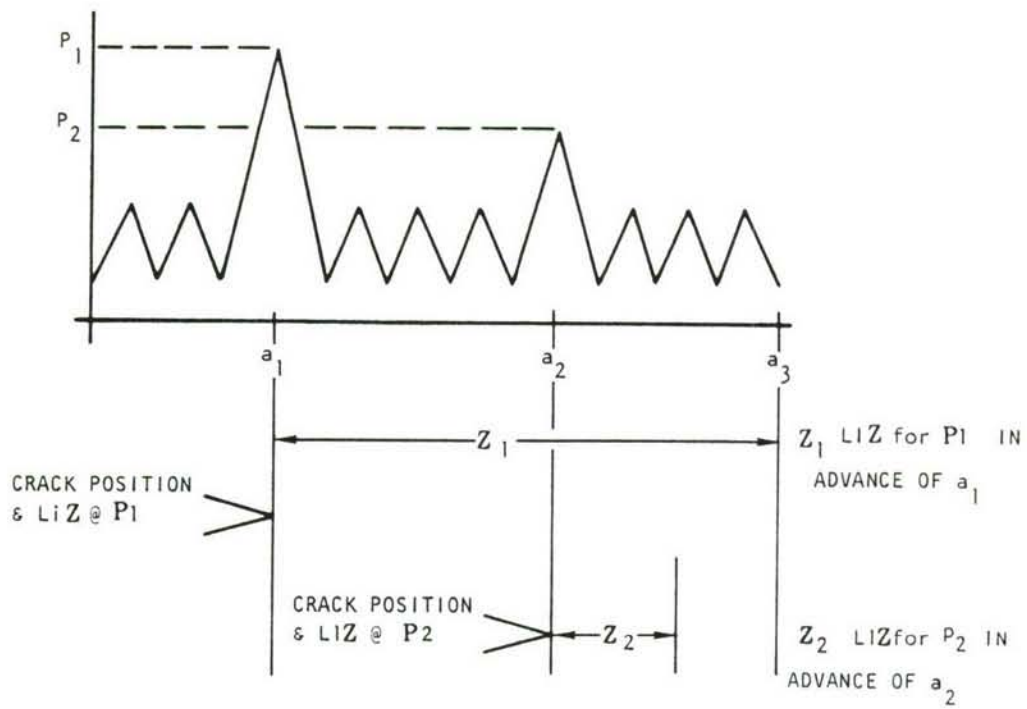
Figure 31. Schematic illustration of the load interaction zone (LIZ) concept.
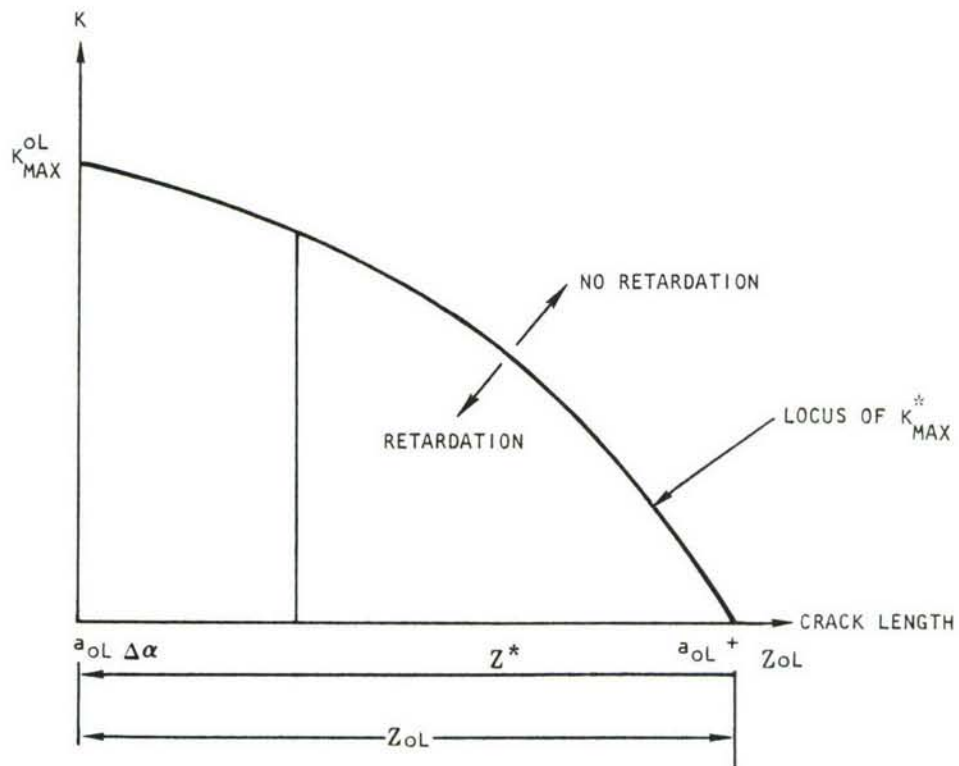
Figure 32. K^*_{MAX} required for coincident load interaction zone (LIZ) boundaries.
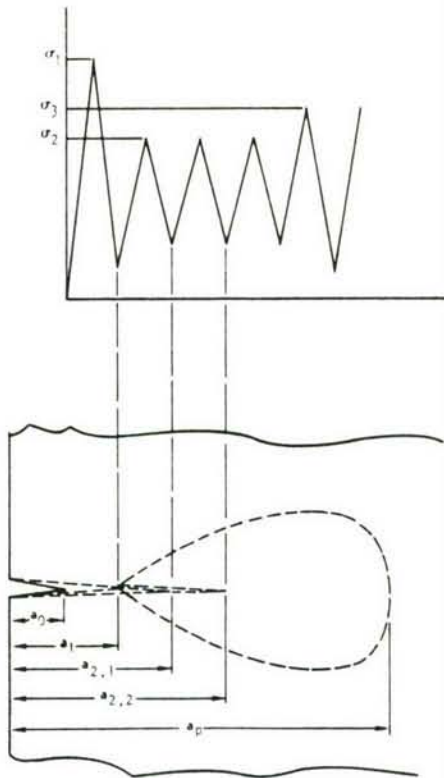
Figure 33.   Spectrum and yield zones.

$$\delta_{K_{MAX}} = \delta_{\sigma_{MAX}} + \delta_{\sigma_o}$$
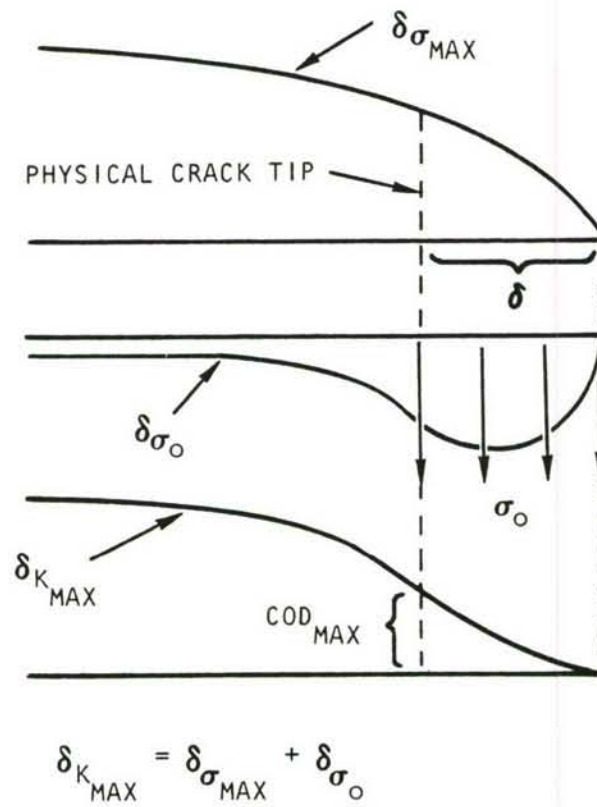
Figure 34.   Elastic crack surface displacement at maximum load.

127
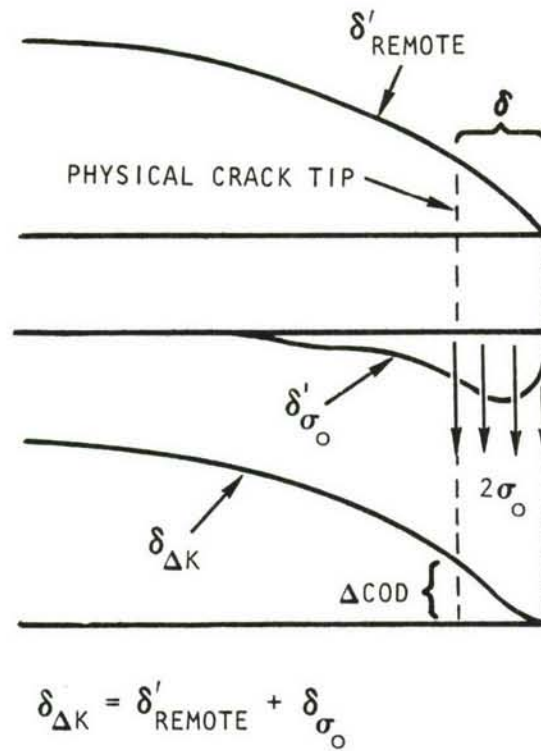
Figure 35. Elastic crack surface displacements during unloading.
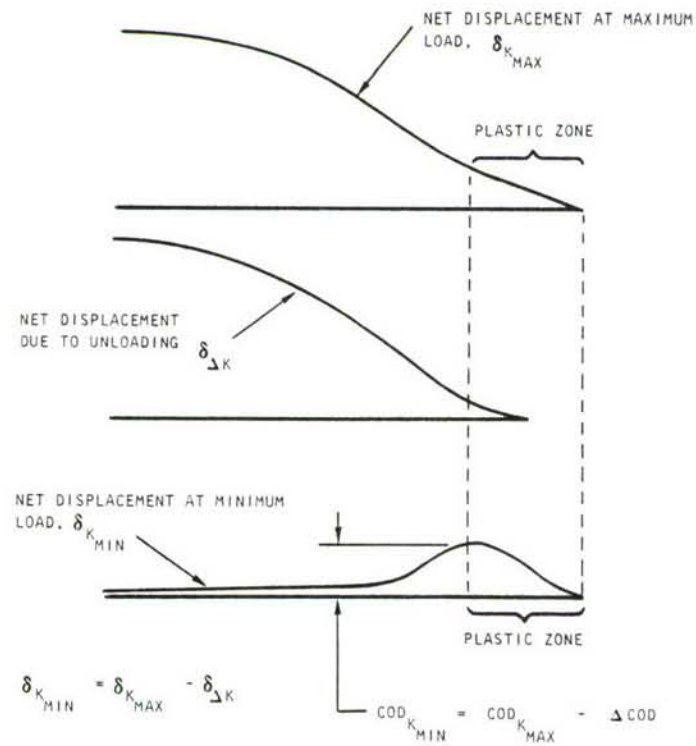
Figure 36. Elastic crack surface displacement at minimum load.
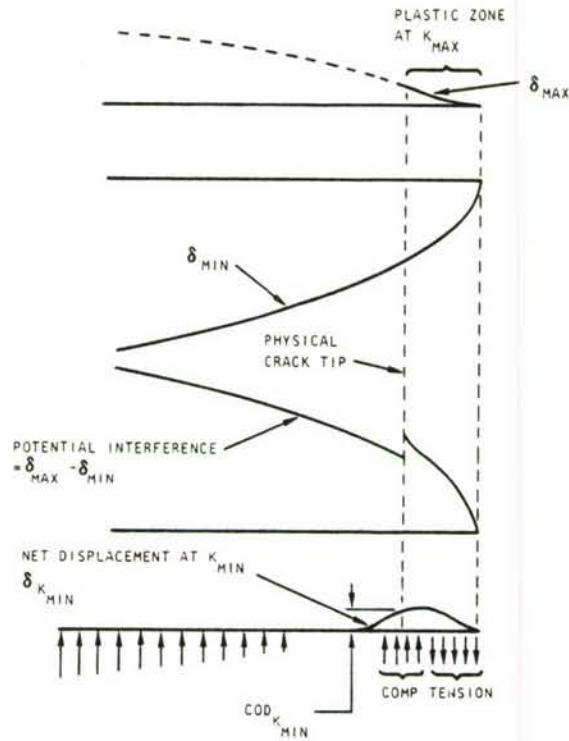
Figure 37. Computation of crack surface displacements under compression load.
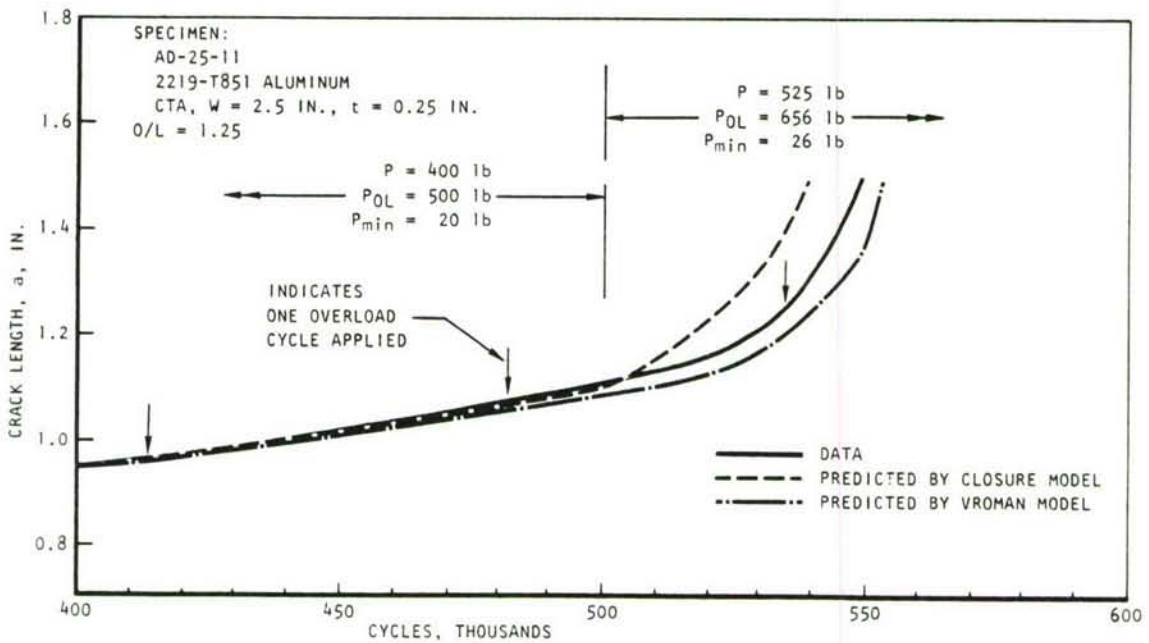
Figure 38. Predicted a versus N for O/L = 1.25, single overload, 2219-T851 aluminum.
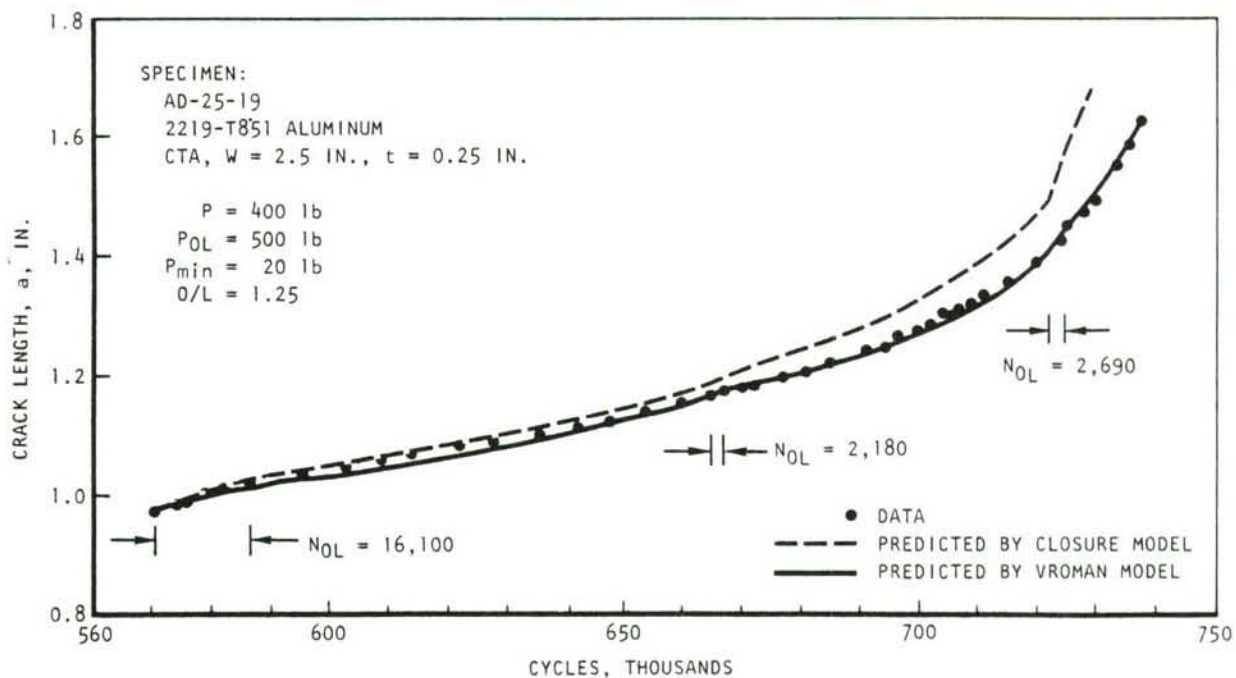
Figure 39.   Predicted a versus N for O/L = 1.25, multiple overloads, 2219-T851 aluminum.
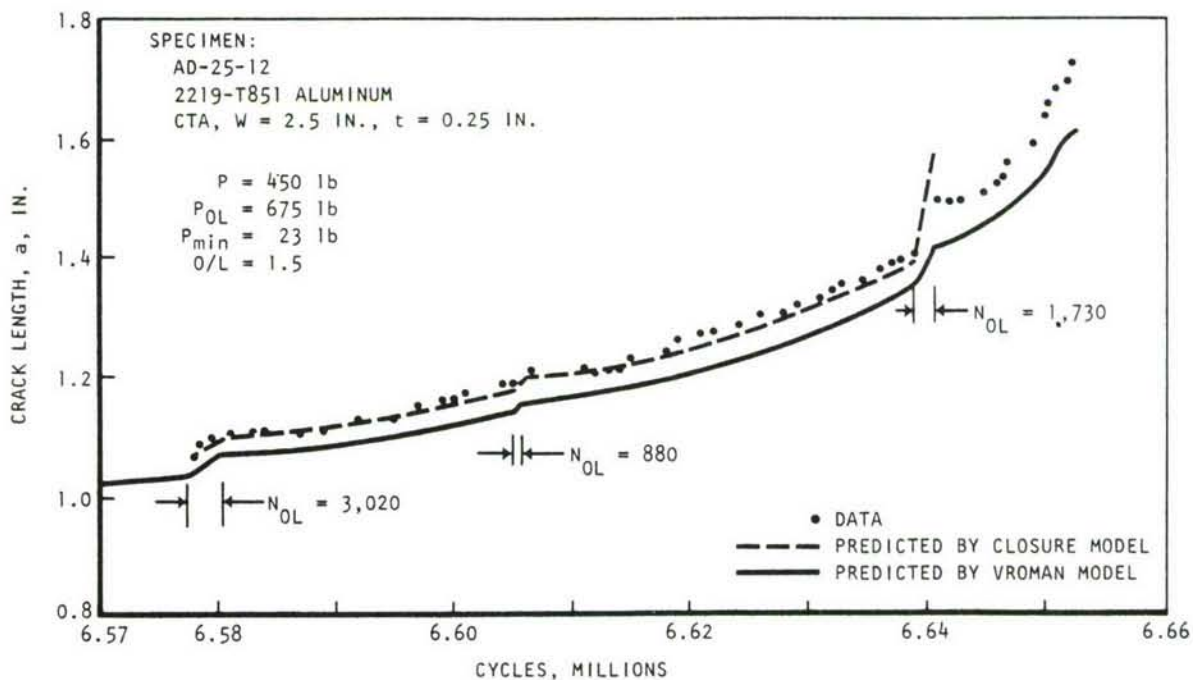
Figure 40.   Predicted a versus N for O/L = 1.5, multiple overloads, 2219-T851 aluminum.
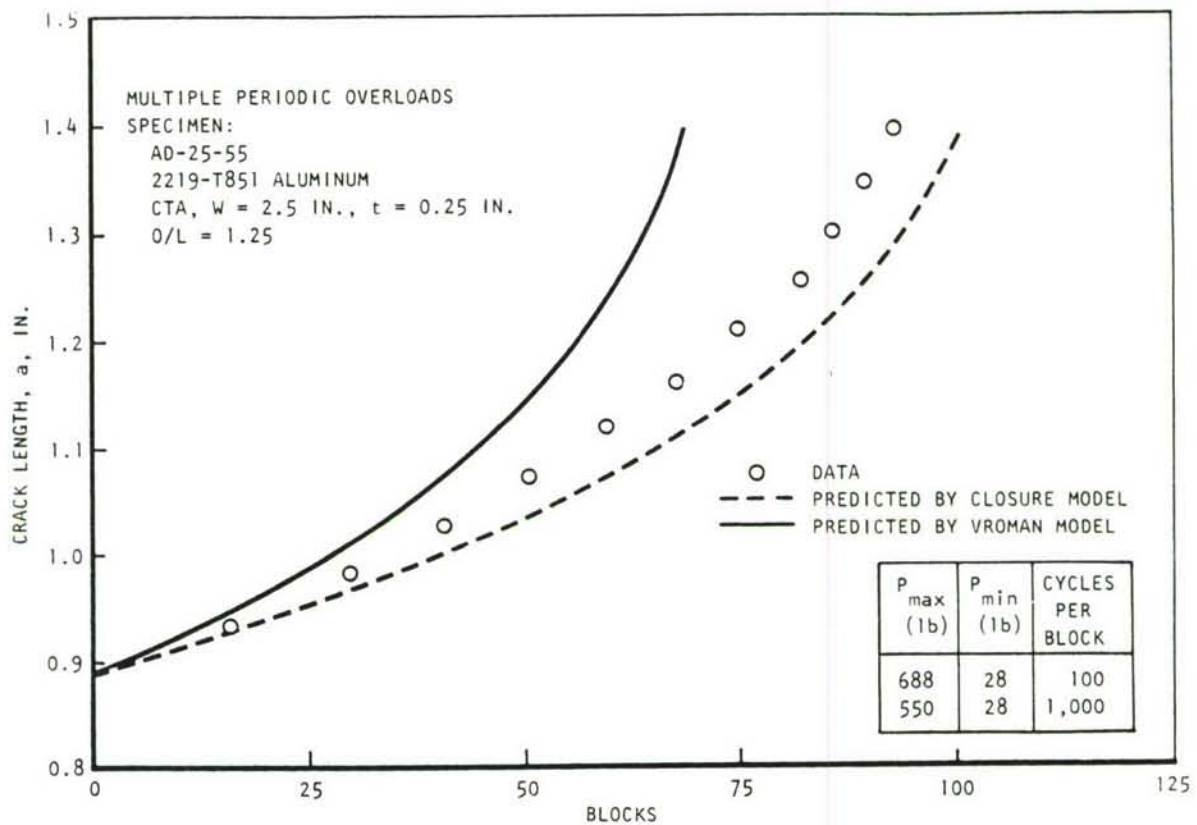
Figure 41. Predicted a versus B for O/L = 1.25 and $N_{OL}/N = 100/1000$, 2219-T851 aluminum.
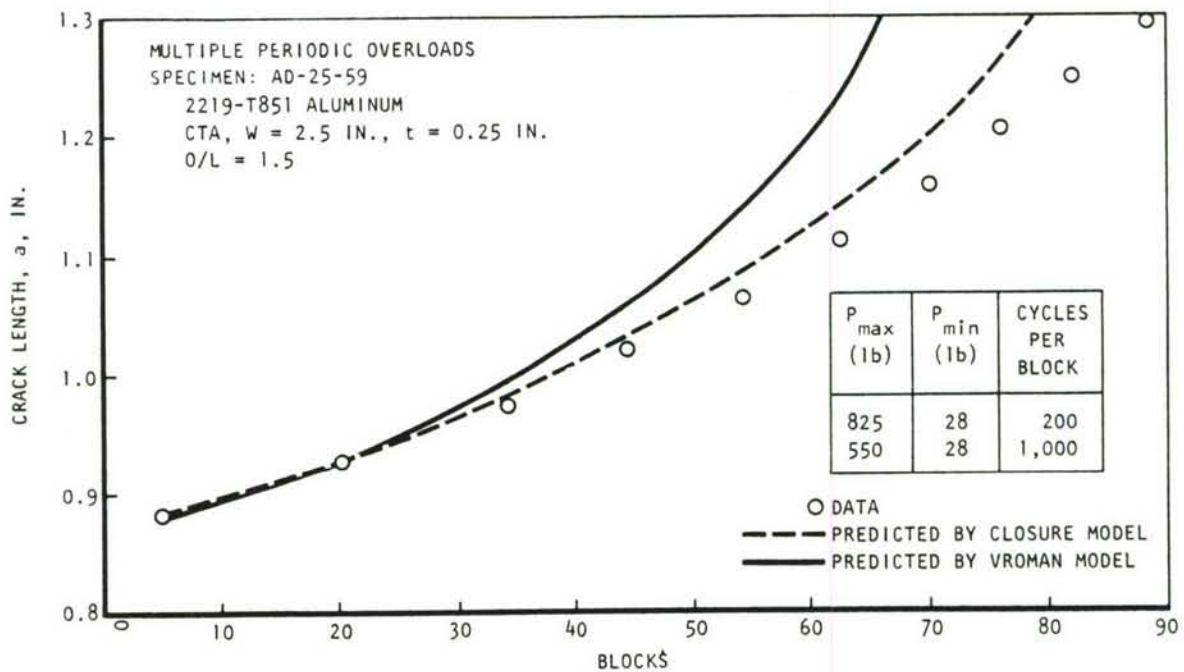
Figure 42. Predicted a versus B for O/L = 1.5 and $N_{OL}/N = 200/1000$, multiple periodic overloads, 2219-T851 aluminum.
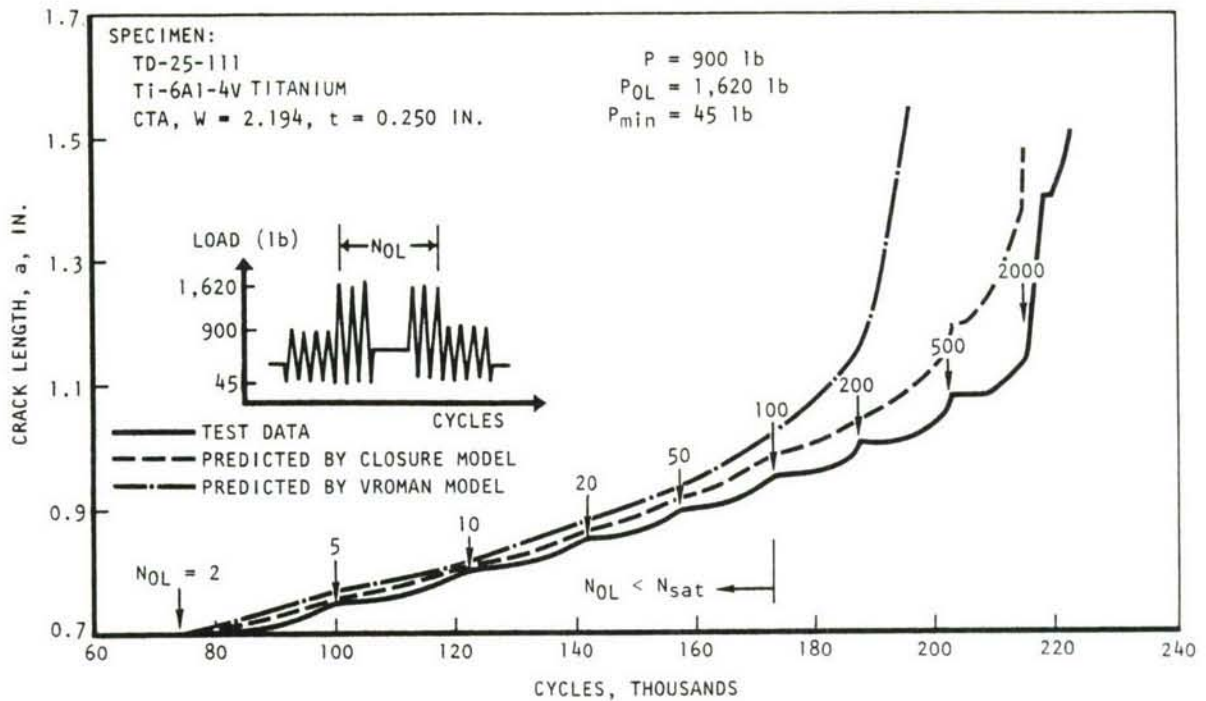
Figure 43.   Predicted a versus N for O/L = 1.8 and $N_{OL} < N_{sat}$,
Ti-6Al-4V titanium.
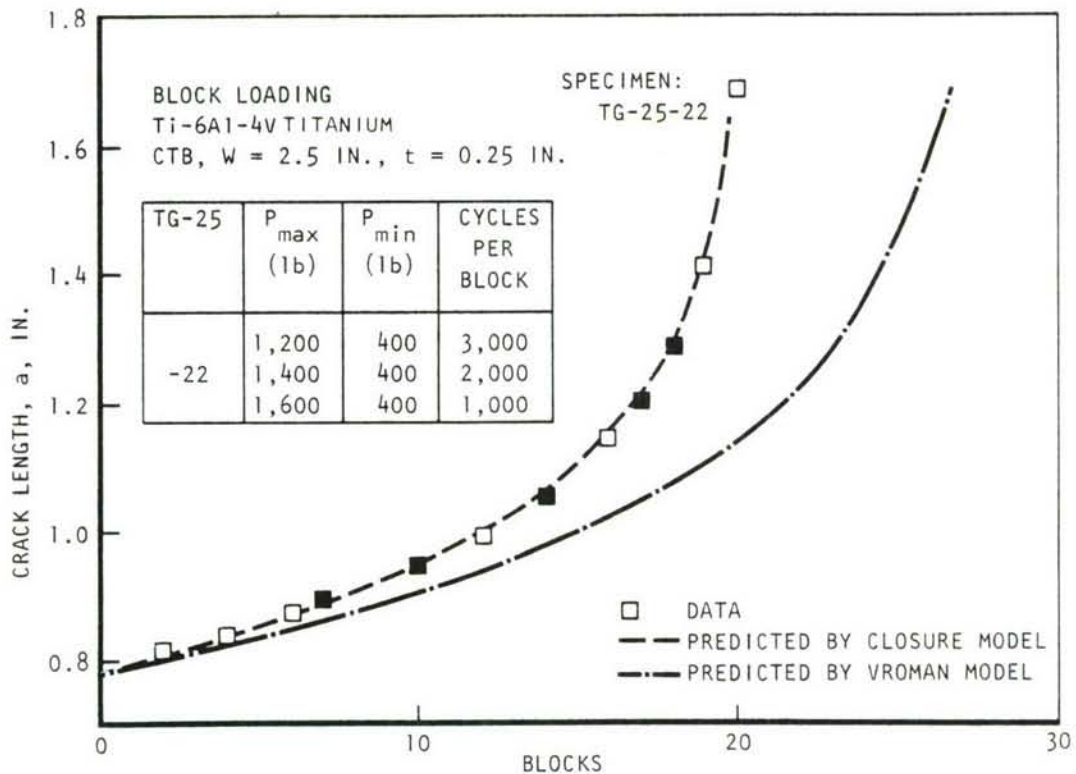
Figure 44.   Predicted a versus B for high-low and low-high block loading,
R_{min} = 0.333, Ti-6Al-4V titanium.

TEST 588, SPECIMEN 66-61
SURFACE FLAW - DEEP - $a/2c_i$ = 1/2
HP-9-4-20 STEEL PLATE
FLIGHT-BY-FLIGHT HORIZONTAL TAIL SPECTRUM (HS)
MAX SPECTRUM STRESS = 125 KSI TENS., -50 KSI COMP
DRY-AIR ENVIRONMENT
TEST LIFE 1,332 MISSIONS

●─────● TEST DATA
────── PREDICTED BY VROMAN/CHANG MODEL

a_i = 0.06
$a/2c_i$ = 1/2
C_{CR} = 0.90

0.500
4
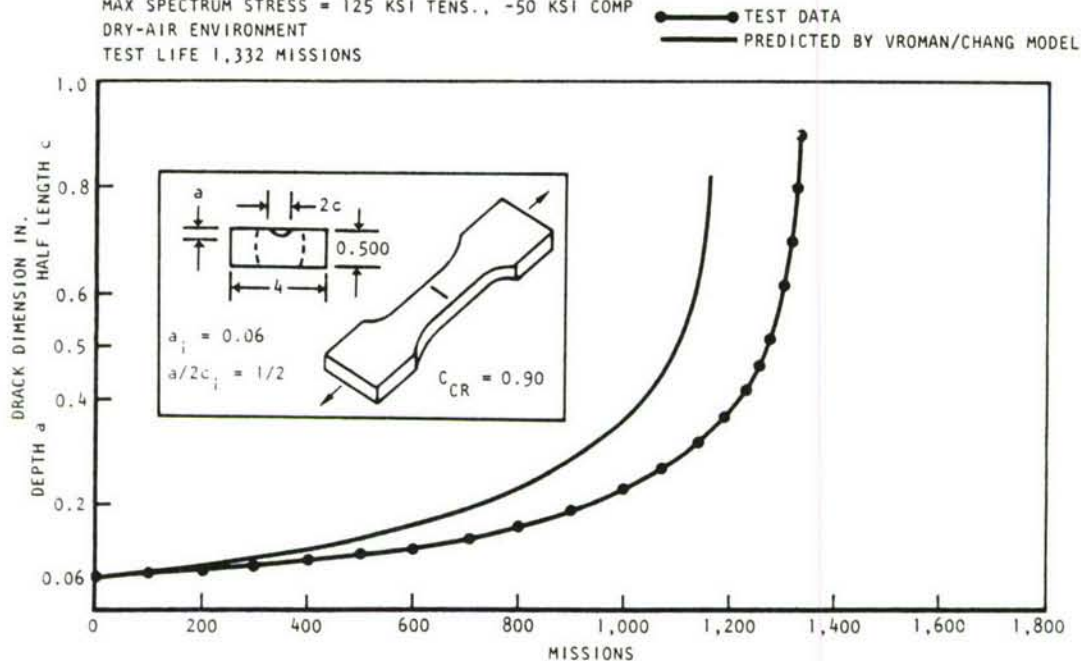
Figure 45.   Predicted a versus N, flight-by-flight tail spectrum
σ_{max} = 125 ksi, σ_{min} = -50 ksi, HP-9-4-20 steel.

TEST 599, SPECIMEN 66-62
SURFACE FLAW-DEEP - $a/2c_i$ = 1/2
HP-9-4-20 STEEL PLATE
FLIGHT-BY-FLIGHT HORIZONTAL TAIL SPECTRUM (HS)
MAX SPECTRUM STRESS = 150 KSI TENS., -60 KSI COMP
DRY-AIR ENVIRONMENT
TEST LIFE 800 MISSIONS

●─────● TEST DATA
────── PREDICTED BY VROMAN/CHANG MODEL

a_i = 0.06
$a/2c_i$ = 1/2
C_{CR} = 0.68

0.500
4
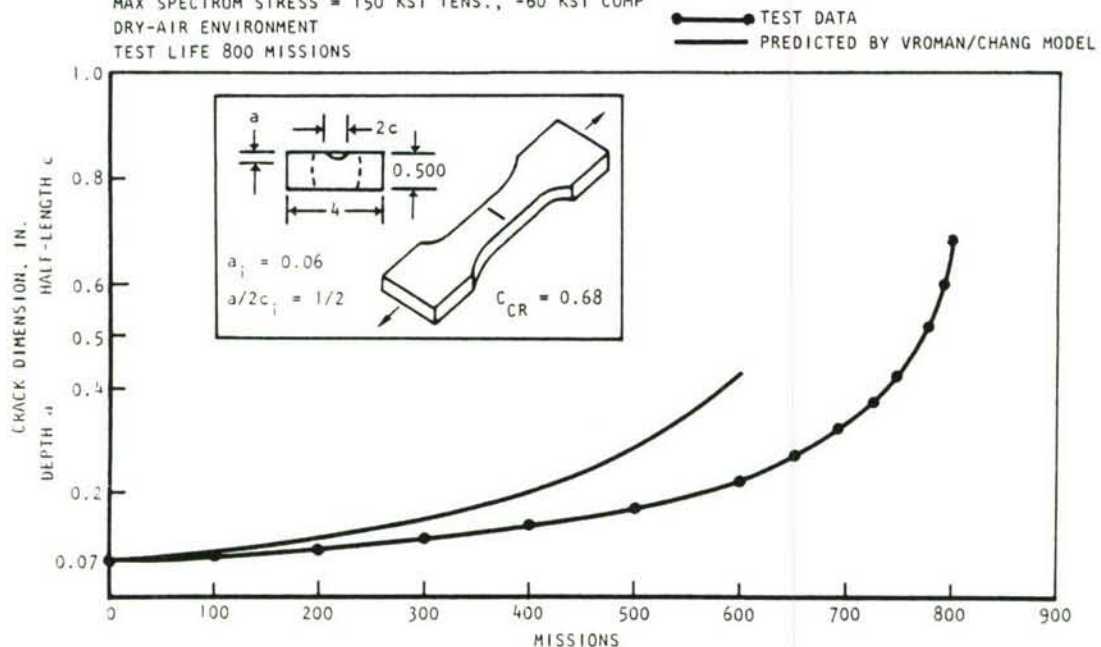
Figure 46.   Predicted a versus N, flight-by-flight tail spectrum
σ_{max} = 150 ksi, σ_{min} = -60 ksi, HP-9-4-20 steel.

133

$\sigma = 10,000$ psi

4.00 in.

←1.00→ 2.00 →←1.00→

4.00 in.
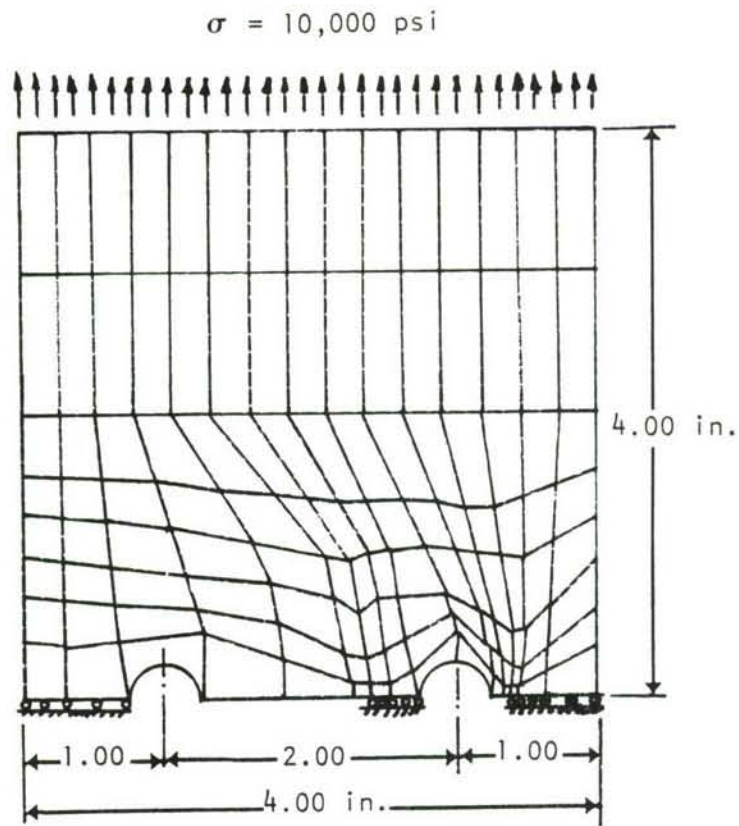
Figure 47. The finite-element model.
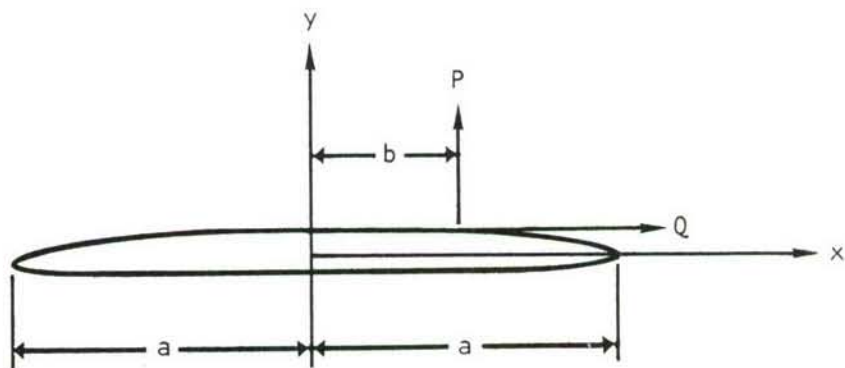
Figure 48. Concentrated force on crack surface.

134
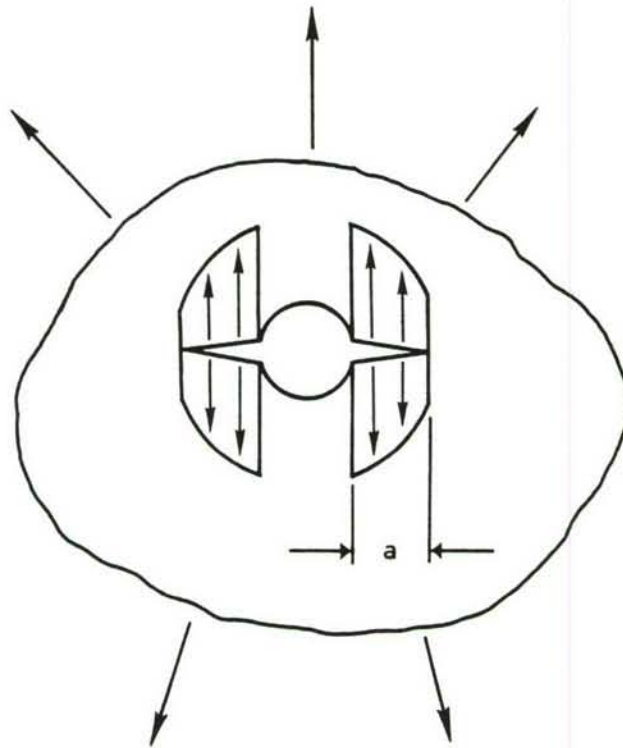
Figure 49. Distributed force on crack surface.

(A)   (B)   (C)
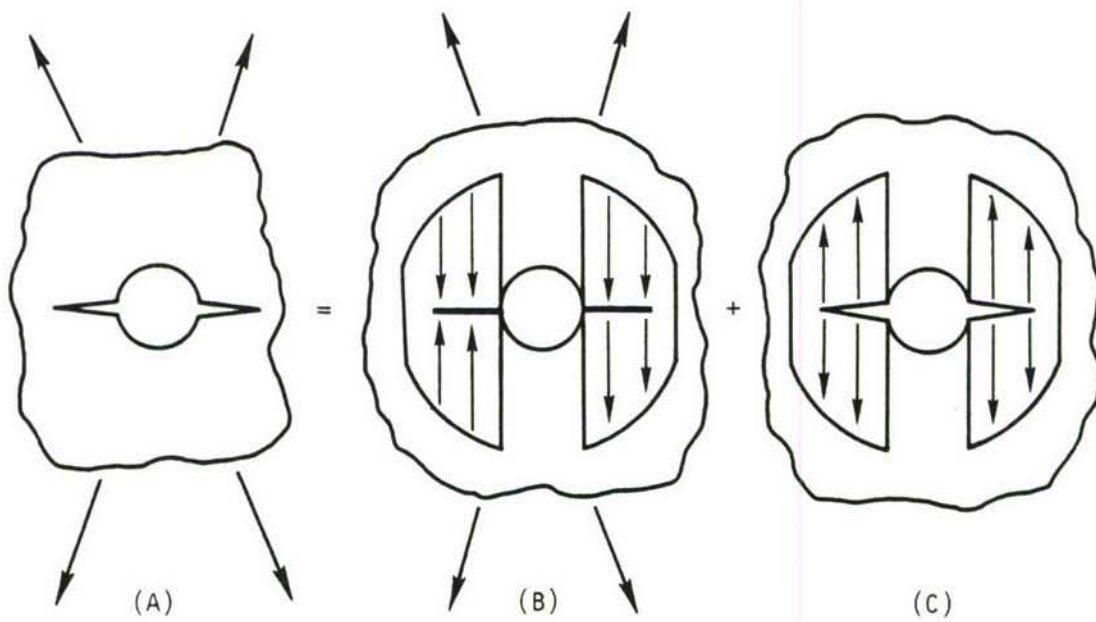
Figure 50. Schematic of linear superposition method.

135
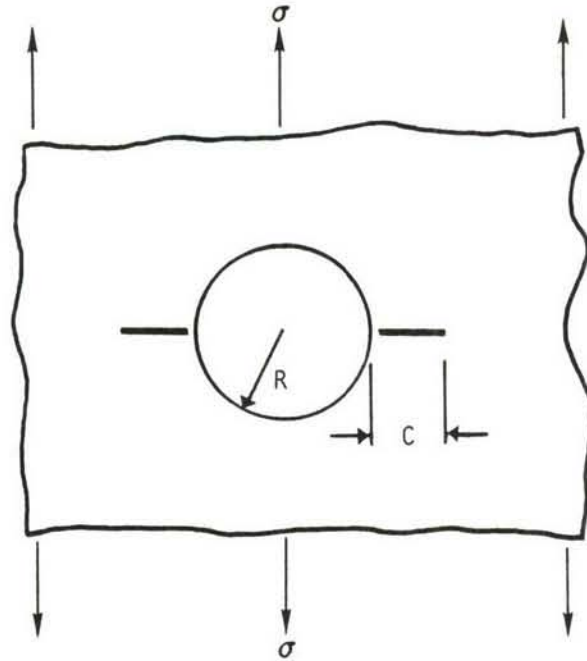
Figure 51.   A single crack emanating from an open hole
subjected to uniform tension.
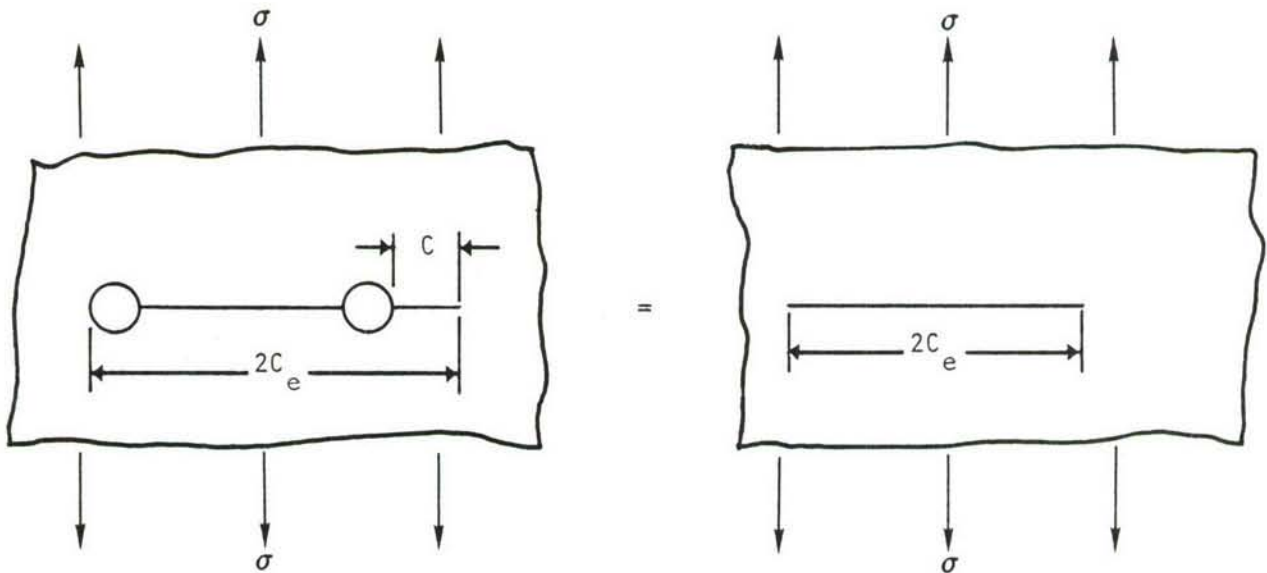
Figure 52.   Two approximately equivalent cases.

136
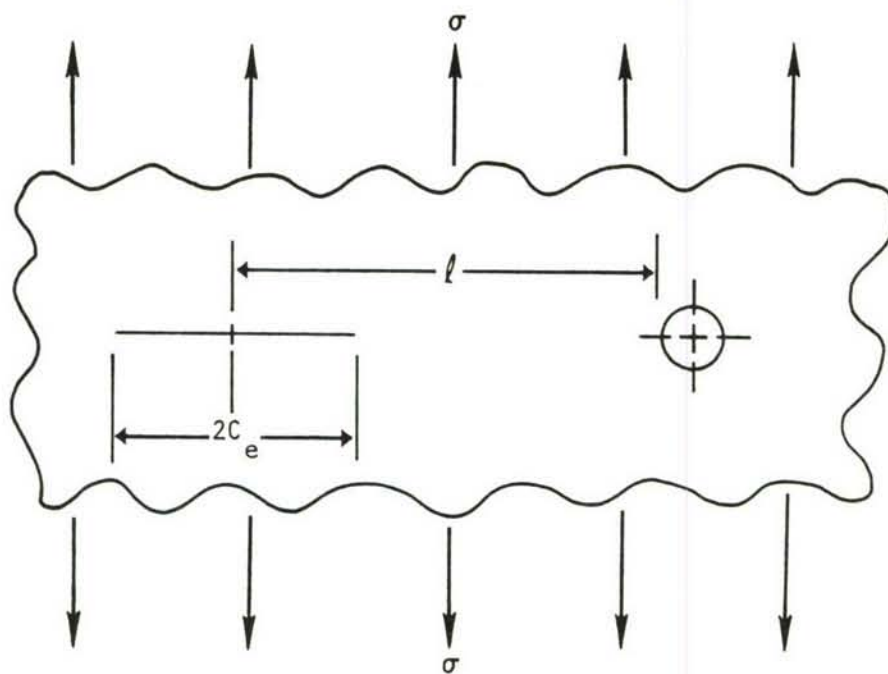
Figure 53.   Crack approaches a hole.
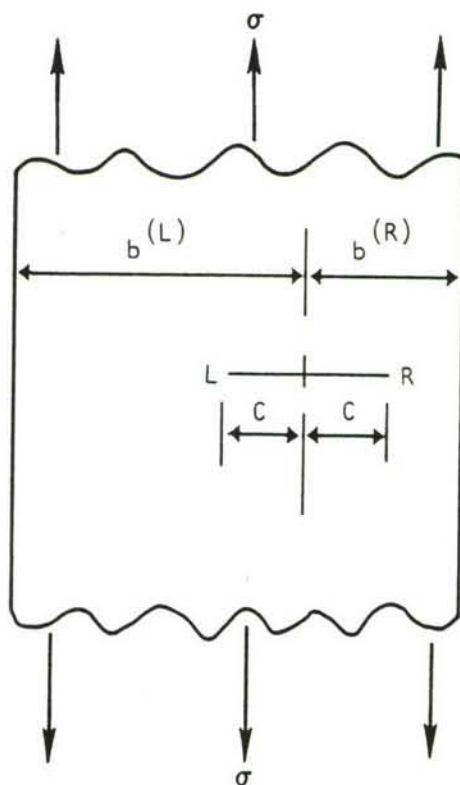
Figure 54.   Eccentrically located crack in a finite-width strip under uniform tension load.

137
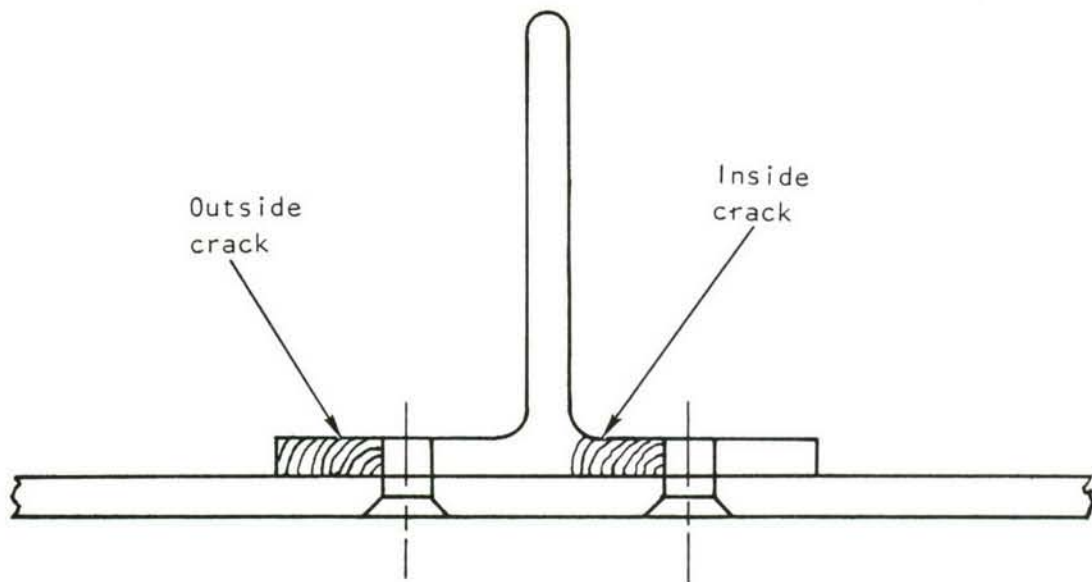
Figure 55.   Inside and outside cracks in the stringer.
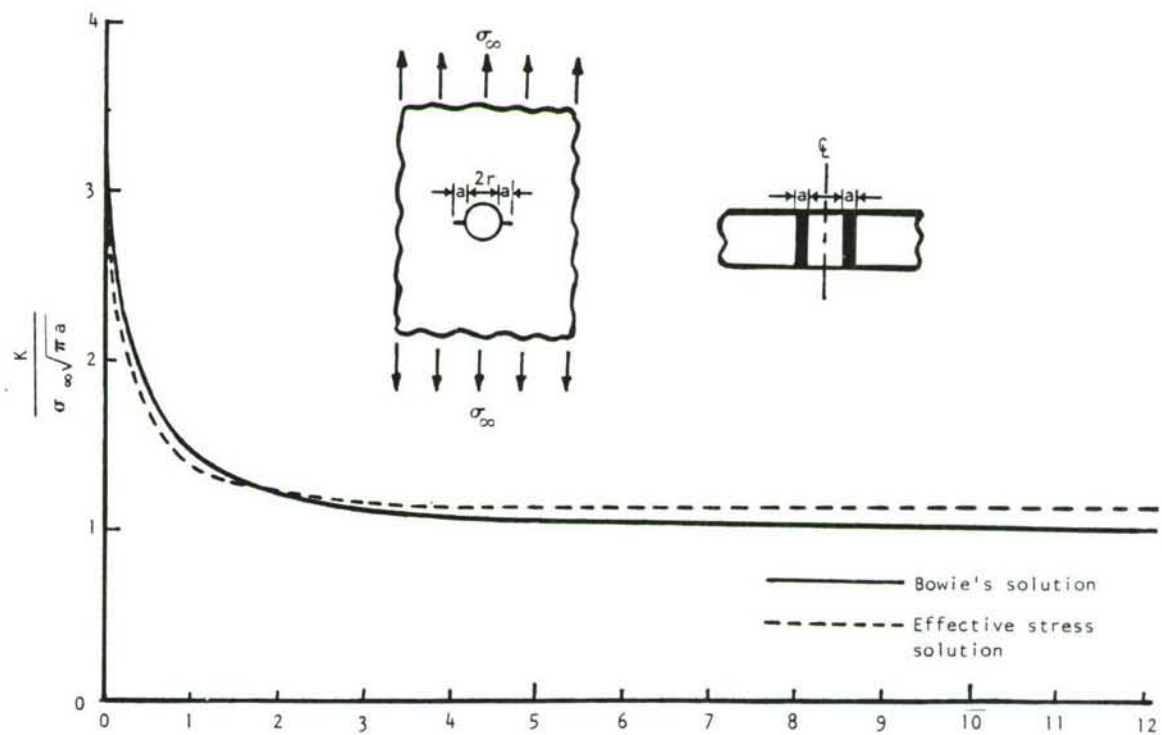
Figure 56.   Comparison of solutions, two-cracks emanating from an open hole contained in an infinite plate in tension.

138
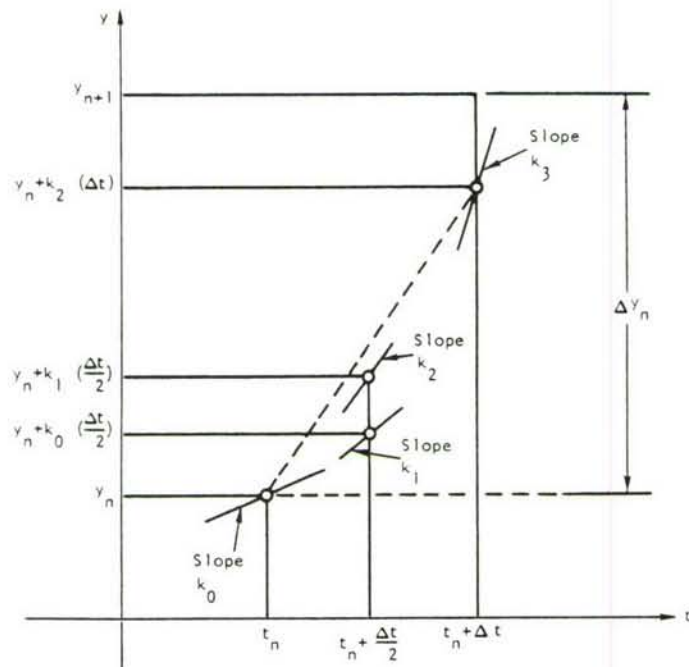
Figure 57. Four slopes used in Runge-Kutta method.
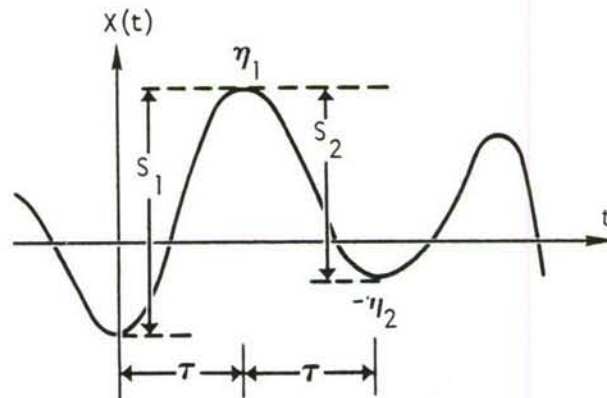
Figure 58. Definition of rise S_1 and fall S_2.

139
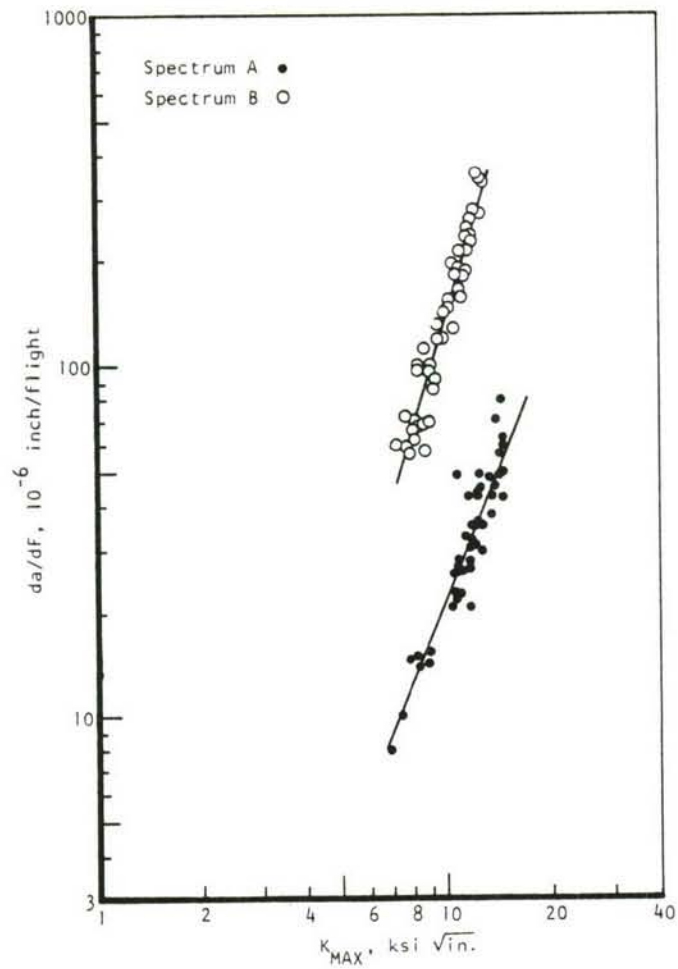
Figure 59. Crack growth rate behavior of spectra A and B.
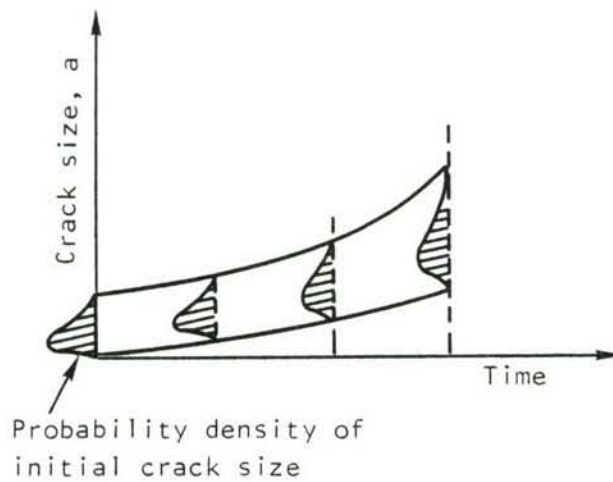
Figure 60. Probability density function of crack size in service.
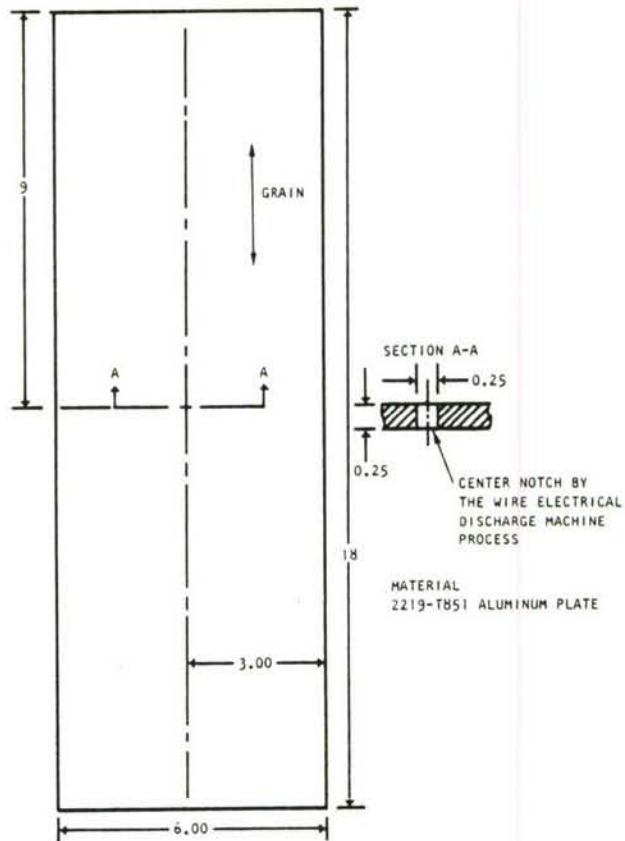
Figure 61.   Test Specimen Configuration
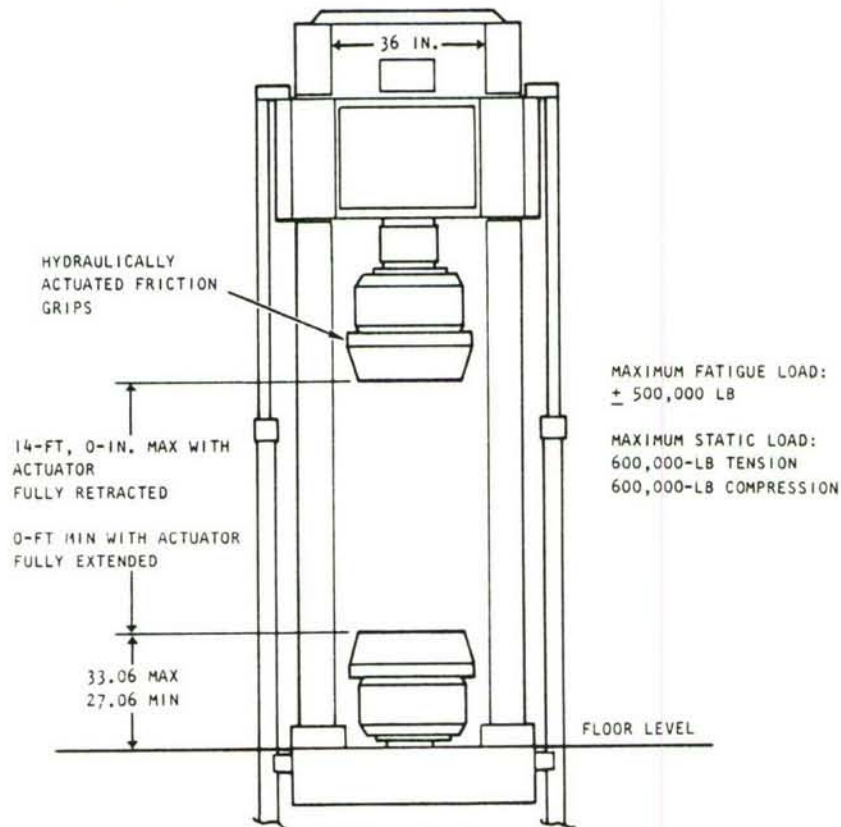
Figure 62.   500-KIP Materials Test System
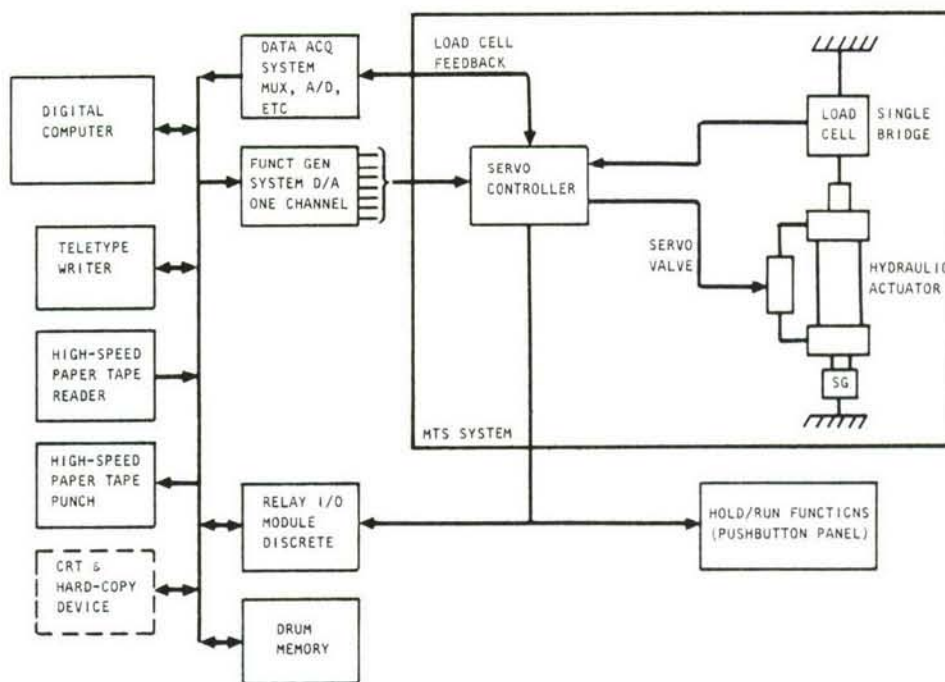
Figure 63.   Schematic of MTS System/Datum System 70
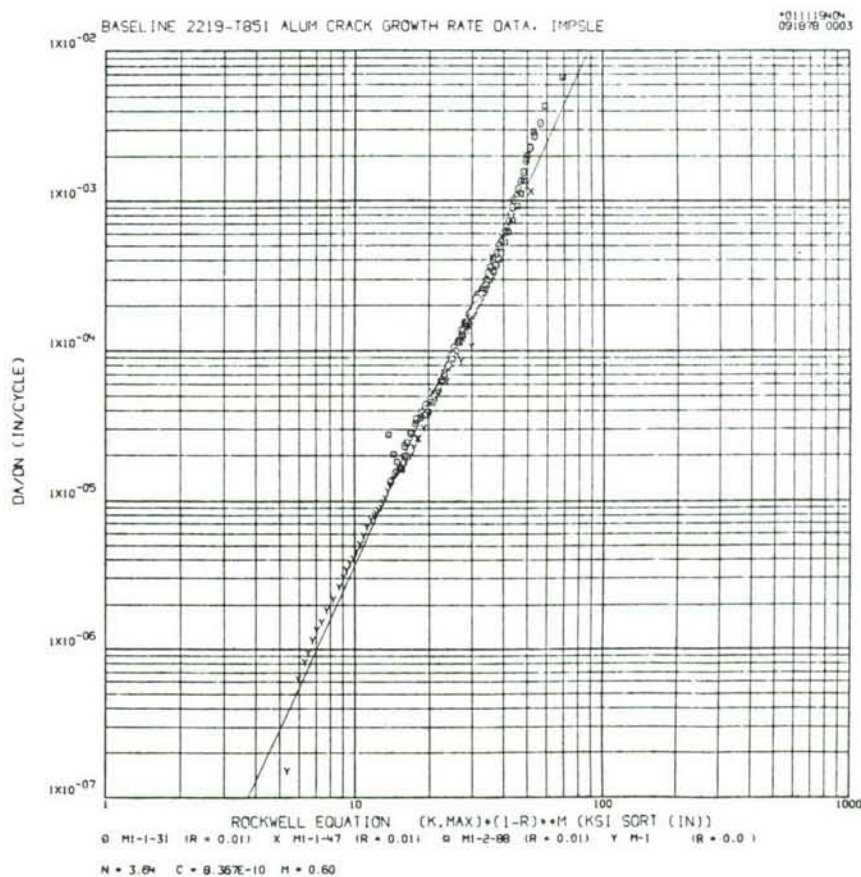
Figure 64.   Baseline Fatigue Crack Growth Rate Data

142

PLOTRATE CRACK GROWTH ANALYSIS
SINGLE OVERLOAD   R = 0
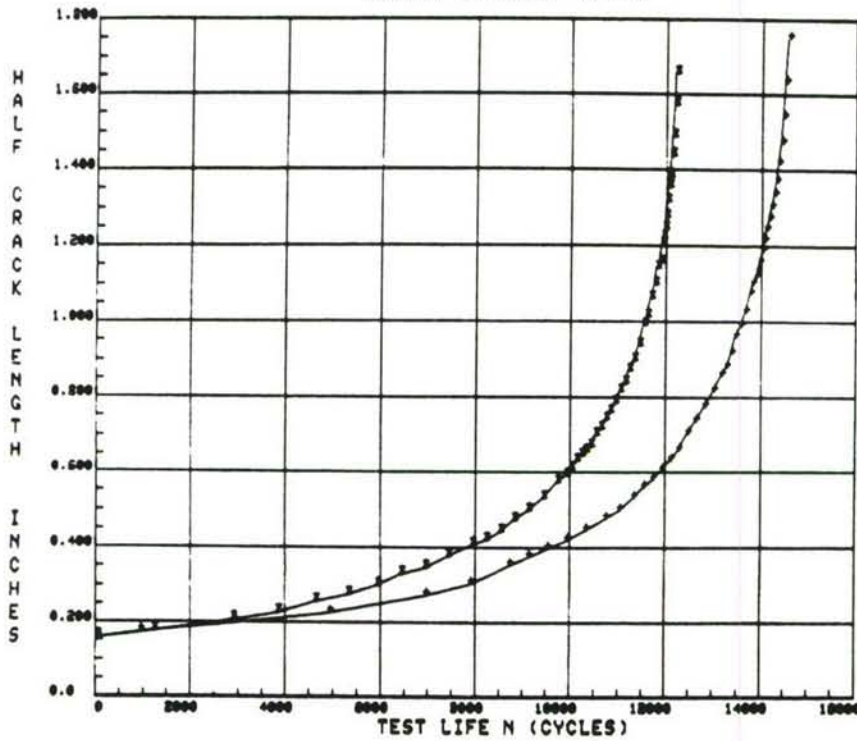
Figure 65.   Single overload effect R = 0.

PLOTRATE CRACK GROWTH ANALYSIS
PERIODIC OVERLOAD   R = 0
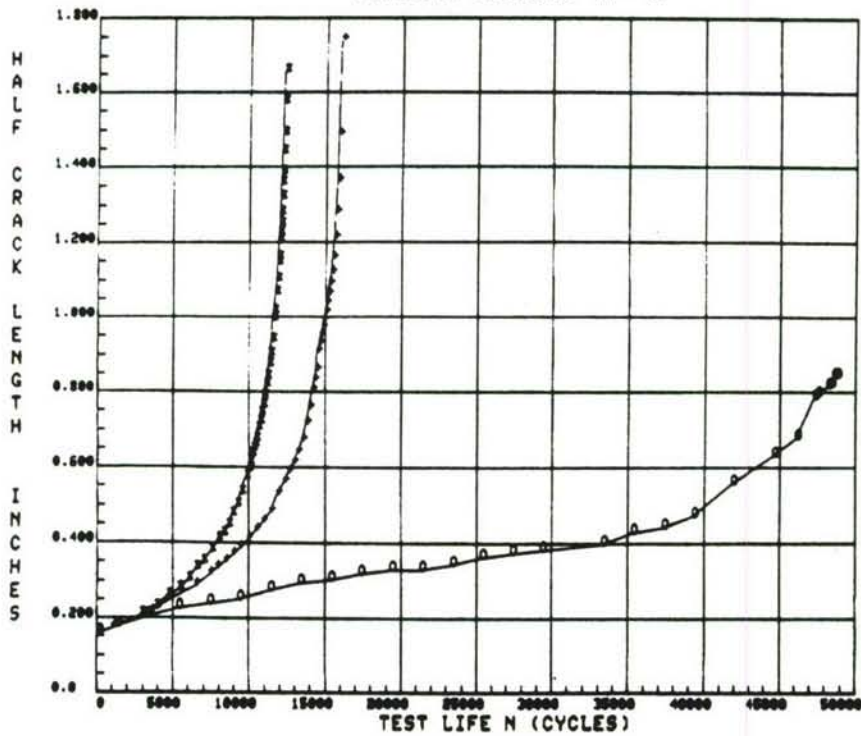
Figure 66.   Periodic overload effect R = 0.

143
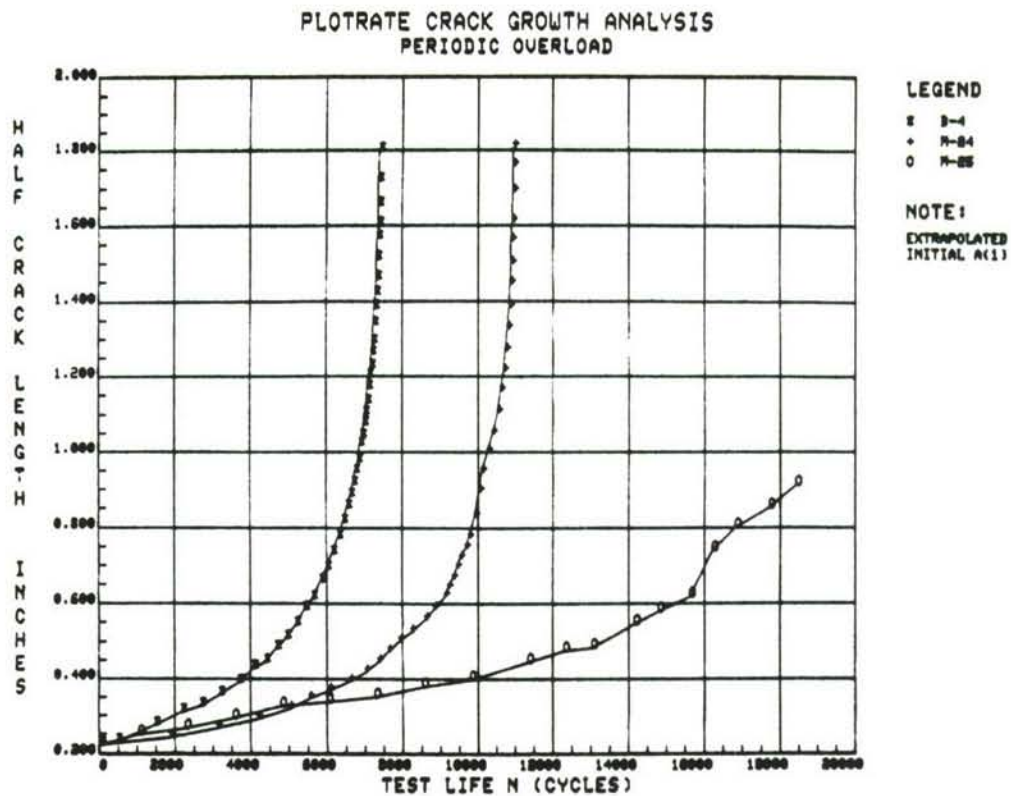
Figure 67.   Periodic overload effect.
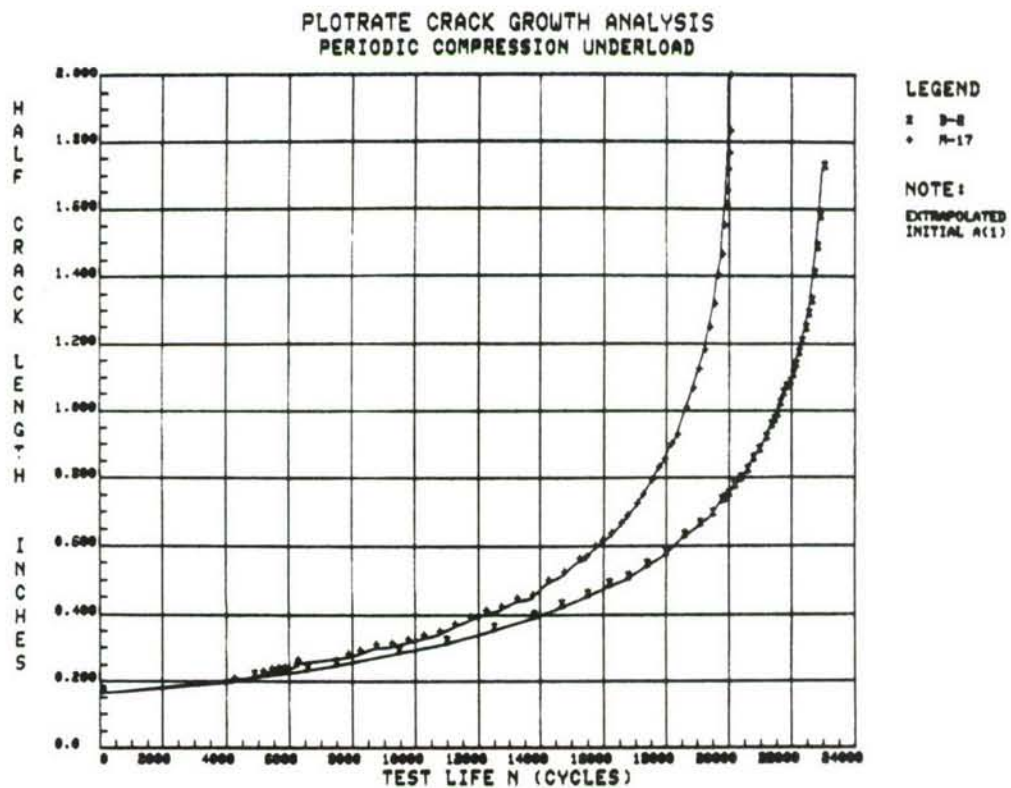
Figure 68.   Periodic compression underload effect.

144
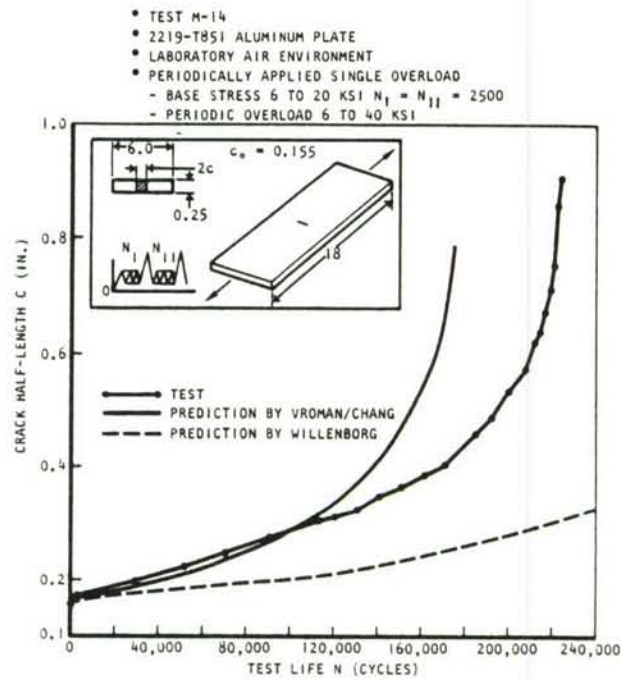
Figure 69.   Crack Growth Curve and Predictions for Test M-14
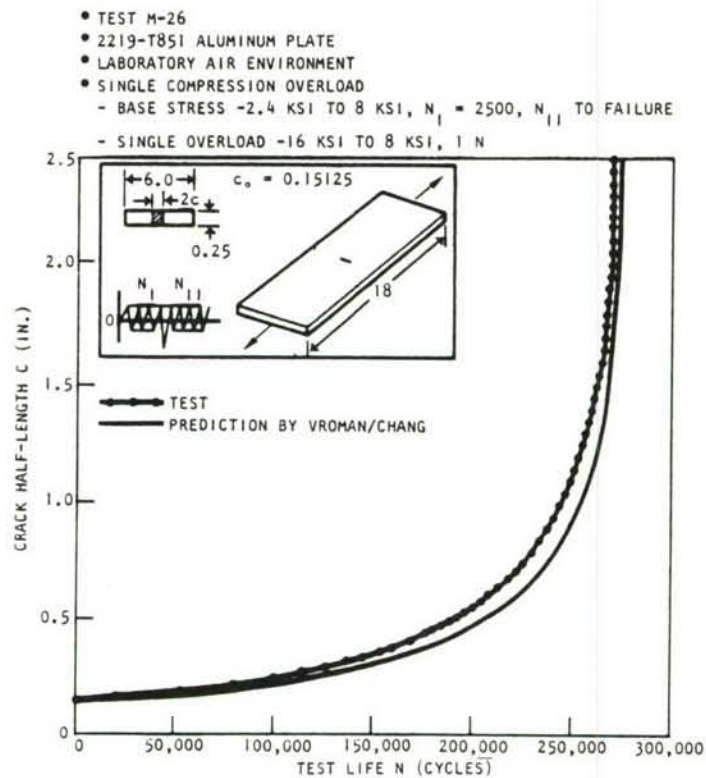
Figure 70.   Crack Growth Curve and Prediction for Test M-26

145
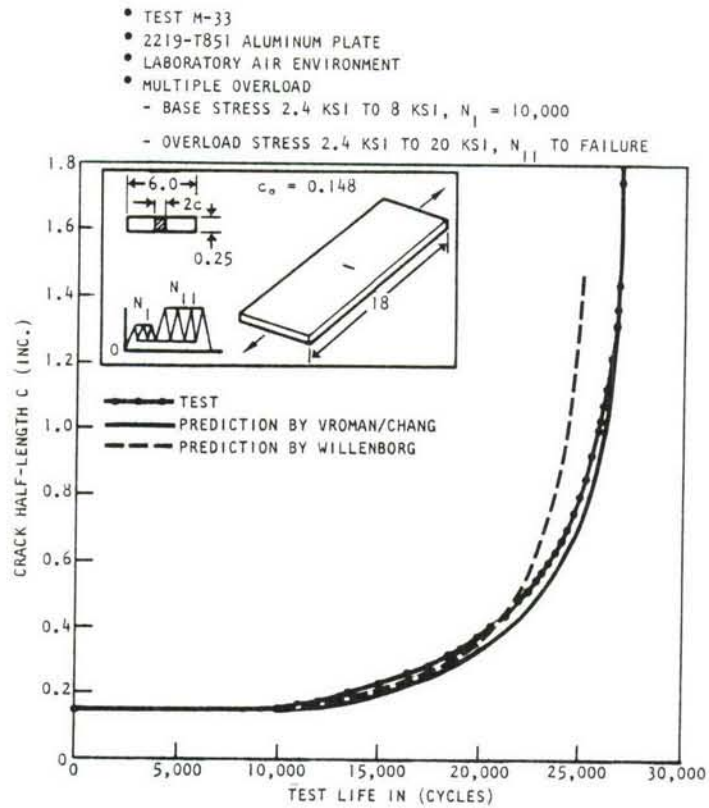
Figure 71. Crack Growth Curve and Predictions for Test M-33
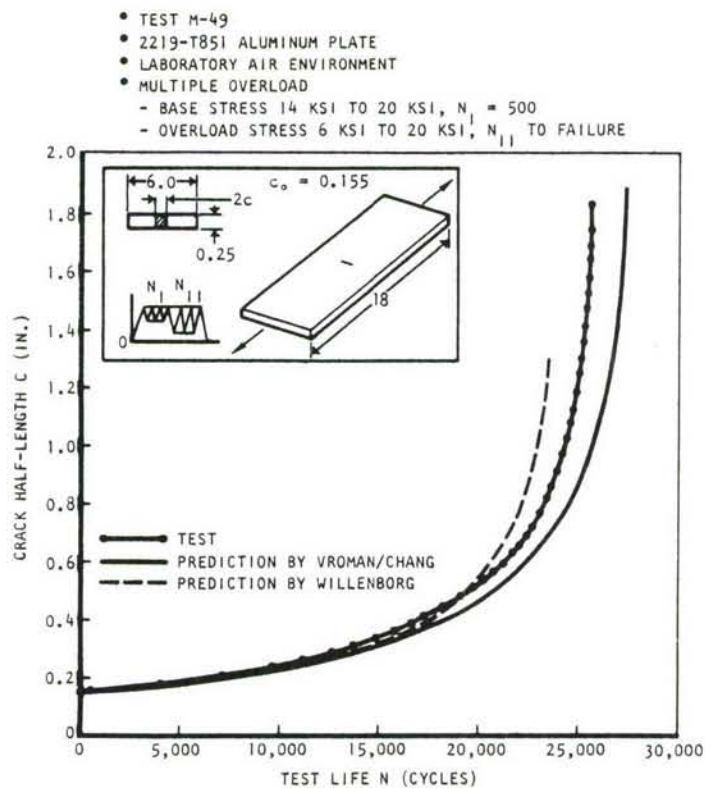
Figure 72. Crack Growth Curve and Predictions for Test M-49
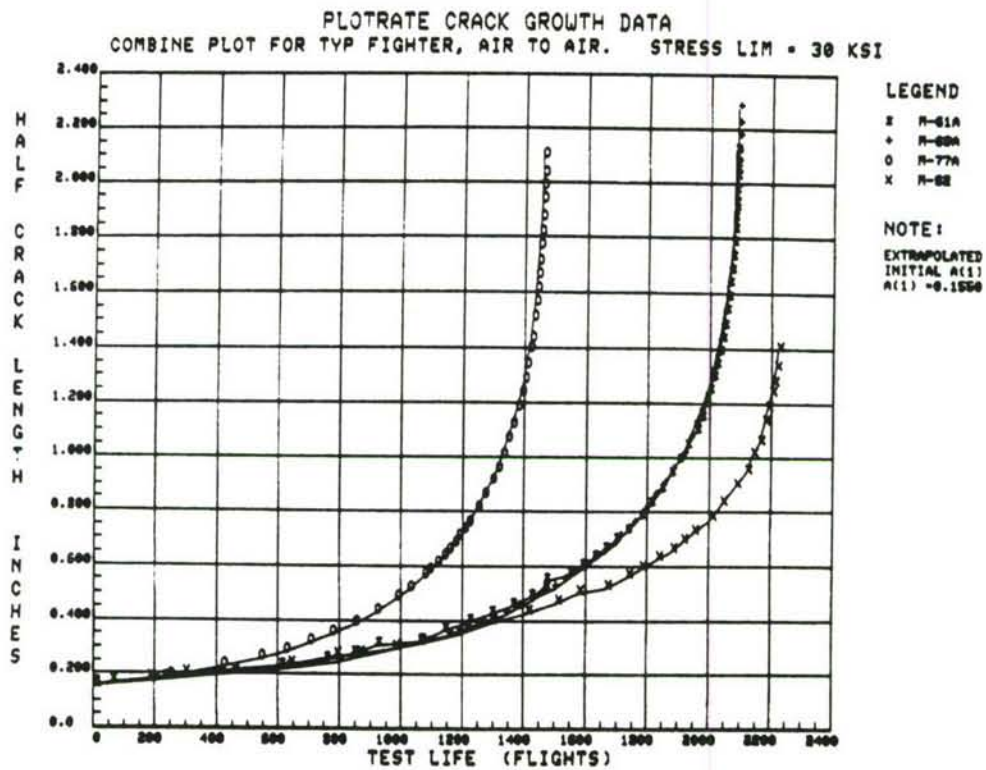
Figure 73.   Combine plot for typical fighter, air-to-air.
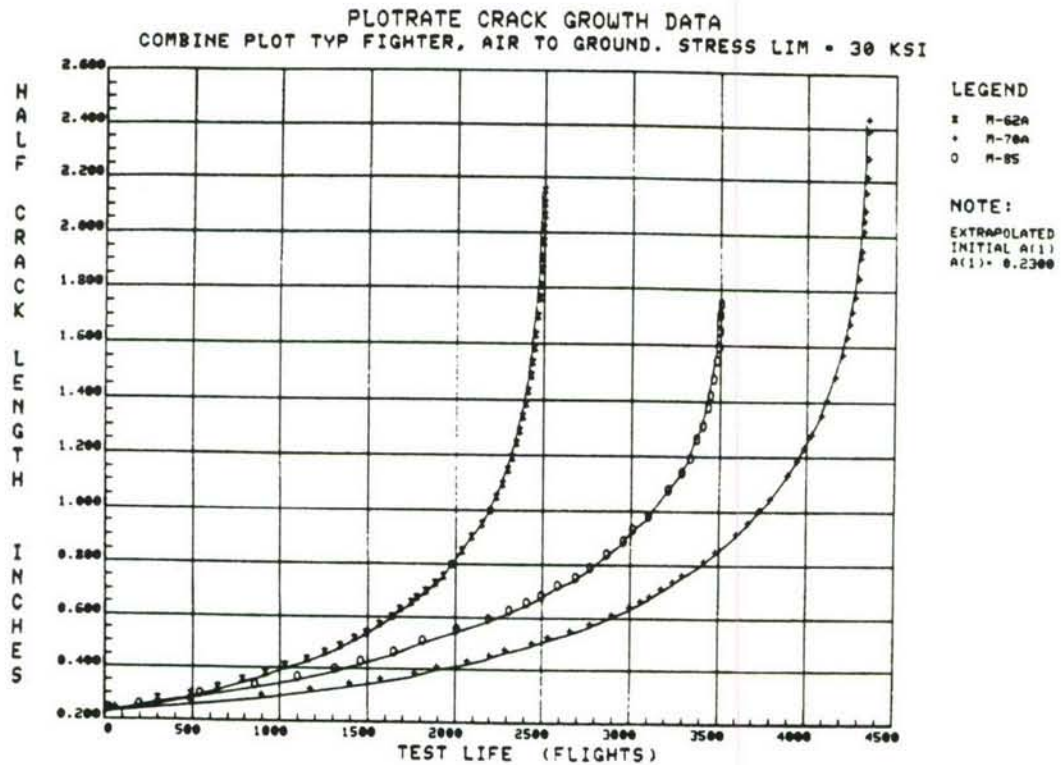
Figure 74.   Combine plot for typical fighter, air-to-ground.

147
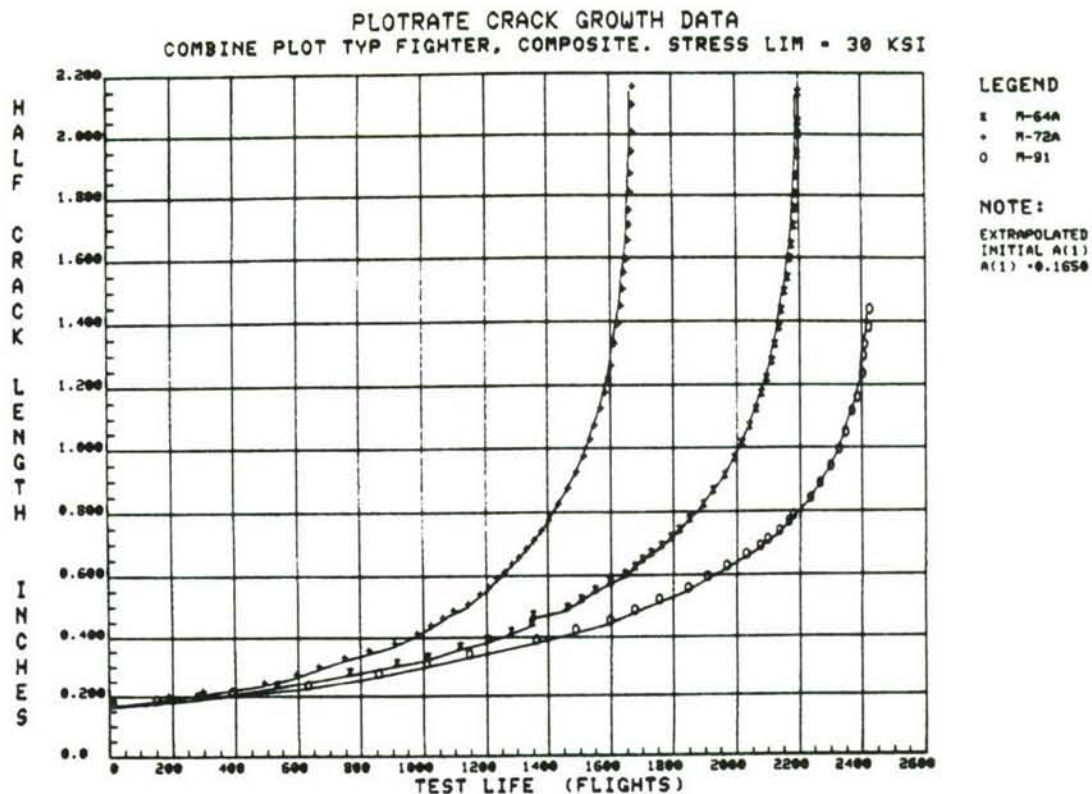
Figure 75. Combine plot for typical fighter, composite, stress limit = 30 ksi.
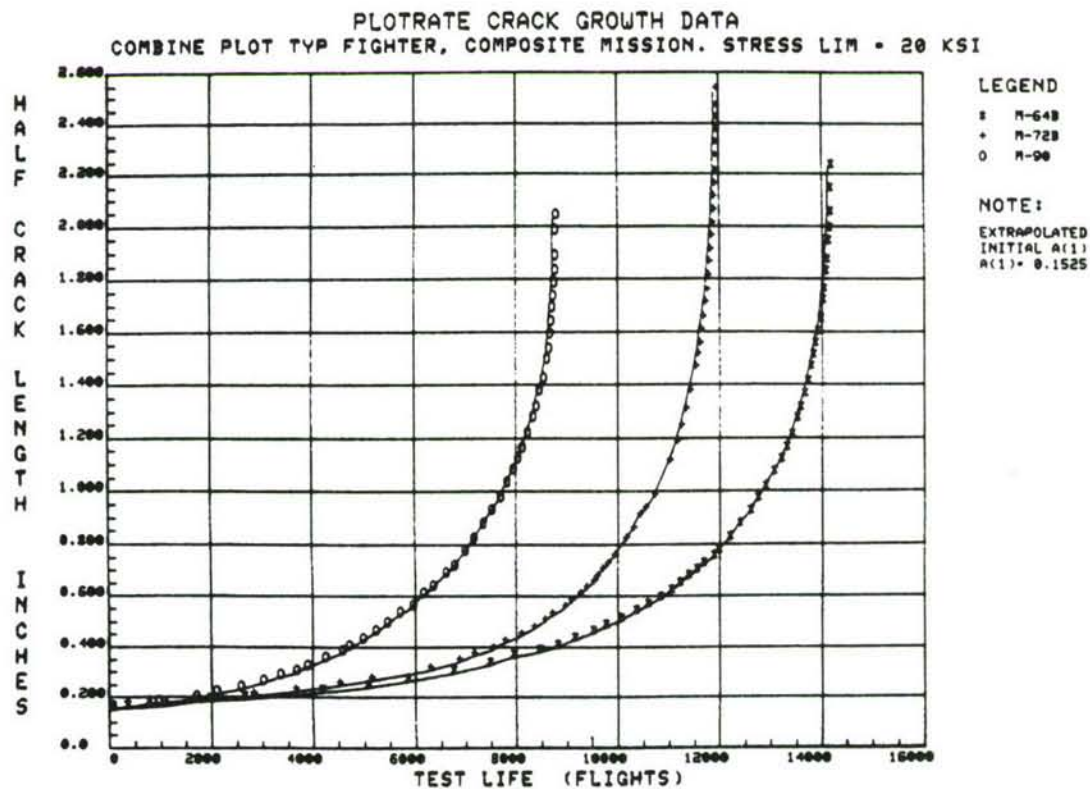
Figure 76. Combine plot for typical fighter, composite mission, stress limit = 20 ksi.

148

PLOTRATE CRACK GROWTH DATA
COMBINE PLOT TYP FIGHTER, COMPOSITE. STRESS LIM = 40 KSI
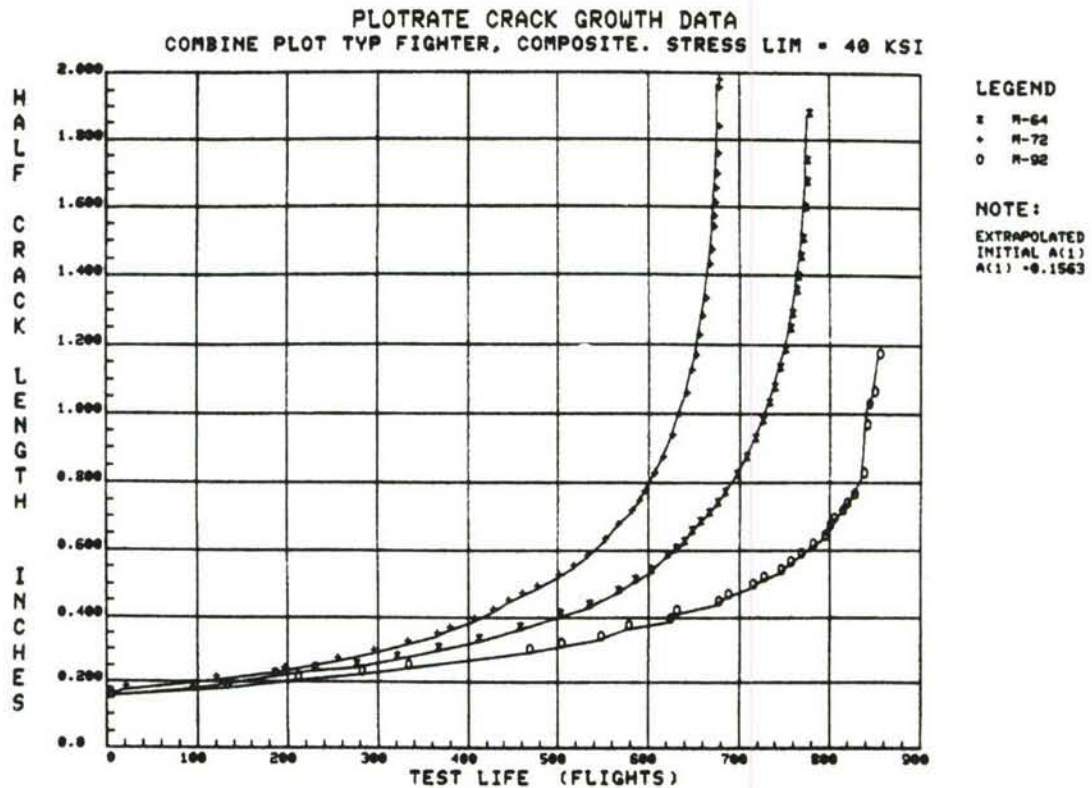
Figure 77. Combine plot for typical fighter, composite, stress limit = 40 ksi.

PLOTRATE CRACK GROWTH DATA
COMBINE PLOT, TYP TRANSPORT. MAX STRESS = 14 KSI
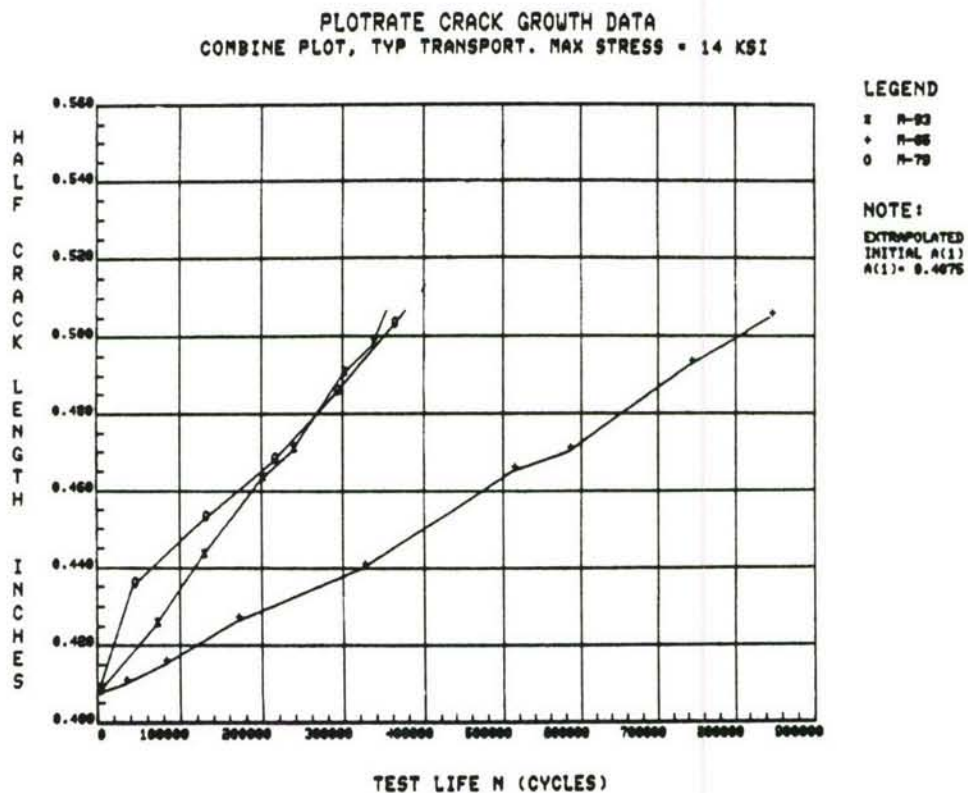
Figure 78. Combine plot for typical transport, maximum stress = 14 ksi.

149
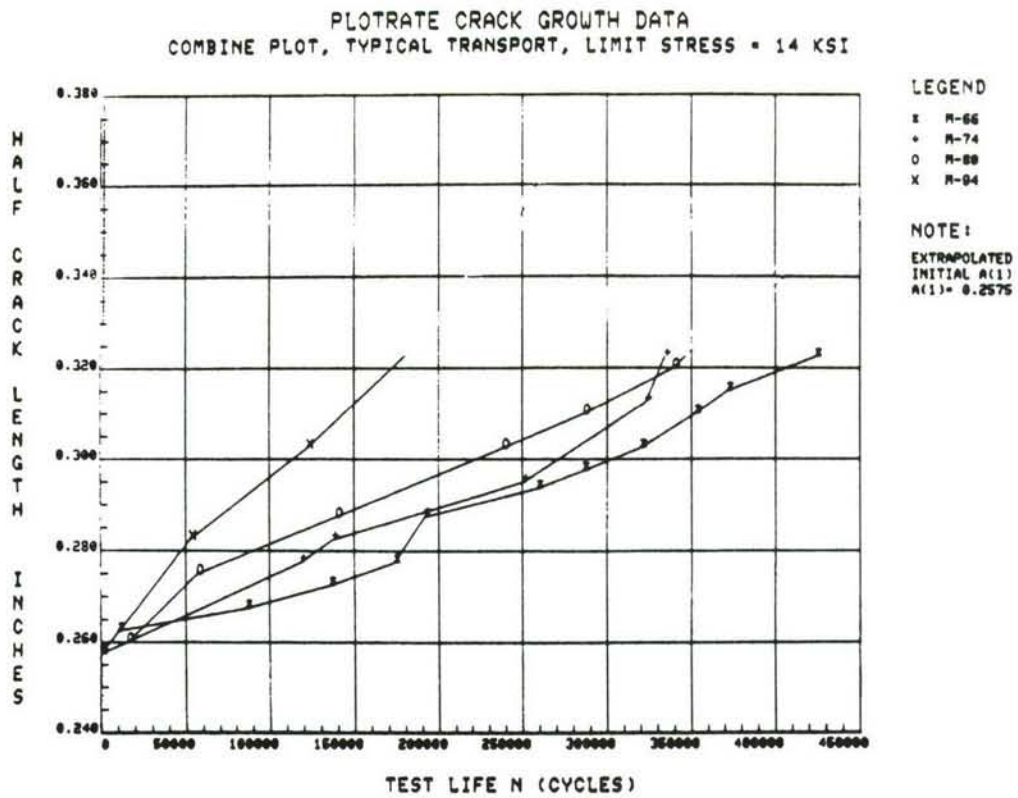
Figure 79. Combine plot for typical transport, limit stress = 14 ksi.
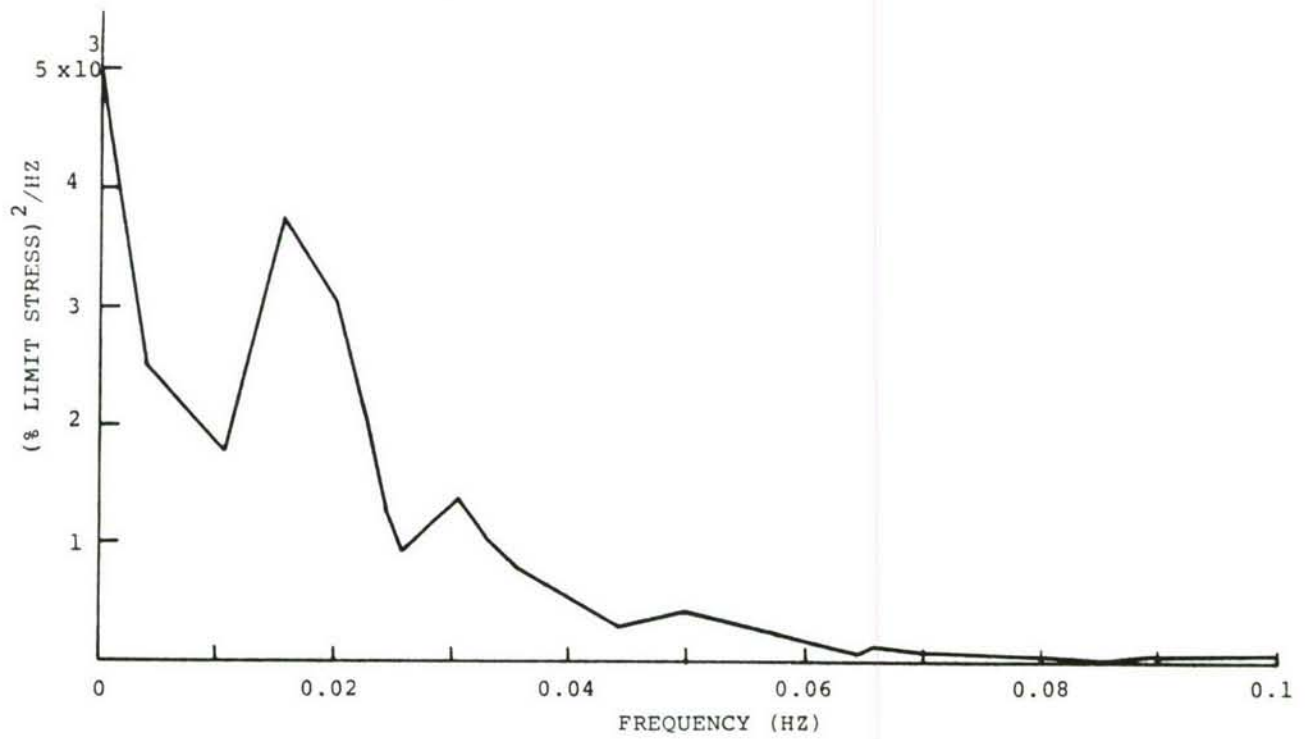
Figure 80. Power spectral density for air-to-air maneuvers.
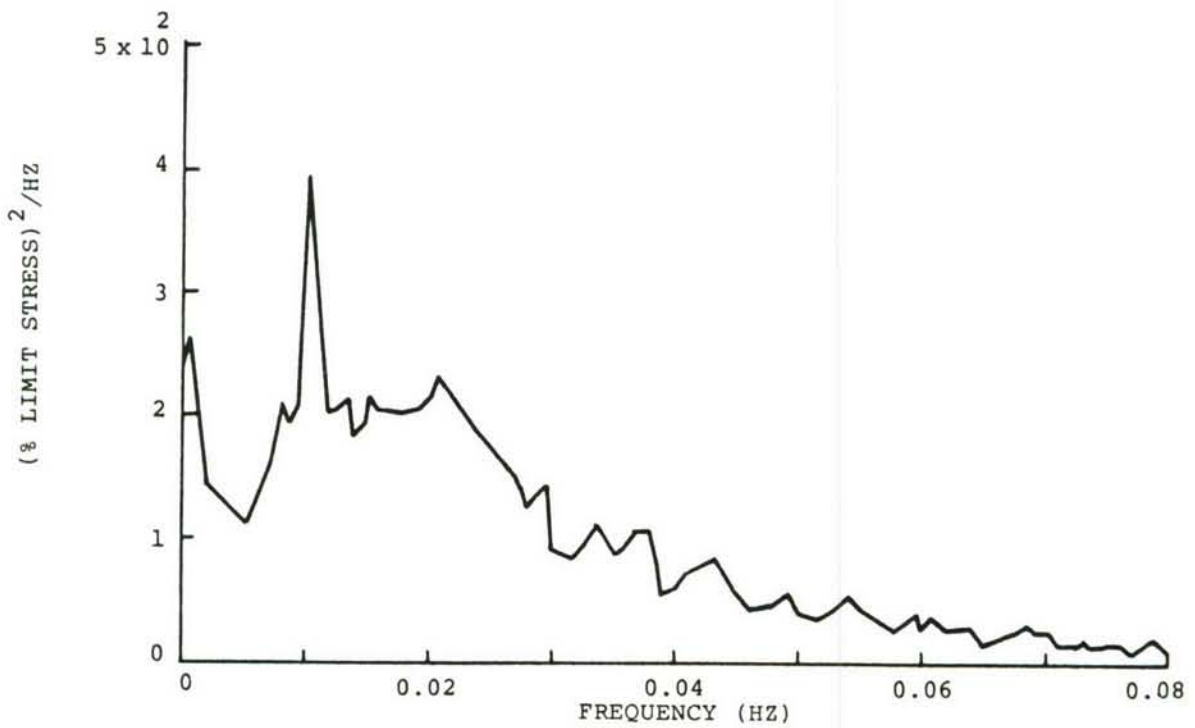
Figure 81. Power spectral density for air-to-ground maneuvers.

151
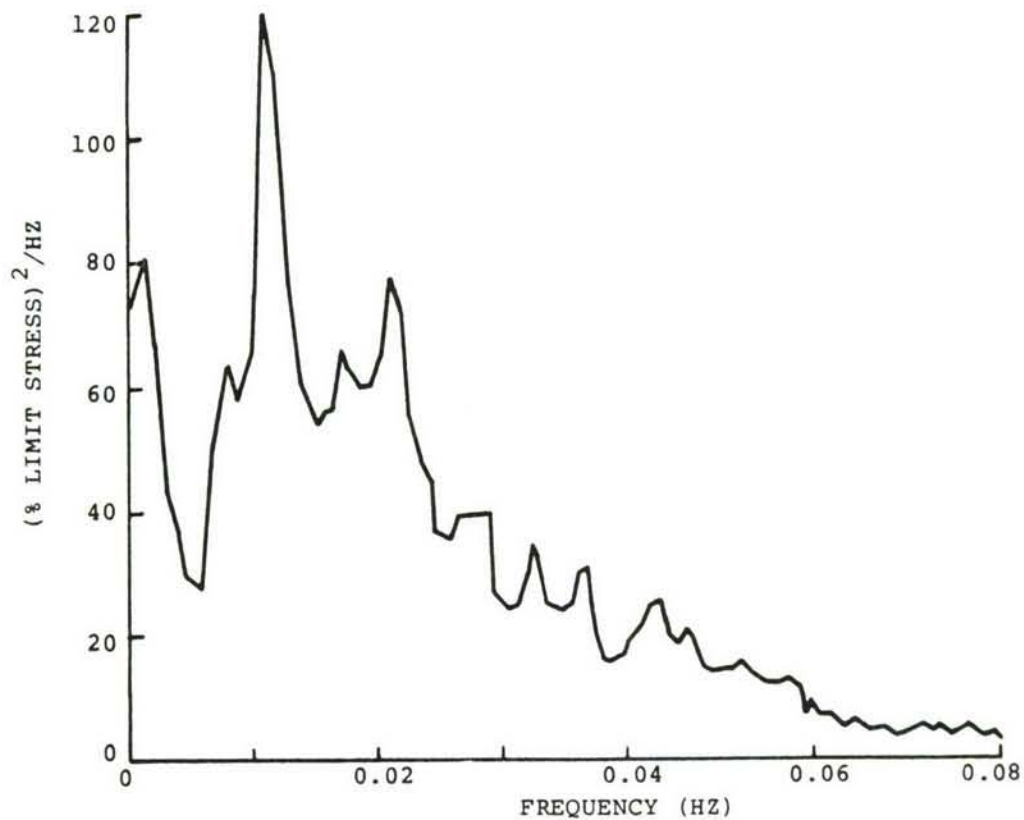
Figure 82. Power spectral density for instrumentation and navigation maneuvers.
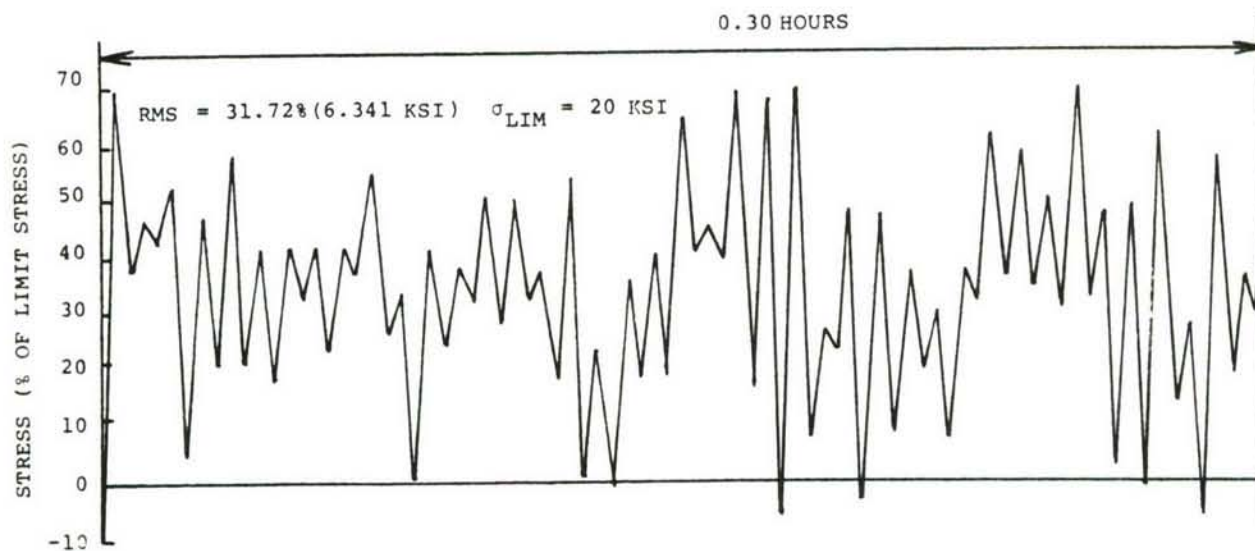
Figure 83. A sample history of air-to-air maneuver spectra.
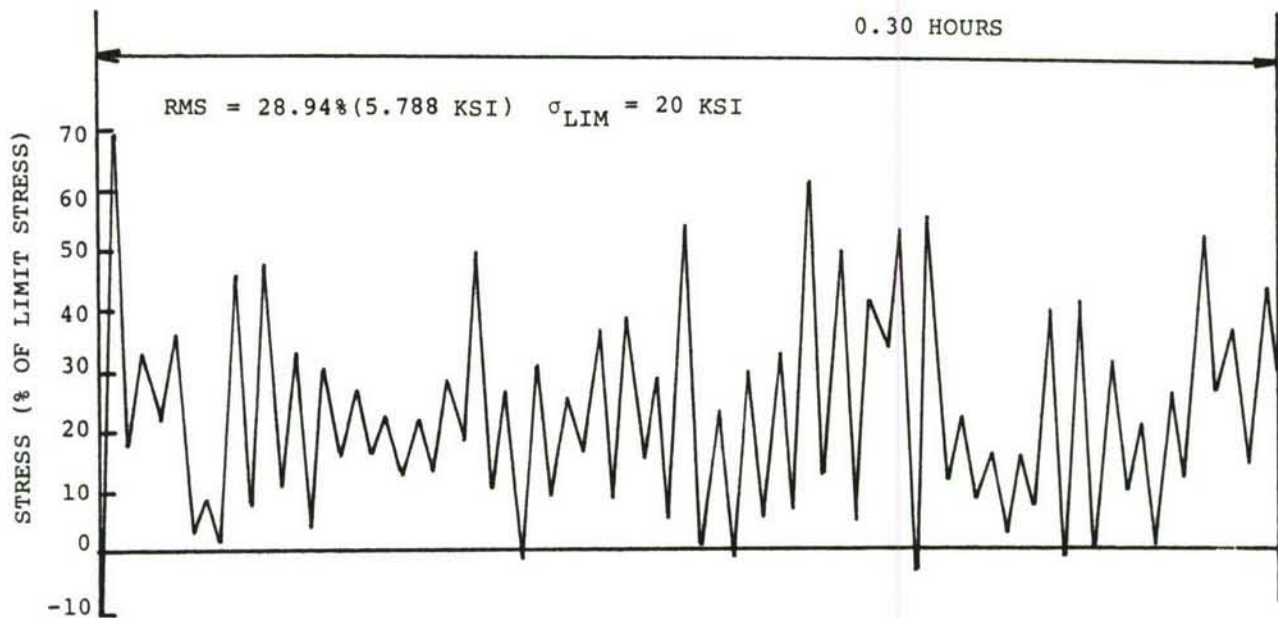
Figure 84. A sample history of air-to-ground maneuver spectra.
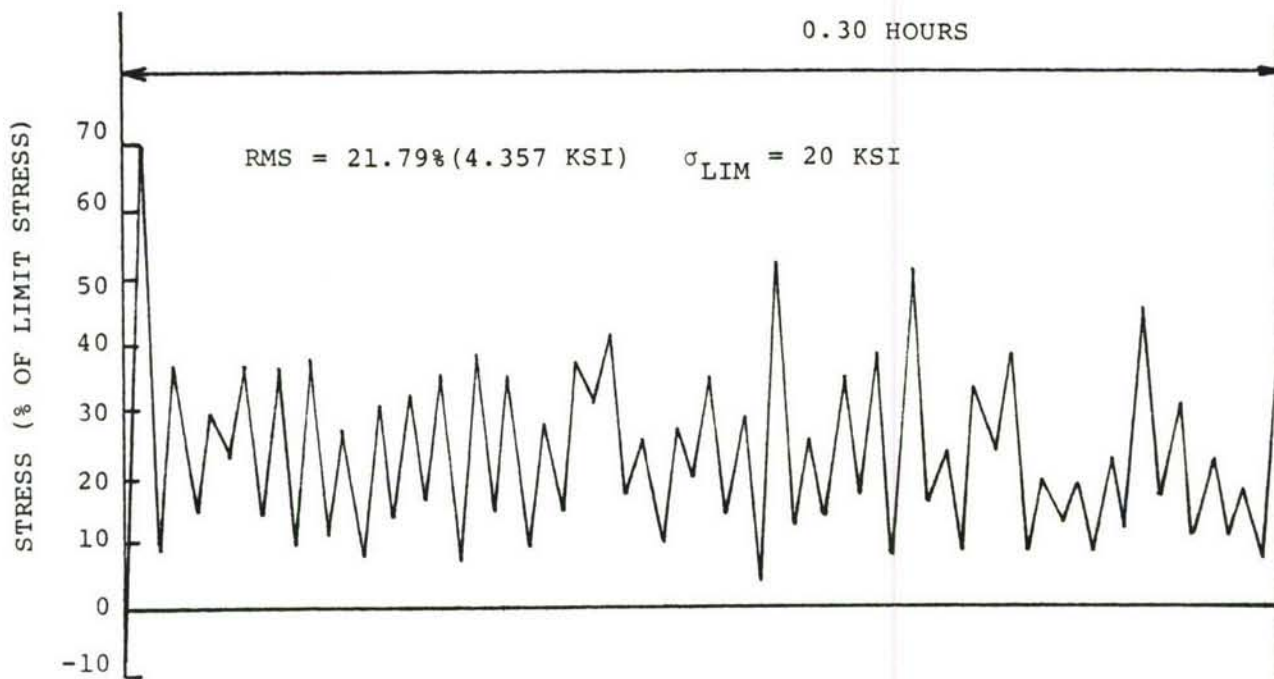
Figure 85. A sample history of instrumentation and navigation
maneuver spectra.

153
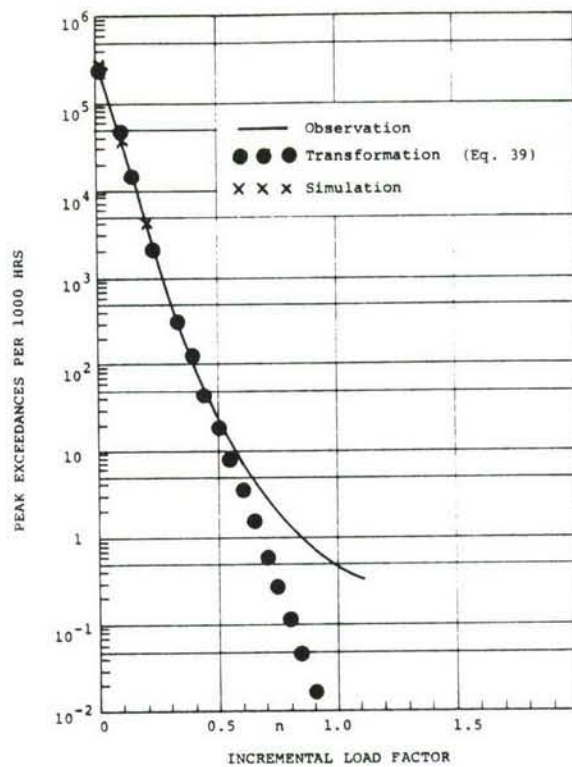
Figure 86. Positive peak exceedances for transport aircraft (assault - climb).
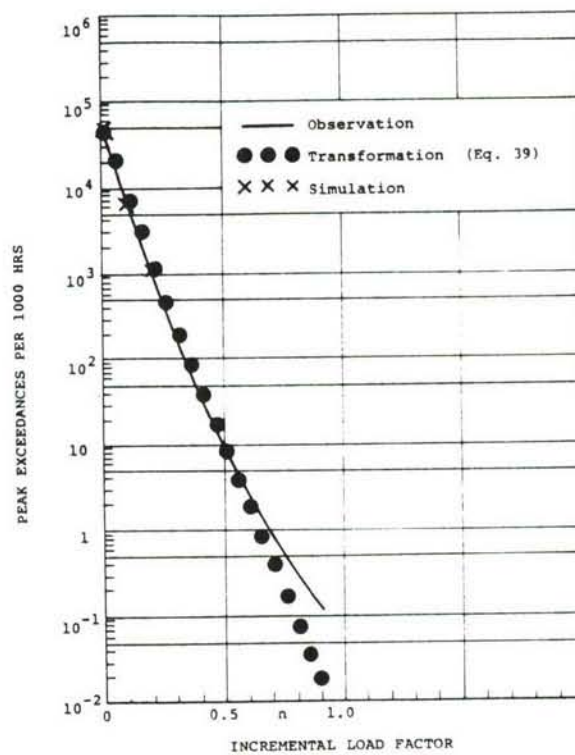
Figure 87. Positive peak exceedances for transport aircraft (assault - cruise).

154
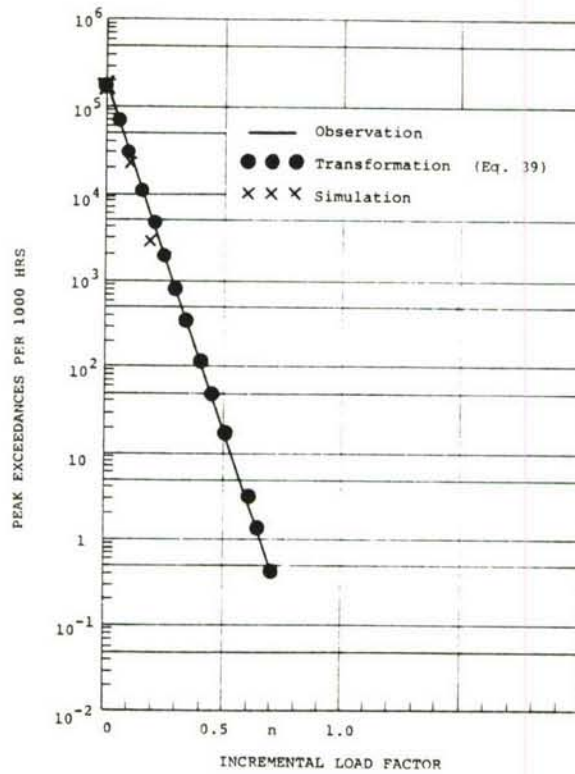
Figure 88. Positive peak exceedances for transport aircraft
(assault - descent).
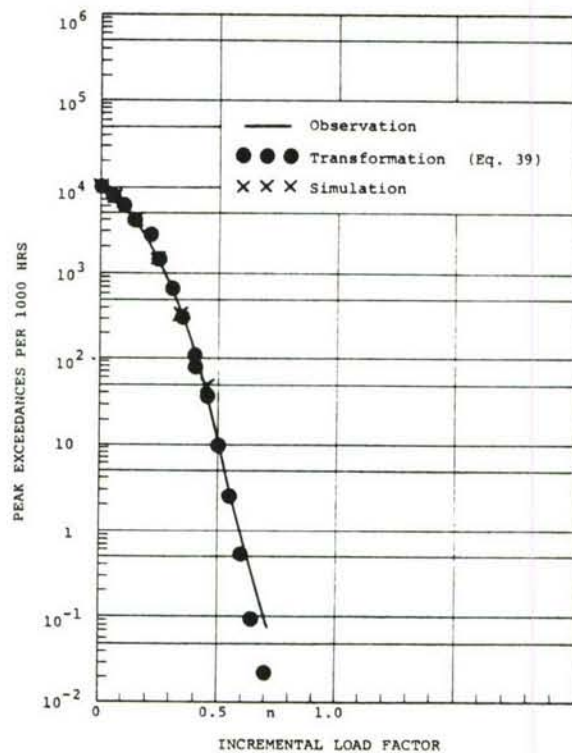
Figure 89. Positive peak exceedances for transport aircraft
(logistics - climb).

155
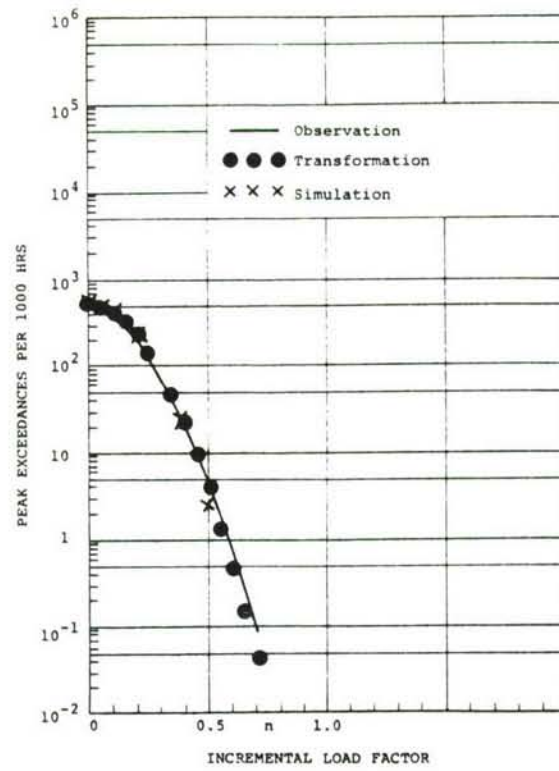
Figure 90. Positive peak exceedances for transport aircraft (logistics - cruise).
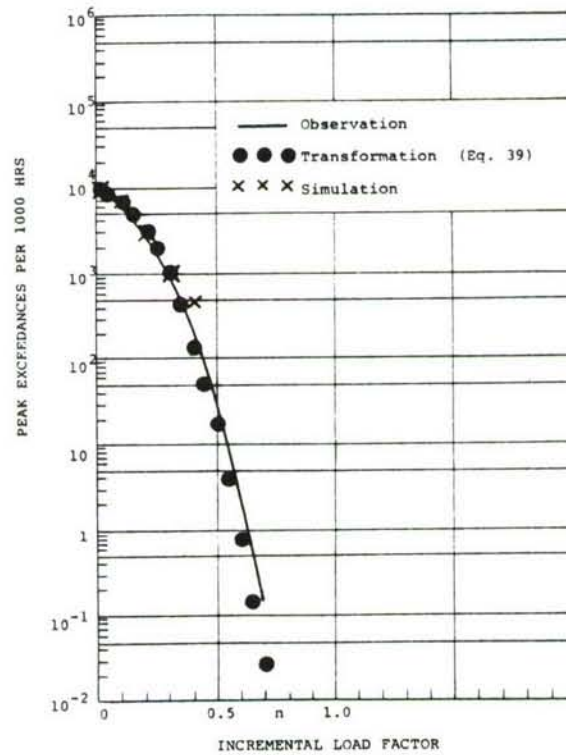
Figure 91. Positive peak exceedances for transport aircraft (logistics - descent).

156
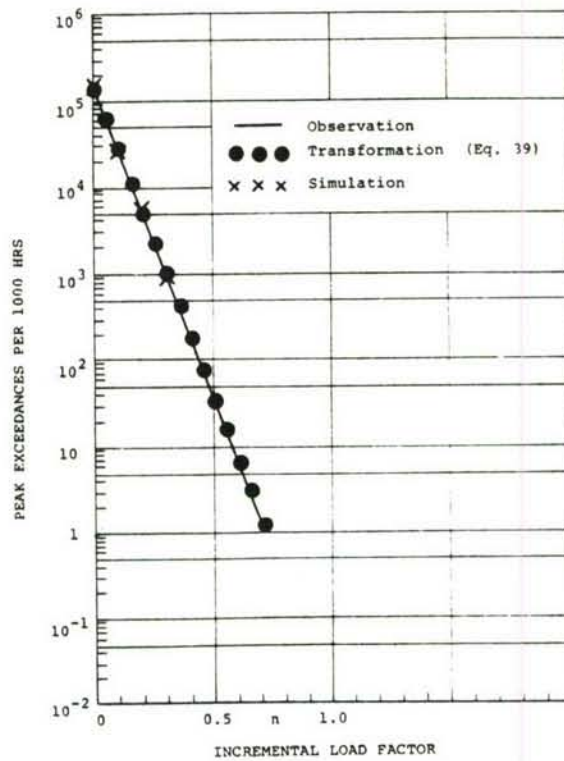
Figure 92. Positive peak exceedances for transport aircraft
(training - ascent).
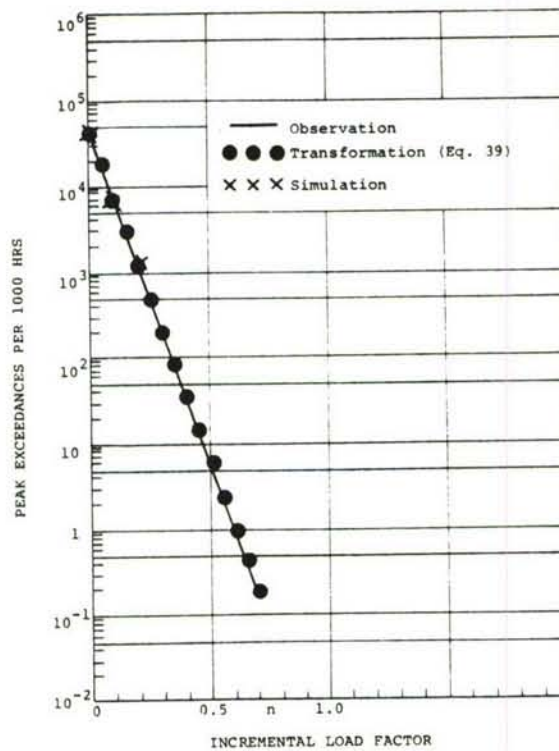
Figure 93. Positive peak exceedances for transport aircraft
(training - cruise).

157
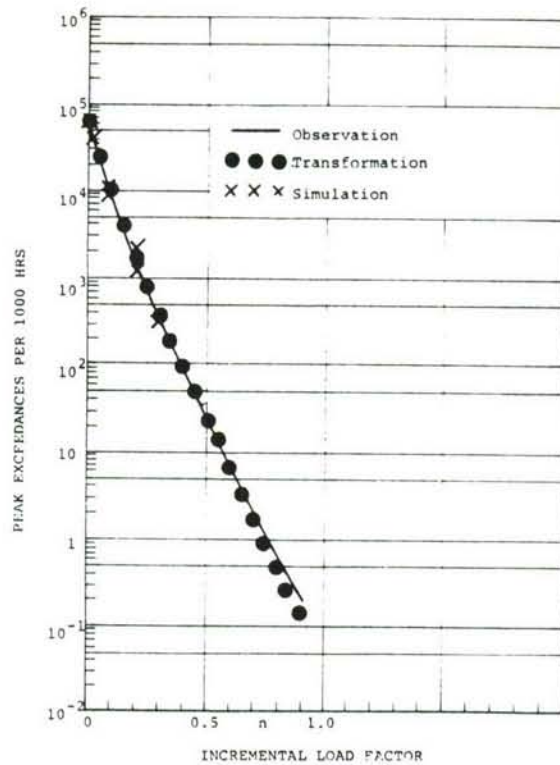
Figure 94.   Positive peak exceedances for transport aircraft
(training - descent).
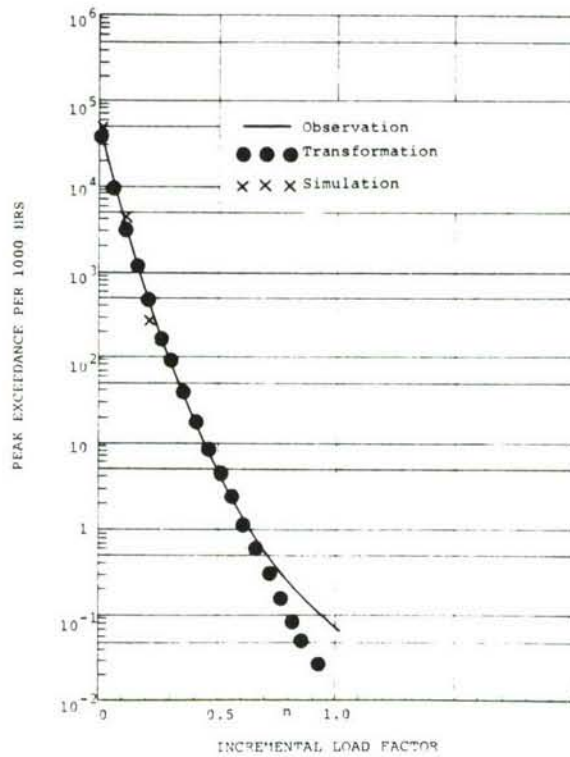
Figure 95.   Positive peak exceedances
for C-5A aircraft (gust).

158
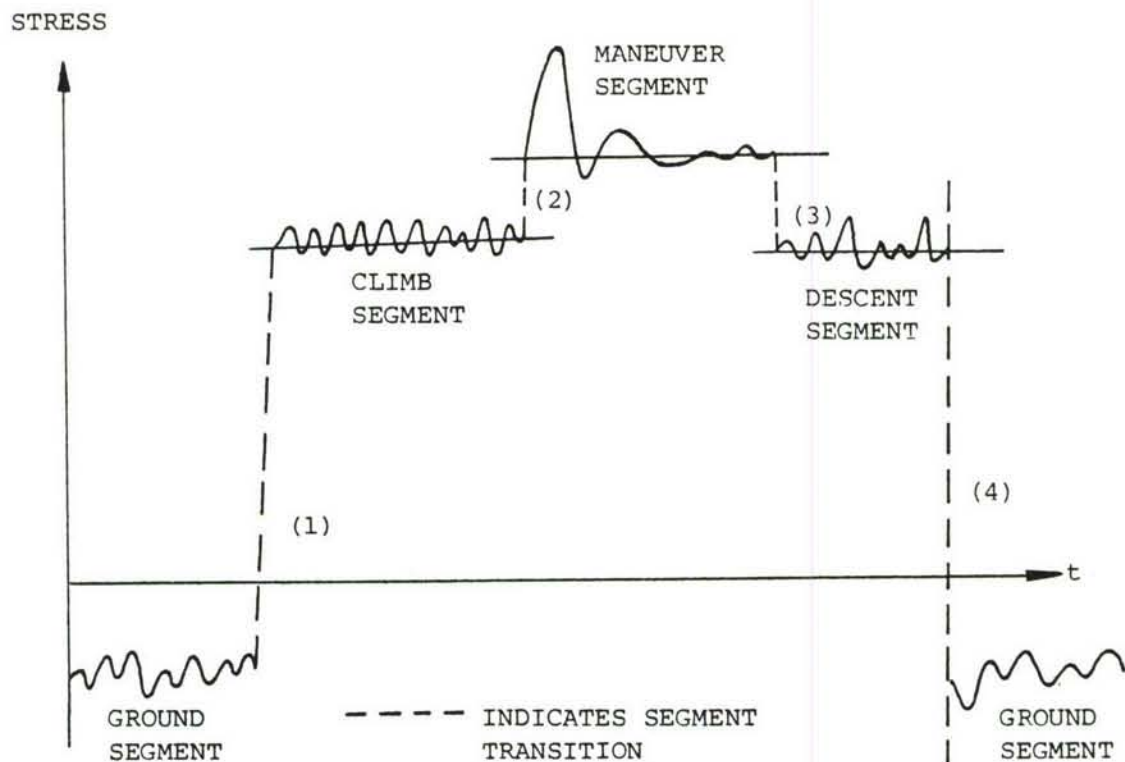
Figure 96a.   Schematic Flight Spectrum

$$dc/dF = C_A (\overline{K}_A)^{\lambda_A}$$

$$\overline{K}_A = \left(\overline{\sigma \frac{b_A}{A}} \right)^{1/b_A} \psi(c)$$

$$\sigma_+ - \sigma_- = \left(\overline{\sigma \frac{b_A}{A}} \right)^{1/b_A}$$
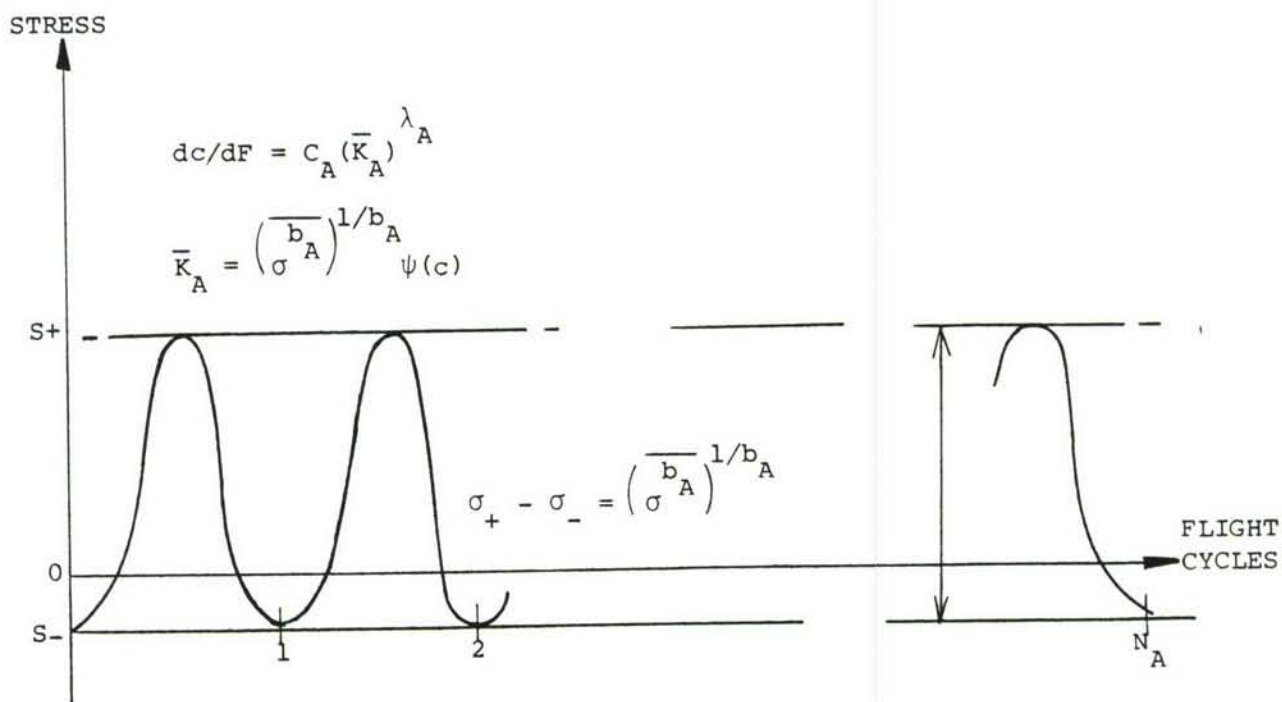
Figure 96b.   Equivalent Stress History

159
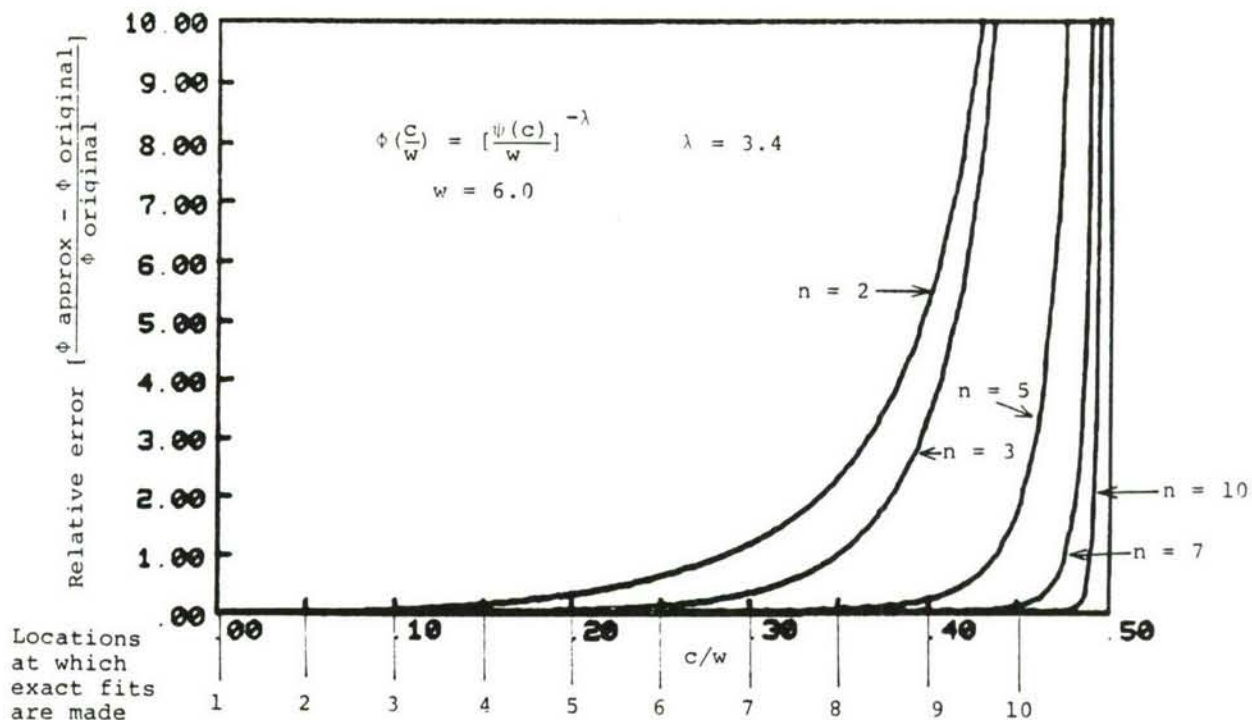
Figure 97. Effect of number of polynomial terms on the accuracy of expansion.
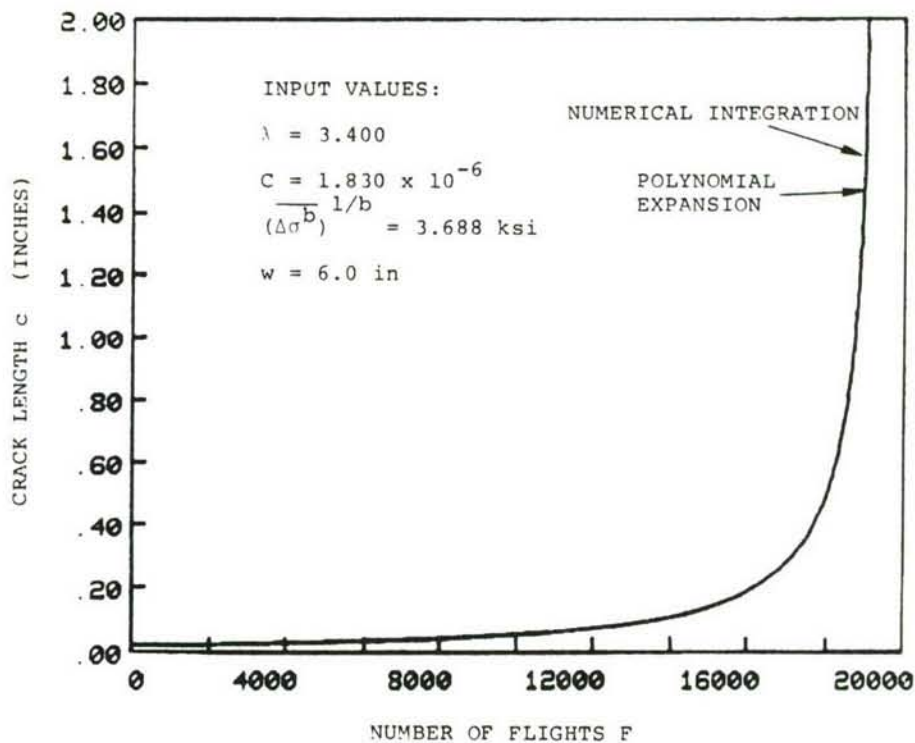
Figure 98. Crack growth as a function of number of flights using numerical solution and polynomial expansion.
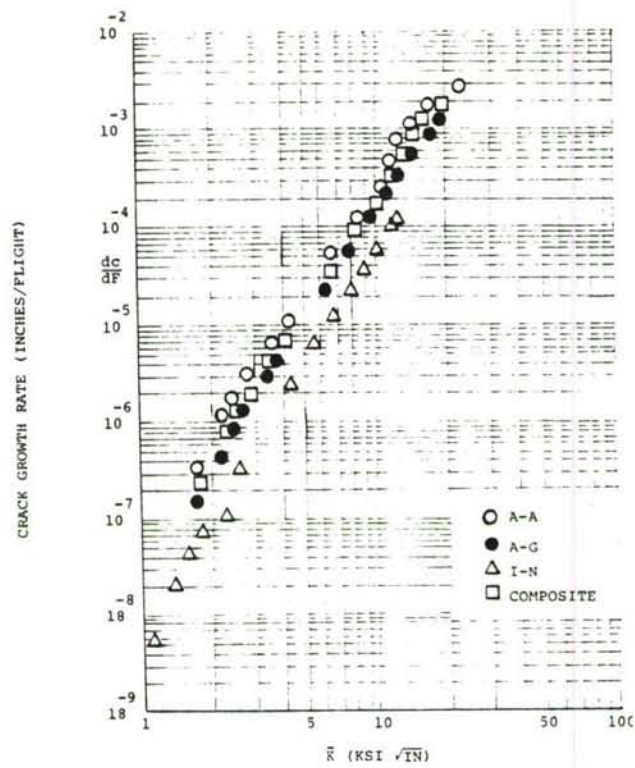
Figure 99. Crack growth rate (different flights in unitblock; compressive stresses included, σ_{LIM} = 20 ksi).
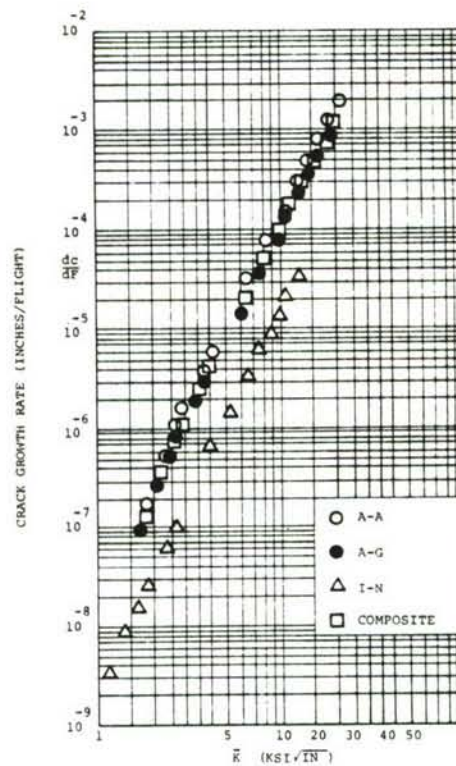
Figure 100. Crack growth rate (different flights in unitblock; compressive stresses deleted).

161
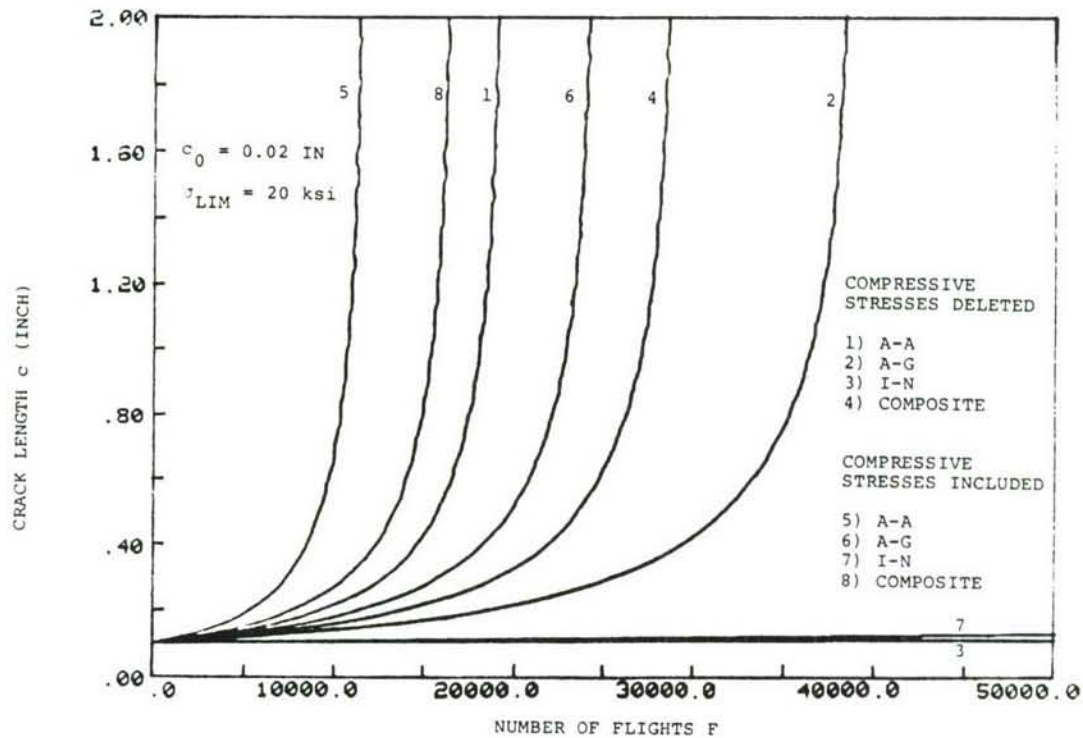
Figure 101. Crack growth as a function of number of flights for random loading $(c_0 = 0.02$ in., $\sigma_{LIM} = 20$ ksi$)$.
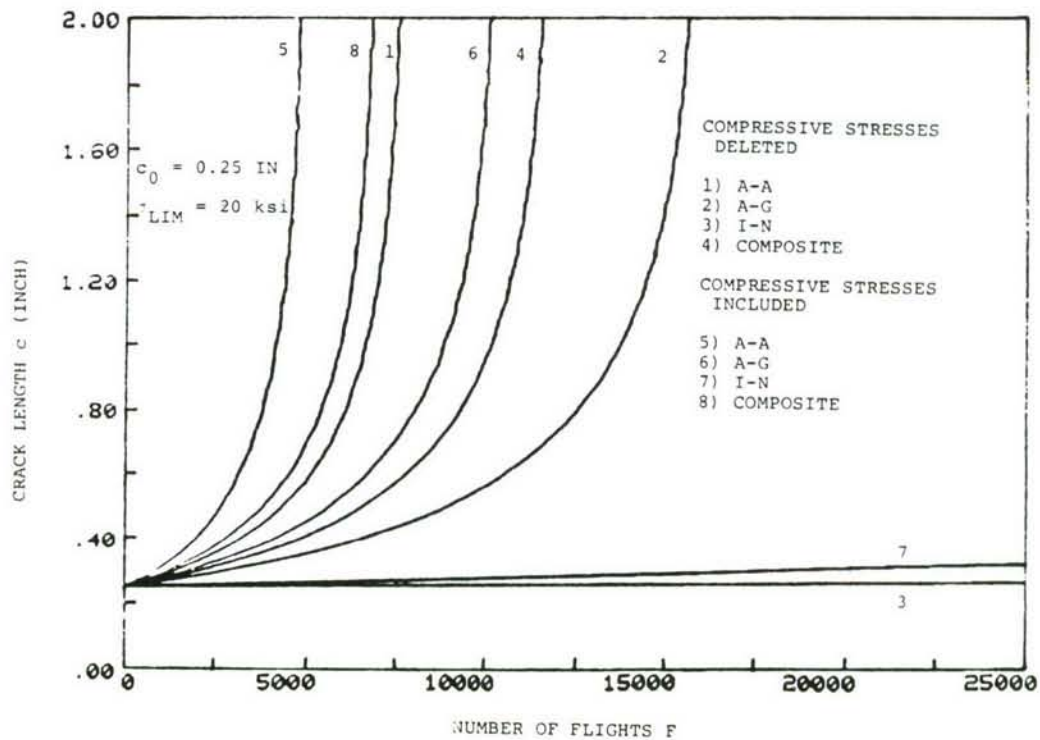
Figure 102. Crack growth as a function of number of flights for random loading $(c_0 = 0.25$ in., $\sigma_{LIM} = 20$ ksi$)$.

162
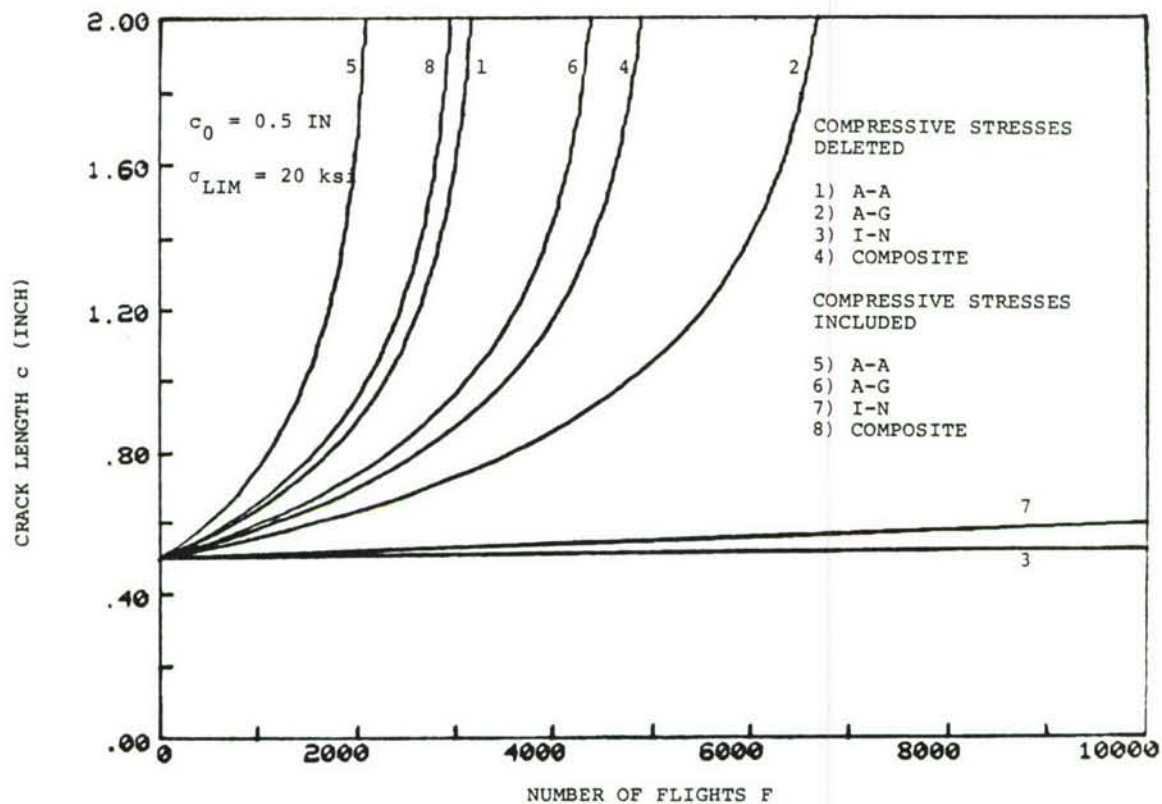
Figure 103. Crack growth as a function of number of flights for random loading ($c_0 = 0.5$ in., $\sigma_{LIM} = 20$ ksi).
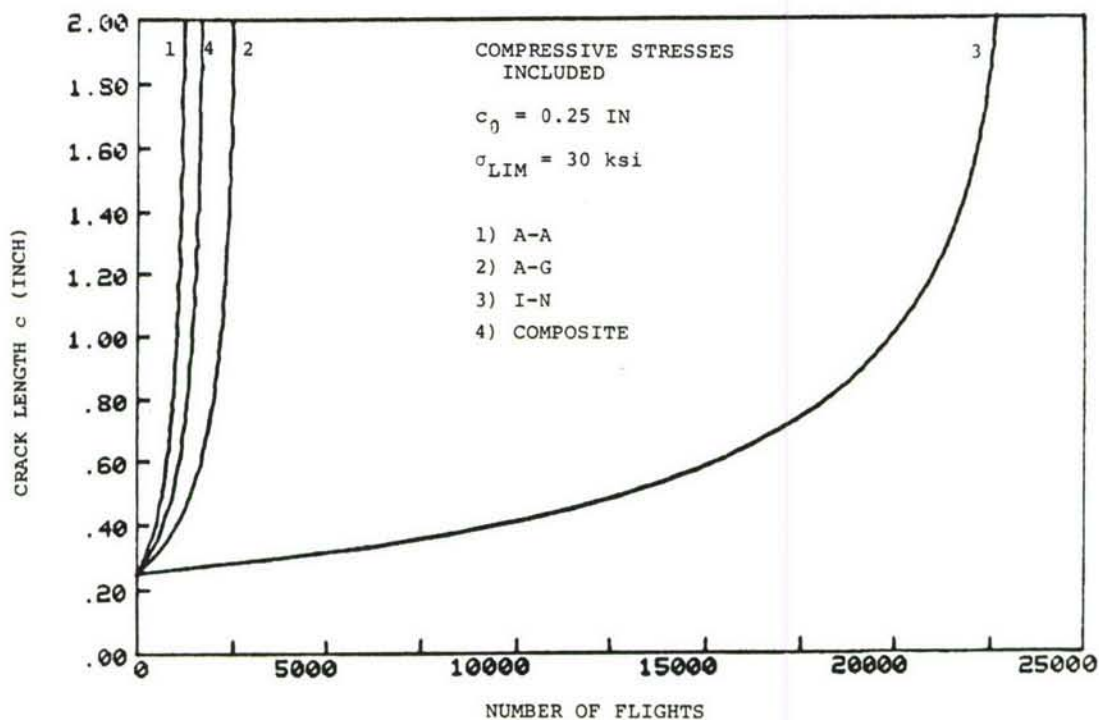
Figure 104. Crack growth as a function of number of flights for random loading ($c_0 = 0.25$ in., $\sigma_{LIM} = 30$ ksi).

163
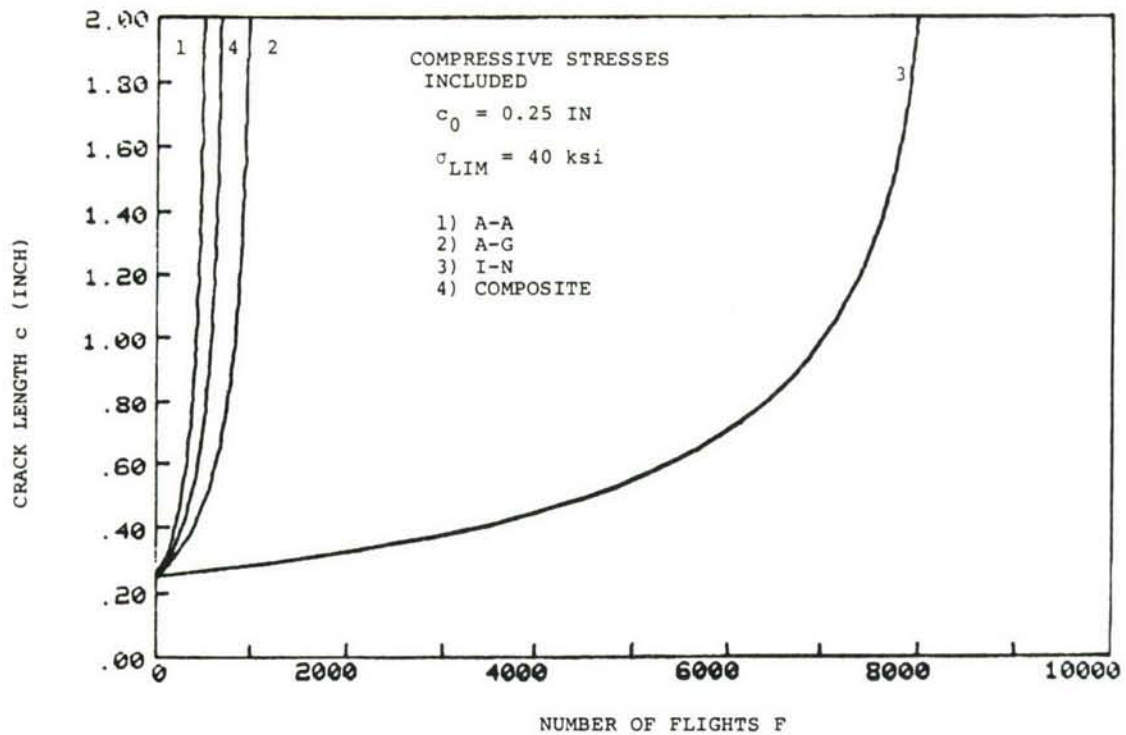
Figure 105. Crack growth as a function of number of flights for random loading (c_0 = 0.25 in., σ_{LIM} = 40 ksi).
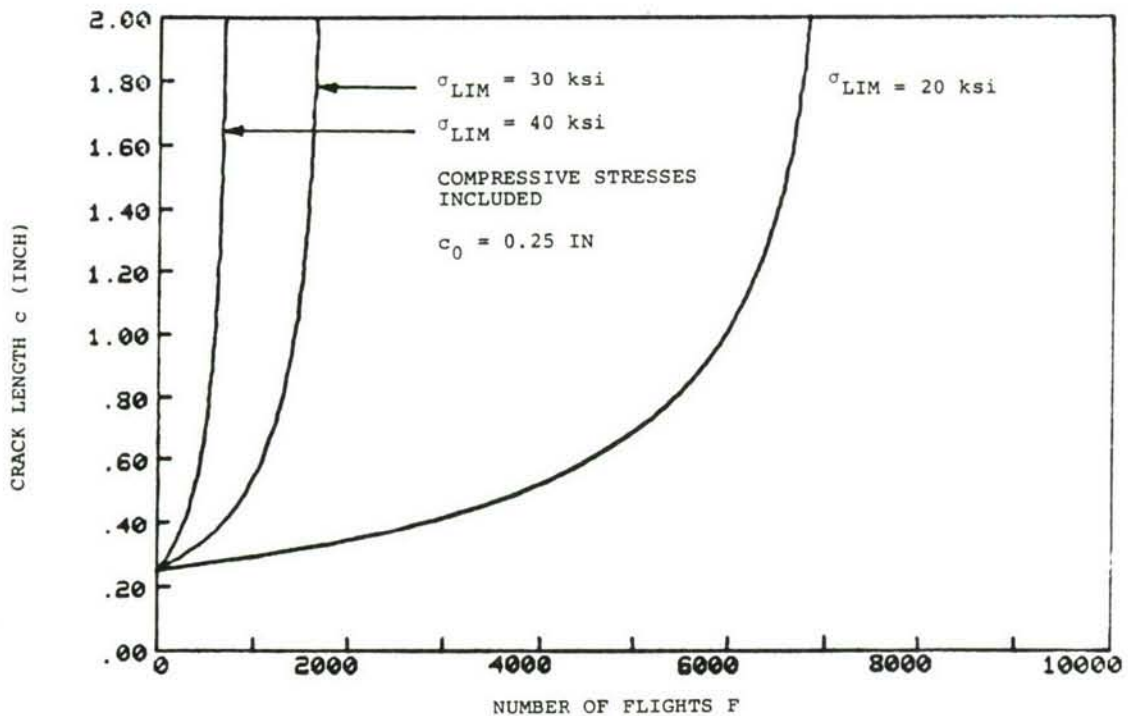
Figure 106. Crack growth as a function of number of flights for random loading (composite maneuver spectra, c_0 = 0.25 in.).

164
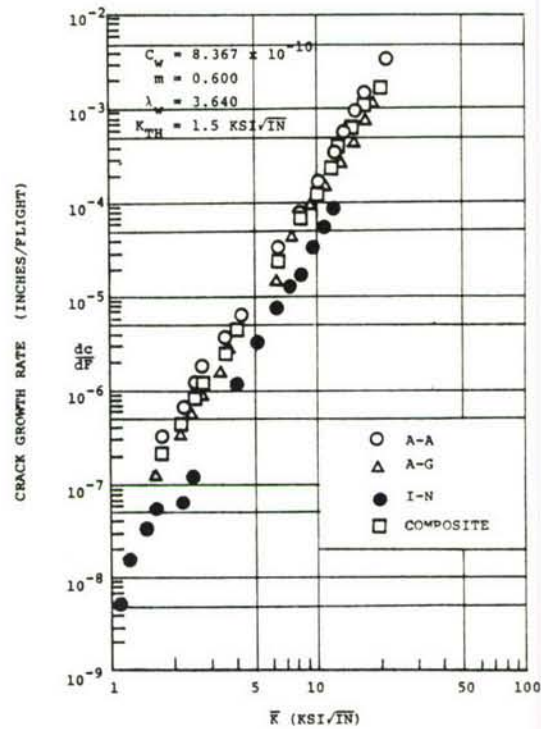
Figure 107. Crack growth rate per flight dc/dF as a function
of average stress intensity factor $\bar{K}$ for different
types of random loadings (σ_{LIM} = 20 ksi).
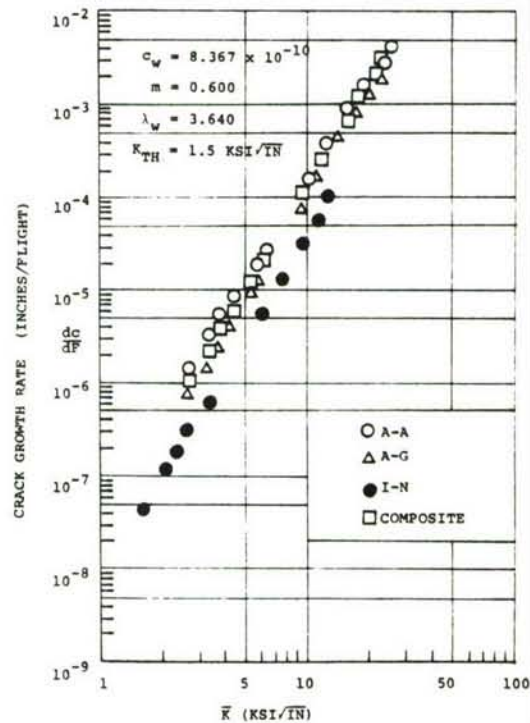
Figure 108. Crack growth rate per flight dc/dF as a function
of average stress intensity factor $\bar{K}$ for different
types of random loadings (σ_{LIM} = 30 ksi).

165
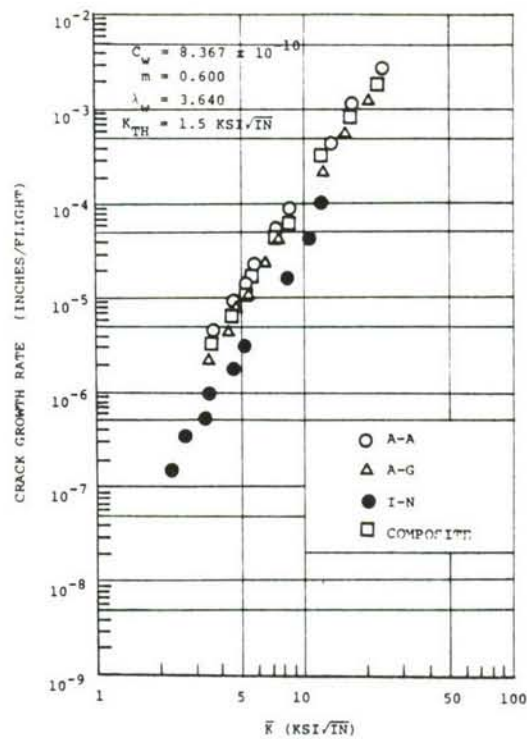
Figure 109. Crack growth rate per flight dc/dF as function of average stress intensity factor $\bar{K}$ for different types of random loadings (σ_{LIM} = 40 ksi).
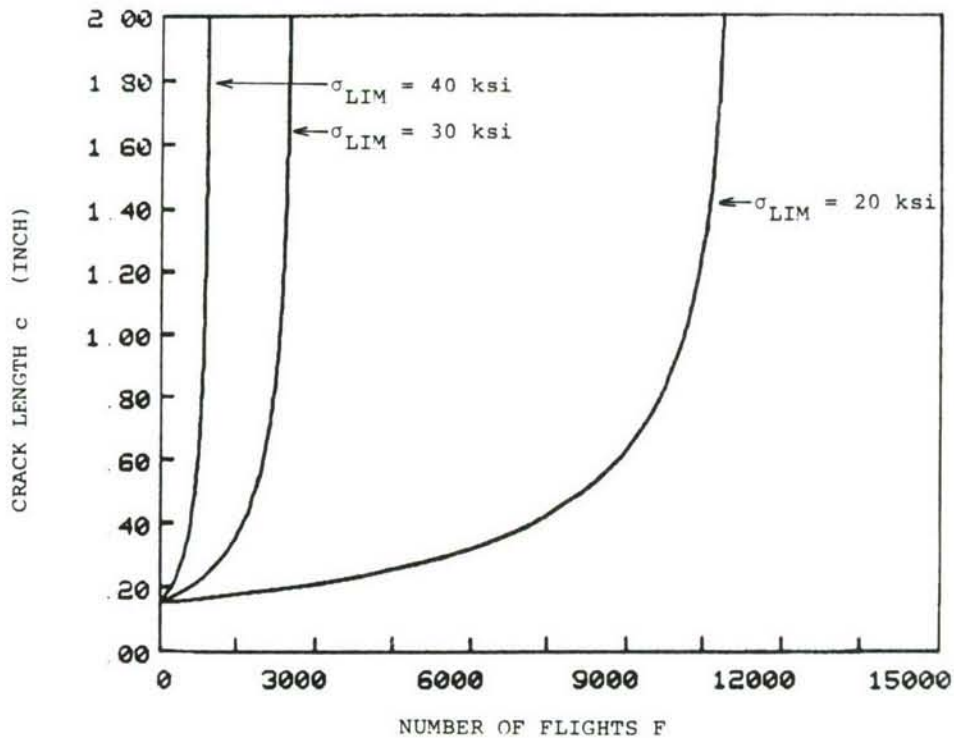
Figure 110. Crack growth as a function of number of flights for random loading (air-to-air, c_0 = 0.155 in.).
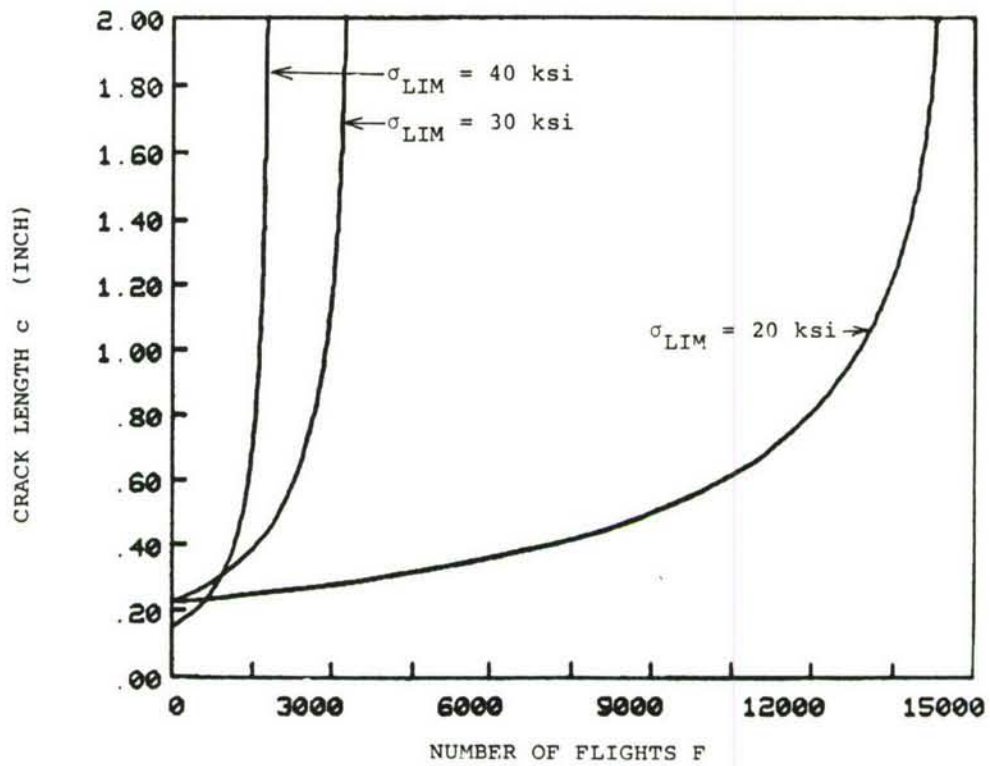
Figure 111. Crack growth as a function of number of flights for random loading (air-to-ground, c_0 = 0.155 and c_0 = 0.23 in.).
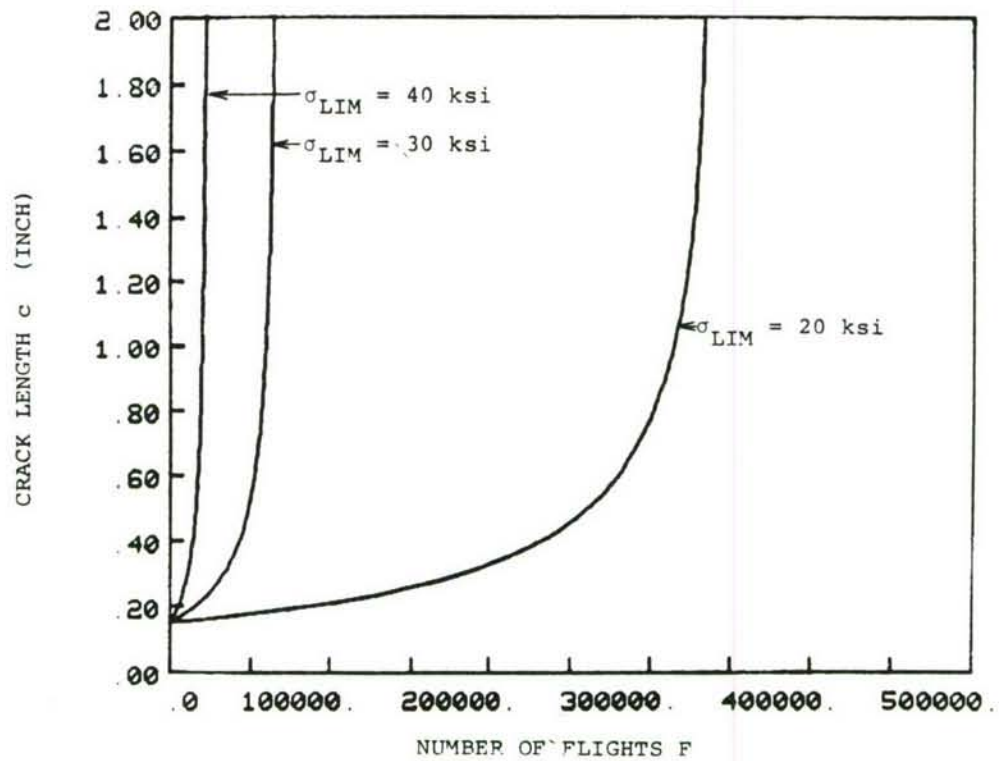
Figure 112. Crack growth as a function of number of flights for random loading (instrumentation and navigation, c_0 = 0.155 in.).

167
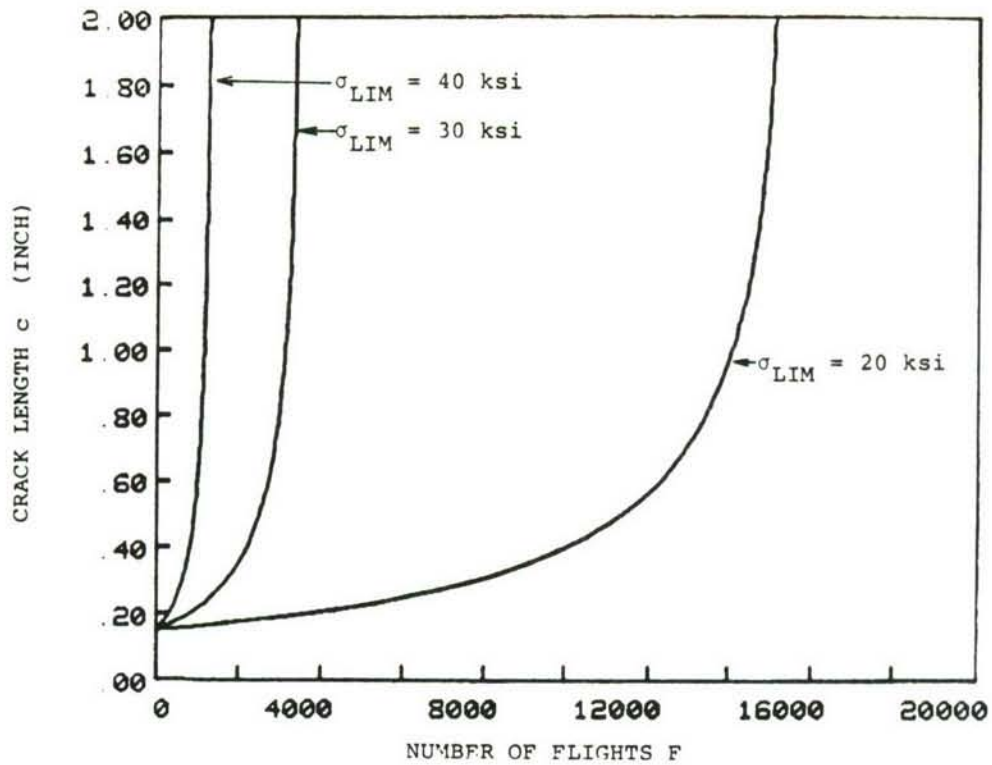
Figure 113. Crack growth as a function of number of flights for random loading (composite, c_0 = 0.155 in.).
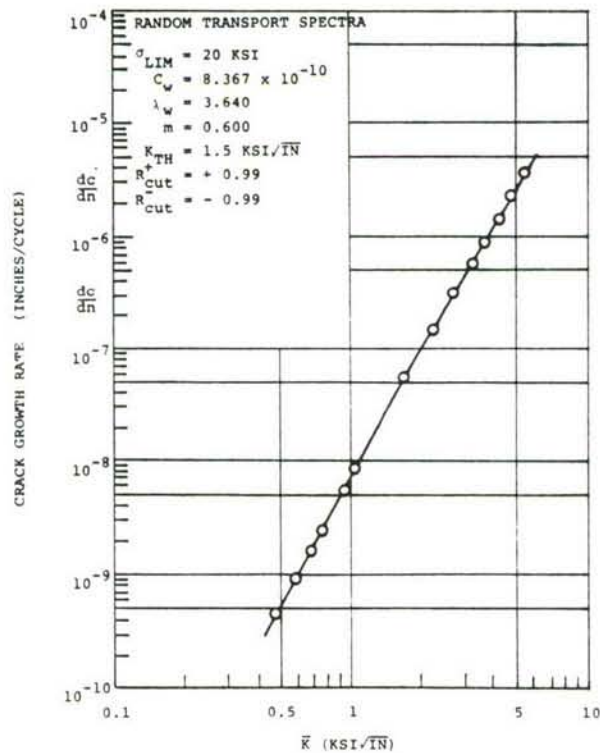
Figure 114. Crack growth rate per cycle dc/dN as a function of average stress intensity factor $\overline{K}$ for random load spectra of transport aircraft.
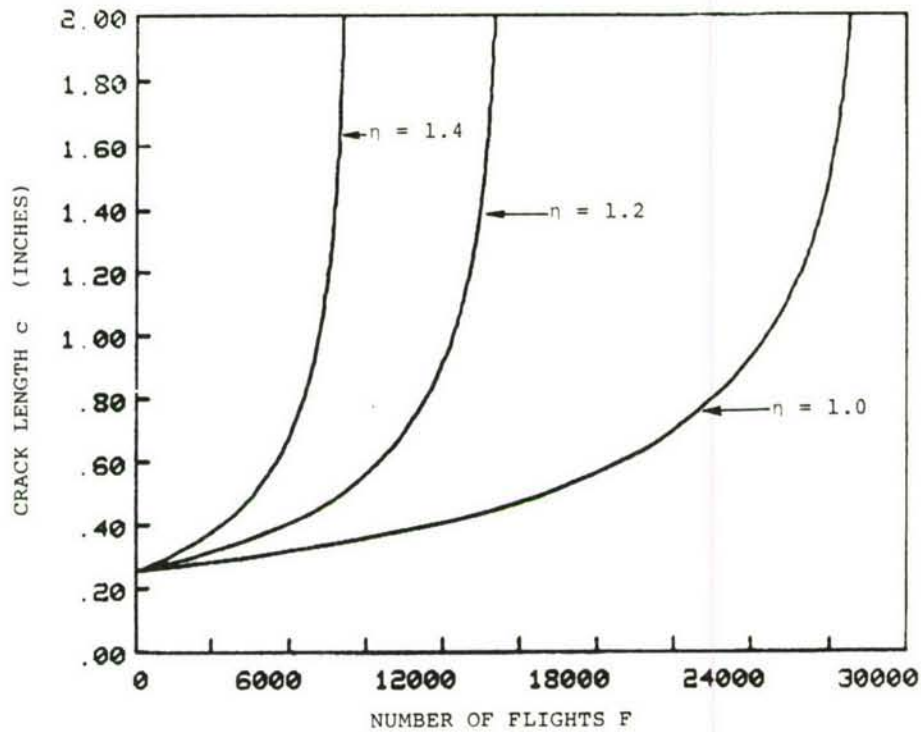
Figure 115.   Crack growth as a function of number of flights
for transport aircraft (c_0 = 0.258 in. σ_{LIM} = 20 ksi).
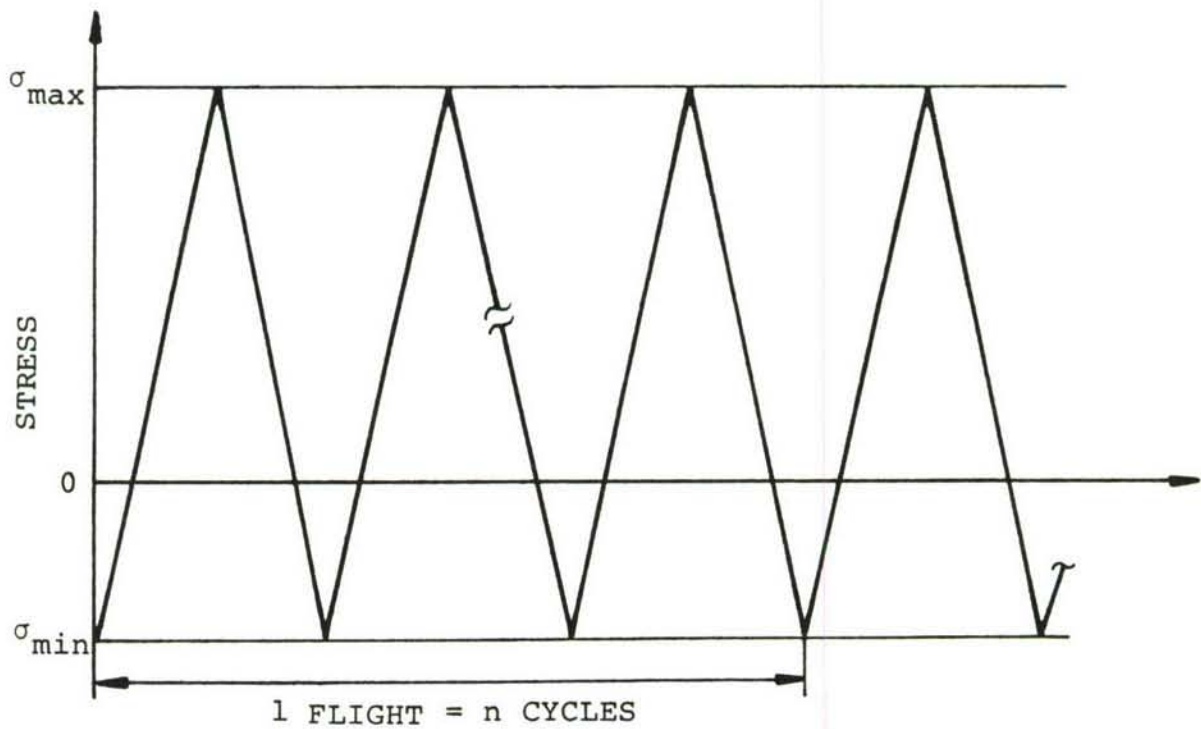
Figure 116.   Constant-amplitude n cycles per flight load spectra.
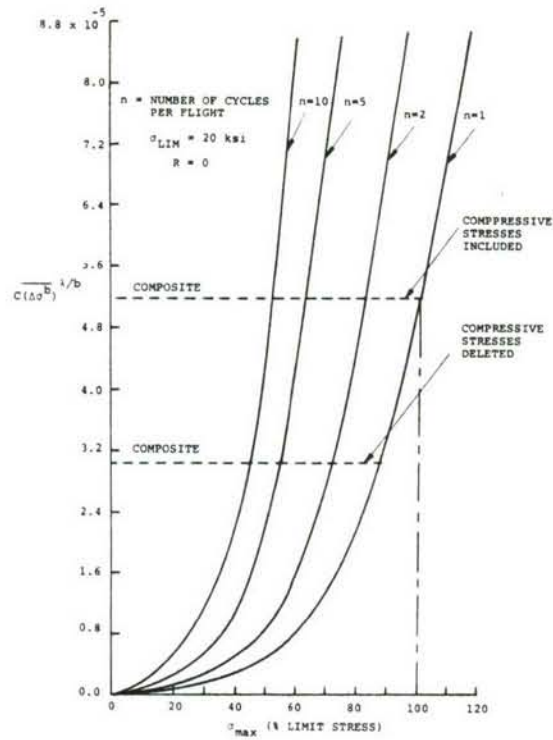
Figure 117. Product C $\overline{(\Delta\sigma^b)}$ $^{\lambda/b}$ for constant amplitude n cycles per flight load spectra (R = 0).
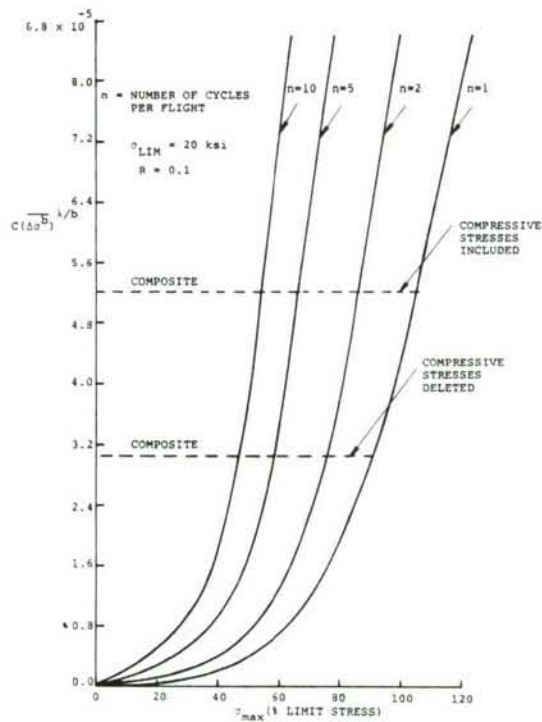
Figure 118. The product $C\overline{(\Delta\sigma^b)}$ $^{\lambda/b}$ for constant amplitude n cycles per flight load spectra (R - 0.1).

170
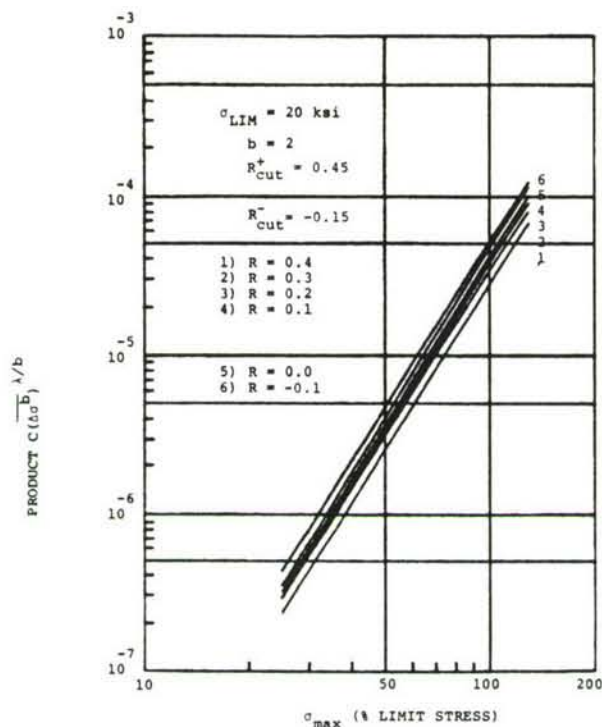
Figure 119. The product $C(\overline{\Delta\sigma^b})^{\lambda/b}$ for constant amplitude loading with compressive stresses included $(\sigma_{LIM} = 20 \text{ ksi})$.
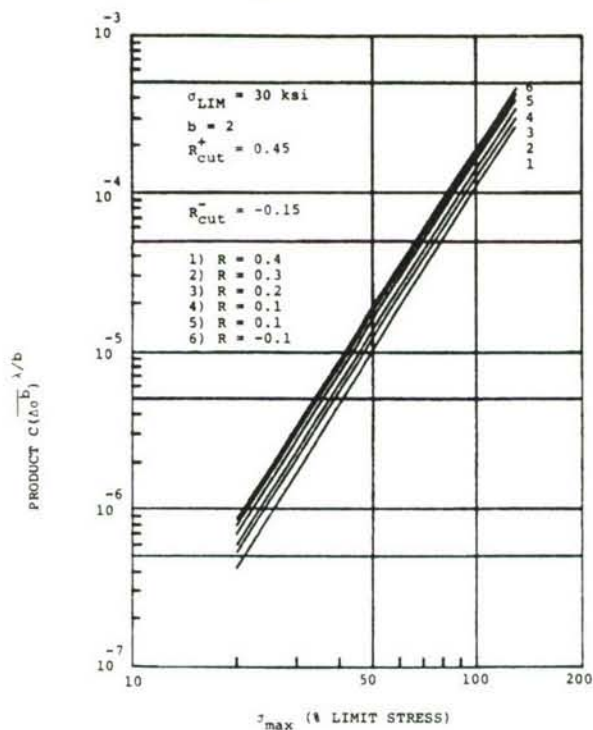
Figure 120. The product $C(\overline{\Delta\sigma^b})^{\lambda/b}$ for constant amplitude loading with compressive stress included $(\sigma_{LIM} = 30 \text{ ksi})$.

171
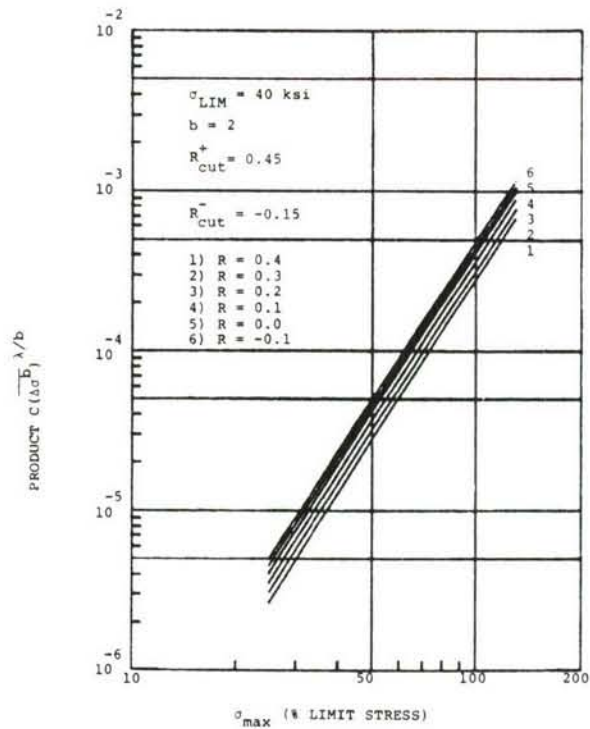
Figure 121. The product $C\overline{(\Delta\sigma^b)}^{\lambda/b}$ for constant amplitude loading with compressive stresses included (σ_{LIM} = 40 ksi).
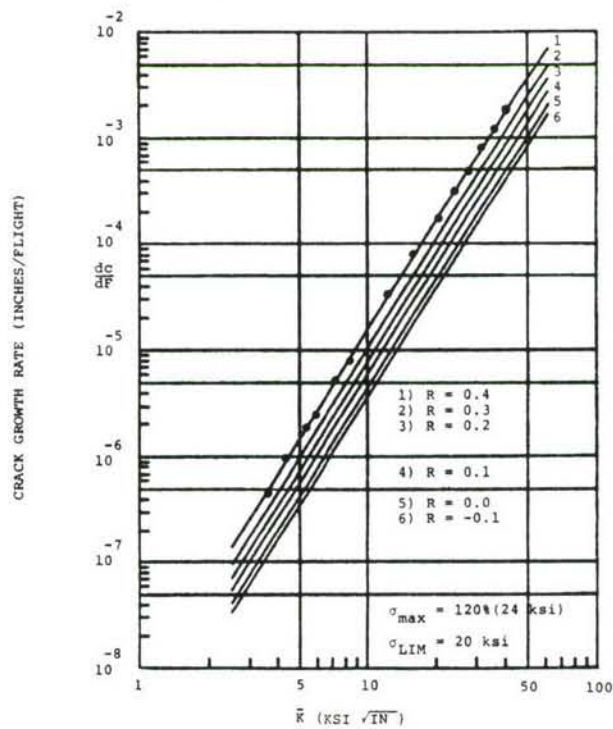
Figure 122. Crack growth rate behavior for constant amplitude loading with compressive stresses included (σ_{max} = 24 ksi, σ_{LIM} = 20 ksi).
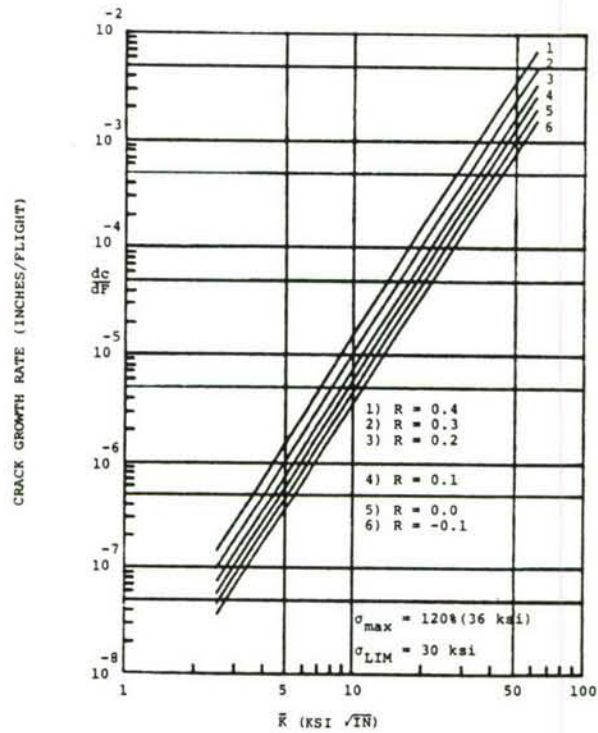
Figure 123. Crack growth rate behavior for constant amplitude loading with compressive stresses included (σ_{max} = 36 ksi, σ_{LIM} = 30 ksi).
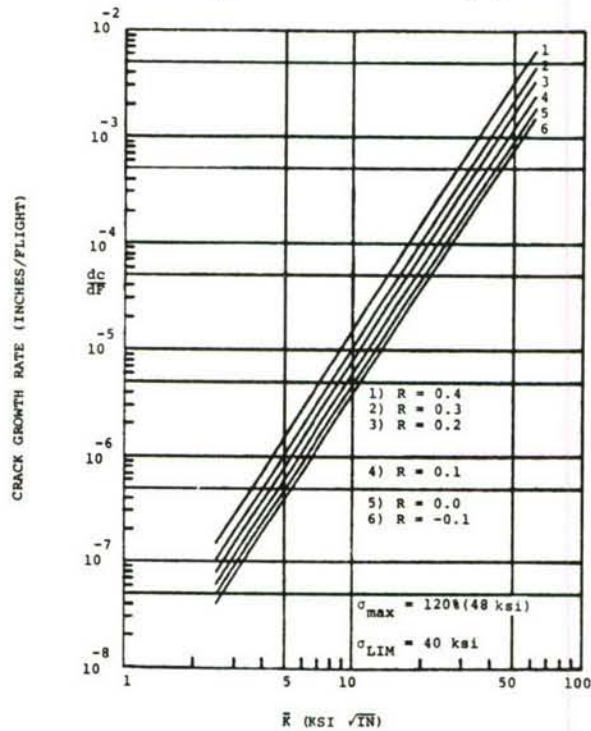
Figure 124. Crack growth rate behavior for constant amplitude loading with compressive stresses included (σ_{max} = 48 ksi, σ_{LIM} = 40 ksi).
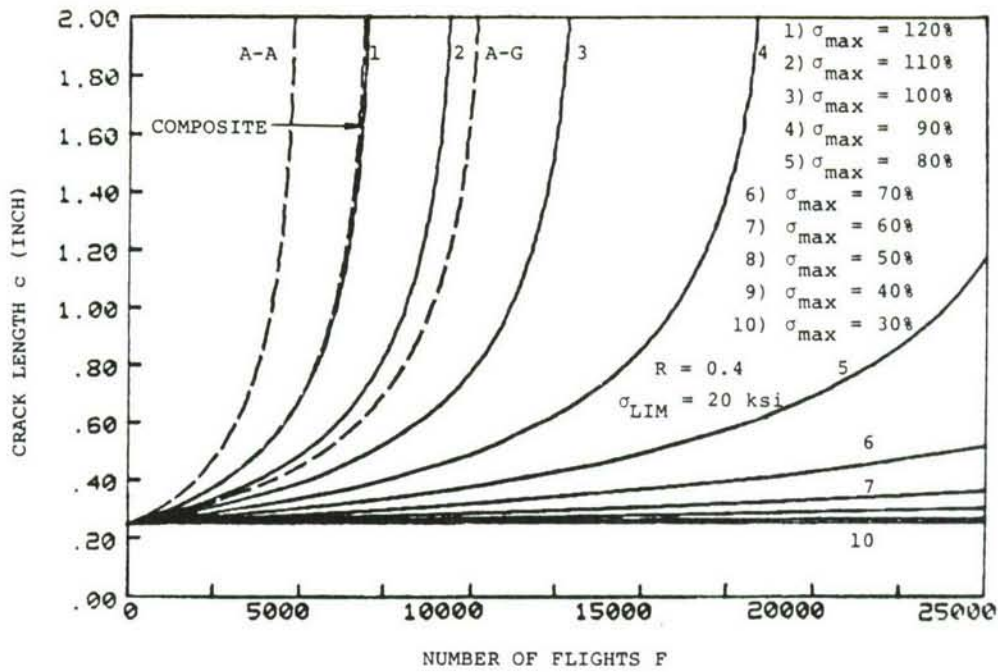
Figure 125. Crack growth as a function of number of flights
for constant amplitude loading (c_0 = 0.25 in., R = 0.4, σ_{LIM} = 20 ksi).
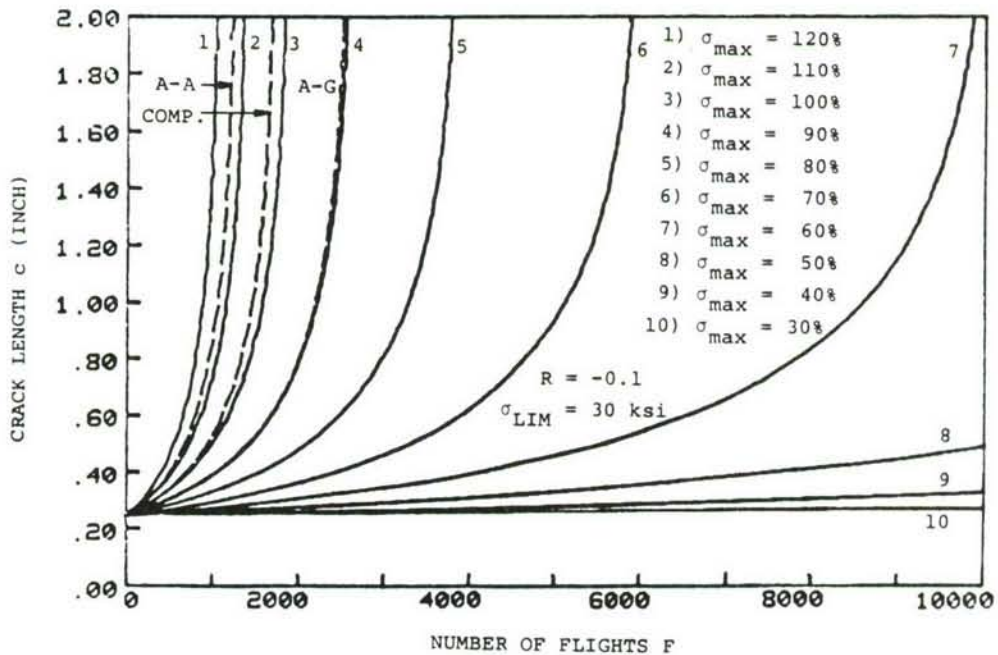
Figure 126. Crack growth as a function of number of flights
for constant amplitude loading (c_0 = 0.25 in., R = -0.1, σ_{LIM} = 30 ksi).

174
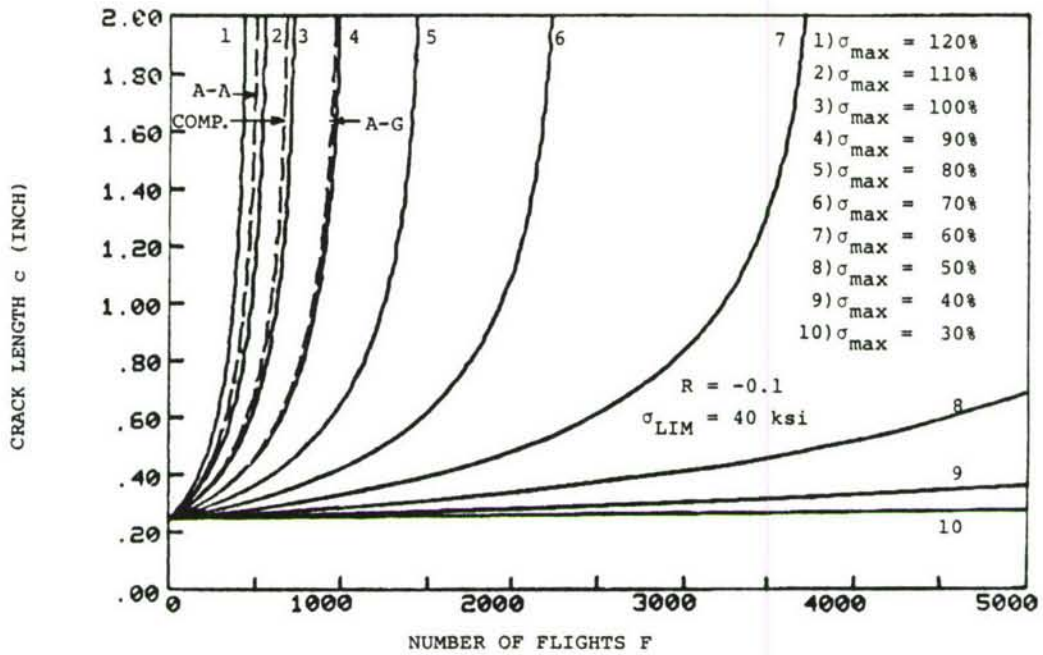
Figure 127. Crack growth as a function of number of flights
for constant amplitude loading ($c_0 = 0.25$ in., R= 0.1, σ_{LIM} = 40 ksi).
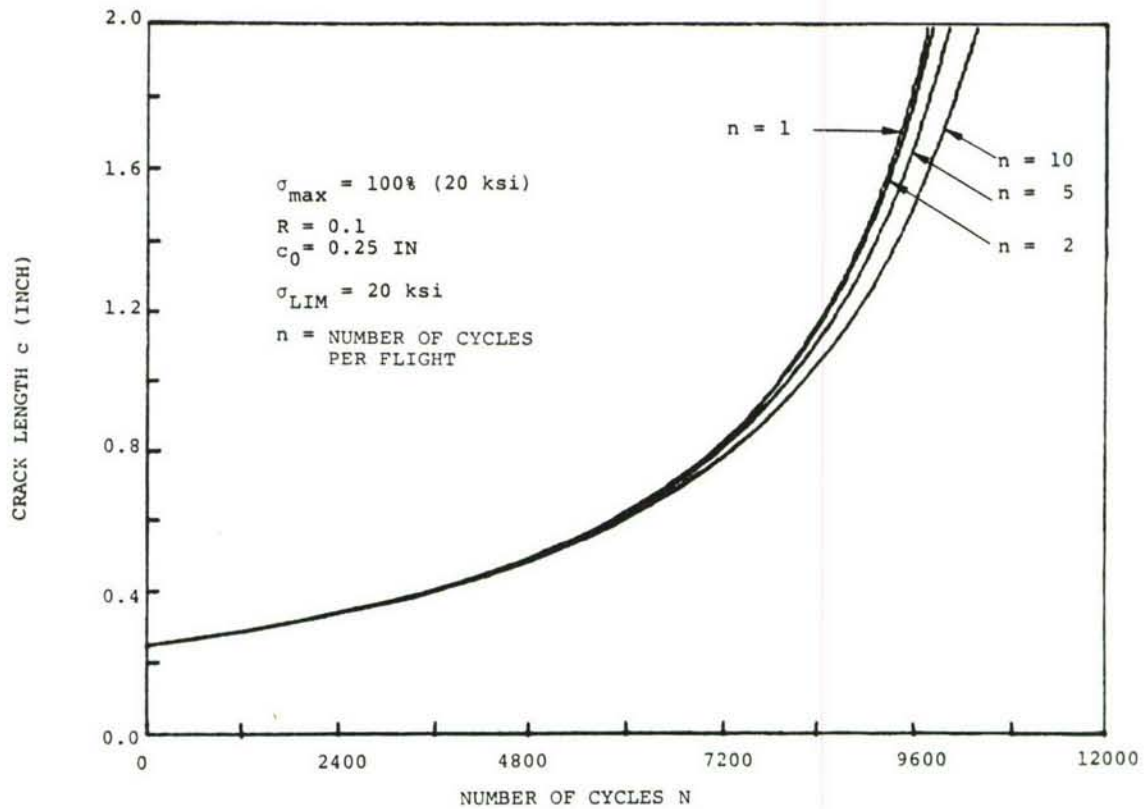
Figure 128. Crack growth as a function of number
of cycles for constant amplitude loading

175

Figure 129.   Simplified amplitude
flight-by-flight load spectra.

Figure 130.   Flight-by-flight, two-step flight load spectra.

176
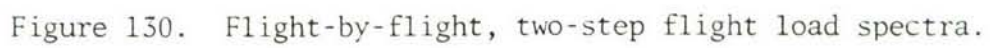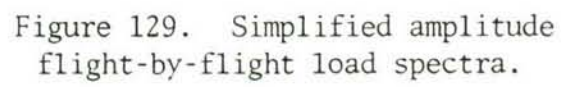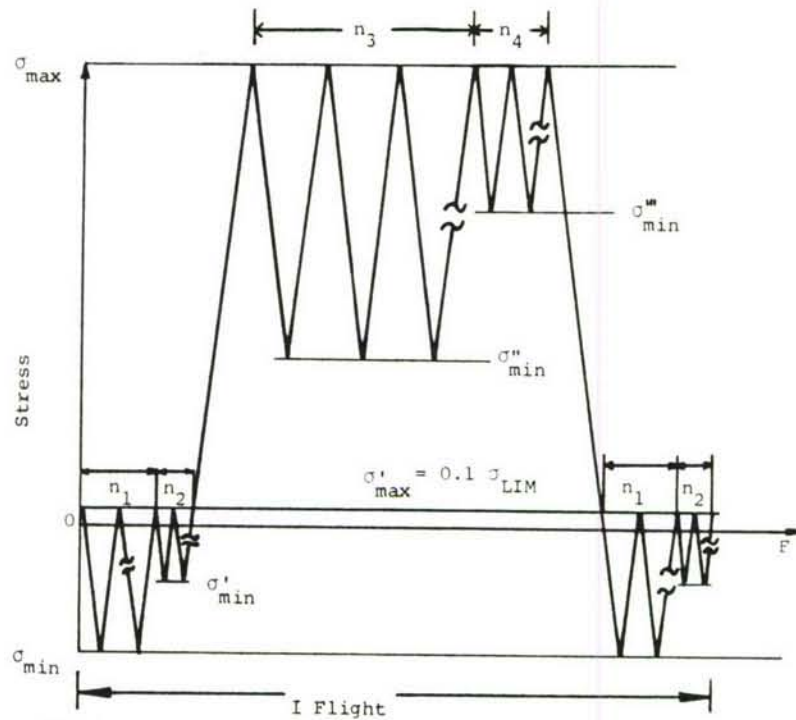
Figure 131. Two-step flight, two-step ground flight-by-flight load spectra.
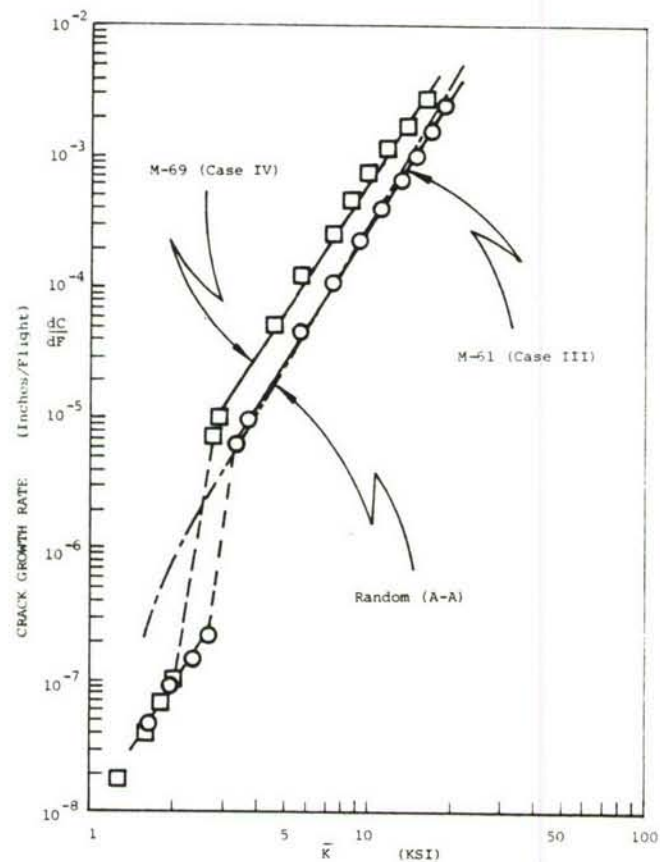
Figure 132. Crack growth rate (M-61, Case III and M-69, Case IV).

177
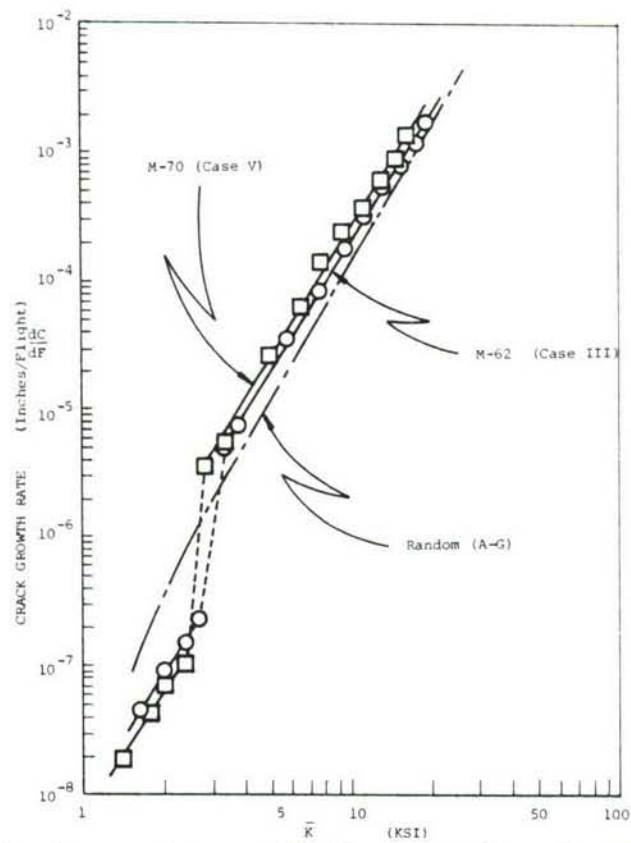
Figure 133. Crack growth rate (M-62, Case III and M-70, Case V).
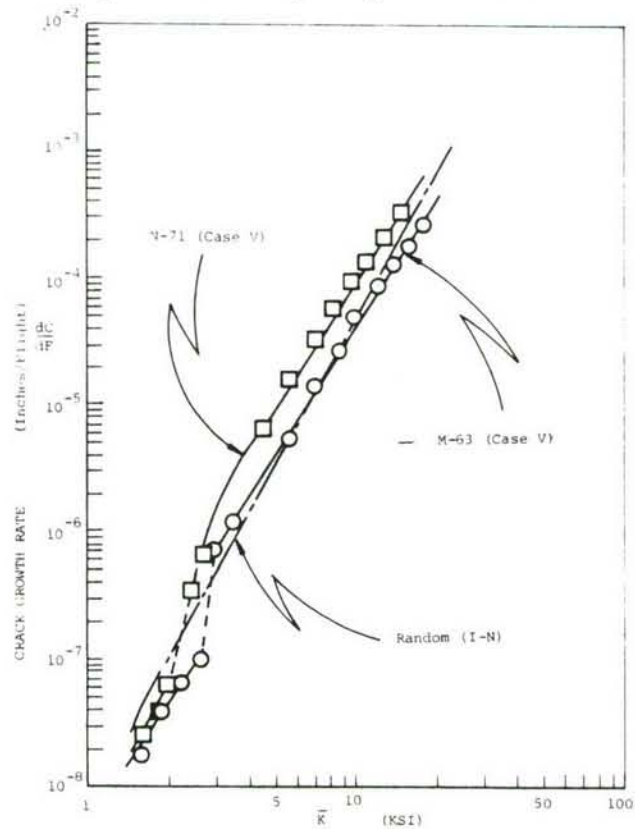
Figure 134. Crack growth rate (M-63, Case V and M-71, Case V).

178
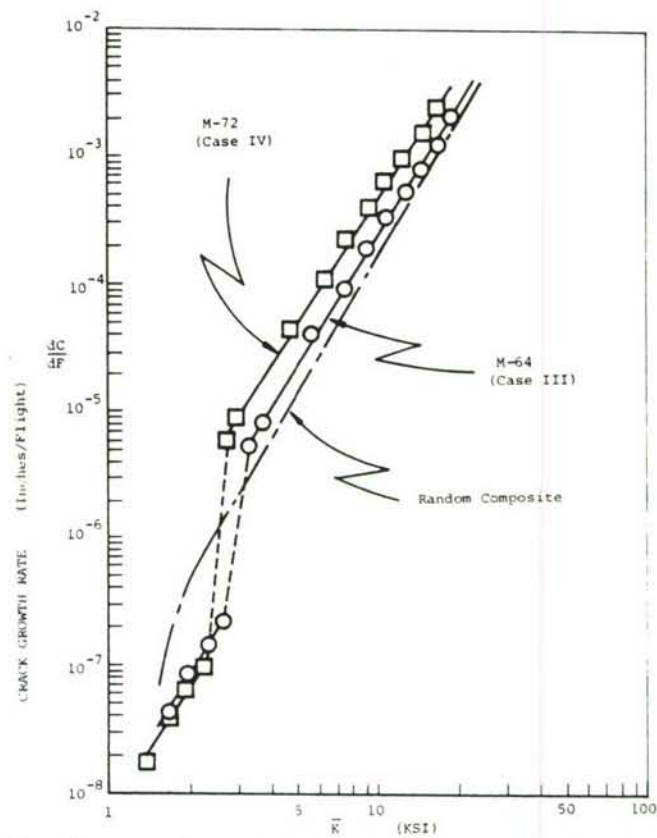
Figure 135. Crack growth rate (M-64, Case III and M-72, Case IV).
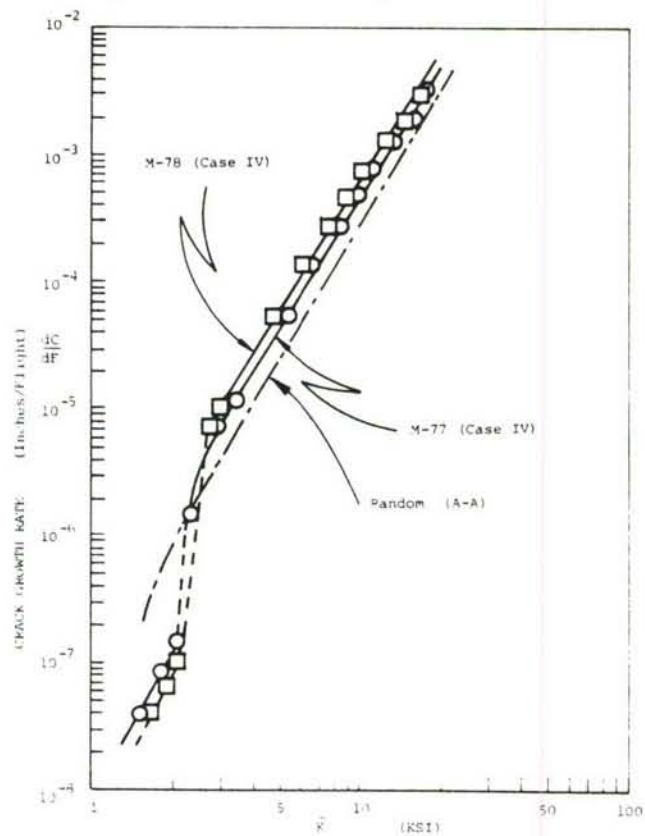
Figure 136. Crack growth rate (M-77, Case IV and M-78, Case IV).

179
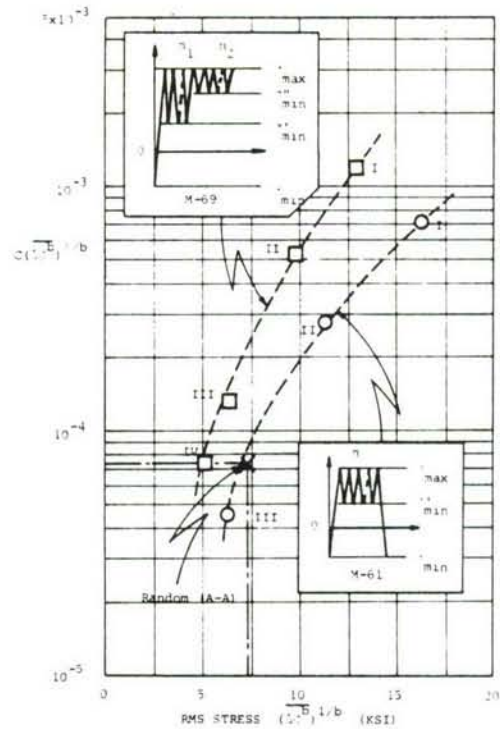
Figure 137. Product $C(\overline{\Delta\sigma^b})^{\lambda/b}$ under load sequences M-62 and M-69 (simplified spectra for air-to-air fighter mission, σ_{LIM} = 20 ksi, b = 2).
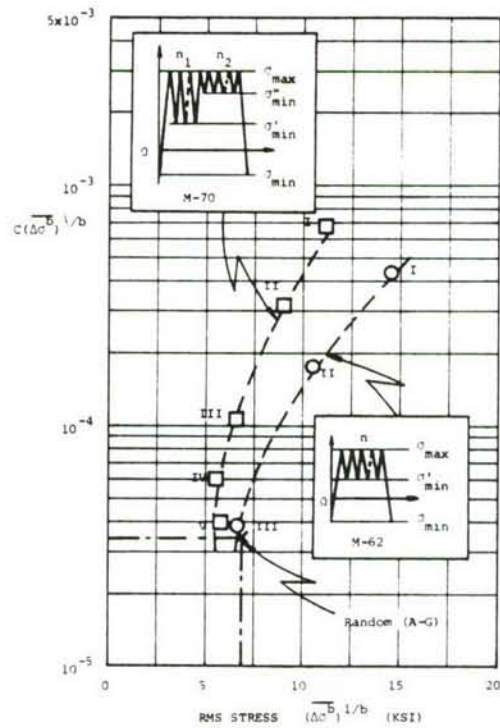
Figure 138. Product $C(\overline{\Delta\sigma^b})^{\lambda/b}$ under load sequences M-62 and M-70 (simplified spectra for air-to-ground fighter mission, σ_{LIM} = 20 ksi, b = 2).
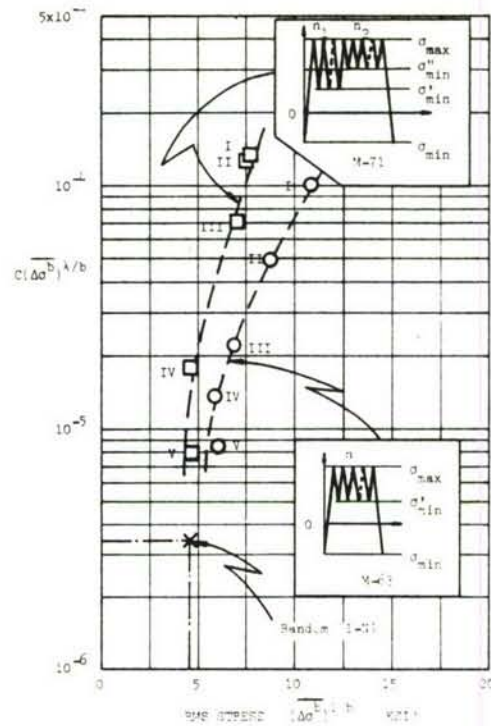
Figure 139. Product $C(\overline{\Delta\sigma^b})^{\lambda/b}$ under load sequences M-63 and M-71 (simplified spectra for instrumentation-and-navigation fighter mission, σ_{LIM} = 20 ksi, b = 2).
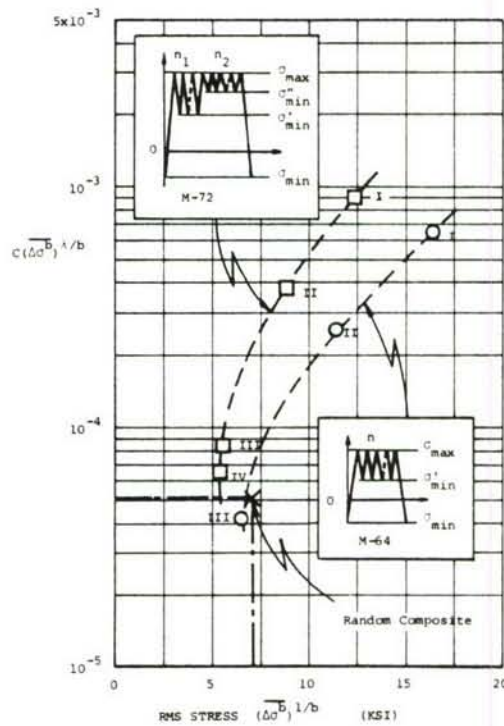
Figure 140. Product $C(\overline{\Delta\sigma^b})^{\lambda/b}$ under load sequences M-64 and M-72 (simplified spectra for composite fighter mission, σ_{LIM} = 20 ksi, b = 2).

181

Figure 141. Product $C(\overline{\Delta\sigma^b})^{\lambda/b}$ under load sequences M-77 and M-78 (simplified spectra for typical fighter mission, σ_{LIM} = 20 ksi, b = 2).

Figure 142. Crack growth as a function of number of flights for simplified spectra loading (M-61, c_0 =0.155 in.).
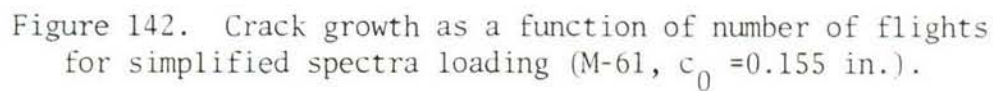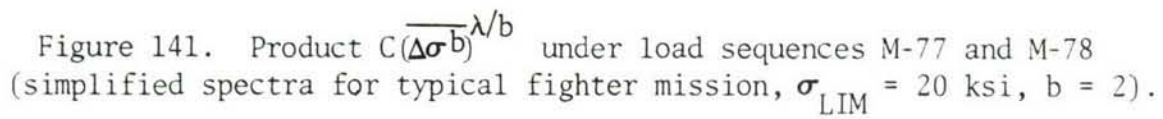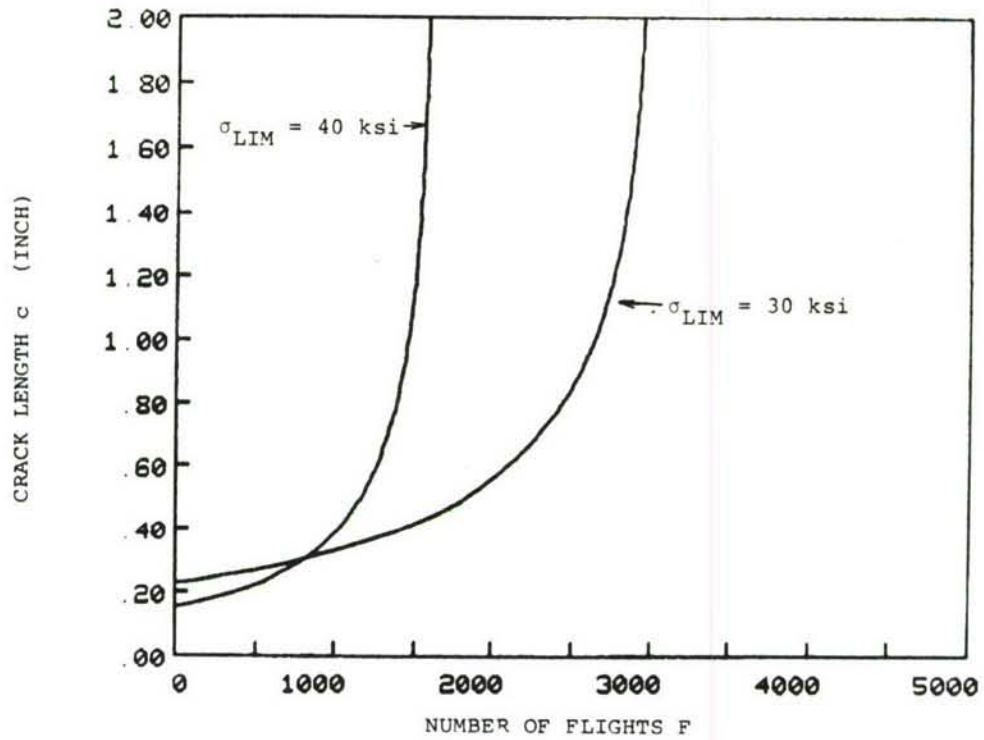
Figure 143. Crack growth as a function of number of flights
for simplified spectra loading (M-62, c_0 = 0.155 in. and c_0 = 0.23 in.).
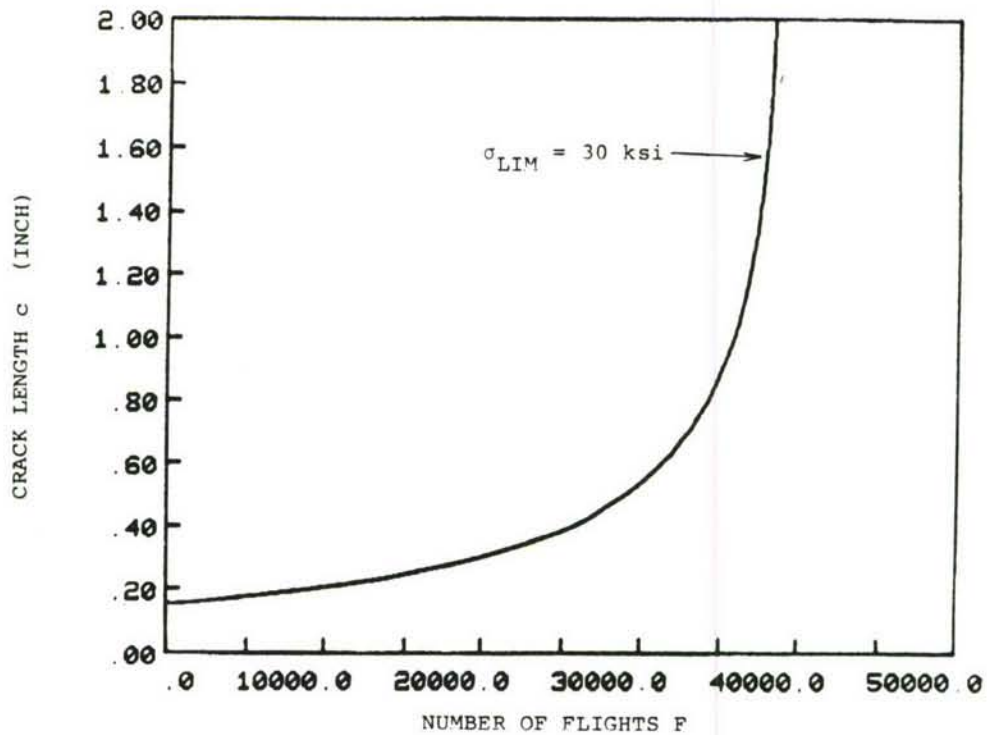
Figure 144. Crack growth as a function of number of flights
for simplified spectra loading (M-63, c_0 = 0.155 in.).

183
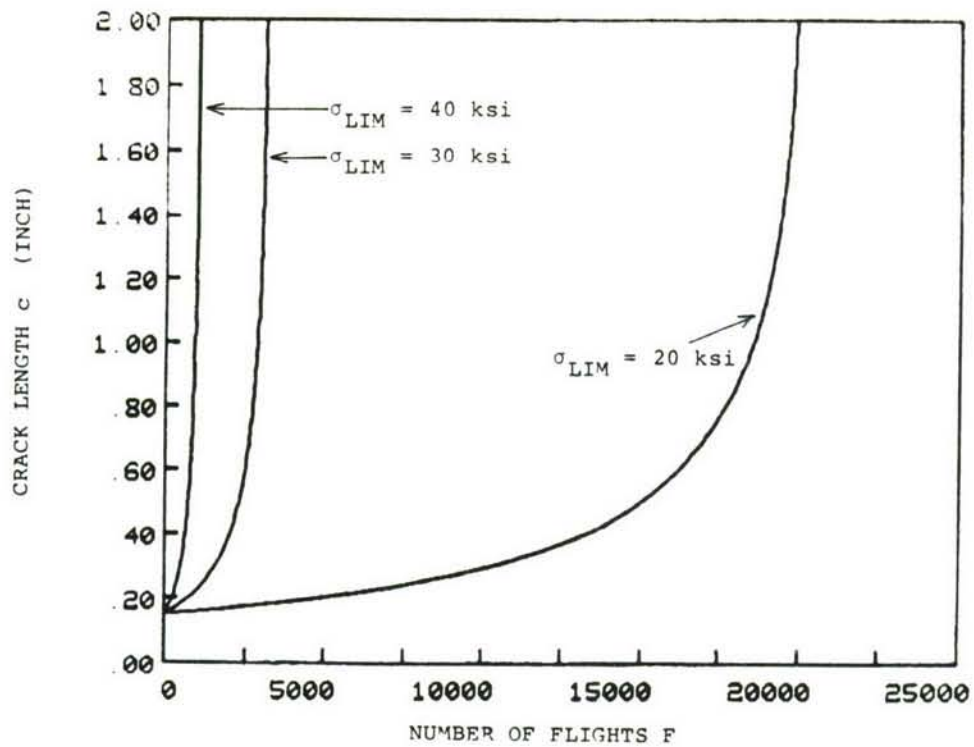
Figure 145. Crack growth as a function of number of flights for simplified spectra loading (M-64, c_0 = 0.155 in.).
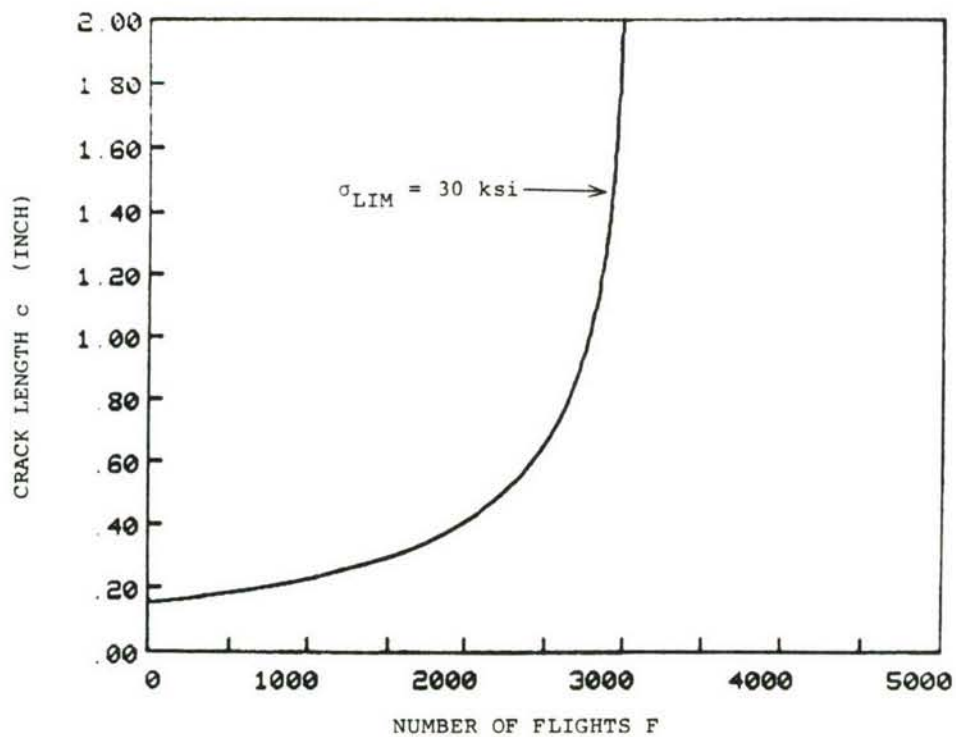
Figure 146. Crack growth as a function of number of flights for simplified spectra loading (M-69, c_0 = 0.155 in.).

184
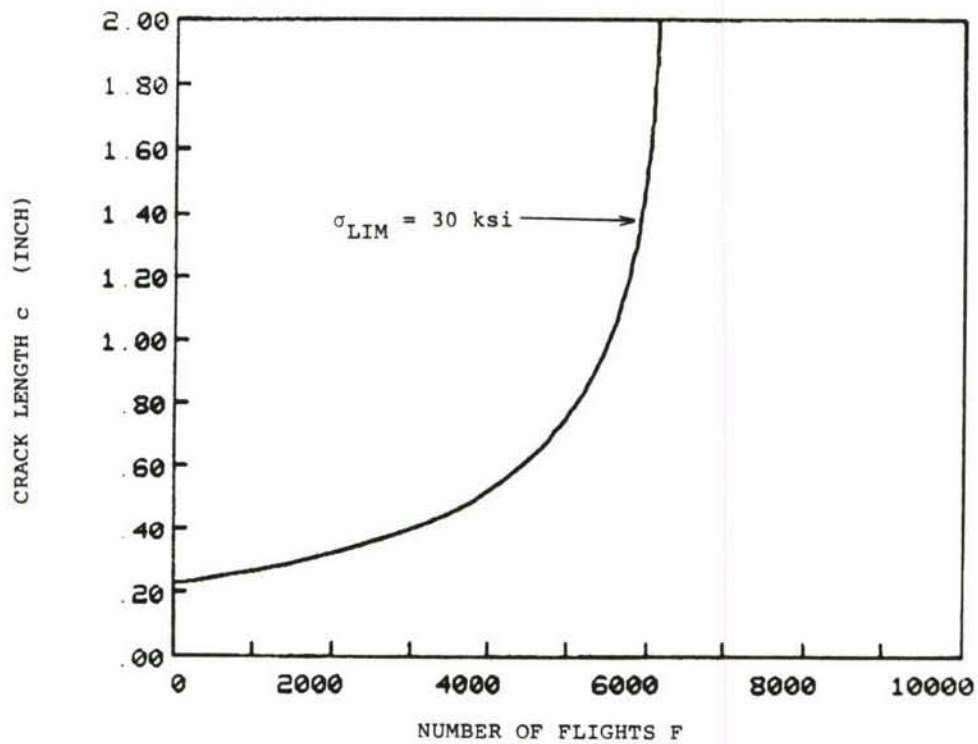
Figure 147. Crack growth as a function of number of flights for simplified spectra loading (M-70, $c_0 = 0.155$ in.).
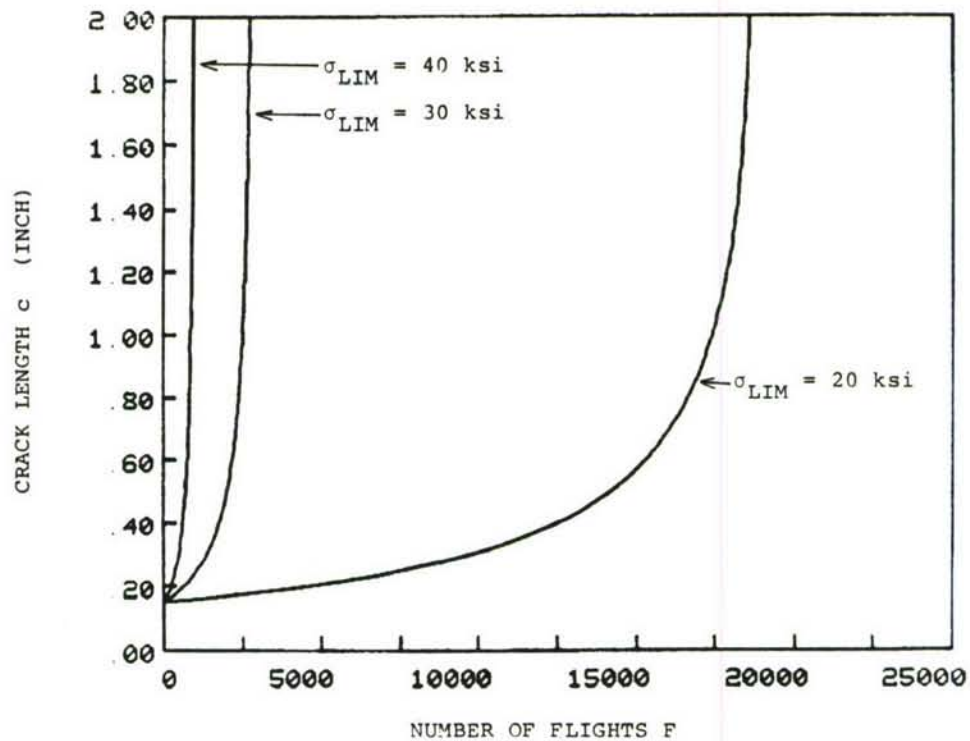
Figure 148. Crack growth as a function of number of flights for simplified spectra loading (M-72, $c_0 = 0.155$ in.).
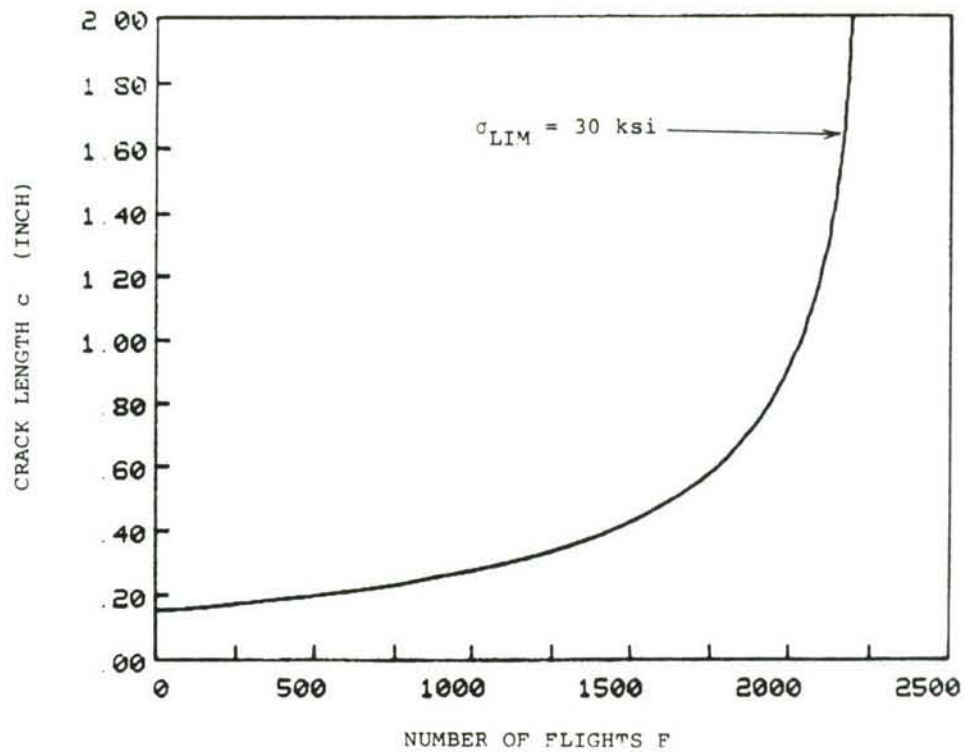
Figure 149. Crack growth as a function of number of flights for simplified spectra loading (M-77, $c_0 = 0.155$ in.).
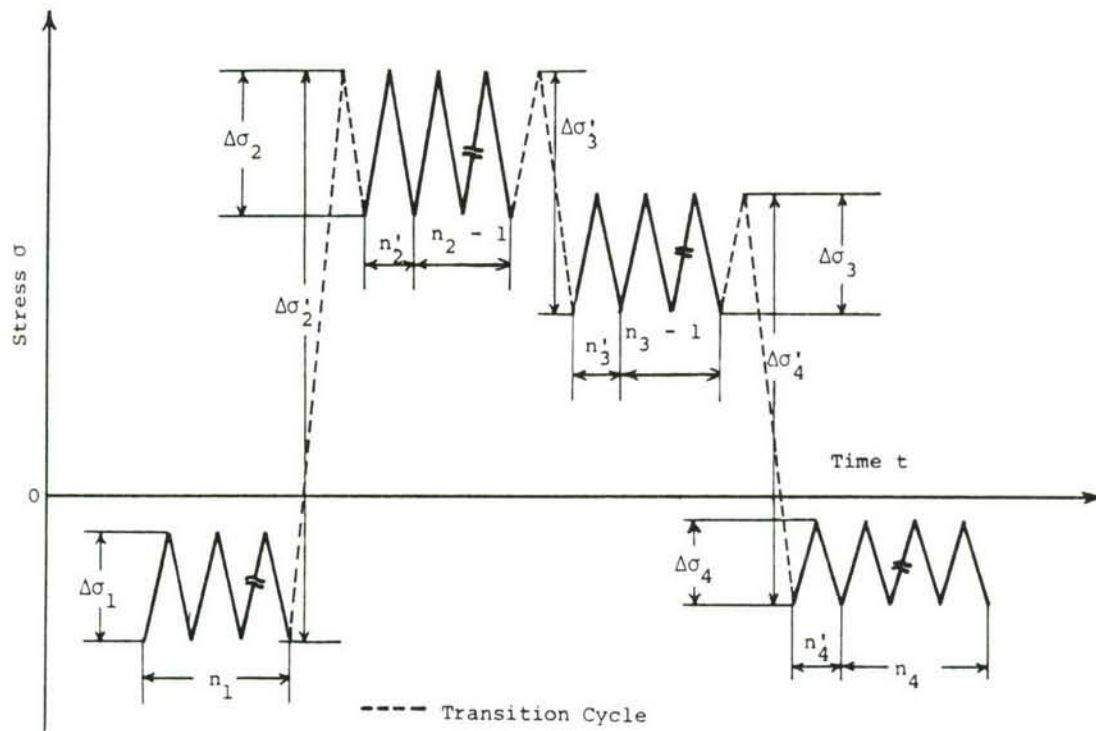
Figure 150. Simplified load spectra for a transport-type aircraft.

186
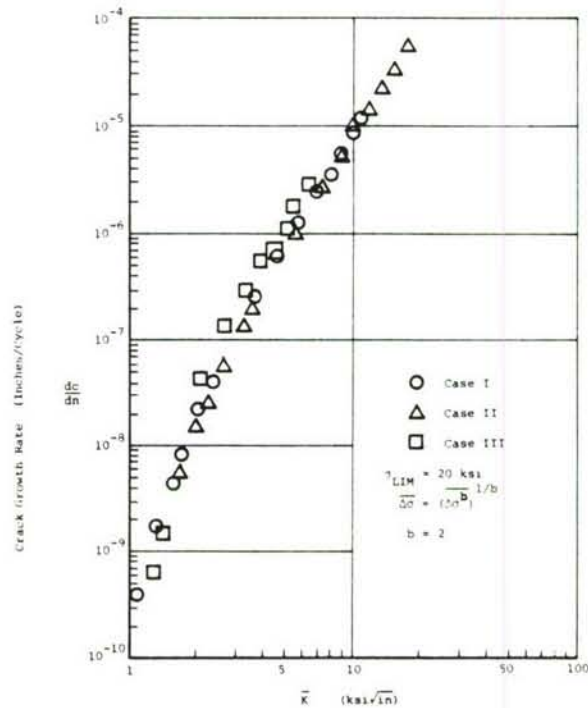
Figure 151. Crack growth rate behavior under random loading with compressive stresses included for average stress ratio $\overline{R} = 0$. ($\sigma_{LIM} = 20$ ksi, $\overline{\Delta\sigma}$ = RMS stress range).
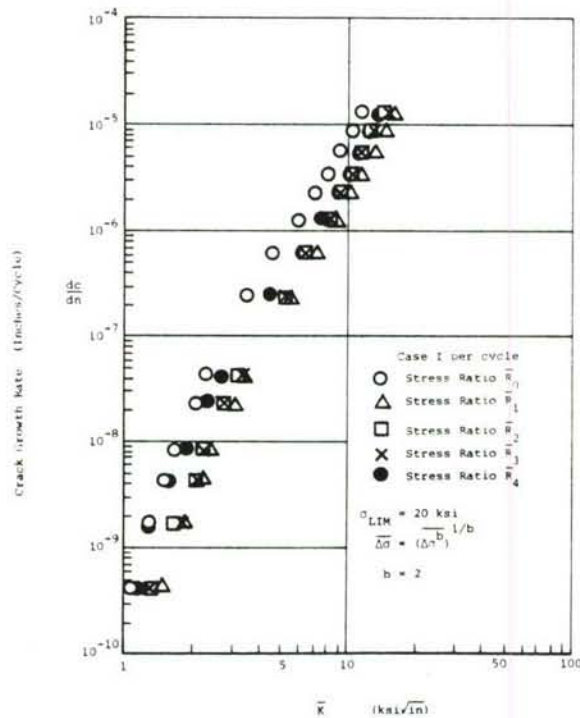
Figure 152. Crack growth rate per cycle dc/dN as a function of average stress intensity factor $\overline{K}$ under different definitions of average stress ratio $\overline{R}$ for Case I ($\sigma_{LIM} = 20$ ksi, $\overline{\Delta\sigma}$ = RMS stress range).

187
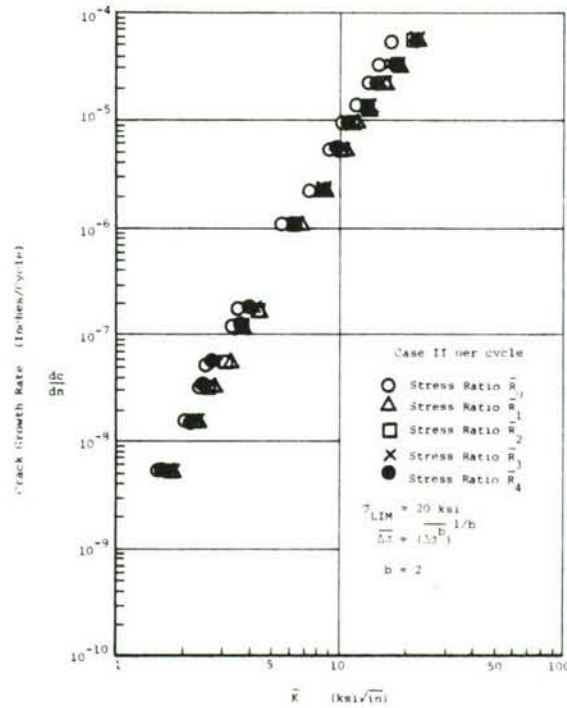
Figure 153. Crack growth rate per cycle dc/dN as a function of average stress intensity factor $\bar{K}$ under different definitions of average stress ratio $\bar{R}$ for Case II (σ_{LIM} = 20 ksi, $\overline{\Delta\sigma}$ = RMS stress range).
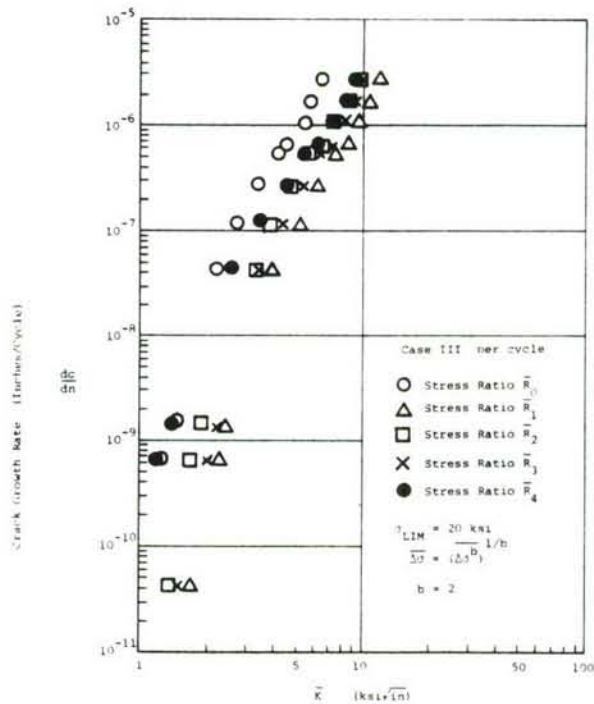
Figure 154. Crack growth rate per cycle dc/dN as a function of average stress intensity factor $\bar{K}$ under different definitions of average stress ratio $\bar{R}$ for Case III (σ_{LIM} = 20 ksi, $\overline{\Delta\sigma}$ = RMS stress range).

188
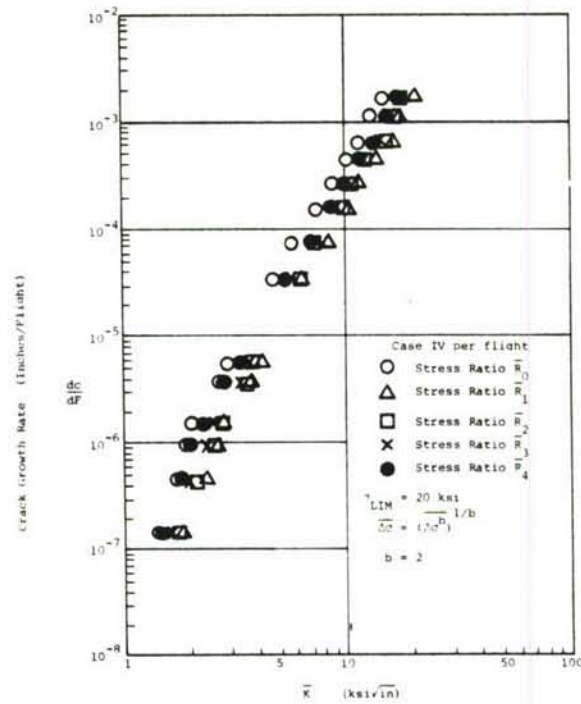
Figure 155. Crack growth rate per flight dc/dF as a function of average stress intensity factor $\bar{K}$ under different definitions of average stress ratio $\bar{R}$ for Case IV (composite flight spectra, σ_{LIM} = 20 ksi).
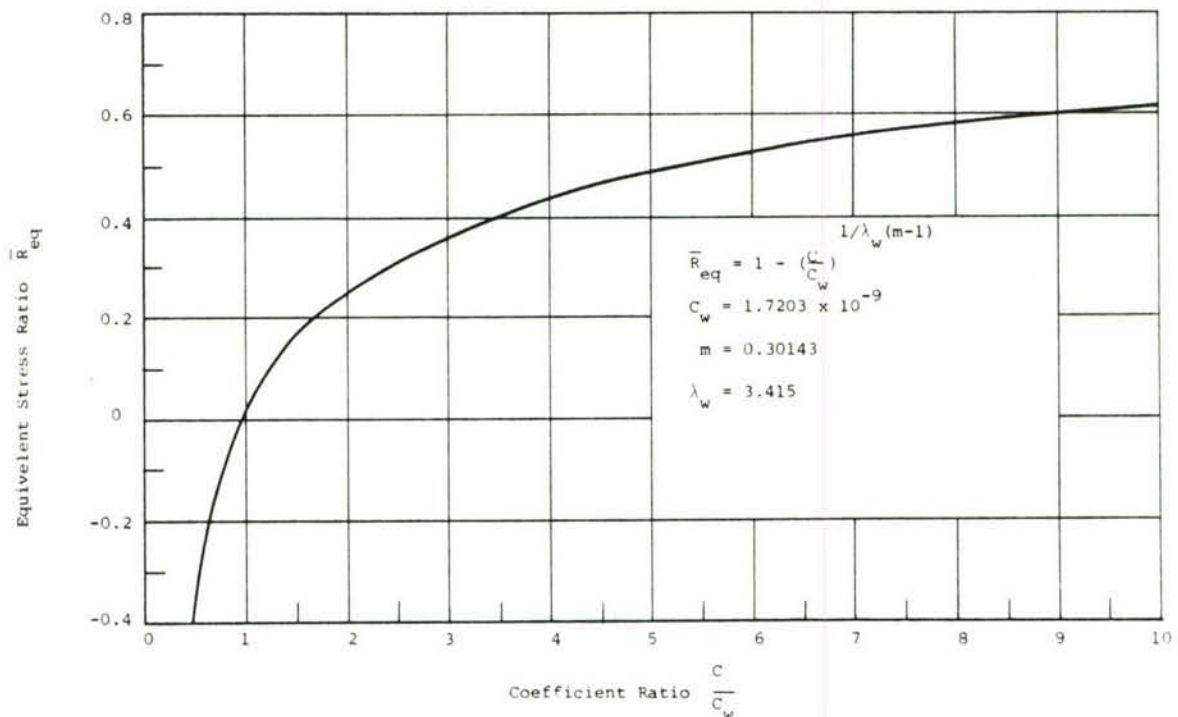
Figure 156. Equivalent average stress ratio $\bar{R}_{eq}$ as a function of coefficient ratio C/C_W, where C = estimated constant by unitblock approach, and C_W = constant in Walker's Equation.

189
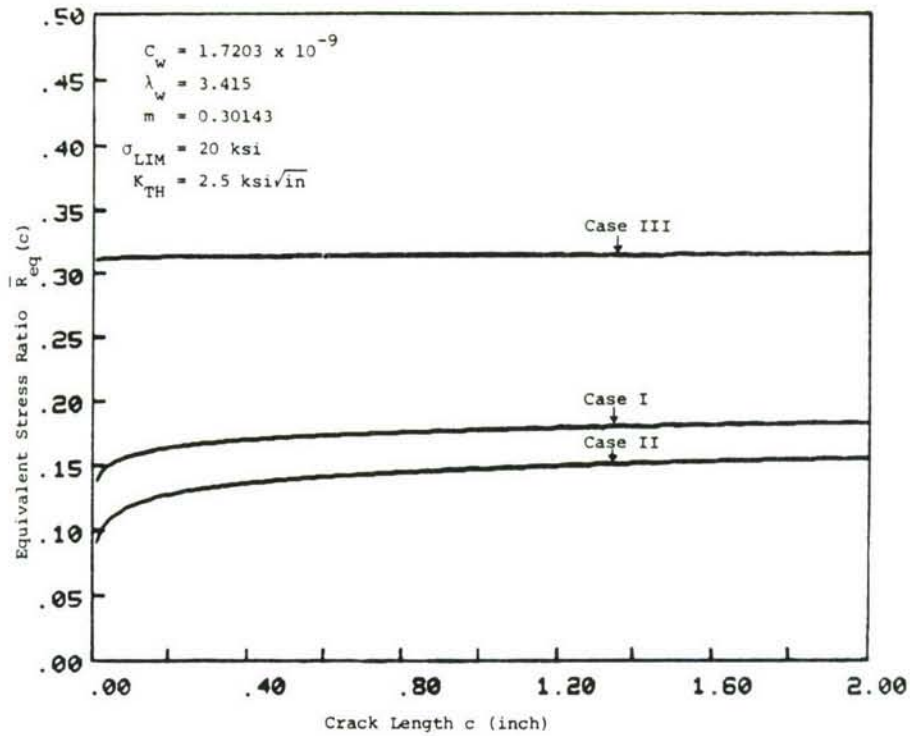
Figure 157. Equivalent stress ratio $\overline{R}_{eq}$ (c) for random loading.
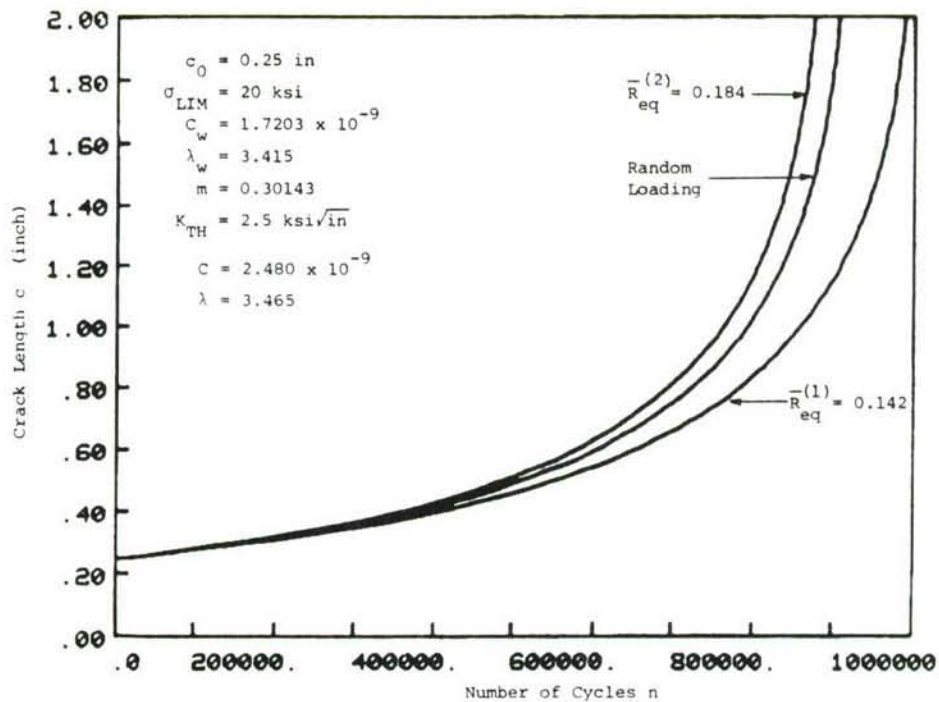
Figure 158. Crack growth as a function of number of cycles (Case I).

190
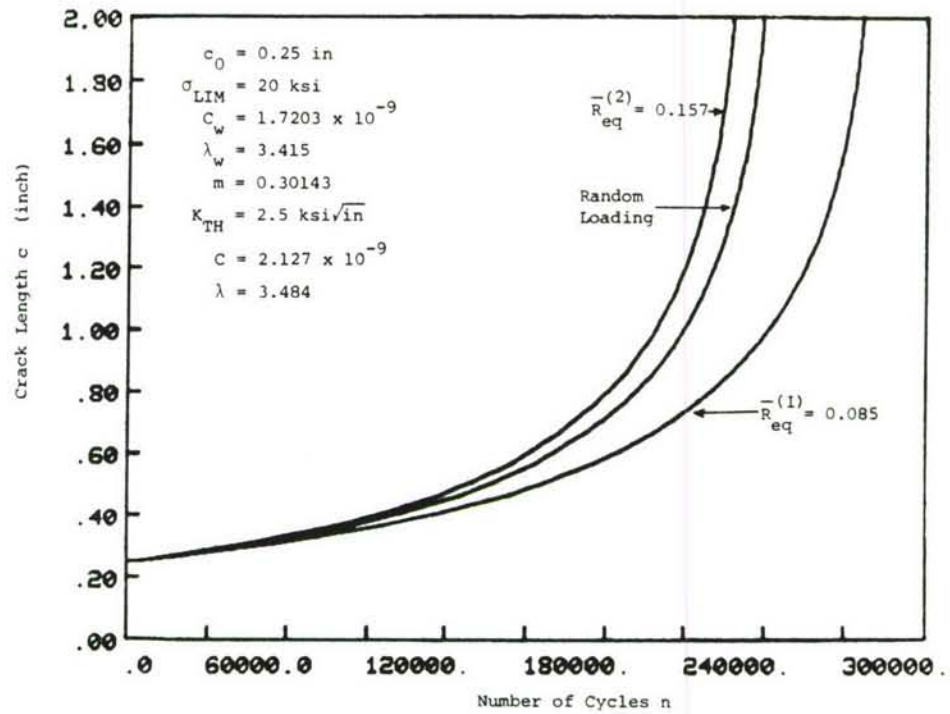
Figure 159. Crack growth as a function of number of cycles (Case II).
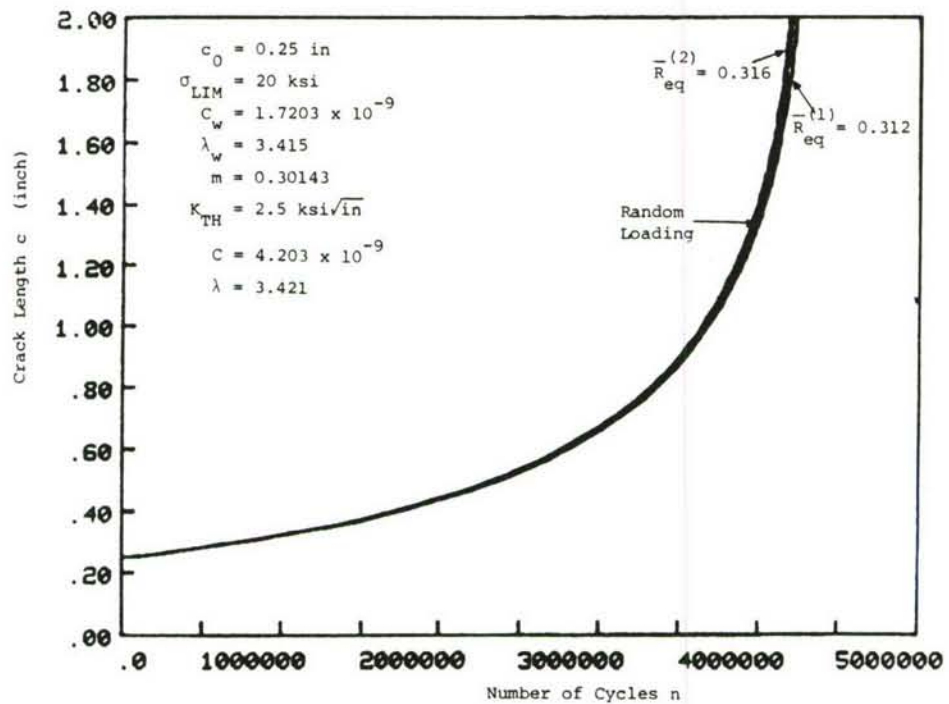
Figure 160. Crack growth as a function of number of cyles (Case III).

191
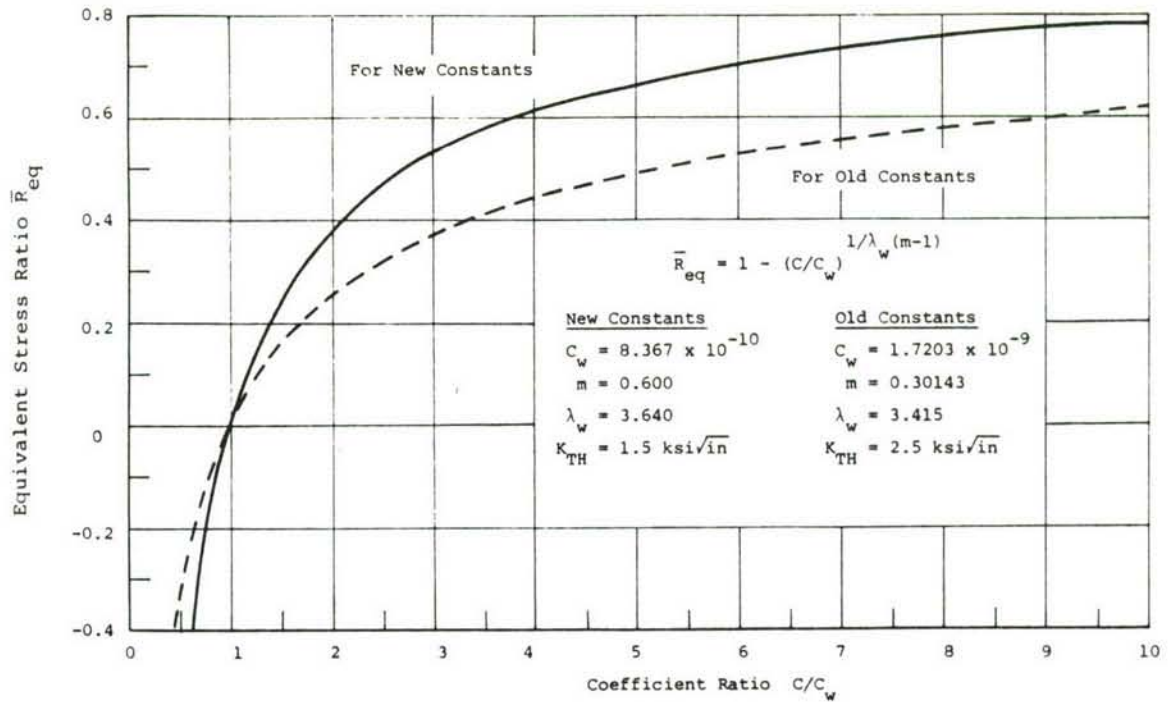
Figure 161. Equivalent average stress ratio $\overline{R}_{eq}$ as a function of coefficient ratio C/C_W where C = estimated constant by unitblock approach, and C_W = constant in Walker's Equation (two sets of constants).
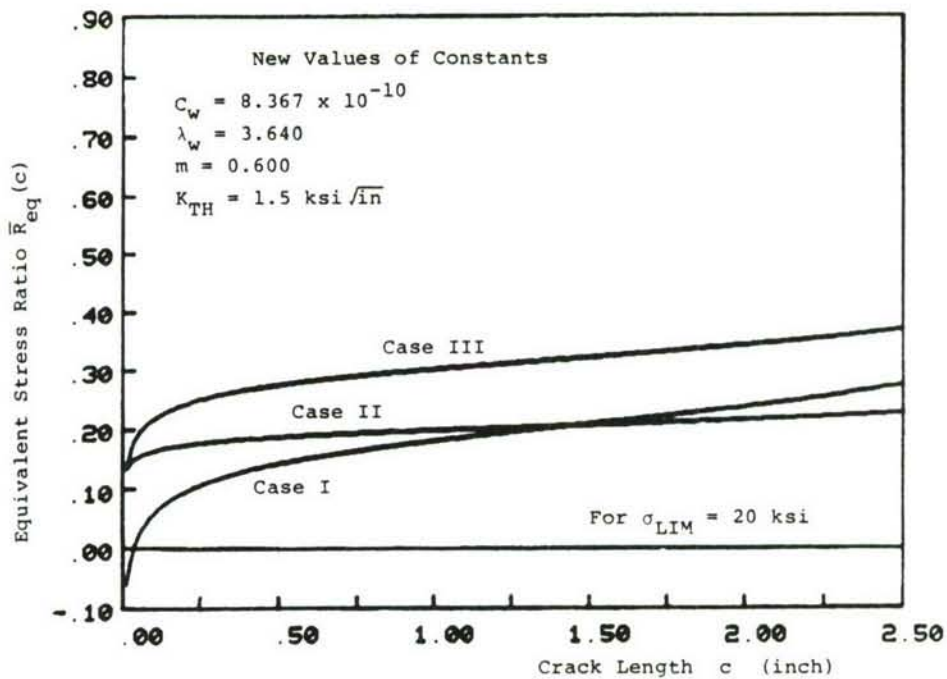
Figure 162. Equivalent stress ratio $\overline{R}_{eq}$ (c) as a function of crack length c for random loading (σ_{LIM} = 20 ksi, for new constants).
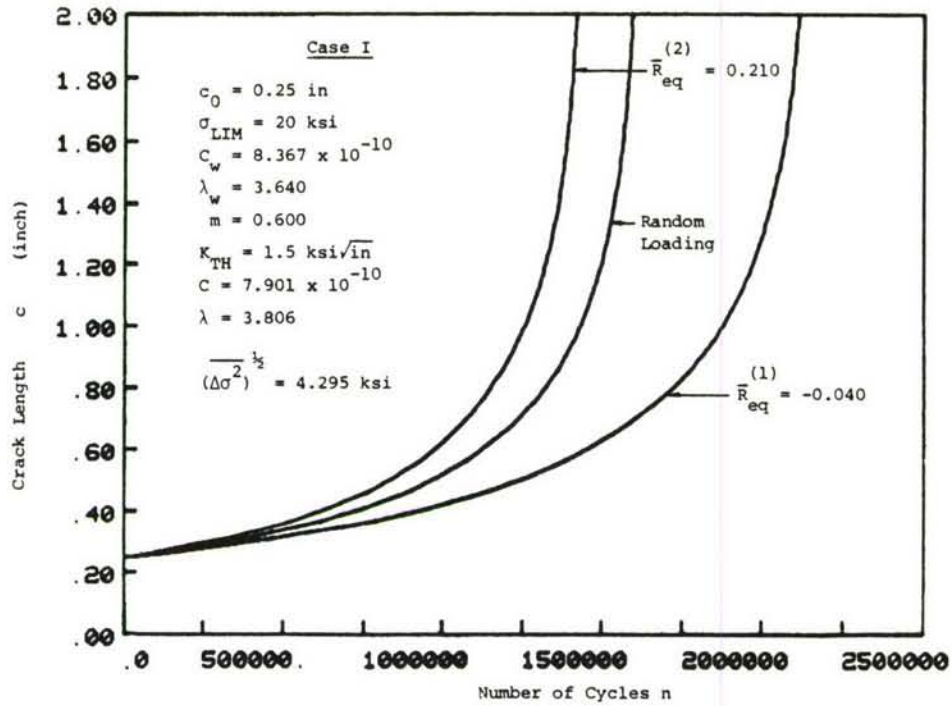
Figure 163. Crack growth as a function of number of cycles (Case I, for new values of constants).
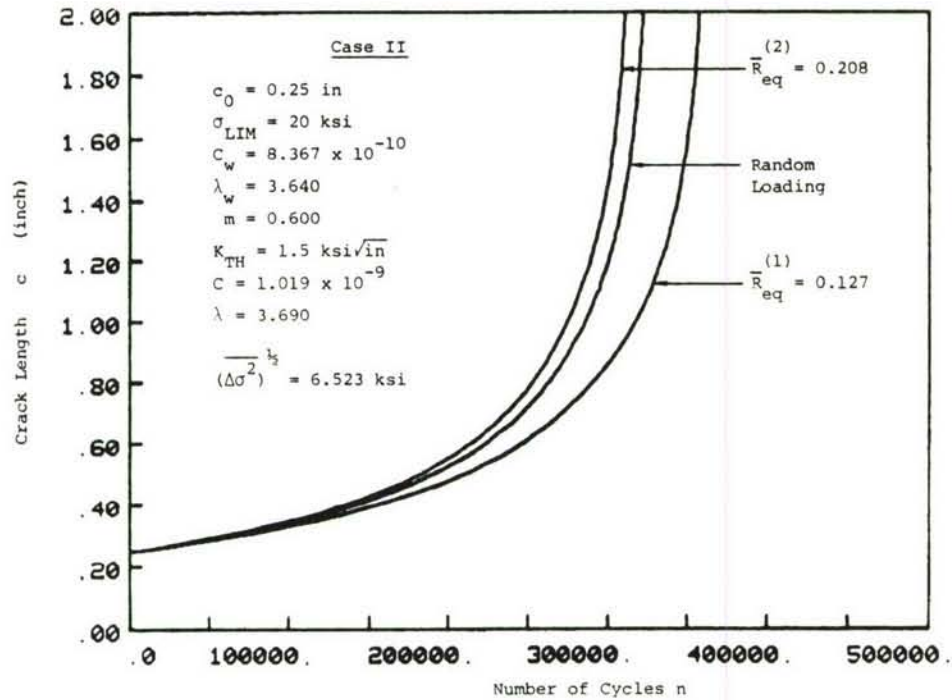
Figure 164. Crack growth as a function of number of cycles (Case II, for new values of constants).

193
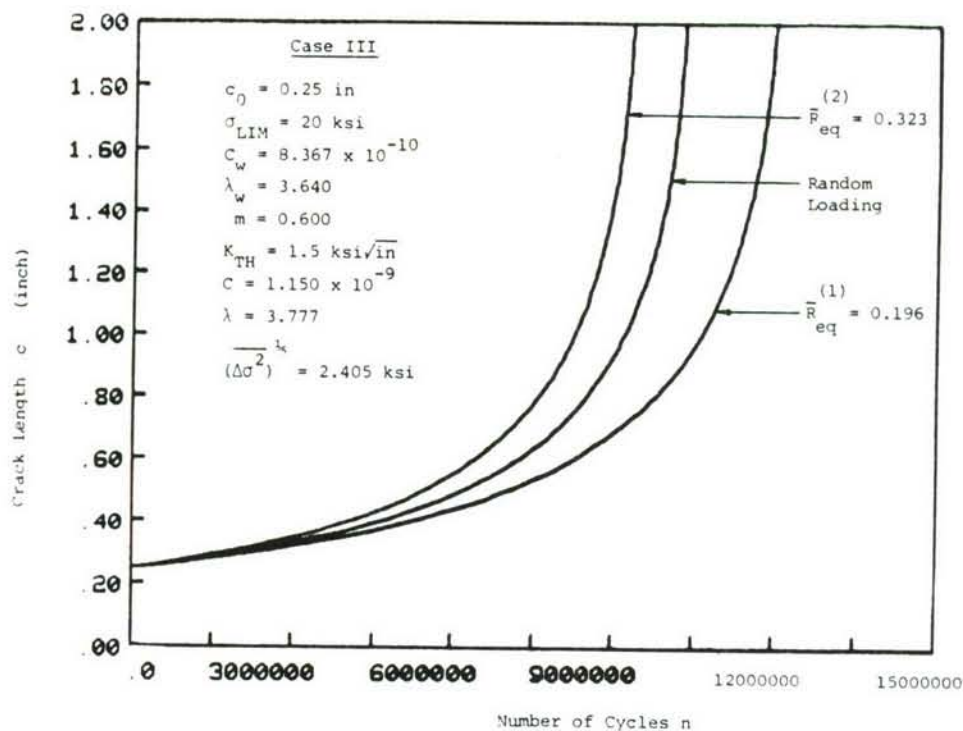
Figure 165. Crack growth as a function of number of cycles
(Case III, for new values of constants).
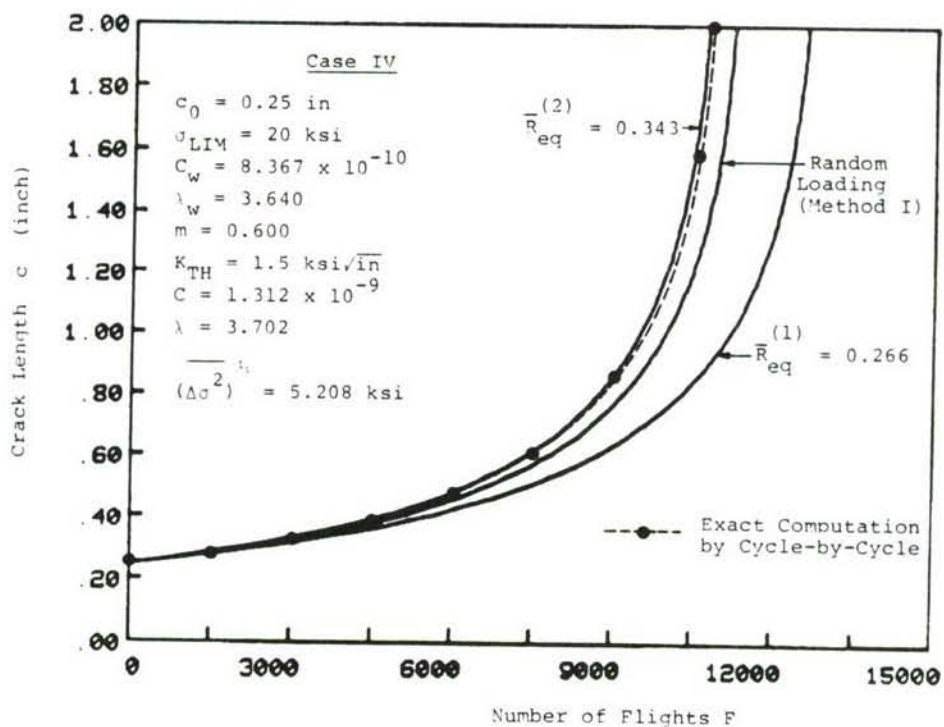
Figure 166. Crack growth as a function of number of cycles
(Case IV, for new values of constants).

194
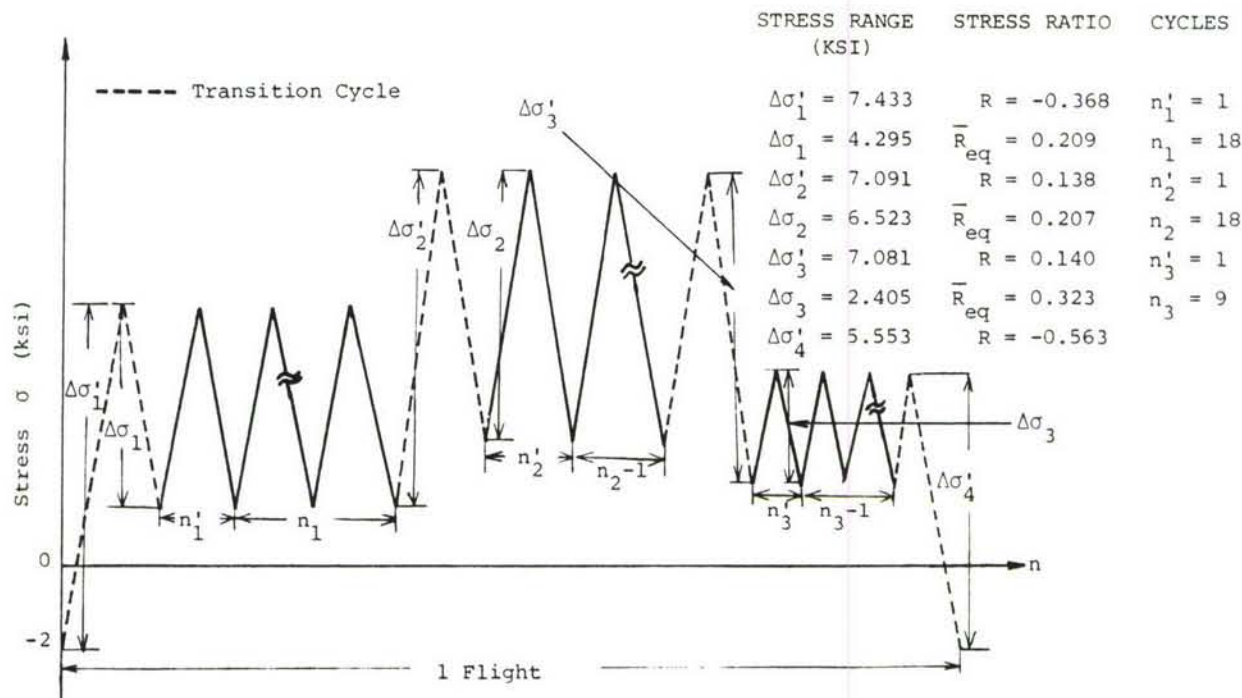
Figure 167. Simplified load spectra for case IV (Method II).
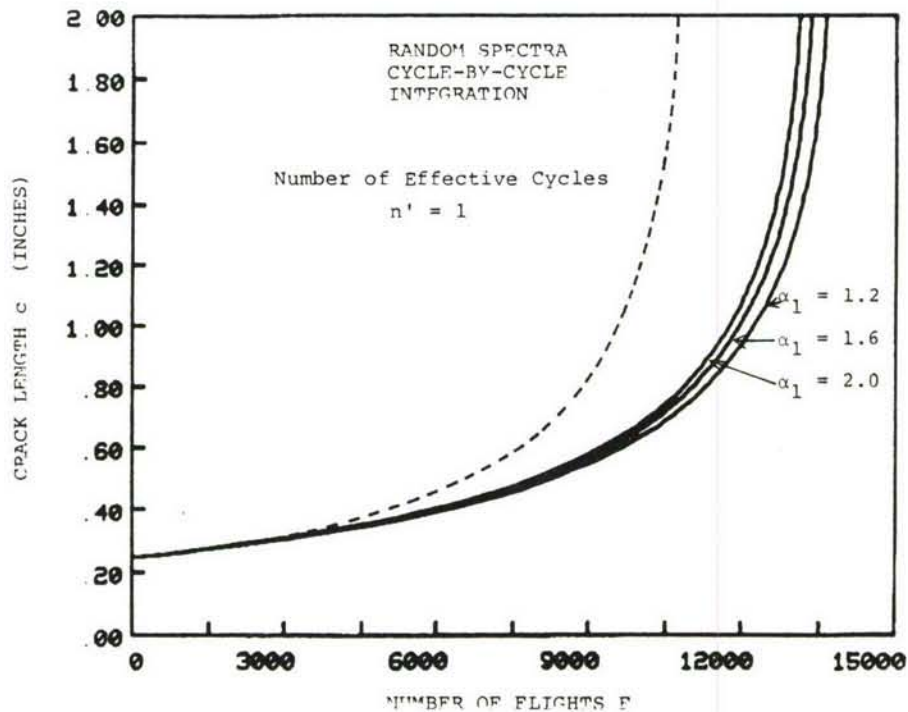
Figure 168. Crack growth as a function of number of flights
for n' = 1 and different values of α_1.

195
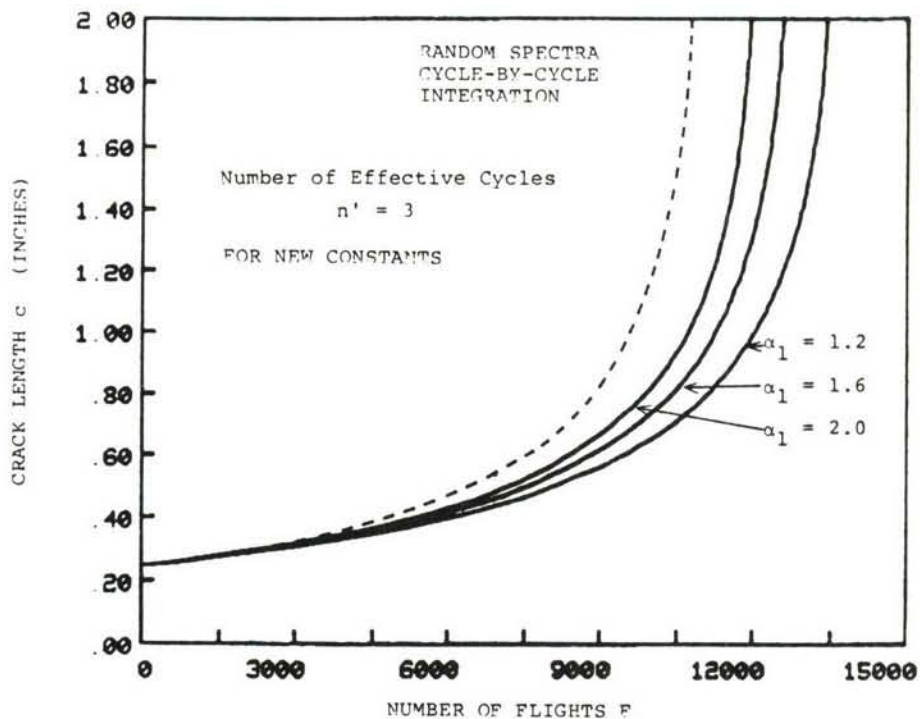
Figure 169. Crack growth as a function of number of flights for n' = 3 and different values of α_1.
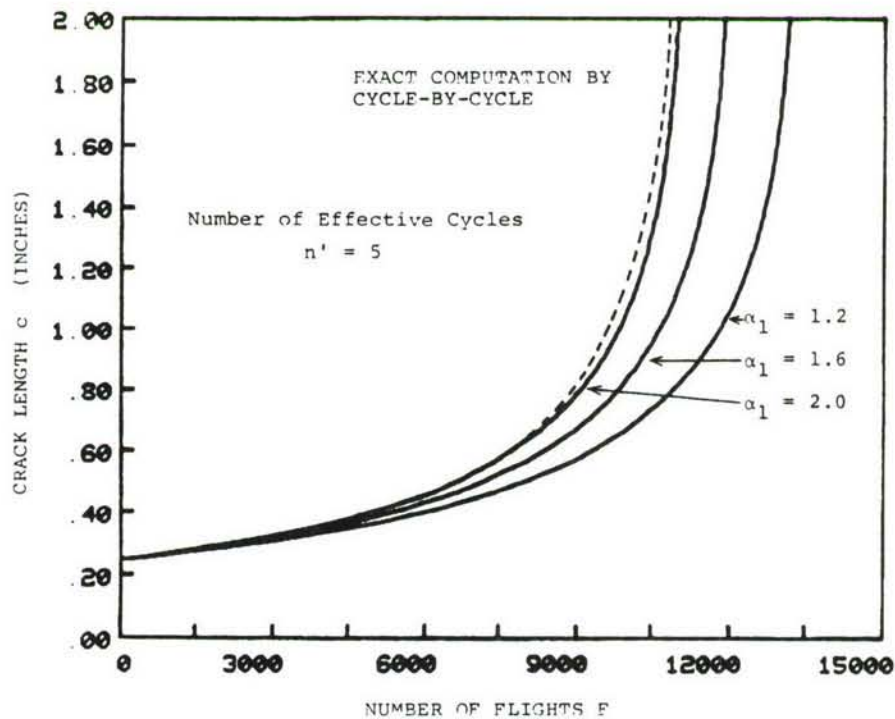
Figure 170. Crack growth as a function of number of flights for n' = 5 and different values of α_1.

196
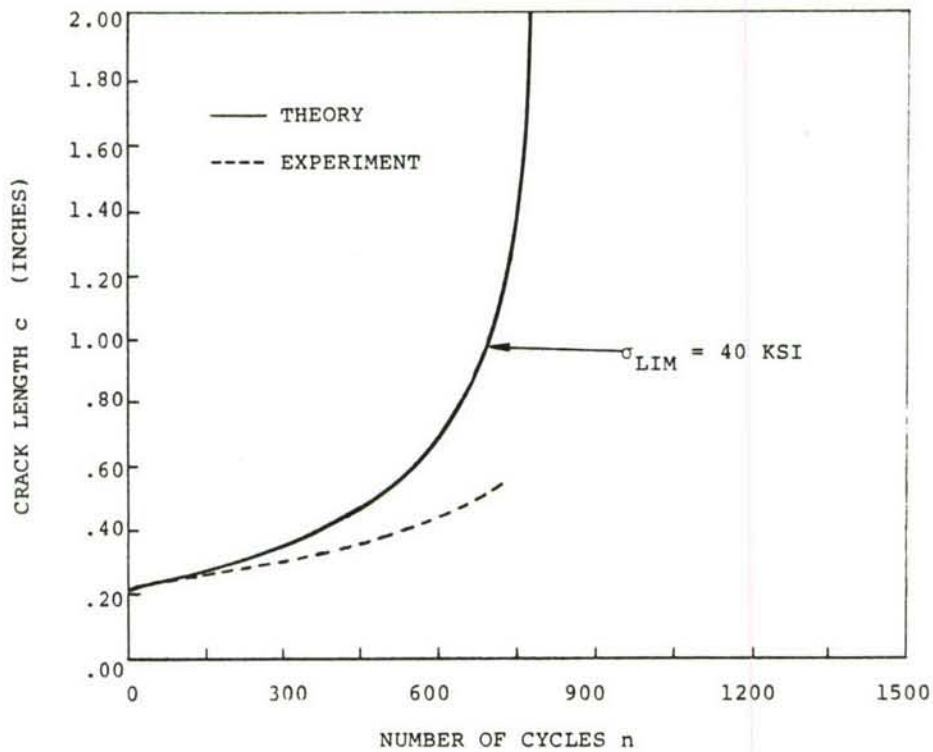
Figure 171. Crack growth as a function of number of cycles for constant amplitude loading (M-5, c_0 = 0.15 in.).
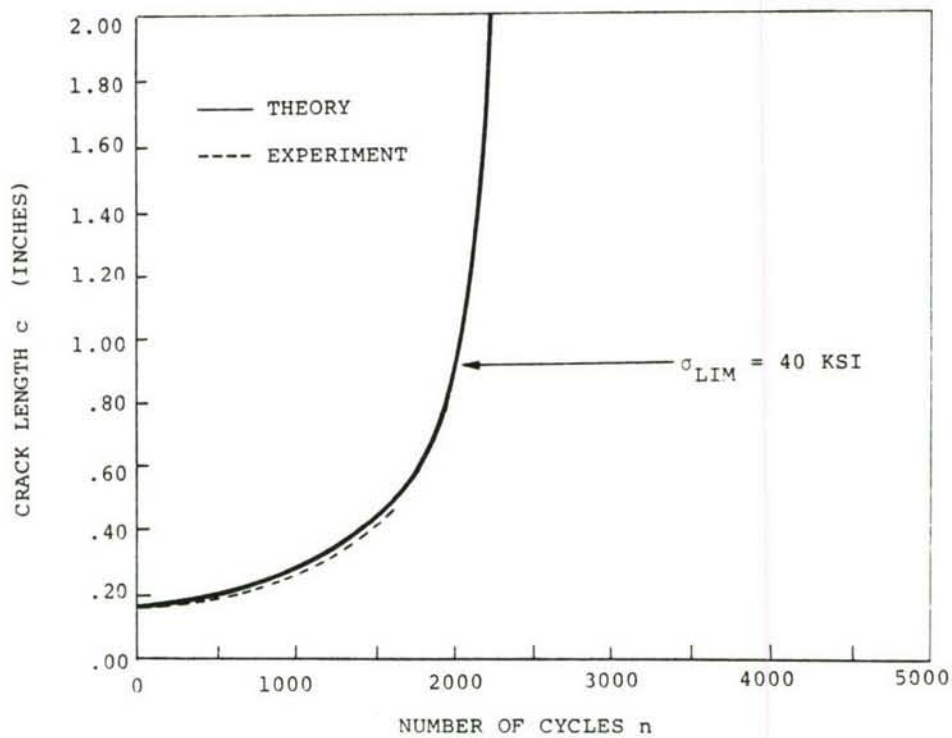
Figure 172. Crack growth as a function of number of cycles for constant amplitude loading (M-6, c_0 = 0.155 in.).

197
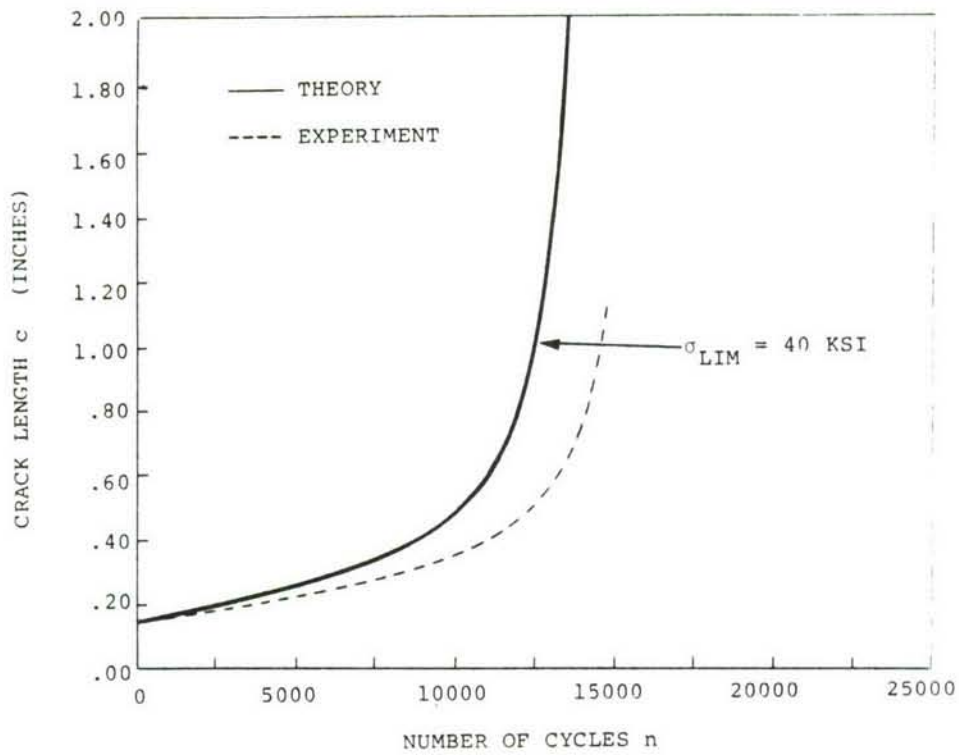
Figure 173.   Crack growth as a function of number of cycles for constant amplitude loading (M-7, c_0 = 0.155 in.).
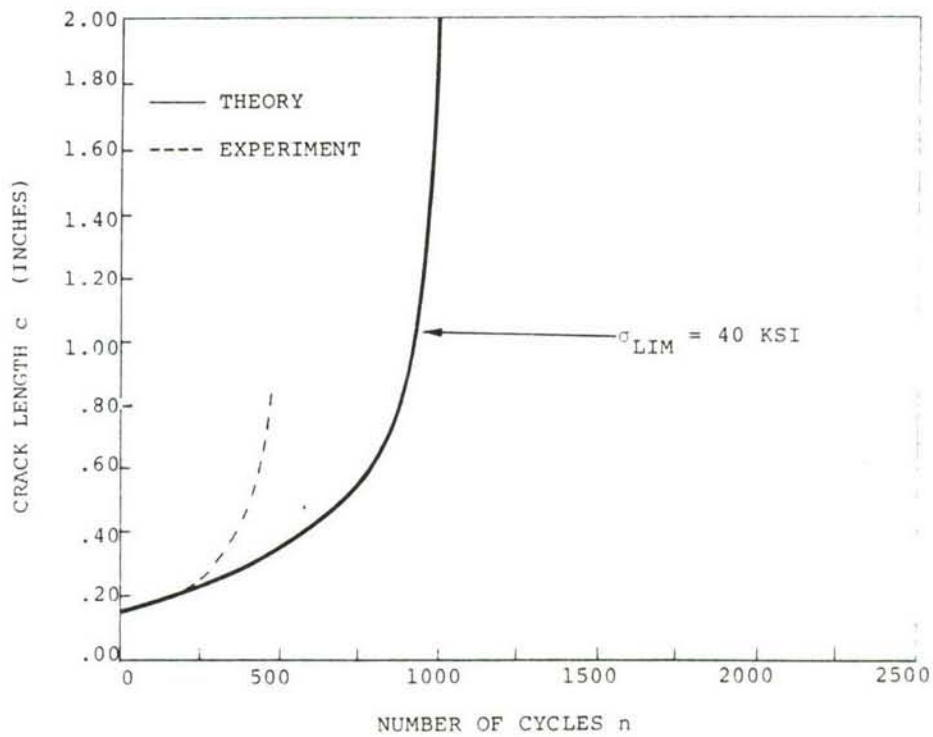
Figure 174.   Crack growth as a function of number of cycles for constant amplitude loading (M-8, c_0 = 0.155 in.).
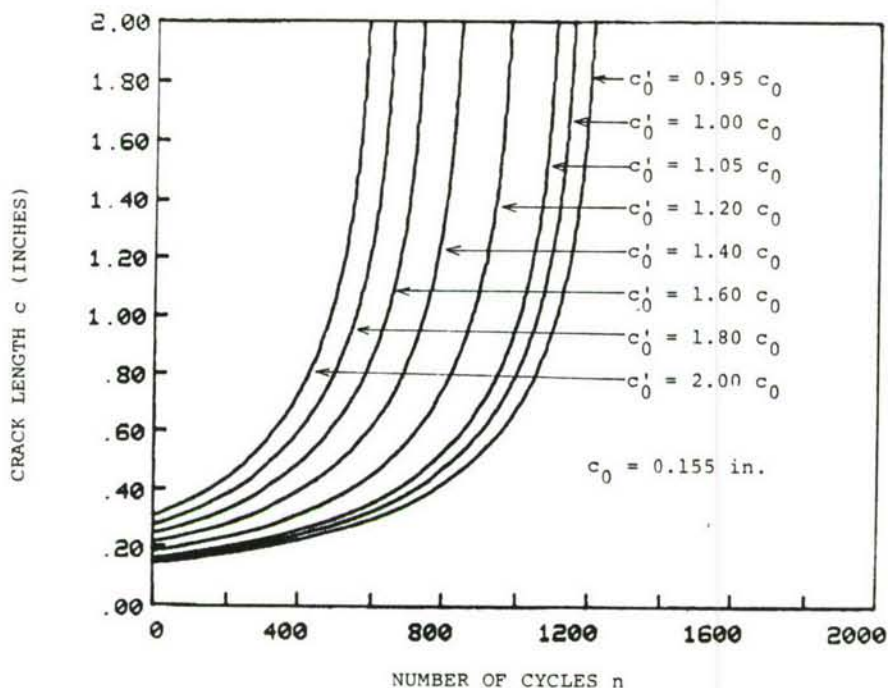
Figure 175. Crack growth as a function of number of cycles for different initial crack sizes (M-8, σ_{LIM} = 20 ksi).
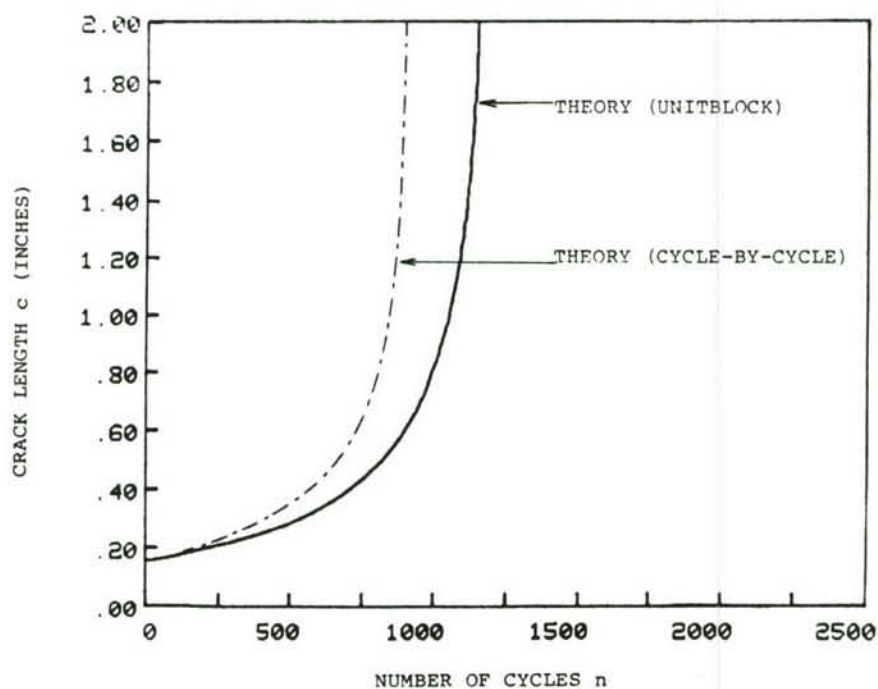
Figure 176. Crack growth as a function of number of cycles for constant amplitude loading evaluated by unitblock approach and cycle-by-cycle integration (M-8, c_0 = 0.155 in., σ_{LIM} = 20 ksi).

199
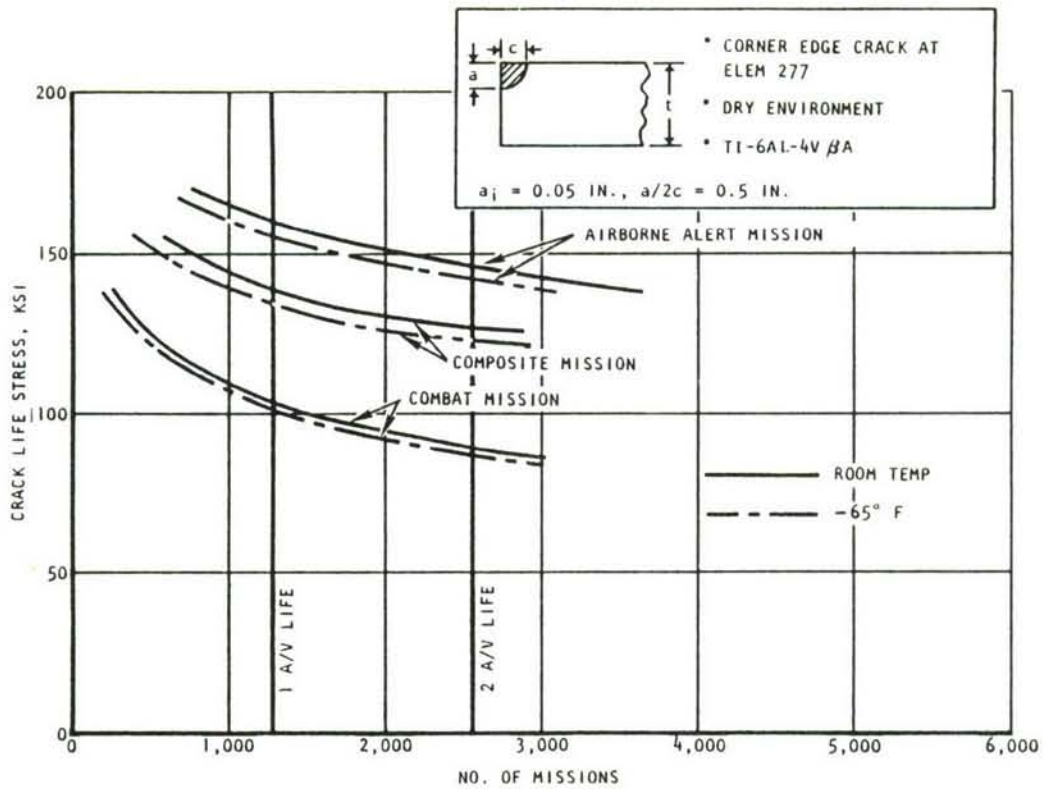
Figure 177. Crack life allowable stresses under various spectrum loading.
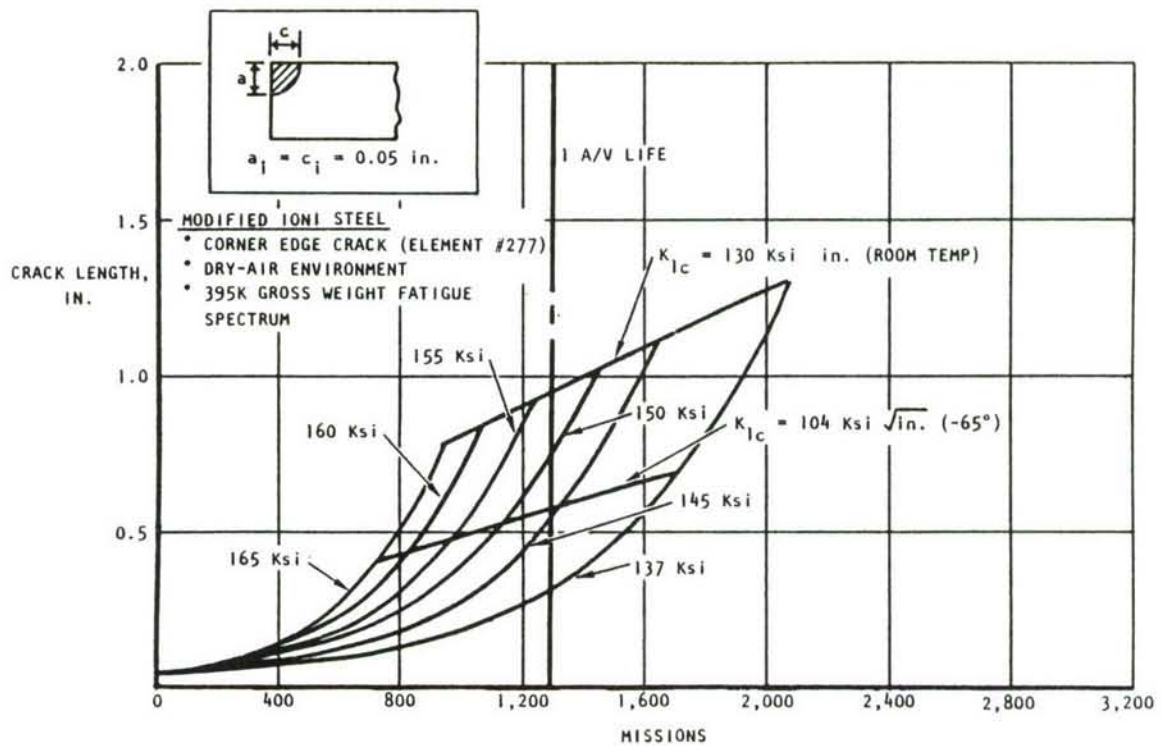
Figure 178. Parametric crack growth analysis for various limit stress levels.

200

TABLE 1. SUMMARY OF CRACK GROWTH RATE EQUATIONS AND CORRESPONDING GROWTH RATE CONSTANTS USED IN BASELINE CRACK GROWTH DATA CORRELATIONS AND CROSS-CORRELATIONS

Material / Rate Equation	2219-T851 Aluminum	Ti-6Al-4V Titanium	9Ni-4Co-0.2c Steel	Data Source
Boeing Equation $$da/dN = C(K_{max} - K_{th})^{\alpha} (\Delta K)^{n}$$	$C = 0.34 \times 10^{-8}$ $\alpha = 0.84$ $n = 2.4$ $K_{th} = 1.5$ ksi $\sqrt{in.}$	$C = 0.33 \times 10^{-10}$ [b] $\alpha = 1.02$ $n = 3.0$ $K_{th} = 5$ ksi $\sqrt{in.}$	$C = 0.4 \times 10^{-8}$ $\alpha = 0.57$ $n = 1.76$ $K_{th} = 10$ ksi $\sqrt{in.}$	Reference 3
Grumman Equation $$da/dN = C[(1 + q\overline{R})\Delta K]^{n}$$ $R \leq R_{co}, \overline{R} = R$ $R > R_{co}, \overline{R} = R_{co}$	$C = 1.96 \times 10^{-9}$ $n = 3.34$ $q = 0.6$ $R_{co} = 0.5$	$C = 5.9 \times 10^{-10}$ [c] $n = 3.08$ $q = 0.7$ $R_{co} = 0.7$	--	Reference 4
Rockwell Equation[a] $$da/dN = C\left[\frac{\Delta K}{(1-\overline{R})^{1-m}} \right]$$ $R \leq R_{co}, \overline{R} = R$ $R > R_{co}, \overline{R} = R_{co}$ $da/dN = 0, \Delta K \leq \Delta K_{th}$	$C = 1.72 \times 10^{-9}$ $n = 3.415$ $m = 0.65$ $R_{co} = 0.6$ $\Delta K_{th} = 1.5$ ksi $\sqrt{in.}$	--	--	Reference 21

[a] Used for cross-correlation only

[b] Beta annealed

[c] Mill annealed

TABLE 2. SUMMARY OF STATIC & FRACTURE PROPERTIES USED IN BASELINE CRACK GROWTH DATA CORRELATIONS & CROSS-CORRELATIONS

	Static Properties Materials	TYS (ksi)	TUS (ksi)	Elong (%)	RA (%)	E (ksi)	K_{Ic} or K_C (ksi $\sqrt{in.}$)	Data Source
2219-T851 Alum	Boeing Data	52.6 (L) / 51.3 (T)	66.1 (L) / 66.3 (T)	16 (L) / 15 (T)	28 (L) / 25 (T)	10×10^3	45 (K_{Ic}) / 76 (K_C)	Reference 3
2219-T851 Alum	Grumman Data	54.7	66.9	10.3			30 (K_{Ic}) / 57.5 (K_C)	Reference 4
2219-T851 Alum	Rockwell Data[a]	48	62	8		10.5×10^3	45 (K_{Ic}) / 76 (K_C)	Reference 6
Ti-6Al-4V	Boeing Data[b]	125.3 (L) / 128 (T)	138.4 (L) / 138.6 (T)	16 (L) / 16 (T)	26 (L) / 25 (T)		80 (K_{Ic}) / 160 (K_C)	Reference 3
Ti-6Al-4V	Grumman Data[c]	130.0 (1/4 in.) / 135.3 (3/4 in.)	132.6 (1/4 in.) / 137.6 (3/4 in.)	17.8 (1/4 in.) / 12.6 (3/4 in.)			77 (K_{Ic})	Reference 4
9Ni-4Co-0.2c steel	Boeing Data	185.3 (L) / 186.6 (T)	203.2 (L) / 203.5 (T)	23 (L) / 23 (T)	56 (L) / 55 (T)		140 (K_{Ic}) / 180 (K_C)	Reference 3

[a] Used for cross-correlation only
[b] Beta annealed
[c] Mill annealed

TABLE 3. SUMMARY, CORRELATION OF BOEING 2219-T851 ALUMINUM BASELINE CRACK GROWTH RATE DATA

Test specimen No.	Load condition		N_{Test} (cyc)	N_{Pred} (cyc)	$R = \dfrac{N_{Pred}}{N_{Test}}$
	σ (ksi)	R			
SBTA1-1 (flaw 1) 1	16	0.1	7100	13700	1.93
2	24		1950	1540	0.79
3	30		280	245	0.88
SBTA1-1 (flaw 2) 1	16		7100	9000	1.27
2	24		1950	1505	0.77
3	30		280	248	0.89
SBTA1-2 1	16		4980	4070	0.82
2	24		545	360	0.66
3	30		111	209	1.88
SBTA3-1 (flaw 1) 1	20	0.3	6260	5920	0.95
2	30		920	800	0.87
3	38		130	178	1.37
SBTA3-1 (flaw 2) 1	20		6260	5950	0.95
2	30		920	792	0.86
3	38		130	279	2.15
SBTA3-2 1	20		2820	2350	0.83
2	30		301	328	1.09
SBTA5-1 (flaw 1) 1	20	0.5	14100	11550	0.82
2	30		2360	2200	0.93
3	40		200	334	1.67
SBTA5-1 (flaw 2) 1	20		14100	15100	1.07
2	30		2360	1640	0.69
3	40		200	550	2.75
SBTA5-2 1	20		8300	6750	0.81
2	30		900	760	0.84

TABLE 4.   SUMMARY, CORRELATION OF GRUMMAN 2219-T851 ALUMINUM BASELINE CRACK GROWTH RATE DATA

Test specimen No.	Loading cond P(kips)	R	N_{Test} (cyc)	N_{Pred} (cyc)	$R = \dfrac{N_{Pred}}{N_{Test}}$	Remarks
AG-25-01-CTB 1	0.950	0.7	489,000	570,000	1.16	Grumman's
2	0.950	0.5	5,000	7,750	1.55	CT specimen
3	0.950	0.3	8,300	8,800	1.06	
4	0.500	0.1	30,450	13,250	0.43	
AG-25-02A-CTB 1	0.500	-1.0	264,160	327,000	1.24	
AG-25-20-CTB 1	0.700	-1.0	65,120	78,400	1.20	
AG-25-21-CTB 1	0.500	-1.0	286,820	250,600	0.87	
AG-25-27-CTB 1	0.420	0.05	677,400	522,000	0.77	
AG-25-29-CTB 1	0.998	0.7	195,000	122,000	0.63	
2	0.998	0	19,300	17,300	0.90	
AG-25-30-CTB 1	0.951	0.7	424,100	341,000	0.80	
2	0.951	0.5	51,900	43,000	0.83	
3	0.951	0.3	7,600	7,720	1.01	
4	0.951	0.1	2,550	1,830	0.78	
5	0.500	0.1	139,050	6,300	0.04	
6	0.500	-0.1	1,046	1,090	1.04	
AG-50-01-CTB 1	1.400	0.05	90,020	106,600	1.18	
AD-25-06-CTA 1	0.880	0.7	325,880	417,000	1.28	ASTM
2	0.880	0.5	47,607	41,100	0.86	CT specimen
3	0.710	0.3	15,210	23,800	1.56	
4	0.710	0.05	6,724	8,000	1.19	
5	0.580	0.7	131,960	215,500	1.63	
6	0.580	0.5	70,100	34,700	0.50	
7	0.490	0.3	12,275	16,800	1.38	
8	0.490	0.05	7,310	7,550	1.03	
9	0.400	0.5	36,980	61,000	1.65	
10	0.400	0.05	15,450	9,200	0.60	
11	0.330	0.3	20,540	35,230	1.71	
12	0.330	0.05	11,355	11,800	1.04	
13	0.280	-1.0	8,109	6,300	0.78	
14	0.280	0.5	26,890	38,650	1.44	
15	0.200	0.05	27,820	27,150	0.97	
AD-25-08-CTA 1	1.657	0.7	46,072	89,500	1.94	ASTM
2	1.321	0.3	2,251	1,850	0.82	CT specimen
3	1.321	0.05	892	970	1.09	
4	1.055	0.7	25,238	38,400	1.52	
5	1.055	0.5	4,006	4,300	1.07	
6	0.839	0.3	3,650	2,990	0.82	
7	0.839	0.05	1,246	1,140	0.91	
8	0.671	0.5	6,163	6,550	1.06	
9	0.671	0.05	1,145	1,010	0.88	
10	0.535	0.3	3,562	3,380	0.95	

TABLE 4. SUMMARY, CORRELATION OF GRUMMAN 2219-T851 ALUMINUM
BASELINE CRACK GROWTH RATE DATA (CONCL)

Test specimen No.	Loading cond P(kips)	R	N_{Test}(cyc)	N_{Pred}(cyc)	$R = \dfrac{N_{Pred}}{N_{Test}}$	Remarks
11	0.535	0.05	1,296	1,150	0.89	
12	0.427	0.05	2,609	1,740	0.67	
13	0.427	0.5	5,658	6,040	1.07	
14	0.340	0.05	5,527	4,150	0.75	
AD-25-09-CTA 1	0.450	0.1	146,260	242,100	1.66	
2	0.500	0.1	40,750	66,470	1.63	
3	0.600	0.1	19,950	23,560	1.18	
AD-25-10-CTA 1	0.300	0.5	1,336,700	1,414,000	1.06	
2	0.442	0.05	44,610	61,900	1.39	
3	0.442	0.5	124,840	145,000	1.16	
4	0.442	0.05	10,805	11,180	1.03	
5	0.442	0.05	6,700	6,010	0.90	
AD-25-18-CTA 1	1.080	0.05	4,050	2,840	0.70	
2	0.855	0.05	4,000	9,400	2.35	
3	0.690	0.05	12,480	24,000	1.92	
4	0.550	0.05	8,000	14,900	1.86	
5	0.500	0.05	12,000	18,900	1.58	
6	0.470	0.05	16,000	30,800	1.92	
7	0.425	0.05	8,000	26,200	3.27	
8	0.375	0.05	24,090	52,900	2.20	
9	0.350	0.05	24,010	21,350	0.89	
10	0.325	0.05	28,010	24,100	0.86	
11	0.300	0.05	47,360	61,450	1.30	
12	0.320	0.05	30,000	47,100	1.57	
13	0.340	0.05	35,000	33,700	0.96	ASTM
14	0.360	0.05	22,000	26,500	1.20	CT specimen
AD-25-18-CTA 15	0.380	0.05	14,000	19,700	1.41	ASTM
16	0.400	0.05	9,000	14,950	1.66	CT specimen
17	0.420	0.05	6,750	11,450	1.70	
18	0.470	0.05	4,000	6,740	1.68	
19	0.490	0.05	4,000	5,530	1.38	
20	0.510	0.05	4,000	4,360	1.09	
21	0.530	0.05	2,580	3,460	1.34	
22	0.550	0.05	2,010	2,740	1.36	ASTM
23	0.580	0.5	59,610	64,000	1.07	CT specimen
AG-25-1P-CA 2	10.0	0.05	44,000	35,400	0.80	Center
3	6.0	0.05	62,000	55,300	0.89	cracked
4	6.0	0.5	81,000	71,000	0.87	panel
5	6.0	0.7	95,760	118,300	1.24	specimen
AG-25-7P-CA 3	10.0	0.05	45,000	40,000	0.88	
4	6.0	-1.0	290,900	184,200	0.63	
AG-25-12P-CA 2	16.0	0.3	7,960	3,330	0.42	
3	12.0	0.4	11,515	9,100	0.79	
4	8.0	0.6	144,285	137,300	0.95	

TABLE 5.   SUMMARY,   CORRELATION OF BOEING TI-6AL-4V BETA-ANNEALED
TITANIUM BASELINE CRACK-GROWTH RATE DATA

| Test Specimen No. | Load Condition | | N_{Test} | N_{Pred} | $R=\dfrac{N_{Pred}}{N_{Test}}$ |
	σ_{max} ksi	R	Cycles	Cycles	
SBTT1-1(FLAW 1)-1	40.0	.1	7,072	8,100	1.15
2	55.0		1,400	1,810	1.29
3	70.0		550	560	1.02
SBTT1-1(FLAW 2)-1	40.0		7,072	8,800	1.24
2	55.0		1,400	1,140	.81
3	70.0		500	400	.73
SBTT1-2-1	40.0		3,123	3,200	1.02
2	55.0		700	640	.91
3	70.0		545	350	.64
SBTT3-1(FLAW 1)-1	51.5	.3	6,023	10,100	1.68
2	64.0		1,700	1,380	0.81
3	90.0		600	310	.52
SBTT3-1(FLAW 2)-1	51.5		6,023	3,040	.50
2	64.0		1,700	1,920	1.13
3	90.0		600	220	.37
SBTT3-2-1	51.5		4,000	1,200	.30
2	64.0		700	810	1.16
3	90.0		200	240	1.20
SBTT5-1(FLAW 1)-1	72.0	.5	4,000	4,100	1.02
2	85.0		620	520	.84
3	98.0		290	290	1.00
SBTT5-1(FLAW 2)-1	72.0		4,000	3,500	.88
2	85.0		620	540	.87
3	98.0		290	320	1.10
SBTT5-2-1	72.0		2,300	1,900	.83
2	85.0		800	440	.55
3	98.0		100	140	1.40

TABLE 6.   SUMMARY, CORRELATION OF GRUMMAN TI-6AL-4V MILL-ANNEALED
TITANIUM BASELINE CRACK-GROWTH RATE DATA

| Test Specimen No. | Loading Cond | | N_{Test} Cycles | N_{Pred} Cycles | $R = \frac{N_{Pred}}{N_{Test}}$ | Remarks |
	P_{max}, kips	R				
TG-25-01 CTB-1	2.577	.02	2,000	2,500	1.25	Grumman's
2	.400	.05	103,000	No growth	1.00	CT
3	1.300	.05	39,000	26,900	.69	Specimens
4	.800	.05	78,000	67,000	.86	
5	.600	.05	1,790,250	955,000	.53	
TG-25-02 CTB-1	2.580	.02	3,000	1,670	.56	
2	1.100	.05	328,300	145,000	.44	
TG-25-06 CTB-1	2.580	.02	12,000	4,500	.38	
2	1.100	.045	18,000	15,700	.87	
3	.700	.057	525,000	125,000	.24	
4	.470	.05	680,000	37,000	.05	
5	.700	.3	1,123,000	370,000	.33	
TG-75-01 CTB-1	7.730	.5	70,000	65,000	.93	
2	6.720	.5	48,000	59,000	1.23	
3	5.840	.5	72,000	67,800	.94	
4	7.730	.01	5,958	11,850	1.99	
5	5.840	.01	3,202	3,900	1.22	
6	5.070	.01	1,367	4,270	3.12	
7	4.410	.01	2,932	5,400	1.84	
8	3.840	.01	2,548	4,840	1.89	
9	5.560	.01	141	350	2.48	
TD-25-01 CTA-1	.550	.05	646,880	364,000	.56	ASTM
2	.625	.05	125,420	151,000	1.20	CT
3	.700	.05	33,300	45,900	1.38	Specimens
4	.750	.05	8,627	10,180	1.18	
5	.800	.05	5,533	6,340	1.15	
TD-25-03 CTA-1	1.200	.05	29,120	15,200	.52	
2	2.602	.05	2,130	2,270	1.07	
3	2.295	.05	2,340	2,500	1.07	
4	2.013	.05	2,390	2,500	1.05	
5	1.784	.05	2,650	2,780	1.05	
6	1.572	.05	2,910	3,120	1.07	
7	1.376	.05	3,467	3,520	1.02	
8	1.220	.5	8,160	9,000	1.10	
9	1.075	.5	12,040	12,470	1.04	
10	.941	.5	11,600	12,800	1.10	
11	.837	.5	12,600	13,500	1.07	
12	.740	.5	13,300	15,120	1.14	

TABLE 6. SUMMARY, CORRELATION OF GRUMMAN TI-6AL-4V MILL-ANNEALED
TITANIUM BASELINE CRACK-GROWTH RATE DATA (CONCL)

Test Specimen No.	Loading Cond $P_{Max,}$ kips	R	N_{Test} Cycles	N_{Pred} Cycles	$R = \dfrac{N_{Pred}}{N_{Test}}$	Remarks
TD-25-03 CTA-13	.650	.5	15,000	16,950	1.13	ASTM
14	.566	.5	17,000	19,100	1.12	CT
15	.504	.5	15,500	16,180	1.04	Specimens
16	.446	.5	6,900	9,550	1.38	
TD-25-04 CTA-1	.500	.1	364,640	220,000	.60	
2	.550	.1	85,320	74,000	.87	
3	.650	.1	81,650	131,000	1.60	
4	.750	.1	108,320	104,000	.96	
5	.900	.1	61,460	65,900	1.07	
TD-25-17 CTA-1	.900	.05	34,730	54,000	1.55	
2	1.000	.5	125,080	145,000	1.15	
3	1.100	.7	229,520	180,000	.78	
4	1.250	.5	10,790	12,920	1.20	
TD-25-25 CTA-1	.750	.05	242,500	310,000	1.28	
2	.750	.3	70,580	84,800	1.20	
3	.750	.5	43,450	53,400	1.23	
TG-25-6P CCP-1	39.0	.5	32,500	9,500	.29	Center
2	19.5	.05	24,250	4,500	.19	Cracked
3	13.0	.044	99,100	66,900	.68	Panels
TG-25-2P CCP-1	10.0	.05	152,500	175,000	1.15	
2	6.0	.05	385,000	345,000	.90	
3	6.0	.5	396,000	396,000	.93	
4	6.0	.7	655,000	544,000	.83	
TG-25-5P CCP-1	10.0	.05	230,000	141,000	.61	
2	10.0	-1.0	148,800	162,000	1.09	

TABLE 7. SUMMARY, CORRELATION OF BOEING HP-9-4-.20 STEEL BASELINE
CRACK-GROWTH RATE DATA

| Test Specimen No. | Load Condition | | N_{Test} Cycles | N_{Pred} Cycles | $R=\frac{N_{Pred}}{N_{Test}}$ |
	σ_{max}, ksi	R			
SBTS1-1(FLAW 1)-1	30.	.1	17,600	18,200	1.03
2	60.		3,100	2,980	.96
3	90.		1,200	890	.74
SBTS1-1(FLAW 2)-1	30.		17,600	17,600	1.00
2	60.		3,100	2,740	.88
3	90.		1,200	900	.75
SBTS1-2-1	30.		14,700	16,900	1.15
2	60.		1,830	1,960	1.07
3	90.		420	440	1.05
SBTS3-1(FLAW 1)-1	39.	.3	18,500	15,900	.86
2	70.		6,200	5,860	.95
3	116.		1,200	1,060	.88
SBTS3-1(FLAW 2)-1	39.		18,500	19,900	1.08
2	70.		6,200	5,590	.90
3	116.		1,200	1,230	1.03
SBTS3-2-1	39.		14,580	20,130	1.38
2	70.		1,420	730	.51
3	116.		520	460	.88
SBTS5-1(FLAW 1)-1	54.	.5	14,510	13,360	.92
2	93.		5,000	4,520	.90
3	126.		2,300	2,100	.91
SBTS5-1(FLAW 2)-1	54.		14,510	13,900	.96
2	93.		5,000	4,490	.90
3	126.		2,300	2,150	.93
SBTS5-2-1	54.		9,000	8,570	.95
2	93.		2,500	2,110	.84
3	126.		1,700	1,860	1.09

TABLE 8. SUMMARY, CROSS-CORRELATION OF BOEING 2219-T851 ALUMINUM BASELINE CRACK GROWTH RATE DATA

Test Specimen	Test			Boeing Eq.		Grumman Eq.		Rockwell Eq.	
	σ, ksi	R	N, cyc	N, cyc	R	N, cyc	R	N, cyc	R
SBTA1-1 (flaw 1)-1	16	.1	7,100	13,700	1.93	15,060	2.12	14,150	2.18
2	24	↑	1,950	1,540	.79	1,690	.87	1,280	.86
3	30		280	245	.88	275	.98	270	.96
SBTA1-1 (flaw 2)-1	16		7,100	9,000	1.27	9,960	1.40	10,170	1.42
2	24		1,950	1,505	.77	1,650	.85	1,600	.82
3	30		280	248	.89	260	.93	250	.89
SBTA1-2-1	16		4,980	4,070	.82	4,470	.90	4,470	.90
2	24		545	360	.66	390	.72	380	.70
3	30	↓	111	209	1.88	230	2.07	210	1.89
SBTA3-1 (flaw 1)-1	20	.3	6,260	5,920	.95	5,780	.98	6,280	1.06
2	30	↑	920	800	.87	770	.96	800	.87
3	38		130	178	1.37	170	1.31	170	1.31
SBTA3-1 (flaw 2)-1	20		6,260	5,950	.95	5,840	.93	6,260	1.01
2	30		920	792	.86	760	.83	780	.85
3	38		130	279	2.15	260	2.00	270	2.07
SBTA-3-2-1	20		2,820	2,350	.83	2,280	.81	2,420	.86
2	30	↓	301	328	1.09	320	1.06	330	1.10
SBTA5-1 (flaw 1)-1	20	.5	14,100	11,550	.82	11,300	.80	11,670	.83
2	30	↑	2,360	2,200	.93	2,120	.90	2,110	.89
3	40		200	334	1.67	330	1.65	320	1.60
SBTA5-1 (flaw 2)-1	20		14,100	13,800	.98	13,280	.94	13,500	.96
2	30		2,360	1,640	.69	1,580	.67	1,560	.66
3	40		200	550	2.75				
SBTA5-2-1	20		8,300	6,950	.83	6,600	.80	6,630	.80
2	30	↓	900	760	.84	720	.80	700	.78

$$R = \frac{N_{Pred}}{N_{Test}}$$

TABLE 9. CRACK GROWTH CROSS-CORRELATION OF BOEING 2219-T851
ALUMINUM BASELINE DATA

Range of R		Grumman Equation	Boeing Equation	Rockwell Equation
From	To			
0.70	1.30	68%	68%	68%
0.85	1.15	44%	36%	48%
0.70	1.00	64%	60%	56%
0.85	1.00	40%	32%	36%
Mean		1.05	1.14	1.05
Standard Deviation		0.48	0.53	0.47

$$R = \frac{N_{Pred}}{N_{Test}}$$

TABLE 10. SUMMARY, CROSS-CORRELATION OF GRUMMAN 2219-T851 ALUMINUM BASELINE CRACK GROWTH RATE DATA

Test Specimen No.	Test			Grumman Eq.		Boeing Eq.		Rockwell Eq.	
	P, Kips	R	N, Cyc	N_{Pred},Cyc	R	N_{Pred},Cyc	R	N_{Pred},Cyc	R
AG-25-01-CTB -1	.950	.7	489,000	570,000	1.16	367,000	.75	472,000	.97
2	.950	.5	5,000	7,750	1.55	8,100	1.62	7,860	1.57
3	.950	.3	8,300	8,800	1.06	9,110	1.10	3,340	1.13
4	.500	.1	30,450	13,250	.43	12,000	.39	13,400	.44
AG-25-02A-CTB-1	.500	-1.	264,100	327,000	1.24	-	-	312,000	1.18
AG-25-20-CTB -1	.700	-1.	65,100	78,000	1.20	-	-	72,500	1.11
AG-25-21-CTB -1	.500	-1.	286,800	250,600	.87	-	-	236,000	.82
AG-25-27-CTB -1	.420	.05	677,400	522,000	.77	472,000	.70	535,000	.79
AG-25-29-CTB -1	.998	.7	195,000	122,000	.63	77,800	.40	100,800	.52
2	.998	0	19,300	17,300	.90	14,300	.74	16,090	.83
AG-25-30-CTB -1	.951	.7	424,100	341,000	.80	219,000	.52	282,000	.66
2	.951	.5	51,900	43,000	.83	44,300	.85	43,800	.84
3	.951	.3	7,600	7,720	1.01	7,970	1.05	8,150	1.07
4	.951	.1	2,550	1,830	.78	1,690	.66	1,760	.69
5	.500	.1	139,050	6,300	.04	5,900	.04	6,300	.04
6	.500	-.1	1,025	1,090	1.06	-	-	810	.79
AG-50-01-CTB -1	1.400	.05	89,500	106,000	1.18	92,800	1.04	105,500	1.18
AD-25-06-CTA -1	.880	.7	348,774	306,600	.88	196,000	.56	253,700	.73
2	.880	.5	26,911	28,000	1.04	28,900	1.07	28,800	1.07
3	.710	.3	13,015	15,200	1.17	15,600	1.20	16,500	1.27
4	.710	.05	5,010	6,170	1.23	5,360	1.07	6,030	1.20
5	.580	.7	169,609	183,600	1.08	116,900	.69	152,300	.90
6	.580	.5	32,480	26,500	.82	27,500	.85	27,600	.85
7	.490	.3	14,658	16,850	1.15	17,340	1.18	18,660	1.27

NOTE $R = \dfrac{N_{Pred}}{N_{Test}}$

TABLE 10. SUMMARY, CROSS-CORRELATION OF GRUMMAN 2219-T851 ALUMINUM BASELINE
CRACK GROWTH RATE DATA (CONT)

Test Specimen No.	Test			Grumman Eq.		Boeing Eq.		Rockwell Eq.	
	P, Kips	R	N, Cyc	$N_{Pred,}$Cyc	R	$N_{Pred,}$Cyc	R	$N_{Pred,}$Cyc	R
AD-25-06-CTA -8	.490	.05	5,343	6,160	1.15	5,350	1.00	6,060	1.13
9	.400	.5	45,805	49,400	1.08	51,500	1.12	52,360	1.14
10	.400	.05	8,939	9,500	1.06	8,260	.92	9,390	1.05
11	.330	.3	20,549	24,670	1.20	25,470	1.24	27,600	1.34
12	.330	.05	9,968	10,430	1.05	9,050	.91	10,320	1.04
13	.280	-1.	8,842	7,750	.88	-	-	7,190	.81
14	.280	.5	28,699	34,400	1.20	35,700	1.24	36,100	1.26
15	.200	.05	27,326	24,440	.89	21,540	.79	24,700	.90
AD-25-08-CTA -1	1.657	.7	30,942	42,100	1.36	27,500	1.13	33,100	1.07
2	1.321	.3	2,251	1,330	.59	1,440·	.64	1,440	.64
3	1,321	.05	892	750	.84	670	.75	700	.78
4	1.055	.7	25,238	33,400	1.32	19,460	.77	23,960	.95
5	1.055	.5	4,006	3,490	.87	3,650	.91	3,460	.86
6	.839	.3	3,650	2,560	.70	2,640	.72	2,700	.74
7	.839	.05	1,246	1,090	.87	960	.77	1,020	.82
8	.671	.5	6,163	5,580	.91	5,800	.94	5,610	.91
9	.671	.05	1,145	900	.79	790	.69	850	.74
10	.535	.3	3,662	3,210	.88	3,300	.90	3,430	.94
11	.535	.05	1,296	1,100	.85	970	.75	1,050	.81
12	.427	.05	2,609	1,800	.69	1,570	.60	1,730	.66
13	.427	.5	5,658	5,360	.95	5,550	.98	5,390	.95
14	.340	.05	5,527	4,020	.73	3,500	.63	3,850	.70

NOTE $R = \dfrac{N_{Pred}}{N_{Test}}$

TABLE 10. SUMMARY, CROSS-CORRELATION OF GRUMMAN 2219-T851 ALUMINUM BASELINE
CRACK GROWTH RATE DATA (CONT)

Test Specimen No.	Test			Grumman Eq.		Boeing Eq.		Rockwell Eq.	
	P, Kips	R	N, Cyc	N_{Pred}, Cyc	R	N_{Pred}, Cyc	R	N_{Pred}, Cyc	R
AD-25-09-CTA -1	.450	.1	146,260	169,800	1.16	160,100	1.09	180,300	1.23
2	.500	.1	40,750	44,400	1.09	40,380	.99	45,780	1.12
3	.600	.1	19,950	20,430	1.02	18,540	.93	20,680	1.04
AD-25-10-CTA -1	.300	.05	1,336,700	997,000	.75	975,000	.73	1,052,000	.79
2	.442	.05	44,610	49,300	1.11	43,300	.97	49,500	1.11
3	.442	.5	124,840	126,900	1.02	131,400	1.05	132,700	1.06
4	.442	.05	10,805	10,630	.98	9,230	.85	10,250	.95
5	.442	.05	6,700	5,830	.87	6,090	.91	6,510	.97
AD-25-18-CTA -1	1.080	.05	4,050	1,900	.47	1,650	.41	1,840	.45
2	.855	.05	4,000	6,300	1.57	5,480	1.37	6,220	1.56
3	.690	.05	12,480	16,920	1.36	14,800	1.19	16,880	1.35
4	.550	.05	8,000	10,350	1.29	9,140	1.14	10,460	1.31
5	.500	.05	12,000	13,250	1.10	11,800	.98	13,500	1.12
6	.470	.05	16,000	21,850	1.37	19,500	1.22	22,260	1.39
7	.425	.05	8,000	18,800	2.35	16,900	2.11	19,200	2.40
8	.375	.05	24,090	38,300	1.59	34,900	1.45	39,500	1.64
9	.350	.05	24,010	15,700	.65	14,400	.60	16,200	.67
10	.325	.05	28,010	17,700	.63	16,400	.58	18,350	.66
11	.300	.05	47,360	45,500	.96	42,850	.90	47,550	1.00
12	.320	.05	30,000	34,500	1.15	32,400	1.08	35,750	1.19
13	.340	.05	35,000	25,700	.73	23,100	.66	26,100	.75
14	.360	.05	22,000	19,950	.91	18,000	.82	20,600	.94

NOTE $R = \dfrac{N_{Pred}}{N_{Test}}$

214

TABLE 10. SUMMARY, CROSS-CORRELATION OF GRUMMAN 2219-T851 ALUMINUM BASELINE CRACK GROWTH RATE DATA (CONCL)

Test Specimen No.	Test			Grumman Eq.		Boeing Eq.		Rockwell Eq.	
	P, Kips	R	N, Cyc	$N_{Pred,}^{Cyc}$	R	$N_{Pred,}^{Cyc}$	R	$N_{Pred,}^{Cyc}$	R
AD-25-18-CTA-15	.380	.05	14,000	15,250	1.09	13,560	.97	15,500	1.11
16	.400	.05	9,000	11,650	1.29	10,300	1.14	11,800	1.31
17	.420	.05	6,750	9,000	1.33	7,940	1.18	9,100	1.35
18	.470	.05	4,000	5,400	1.35	4,700	1.17	5,380	1.35
19	.490	.05	4,000	4,490	1.12	3,900	.97	4,460	1.12
20	.510	.05	4,000	3,590	0.90	3,100	.77	3,530	0.88
21	.530	.05	2,580	2,880	1.11	2,500	.97	2,830	1.10
22	.550	.05	2,010	1,530	.76	2,010	1.00	2,270	1.13
23	.580	.5	59,610	58,100	.97	60,200	1.01	58,800	.99
AG-25-1P-CA -1	10.0	.05	44,000	35,400	.80	30,070	.68	34,300	.78
2	6.0	.05	62,000	55,300	.89	47,800	.77	53,700	.87
3	6.0	.5	81,000	71,000	.87	73,700	.91	72,100	.89
4	6.0	.7	95,760	118,300	1.24	76,800	.81	93,300	.97
AG-25-7P-CA -1	10.0	.05	45,000	40,000	.88	35,100	.78	40,000	.89
2	6.0	-1.0	290,900	184,200	.63	-	-	171,000	.59
AG-25-12P-CA -1	16.0	.3	7,960	3,330	.42	3,480	.44	3,450	.43
2	12.0	.4	11,515	9,100	.79	9,600	.83	9,500	.83
3	8.0	.6	144,285	137,300	.95	116,200	.81	108,500	.74
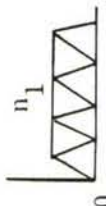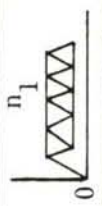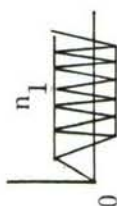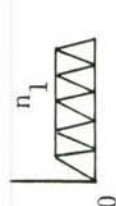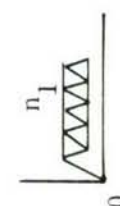
NOTE $R = \dfrac{N_{Pred}}{N_{Test}}$

TABLE 11. CRACK GROWTH CROSS-CORRELATION OF GRUMMAN 2219-T851
ALUMINUM BASELINE DATA

Range of R		Grumman Equation	Boeing Equation	Rockwell Equation
From	To			
0.70	1.30	76%	68%	73%
0.85	1.15	43%	39%	43%
0.70	1.00	40%	41%	41%
0.85	1.00	24%	22%	20%
Mean		0.99	0.84	0.98
Standard Deviation		0.30	0.36	0.31

$$R = \frac{N_{Pred}}{N_{Test}}$$

TABLE 12. SUMMARY, CRACK GROWTH DATA CORRELATIONS, METHODOLOGY DEVELOPMENT TEST PROGRAM, GROUPS I THROUGH III

Test	Test Condition							Test Life N_{Test} (cycle)	Analytical Prediction			
	Applied Base Load			Over-/Under-Load		n_1 Cycle	n_2 Cycle		Vroman/Chang Model		Willenborg Model	
	Loading Profile	σ_{Max} Ksi	σ_{Min} Ksi	σ_{Max} Ksi	σ_{Min} Ksi				Predicted Life N_{pred} (cycle)	R	Predicted Life N_{pred} (cycle)	R
M-1		8	0					403,310	384,600	0.95	387,250	0.96
M-2		8	2.4					260,000	352,000	1.35	357,000	1.37
M-3		8	-8					129,240	120,000	0.93	>200,000	> 2
M-4		8	-2.4					144,000	262,000	1.8	356,000	2.47
M-5		40	0					846	910	1.08	1,030	1.22
M-6		40	12					1,693	1,905	1.2	2,100	1.24
M-7		40	28					14,870	12,050	0.81	12,250	0.82

Note: $R = \dfrac{N_{pred}}{N_{test}}$

TABLE 12. SUMMARY, CRACK GROWTH DATA CORRELATIONS, METHODOLOGY DEVELOPMENT
TEST PROGRAM, GROUPS I THROUGH III (CONT')

Test	Loading Profile	Applied Base Load σMax Ksi	Applied Base Load σMin Ksi	Over-/Under-Load σMax Ksi	Over-/Under-Load σMin Ksi	N_I Cycle	N_{II} Cycle	Test Life N_{Test} (cycle)	Vroman/Chang Model Predicted Life N_{pred} (cycle)	R	Willenborg Model Predicted Life N_{pred} (cycle)	R
M-8	N_I profile	40	-4					469	784	1.68	1,100	2.35
M-9	N_I N_{II} profile	8	-0.8					175,000	313,300	1.79	359,000	2.05
M-10		40	-12					251	624	2.48	950	3.78
M-11		20	0	30	0	2,500	To failure	15,150	13,180	0.87	12,251	0.81
M-12	N_I N_{II} profile	20	0	30	0	2,500	2,500	16,600	13,590	0.82	16,607	1.00
M-13		20	0	45	0	2,500	2,500	49,600	32,500	0.66	>250,100	>>1
M-14	N_I N_{II} profile	20	6	40	6	2,500	2,500	224,100	175,000	0.78	>500,200	>>1
M-15		30	21	40	21	2,500	2,500	124,900	117,500	0.94		

218

TABLE 12. SUMMARY, CRACK GROWTH DATA CORRELATIONS, METHODOLOGY DEVELOPMENT TEST PROGRAM, GROUPS I THROUGH III (CONT')

| | Test Condition | | | | | | | Test Life | Analytical Prediction | | | |
| | Applied Base Load | | Over-Load | Under-Load | | | | | Vroman/Chang Model | | Willenborg Model | |
Test	σMax Ksi	σMin Ksi	σMax Ksi	σMin Ksi	Loading Profile	n_1 Cycle	n_2 Cycle	N_{Test} (cycle)	Predicted Life N_{pred} (cycle)	R	Predicted Life N_{pred} (cycle)	R
M-16	20	0	20	-6.0		2,500	2,500	11,370	12,700	1.12	12,880	1.13
M-17	20	6	20	-6.0		2,500	2,500	20,810	>23,300			
M-18	40	28	40	-12		2,500	2,500	11,600	13,000	1.12	13,005	1.12
M-19	20	0	30	-6.0		2,500	To failure	13,460	13,446	1.0	14,751	1.1
M-20	20	0	30	-6.0		2,500	2,500	36,075	13,414	0.37	19,757	0.55
M-21	20	0	40	-12		2,500	2,500	22,500	15,000	0.67	>75,030	>>1

219

TABLE 12. SUMMARY, CRACK GROWTH DATA CORRELATIONS, METHODOLOGY DEVELOPMENT
TEST PROGRAM, GROUPS I THROUGH III (CONT)
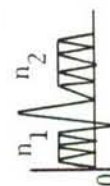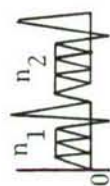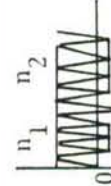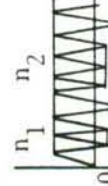
| | | Test Condition | | | | | | | Analytical Prediction | | | |
| | | Applied Base Load | | Over-/Under Load | | | | Test Life | Vroman/Chang Model | | Willenborg Model | |
Test	Loading Profile	σ_{Max} Ksi	σ_{Min} Ksi	σ_{Max} Ksi	σ_{Min} Ksi	n_1 Cycle	n_2 Cycle	N_{Test} (cycle)	Predicted Life N_{pred} (cycle)	R	Predicted Life N_{pred} (cycle)	R
M-22		20	0	30	-6.0	2,500	To failure	13,910	12,334	0.89	13,502	0.97
M-23		20	0	30	-6.0	2,500	2,500	17,200	13,319	0.77	19,514	1.14
M-24		20	-6	30	-6	2,500	2,500	10,950	6,430	0.59	12,504	1.14
M-25		20	-6	40	-16	2,500	2,500	22,400	9,513	0.42	>75,030	>>1
M-26		8	-2.4	8	-16	2,500	To failure	269,840	270,102	1.00	387,501	1.44
M-27		8	-2.4	8	-16	2,500	2,500	194,016	228,900	1.18	>300,120	>1.5

220

TABLE 12. SUMMARY, CRACK GROWTH DATA CORRELATIONS, METHODOLOGY DEVELOPMENT TEST PROGRAM, GROUPS I THROUGH III (CONT)

| | Test Condition | | | | | | | Test Life | Analytical Prediction | | | |
| | Applied Base Load | | | Over-/Under-Load | | | | | Vroman/Change Model | | Willenborg Model | |
Test	Loading Profile	σ_{Max} Ksi	σ_{Min} Ksi	σ_{Max} Ksi	σ_{Min} Ksi	n_1 Cycle	n_2 Cycle	N_{Test} (cycle)	Predicted Life N_{pred} (cycle)	R	Predicted Life N_{pred} (cycle)	R
M-28		20	-6	30	-15	2,500	2,500	9,975	5,975	0.6	10,003	1.00
M-29		20	-6	40	-15	2,500	2,500	14,900	8,960	0.6	>75,030	>>1
M-30		20	-6	40	-15	2,500	2,500	19,914	9,906	0.5	>75,030	>>1
M-31		8	0	20	0	10,000	To failure	24,425	22,443	0.92	23,000	0.94
M-32		20	0	40	0	5,000	To failure	5,275	5,476	1.04	5,500	1.04
M-33		8	2.4	20	2.4	10,000	To failure	27,000	26,990	1.00	27,000	1.00
M-34		20	6	40	12	5,000	To failure	6,884	6,584	0.96	7,000	1.02

TABLE 12. SUMMARY, CRACK GROWTH DATA CORRELATIONS, METHODOLOGY DEVELOPMENT
TEST PROGRAM, GROUPS I THROUGH III (CONT)
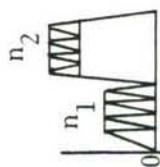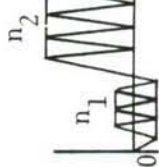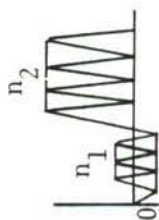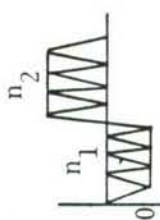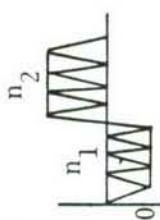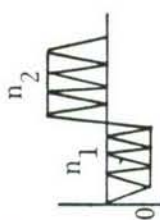
	Test Condition							Test Life N_{Test} (cycle)	Analytical Prediction			
	Applied Base Load		Over-/Under-Load						Vroman/Chang Model		Willenborg Model	
Test	Loading Profile	σ_{Max} Ksi	σ_{Min} Ksi	σ_{Max} Ksi	σ_{Min} Ksi	n_1 Cycle	n_2 Cycle		Predicted Life N_{pred} (cycle)	R	Predicted Life N_{pred} (cycle)	R
M-35		8	0	20	14	10,000	To failure	178,670	191,845	1.1	192,500	1.08
M-36		20	0	40	28	5,000	To failure	9,346	12,051	1.29	12,000	1.28
M-37		8	-2.4	20	0	10,000	To failure	24,200	21,904	0.91	23,000	0.95
M-38		20	-6	40	0	5,000	To failure	5,190	5,376	1.04	5,500	1.06
M-39		0	-6	20	0	5,000	To failure	19,300	17,796	0.92	18,000	0.93
M-40		0	-12	40	0	5,000	To failure	5,653	5,910	1.04	6,000	1.06

222

TABLE 12. SUMMARY, CRACK GROWTH DATA CORRELATIONS, METHODOLOGY DEVELOPMENT TEST PROGRAM, GROUPS I THROUGH III (CONT)
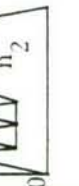
Test	Loading Profile	Applied Base Load σ_{Max} Ksi	Applied Base Load σ_{Min} Ksi	Over-/Under-Load σ_{Max} Ksi	Over-/Under-Load σ_{Min} Ksi	n_1 Cycle	n_2 Cycle	Test Life N_{Test} (cycle)	Vroman/Chang Model Predicted Life N_{pred} (cycle)	Vroman/Chang Model R	Willenborg Model Predicted Life N_{pred} (cycle)	Willenborg Model R
M-41		-3	-6	20	10	5,000	To failure	67,400	63,150	0.94	63,500	0.94
M-42		-3	-12	20	10	5,000	To failure	57,830	61,255	1.06	61,500	1.06
M-43		30	0	20	0	500	To failure	17,808	10,676	0.6	12,500	0.70
M-44		40	0	20	0	500	To failure	50,465	7,394	0.15	29,250	0.58
M-45		30	9	20	6	3,370	To failure	23,620	18,030	0.76	18,120	0.77
M-46		40	12	20	6	500	To failure	133,260	28,453	0.21	50,500	0.38
M-47		20	6	20	14	500	To failure	203,526	144,287	0.71	169,000	0.83
M-48		40	12	40	28	500	To failure	10,350	9,256	0.89	9,500	0.92

TABLE 12. SUMMARY, CRACK GROWTH DATA CORRELATIONS, METHODOLOGY DEVELOPMENT
TEST PROGRAM, GROUPS I THROUGH III (CONT)

Test	Loading Profile	Applied Base Load σMax Ksi	σMin Ksi	Over-/Under-Load σMax Ksi	σMin Ksi	n1 Cycle	n2 Cycle	Test Life N_Test (cycle)	Vroman/Chang Model Predicted Life N_pred (cycle)	R	Willenborg Model Predicted Life N_pred (cycle)	R
M-49		20	14	20	6	500	To failure	25,665	27,401	1.07	27,500	1.07
M-50		40	28	40	12	500	To failure	2,270	2,332	1.03	2,500	1.10
M-51		8	0	20	0	2,500	500	86,600	74,718	0.86	75,000	0.87
M-52		20	0	40	0	500	50	8,238	8,271	1.00	10,950	1.33
M-53		8	2.4	20	2.4	2,500	500	113,540	104,871	0.92	105,000	0.93
M-54		20	6	40	6	500	50	9,316	13,700	1.47	15,350	1.65
M-55		8	0	20	0	2,500	50	551,050	502,000	0.91	231,300	0.42
				0	-6		50					
M-56		20	0	40	0	2,500	50	18,130	10,303	0.57	10,300	0.57
				0	-12		50					

224

TABLE 12. SUMMARY, CRACK GROWTH DATA CORRELATIONS, METHODOLOGY DEVELOPMENT
TEST PROGRAM, GROUPS I THROUGH III (CONCL)
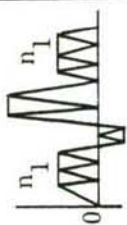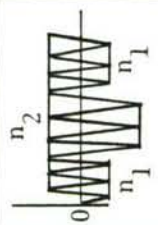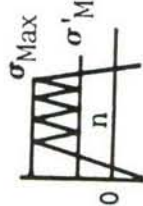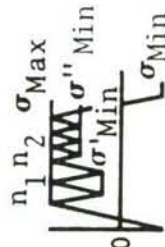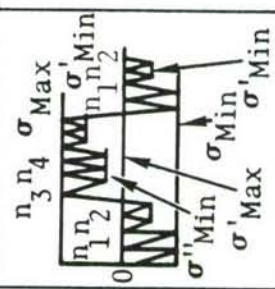
Test	Test Condition								Test Life N_{Test} (cycle)	Analytical Prediction			
	Applied Base Load		Over-/Under-Load							Vroman/Chang Model		Willenborg Model	
	Loading Profile	σ_{Max} Ksi	σ_{Min} Ksi	σ_{Max} Ksi	σ_{Min} Ksi	n_1 Cycle	n_2 Cycle			Predicted Life N_{pred} (cycle)	R	Predicted Life N_{pred} (cycle)	R
M-57		20	0	0	-12	2,500	50		20,760	12,960	0.62	41,600	2.04
				40	0		50						
M-58		20	-6	40	-6	2,500	500		2,774	4,500	1.6	5,750	2.08
M-59		8	-2.4	30	-2.4	5,000	2,500		7,402	7,413	1.0	13,750	1.86
M-60		8	-2.4	8	-16	2,500	2,500		123,180	129,000	1.05	> 250,000	>>1
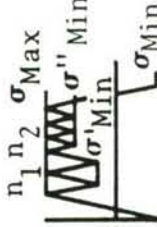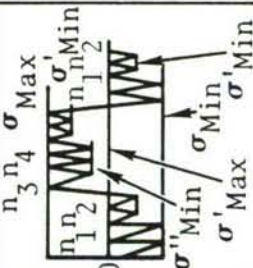
TABLE 13. SUMMARY, CRACK GROWTH DATA CORRELATIONS, METHODOLOGY DEVELOPMENT TEST PROGRAM, GROUPS IV AND V

Text No.	Loading profile	G-A-G step		Flight steps								Test life flights**	Analytical prediction	
		σ_{Max} (ksi)	σ_{Min} (ksi)	σ'_{Min} (ksi)	σ''_{Min} (ksi)	σ'''_{Min} (ksi)	σ'_{Max} (ksi)	n_1 / n_5 (cyc)	n_2 / n_6 (cyc)	n_3 / n_5 (cyc)	n_4 / n_4 (cyc)		Vroman/Chang pred life flight	R*
M-82		Random spectrum, air-to-air, σ_{lim} = 30 ksi										2,227	2,242	1.0
M-61a		15	-2	4	-	-	-	25	-	-	-	2,083	2,541	1.22
M-69a		12	-2	3	4	-	-	20	40	-	-	2,090	2,799	1.4
M-77a		14	-6	-1	4	6	2	4	8	20	40	1,456	1,860	1.28

$$* \quad R = \frac{N_{pred}}{N_{test}}$$

** Counted from common initial crack size

226

TABLE 13. SUMMARY, CRACK GROWTH DATA CORRELATIONS, METHODOLOGY DEVELOPMENT TEST PROGRAM, GROUPS IV AND V (CONT)

Text No.	Loading profile	G-A-G step σ_{Max} (ksi)	σ_{Min} (ksi)	Flight steps σ'_{Min} (ksi)	σ''_{Min} (ksi)	σ'''_{Min} (ksi)	σ'_{Max} (ksi)	n_1 / n_5 (cyc)	n_2 / n_6 (cyc)	n_3 (cyc)	n_4 (cyc)	Test life flights**	Analytical prediction Vroman/Chang pred life flight	R*
M-83	Random spectrum air-to-air, σ_{lim} = 40 ksi											710	733	1.03
M-61		20	-2	4	-	-	-	25	-	-	-	742	757	1.02
M-69		20	-2	6	8	-	-	20	40	-	-	489	526	1.08
M-77		20	-3	-1	6	8	-	2	4	15	35	492	594	1.2

*R = $\dfrac{N_{pred}}{N_{test}}$ ** Counted from common initial crack size
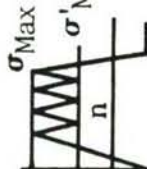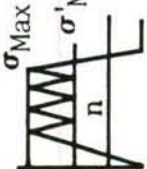
227

TABLE 13. SUMMARY, CRACK GROWTH DATA CORRELATIONS, METHODOLOGY DEVELOPMENT TEST PROGRAM, GROUPS IV AND V (CONT)

Text No.	Loading profile	G-A-G step σ_{Max} (ksi)	σ_{Min} (ksi)	Flight steps σ'_{Min} (ksi)	σ''_{Min} (ksi)	σ'''_{Min} (ksi)	σ'_{Max} (ksi)	n_1 n_5 (cyc)	n_2 n_6 (cyc)	n_3 n_7 (cyc)	n_4 (cyc)	Test life flights**	Vroman/Chang pred life flight	R*
M-85		Random spectrum, air-to-ground, σ_{lim} = 30 ksi										3,498	3,095	0.9
M-62a		14	-4	4	-	-	-	20	-	-	-	2,481	2,744	1.1
M-70a		10	-4	3	4	-	-	15	30	-	-	4,352	5,620	1.3
M-86		Random spectrum, air-to-ground, σ_{lim} = 40 ksi										1,920	1,620	0.84
M-62		18	-4	4	-	-	-	20	-	-	-	1,220	1,441	1.18
M-70		18	-4	6	8	-	-	15	30	-	-	1,151	1,171	1.01

$$*R = \frac{N_{pred}}{N_{test}}$$

**Counted from common initial crack size

228

TABLE 13. SUMMARY, CRACK GROWTH DATA CORRELATIONS, METHODOLOGY DEVELOPMENT TEST PROGRAM, GROUPS IV AND V (CONT)

Text No.	Loading profile	G-A-G step σ_{Max} (ksi)	σ_{Min} (ksi)	Flight steps σ'_{Min} (ksi)	σ''_{Min} (ksi)	σ'''_{Min} (ksi)	σ'_{Max} (ksi)	n_1 n_5 (cyc)	n_2 n_6 (cyc)	n_3 (cyc)	n_4 (cyc)	Test life flights**	Vroman/Chang pred life flight	R*
M-88		Random spectrum, instrumentation & navigation, σ_{lim} = 30 ksi										66,497	61,200	0.92
M-63a		10	-2	4	-	-	-	10	-	-	-	30,270	35,580	1.17
M-89	-	Random spectrum, instrumentation & navigation, σ_{lim} = 40 ksi										26,956	20,260	0.75
M-63	-	14	-2	4	-	-	-	10	-	-	-	6,563	7,663	1.17

$$*R = \frac{N_{pred}}{N_{test}}$$

**Counted from common initial crack size

229

TABLE 13. SUMMARY, CRACK GROWTH DATA CORRELATIONS, METHODOLOGY DEVELOPMENT TEST PROGRAM, GROUPS IV AND V (CONT')
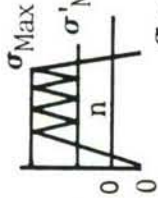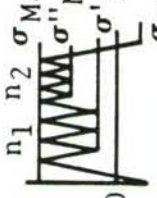
Text No.	Loading profile	G-A-G step		Flight steps								Test life flights**	Analytical prediction	
		σ_{Max} (ksi)	σ_{Min} (ksi)	σ'_{Min} (ksi)	σ''_{Min} (ksi)	σ'''_{Min} (ksi)	σ'_{Max} (ksi)	n_1 n_5 (cyc)	n_2 n_6 (cyc)	n_3 (cyc)	n_4 (cyc)		Vroman/Chang pred life flight	R*
M-90	Random spectrum, composite mission, σ_{lim} = 20 ksi											8,737	13,134	1.5
M-64b		10	-3	4	-	-	-	22	-	-	-	14,144	18,374	1.3
M-72b		8	-3	2	3	-	-	15	35	-	-	11,888	16,121	1.36
M-91	Random spectrum, composite mission, σ_{lim} = 30 ksi											2,419	2,603	1.08
M-64a		15	-3	4	-	-	-	22	-	-	-	2,193	2,663	1.21
M-72a		14	-3	4	6	-	-	15	35	-	-	1,668	2,266	1.36

$*R = \dfrac{N_{pred}}{N_{test}}$

** Counted from common initial crack size
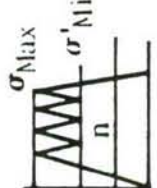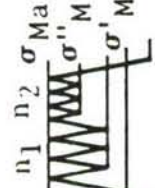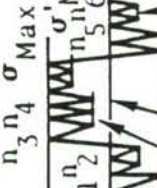
TABLE 13. SUMMARY, CRACK GROWTH DATA CORRELATIONS, METHODOLOGY DEVELOPMENT
TEST PROGRAM, GROUPS IV AND V (CONT)

Text No.	Loading profile	G-A-G step		Flight steps				n_1 n_5 (Cyc)	n_2 n_6 (Cyc)	n_3 (Cyc)	n_4 (Cyc)	Test life flights**	Analytical prediction	
		σ_{Max} (ksi)	σ_{Min} (ksi)	σ'_{Min} (ksi)	σ''_{Min} (ksi)	σ'''_{Min} (ksi)	σ'_{Max} (ksi)						Vroman/Chang pred life flight	R*
M-92		Random spectrum, composite mission, σ_{lim} = 40 ksi										854	896	1.06
M-64		20	-3	4	–	–	–	22	–	–	–	774	831	1.07
M-72		19	-3	6	8	–	–	15	35	–	–	676	803	1.19

$*R = \dfrac{N_{pred}}{N_{test}}$

** Counted from common initial crack size

231

TABLE 13. SUMMARY, CRACK GROWTH DATA CORRELATIONS, METHODOLOGY DEVELOPMENT TEST PROGRAM, GROUPS IV AND V (CONT)

Text No.	Loading profile	G-A-G step σ_{Max} (ksi)	σ_{Min} (ksi)	Flight steps σ'_{Min} (ksi)	σ''_{Min} (ksi)	σ'''_{Min} (ksi)	σ'_{Max} (ksi)	n_1 / n_5 (cyc)	n_2 / n_6 (cyc)	n_3 (cyc)	n_4 (cyc)	Test life flights**	Vroman/Chang pred life flight	R*
M-94		Random spectrum σ_{max} = 19.6 ksi										1,351	1,486	1.1
M-66		16.8	-10.5	16.1	-	-	-	133	-	-	-	3,187	1,829	0.58
M-74		16.8	-10.5	15.4	16.1	-	-	25	108	-	-	2,513	1,858	0.74
M-80		16.8	-10.5	-4.2	16.1	16.1	4.48	2	4	25	108	2,390	1,518	0.61

$*R = \dfrac{N_{pred}}{N_{test}}$

**Counted from common initial crack size

TABLE 13. SUMMARY, CRACK GROWTH DATA CORRELATIONS, METHODOLOGY DEVELOPMENT TEST PROGRAM, GROUPS IV AND V (CONCL)

Text No.	Loading profile	G-A-G step		Flight steps				n_1 n_5 (cyc)	n_2 n_6 (cyc)	n_3 (cyc)	n_4 (cyc)	Test life flights**	Analytical prediction	
		σ_{Max} (ksi)	σ_{Min} (ksi)	σ'_{Min} (ksi)	σ''_{Min} (ksi)	σ'''_{Min} (ksi)	σ'_{Max} (ksi)						Vroman/Chang pred life flight	R*
M-93		Random spectrum σ_{max} = 14 ksi										2,643	3,208	1.21
M-65		12	-7.5	11.5	-	-	-	133	-	-	-	6,361	4,133	0.65
M-79		12	-7.5	-3.0	10	11.5	3.2	2	4	25	108	2,673	3,293	1.23

*R = $\dfrac{N_{pred}}{N_{test}}$

**Counted from common initial crack size

233

TABLE 14. MISSION PROFILE AND STRESS DATA

Mission	Segment	Cycles	1.0 g Stress	Ground Stress ksi
Assault	Climb Cruise Gust Descent	65 15 25 45	10.783 9.075 9.000 10.622	-6.4
Logistics	Climb Cruise Gust Descent	10 5 45 10	9.339 7.458 9.000 10.272	-11.5
Training	Climb Cruise Gust Descent	40 10 45 20	6.559 6.171 9.000 8.648	-8.9

TABLE 15. TRANSFORMATION COEFFICIENT R^*, VARIANCE σ^2 AND ZERO UPCROSSINGS N_0 FOR TRANSPORT LOAD SPECTRA

Mission	Segment	R^*	σ^2	N_0 Cycles per Hour
Assault	Climb Cruise Gust Descent	2.10 2.15 2.66 2.00	2.75×10^{-2} 3.11×10^{-2} 3.20×10^{-2} 2.71×10^{-2}	270 41 47 190
Logistics	Climb Cruise Gust Descent	1.06 1.04 2.66 1.02	1.95×10^{-2} 2.67×10^{-2} 3.20×10^{-2} 1.96×10^{-2}	10 55 47 9
Training	Climb Cruise Gust Descent	2.00 2.00 2.66 2.28	2.99×10^{-2} 2.83×10^{-2} 3.20×10^{-2} 3.49×10^{-2}	160 40 47 65

234

TABLE 16. PARAMETERS λ, C, $(\overline{\Delta\sigma^b})^{1/b}$ AND $C(\overline{\Delta\sigma^b})^{\lambda/b}$ (WITH COMPRESSIVE STRESSES INCLUDED; σ_{LIM} = 20 KSI)

Type of Maneuver	Stress Intensity Factor Range	λ	C	$(\overline{\Delta\sigma^b})^{1/b}$ b = 2 (ksi)	$C(\overline{\Delta\sigma^b})^{\lambda/b}$ b = 2 in$^{-\lambda}\sqrt{in}$/Flight
A-A	(1) $\overline{K} \leqq K_{TH}$	5.139	1.483×10^{-8}		4.354×10^{-4}
	(2) $K_{TH} < \overline{K} < K_{IC}$	3.446	7.449×10^{-8}	7.402	7.384×10^{-5}
	(3) $\overline{K} < K_{IC}$	3.547	5.814×10^{-8}		7.050×10^{-5}
A-G	(1) $\overline{K} \leqq K_{TH}$	4.964	1.083×10^{-8}		1.548×10^{-4}
	(2) $K_{TH} < \overline{K} < K_{IC}$	3.467	4.352×10^{-8}	6.873	3.473×10^{-5}
	(3) $\overline{K} < K_{IC}$	3.583	3.310×10^{-8}		3.298×10^{-5}
I-N	(1) $\overline{K} \leqq K_{TH}$	5.191	2.814×10^{-9}		8.412×10^{-6}
	(2) $K_{TH} < \overline{K} < K_{IC}$	3.633	1.265×10^{-8}	4.672	3.423×10^{-6}
	(3) $\overline{K} < K_{IC}$	4.048	5.400×10^{-9}		2.771×10^{-6}
Composite	(1) $\overline{K} \leqq K_{TH}$	4.980	1.375×10^{-8}		2.514×10^{-4}
	(2) $K_{TH} < \overline{K} < K_{IC}$	3.466	5.562×10^{-8}	7.176	5.145×10^{-5}
	(3) $\overline{K} < K_{IC}$	3.557	4.459×10^{-8}		4.938×10^{-5}

TABLE 17. PARAMETERS λ, C, $(\overline{\Delta\sigma b})^{1/b}$ AND $C(\overline{\Delta\sigma b})^{\lambda/b}$ (DIFFERENT FLIGHTS IN THE UNITBLOCK; σ_{LIM} = 20 KSI)

Type of Maneuver	Stress Intensity Factor Range	λ	C	$(\overline{\Delta\sigma b})^{1/b}$ b = 2 (ksi)	$C(\overline{\Delta\sigma b})^{\lambda/b}$ b = 2 $in^{-\lambda}\sqrt{in}$/Flight
A-A	(1) $\overline{K} \leqq K_{TH}$	–	–		–
	(2) $K_{TH} < \overline{K} < K_{IC}$	3.405	8.171×10^{-8}	11.10	2.964×10^{-4}
	(3) $\overline{K} < K_{IC}$	3.405	8.171×10^{-8}		2.964×10^{-4}
A-G	(1) $\overline{K} \leqq K_{TH}$	–	–		–
	(2) $K_{TH} < \overline{K} < K_{IC}$	3.436	4.652×10^{-8}	10.31	1.408×10^{-4}
	(3) $\overline{K} < K_{IC}$	3.436	4.652×10^{-8}		1.408×10^{-4}
I-N	(1) $\overline{K} \leqq K_{TH}$	4.907	3.721×10^{-9}		5.249×10^{-5}
	(2) $K_{TH} < \overline{K} < K_{IC}$	3.558	1.485×10^{-8}	7.008	1.513×10^{-5}
	(3) $\overline{K} < K_{IC}$	3.727	1.021×10^{-8}		1.448×10^{-5}
Composite	(1) $\overline{K} \leqq K_{IC}$	–	–		–
	(2) $K_{TH} < \overline{K} < K_{IC}$	3.451	5.850×10^{-8}	10.76	2.129×10^{-4}
	(3) $\overline{K} < K_{IC}$	3.451	5.850×10^{-8}		2.129×10^{-4}

TABLE 18. PARAMETERS λ, C, $(\overline{\Delta\sigma b})^{1/b}$ AND $C(\overline{\Delta\sigma b})^{\lambda/b}$ (WITH COMPRESSIVE STRESSES INCLUDED; σ_{LIM} = 30 KSI)

Type of Maneuver	Stress Intensity Factor Range	λ	C	$(\overline{\Delta\sigma b})^{1/b}$ b = 2 (ksi)	$C(\overline{\Delta\sigma b})^{\lambda/b}$ b = 2 in$^{-\lambda}\sqrt{in}$/Flight
A-A	(1) $\overline{K} \leqq K_{TH}$	5.081	8.025×10^{-9}		2.098×10^{-4}
	(2) $K_{TH} < \overline{K} < K_{IC}$	3.597	3.352×10^{-8}	7.402	4.494×10^{-5}
	(3) $\overline{K} < K_{IC}$	3.690	2.669×10^{-8}		4.310×10^{-5}
A-G	(1) $\overline{K} \leqq K_{TH}$	4.878	6.903×10^{-9}		8.363×10^{-5}
	(2) $K_{TH} < \overline{K} < K_{IC}$	3.536	2.420×10^{-8}	6.873	2.206×10^{-5}
	(3) $\overline{K} < K_{IC}$	3.642	1.880×10^{-8}		2.104×10^{-5}
I-N	(1) $\overline{K} \leqq K_{TH}$	4.143	1.954×10^{-9}		1.160×10^{-6}
	(2) $K_{TH} < \overline{K} < K_{IC}$	3.594	3.544×10^{-9}	4.672	9.032×10^{-7}
	(3) $\overline{K} < K_{IC}$	3.774	2.444×10^{-9}		8.219×10^{-7}
Composite	(1) $\overline{K} \leqq K_{TH}$	4.984	7.386×10^{-9}		1.362×10^{-4}
	(2) $K_{TH} < \overline{K} < K_{IC}$	3.554	2.703×10^{-8}	7.176	2.974×10^{-5}
	(3) $\overline{K} < K_{IC}$	3.635	2.223×10^{-8}		2.870×10^{-5}

TABLE 19. PARAMETERS λ, C, $(\overline{\Delta\sigma^b})^{1/b}$ AND $C(\overline{\Delta\sigma^b})^{\lambda/b}$ (WITH COMPRESSIVE STRESSES INCLUDED, σ_{LIM} = 40 KSI)

Type of Manueuver	Stress Intensity Factor Range	λ	C	$(\overline{\Delta\sigma^b})^{1/b}$ b = 2 (ksi)	$C(\overline{\Delta\sigma^b})^{-\lambda/b}$ b = 2 $in^{-\lambda}\sqrt{in}$/Flight
A-A	(1) $\overline{K} \leq K_{TH}$	–	–		–
	(2) $K_{TH} < \overline{K} < K_{IC}$	3.320	9.691×10^{-8}	14.80	7.454×10^{-4}
	(3) $\overline{K} < K_{IC}$	3.320	9.691×10^{-8}		7.454×10^{-4}
A-G	(1) $\overline{K} \leq K_{TH}$	–	–		–
	(2) $K_{TH} < \overline{K} < K_{IC}$	3.390	5.161×10^{-8}	13.75	3.726×10^{-4}
	(3) $\overline{K} < K_{IC}$	3.390	5.161×10^{-8}		3.726×10^{-4}
I-N	(1) $\overline{K} \leq K_{TH}$	–	–		–
	(2) $K_{TH} < \overline{K} < K_{IC}$	3.545	1.564×10^{-8}	9.344	4.312×10^{-5}
	(3) $\overline{K} < K_{IC}$	3.545	1.342×10^{-8}		4.371×10^{-5}
Composite	(1) $\overline{K} \leq K_{TH}$	–	–		–
	(2) $K_{TH} < \overline{K} < K_{IC}$	3.363	6.935×10^{-8}	14.35	5.396×10^{-4}
	(3) $\overline{K} < K_{IC}$	3.363	6.935×10^{-8}		5.396×10^{-4}

TABLE 20. PARAMETERS λ, C, $(\overline{\Delta\sigma^b})^{1/b}$ AND $C(\overline{\Delta\sigma^b})^{\lambda/b}$ FOR NEW VALUES OF CONSTANTS (σ_{LIM} = 20 KSI)

TYPE OF MANEUVER	STRESS INTENSITY FACTOR RANGE		λ	C	$(\overline{\Delta\sigma^b})^{1/b}$ $b = 2$ (KSI)	$C(\overline{\Delta\sigma^b})^{\lambda/b}$ $b = 2$ $in^{-\lambda}\sqrt{in}$/FLIGHT
A – A	(1)	$\overline{K} \leq K < K_{TH}$	-	-		-
	(2)	$K_{TH} < \overline{K} < K_{IC}$	3.652	3.476×10^{-8}	7.381	5.142×10^{-5}
	(3)	$\overline{K} < K_{IC}$	3.652	3.476×10^{-8}		5.142×10^{-5}
A – G	(1)		-	-		-
	(2)		3.680	2.123×10^{-8}	6.873	2.558×10^{-5}
	(3)		3.680	2.123×10^{-8}		2.558×10^{-5}
I – N	(1)		5.724	2.702×10^{-9}		1.495×10^{-5}
	(2)		3.913	4.585×10^{-9}	4.508	1.660×10^{-6}
	(3)		3.949	4.286×10^{-9}		1.638×10^{-6}
COMPOSITE	(1)		-	-		-
	(2)		3.665	2.685×10^{-8}	7.188	3.702×10^{-5}
	(3)		3.665	2.685×10^{-8}		3.702×10^{-5}

TABLE 21. PARAMETERS λ, C, $(\overline{\Delta\sigma^b})^{1/b}$ AND $C(\overline{\Delta\sigma^b})^{\lambda/b}$ FOR NEW VALUES OF CONSTANTS (σ_{LIM} = 30 KSI)

TYPE OF MANEUVER	STRESS INTENSITY FACTOR RANGE		λ	C	$(\overline{\Delta\sigma^b})^{1/b}$ b = 2 (KSI)	$C(\overline{\Delta\sigma^b})^{\lambda/b}$ b = 2 in$^{-\lambda}\sqrt{in}$/FLIGHT
A – A	(1)	$\overline{K} \leqq K_{IC}$	–	–		–
	(2)	$K_{TH} < \overline{K} < K_{IC}$	3.606	3.880 x 10^{-8}	11.07	2.263 x 10^{-4}
	(3)	$\overline{K} < K_{IC}$	3.606	3.880 x 10^{-8}		2.263 x 10^{-4}
A – G	(1)		–	–		–
	(2)		3.629	2.403 x 10^{-8}	10.31	1.142 x 10^{-4}
	(3)		3.629	2.403 x 10^{-8}		1.142 x 10^{-4}
I – N	(1)		–	–		–
	(2)		3.730	7.018 x 10^{-9}	6.762	8.751 x 10^{-6}
	(3)		3.730	7.018 x 10^{-9}		8.751 x 10^{-6}
COMPOSITE	(1)		–	–		–
	(2)		3.641	2.898 x 10^{-8}	10.78	1.669 x 10^{-4}
	(3)		3.641	2.898 x 10^{-8}		1.669 x 10^{-4}

240

TABLE 22. PARAMETERS λ, C, $(\overline{\Delta\sigma^b})^{1/b}$ AND $C(\overline{\Delta\sigma^b})^{\lambda/b}$ FOR NEW VALUES OF CONSTANTS (σ_{LIM} = 40 KSI)

TYPE OF MANEUVER	STRESS INTENSITY FACTOR RANGE		λ	C	$(\overline{\Delta\sigma^b})^{1/b}$ b = 2 (KSI)	$C(\overline{\Delta\sigma^b})^{\lambda/b}$ b = 2 $in^{-\lambda}\sqrt{in}$/FLIGHT
A – A	(1)	$\overline{K} \leqq K_{TH}$	–	–		–
	(2)	$K_{TH} < \overline{K} < K_{IC}$	3.539	4.387×10^{-8}	14.76	6.029×10^{-4}
	(3)	$\overline{K} < K_{IC}$	3.539	4.387×10^{-8}		6.029×10^{-4}
A – G	(1)		–	–		–
	(2)		3.597	2.561×10^{-8}	13.75	3.183×10^{-4}
	(3)		3.597	2.561×10^{-8}		3.183×10^{-4}
I – N	(1)		–	–		–
	(2)		3.679	7.983×10^{-9}	9.016	2.604×10^{-5}
	(3)		3.679	7.983×10^{-9}		2.604×10^{-5}
COMPOSITE	(1)		–	–		–
	(2)		3.573	3.277×10^{-8}	14.38	4.478×10^{-4}
	(3)		3.573	3.277×10^{-8}		4.478×10^{-4}

TABLE 23. PARAMETERS λ, C, $\overline{(\Delta\sigma^b)}^{1/b}$ AND $C\overline{(\Delta\sigma^b)}^{\lambda/b}$ FOR RANDOM LOAD SPECTRA OF TRANSPORT AIRCRAFT ($\overline{\sigma_{LIM}}$ = 20 KSI)

Stress Magnification Factor η	Flight/Cycle	Stress Intensity Factor Range	λ	C	$\overline{(\Delta\sigma^b)}^{1/b}$ $b=2$ (ksi)	$C\overline{(\Delta\sigma^b)}^{\lambda/b}$ $b=2$ $in^{-\lambda}\sqrt{in}$/(Cycle or Flight)
1.0	Per Cycle	(1) $\overline{K} \leqq K_{TH}$	3.686	5.985×10^{-9}	1.950	7.013×10^{-8}
		(2) $K_{TH} < \overline{K} < K_{IC}$	3.664	7.534×10^{-9}		8.699×10^{-8}
		(3) $\overline{K} < K_{IC}$	3.798	6.322×10^{-9}		7.981×10^{-8}
	Per Flight	(1)	3.686	7.960×10^{-7}	1.950	9.327×10^{-6}
		(2)	3.664	1.002×10^{-6}		1.157×10^{-5}
		(3)	3.798	8.409×10^{-7}		1.062×10^{-5}
1.2	Per Cycle	(1)	3.793	6.463×10^{-9}	2.340	1.624×10^{-7}
		(2)	3.647	7.817×10^{-9}		1.735×10^{-7}
		(3)	3.770	6.533×10^{-9}		1.610×10^{-7}
	Per Flight	(1)	3.793	8.596×10^{-7}	2.340	1.062×10^{-5}
		(2)	3.647	1.040×10^{-6}		2.160×10^{-5}
		(3)	3.770	8.689×10^{-7}		2.141×10^{-5}
1.4	Per Cycle	(1)	3.839	6.674×10^{-9}	2.730	3.153×10^{-7}
		(2)	3.681	7.404×10^{-9}		2.985×10^{-7}
		(3)	3.742	6.745×10^{-9}		2.889×10^{-7}
	Per Flight	(1)	3.839	8.876×10^{-7}	2.730	4.193×10^{-5}
		(2)	3.681	9.848×10^{-7}		3.969×10^{-5}
		(3)	3.742	8.970×10^{-7}		3.842×10^{-5}

TABLE 24. SENSITIVITY OF λ, C, $\overline{(\Delta\sigma^b)}^{1/b}$, $C\overline{(\Delta\sigma^b)}^{\lambda/b}$ TO DIFFERENT CONSTANT AMPLITUDE LOADINGS (b=2, $R_{cut}^- = -0.15$, $R_{cut}^+ = 0.45$, $\sigma_{LIM} = 20$ KSI)

σ_{max} %	σ_{min} %	R	$\overline{(\Delta\sigma^b)}^{1/b}$ (ksi)	λ	C	$C\overline{(\Delta\sigma^b)}^{\lambda/b}$
120	48	.4	14.40	3.390	.60740E-08	.51268E-04
120	36	.3	16.80	3.384	.42704E-08	.59849E-04
120	24	.2	19.20	3.379	.31514E-08	.68364E-04
120	12	.1	21.60	3.373	.24203E-08	.76826E-04
120	0	.0	24.00	3.368	.19157E-08	.85230E-04
120	-12	-.1	26.40	3.362	.15563E-08	.93541E-04
110	44	.4	13.20	3.398	.59577E-08	.38289E-04
110	33	.3	15.40	3.394	.41762E-08	.44764E-04
110	22	.2	17.60	3.389	.30773E-08	.51230E-04
110	11	.1	19.80	3.386	.23482E-08	.57653E-04
110	0	.0	22.00	3.382	.18478E-08	.64050E-04
110	-11	-.1	24.20	3.377	.14920E-08	.70390E-04
100	40	.4	12.00	3.404	.58987E-08	.27793E-04
100	30	.3	14.00	3.401	.41148E-08	.32506E-04
100	20	.2	16.00	3.397	.30197E-08	.37227E-04
100	10	.1	18.00	3.396	.22858E-08	.41904E-04
100	0	.0	20.00	3.393	.17984E-08	.46638E-04
100	-10	-.1	22.00	3.390	.14456E-08	.51311E-04
90	36	.4	10.80	3.408	.58463E-08	.19449E-04
90	27	.3	12.60	3.406	.40682E-08	.22776E-04
90	18	.2	14.40	3.404	.29717E-08	.26094E-04
90	9	.1	16.20	3.403	.22493E-08	.29401E-04
90	0	.0	18.00	3.401	.17641E-08	.32747E-04
90	-9	-.1	19.80	3.398	.14148E-08	.36056E-04
80	32	.4	9.60	3.411	.58139E-08	.13032E-04
80	24	.3	11.20	3.410	.40400E-08	.15265E-04
80	16	.2	12.80	3.411	.29240E-08	.17484E-04
80	8	.1	14.40	3.409	.22181E-08	.19736E-04
80	0	.0	16.00	3.408	.17296E-08	.21967E-04
80	-8	-.1	17.60	3.407	.13816E-08	.24203E-04

TABLE 24. SENSITIVITY OF λ, C, $\overline{(\Delta\sigma^b)}^{1/b}$, $C\overline{(\Delta\sigma^b)}^{\lambda/b}$ TO DIFFERENT CONSTANT AMPLITUDE LOADINGS (b=2, $R_{cut}^- = -0.15$, $R_{cut}^+ = 0.45$, $\sigma_{LIM} = 20$ KSI) (CONT)

σ_{max} %	σ_{min} %	R	$\overline{(\Delta\sigma^b)}^{1/b}$ (ksi)	λ	C	$C\overline{(\Delta\sigma^b)}^{\lambda/b}$
70	28	.4	8.40	3.416	.57379E-08	.82479E-05
70	21	.3	9.80	3.421	.39202E-08	.96360E-05
70	14	.2	11.20	3.420	.28562E-08	.11064E-04
70	7	.1	12.60	3.414	.21906E-08	.12522E-04
70	0	.0	14.00	3.415	.16983E-08	.13943E-04
70	-7	-.1	15.40	3.413	.13597E-08	.15364E-04
60	24	.4	7.20	3.436	.54577E-08	.48159E-05
60	18	.3	8.40	3.422	.39205E-08	.56991E-05
60	12	.2	9.60	3.424	.28252E-08	.65232E-05
60	6	.1	10.80	3.429	.20993E-08	.73432E-05
60	0	.0	12.00	3.414	.17048E-08	.82490E-05
60	-6	-.1	13.20	3.415	.13523E-08	.90857E-05
50	20	.4	6.00	3.432	.55167E-08	.25844E-05
50	15	.3	7.00	3.459	.35527E-08	.29748E-05
50	10	.2	8.00	3.442	.26993E-08	.34635E-05
50	5	.1	9.00	3.425	.21299E-08	.39480E-05
50	0	.0	10.00	3.427	.16459E-08	.43958E-05
50	-5	-.1	11.00	3.437	.12696E-08	.48178E-05
40	16	.4	4.80	3.571	.40562E-08	.10978E-05
40	12	.3	5.60	3.486	.33480E-08	.13580E-05
40	8	.2	6.40	3.503	.22949E-08	.15294E-05
40	4	.1	7.20	3.427	.21038E-08	.18236E-05
40	0	.0	8.00	3.455	.15126E-08	.19966E-05
40	-4	-.1	8.80	3.437	.12684E-08	.22350E-05
30	12	.4	3.60	3.416	.55105E-08	.43804E-06
30	9	.3	4.20	3.377	.41870E-08	.53271E-06
30	6	.2	4.80	3.546	.20932E-08	.54474E-06
30	3	.1	5.40	3.575	.14626E-08	.60690E-06
30	0	.0	6.00	3.644	.95508E-09	.65396E-06
30	-3	-.1	6.60	3.490	.11021E-08	.79923E-06

TABLE 24. SENSITIVITY OF λ, C, $\overline{(\Delta\sigma^b)}^{1/b}$, $C\overline{(\Delta\sigma^b)}^{\lambda/b}$ TO DIFFERENT CONSTANT AMPLITUDE LOADINGS (b=2, $R_{cut}^- = -0.15$, $R_{cut}^+ = 0.45$, $\sigma_{LIM} = 20$ KSI) (CONCL)

	$\overline{(\Delta\sigma^b)}^{1/b}$ (ksi)	λ	C	$C\overline{(\Delta\sigma^b)}^{\lambda/b}$
Air-to-Air (A-A)	7.402	3.446	7.449×10^{-8}	7.384×10^{-5}
Air-to-Ground (A-G)	6.873	3.467	4.352×10^{-8}	3.473×10^{-5}
Instrumentation and Navigation (I-N)	4.672	3.633	1.265×10^{-8}	3.423×10^{-6}
Composite	7.176	3.466	5.562×10^{-8}	5.145×10^{-5}

Note: Parameter Values Listed in the Categories A-A, A-G, I-N and Composite for Stress Intensity Factor Range $K_{TH} < \bar{K} < K_{IC}$ are taken from Table 4-III.

TABLE 25. SENSITIVITY OF λ, C, $\overline{(\Delta\sigma^b)}^{1/b}$, $C\overline{(\Delta\sigma^b)}^{\lambda/b}$ TO DIFFERENT CONSTANT AMPLITUDE LOADINGS (b=2, $R_{cut}^- = -0.15$, $R_{cut}^+ = 0.45$, $\sigma_{LIM} = 30$ KSI)

σ_{max} %	σ_{min} %	R	$\overline{(\Delta\sigma^b)}^{1/b}$	λ	C	$C\overline{(\Delta\sigma^b)}^{\lambda/b}$
120	48	.4	21.60	3.362	.64767E-08	.19824E-03
120	36	.3	25.20	3.353	.46009E-08	.23028E-03
120	24	.2	28.80	3.345	.34422E-08	.26180E-03
120	12	.1	32.40	3.335	.26822E-08	.29260E-03
120	0	.0	36.00	3.324	.21626E-08	.32258E-03
120	-12	-.1	39.60	3.317	.17712E-08	.35281E-03
110	44	.4	19.80	3.374	.62899E-08	.14930E-03
110	33	.3	23.10	3.368	.44425E-08	.17376E-03
110	22	.2	26.40	3.362	.32958E-08	.19805E-03
110	11	.1	29.70	3.355	.25429E-08	.22205E-03
110	0	.0	33.00	3.348	.20243E-08	.24571E-03
110	-11	-.1	36.30	3.343	.16430E-08	.26928E-03
100	40	.4	18.00	3.385	.61491E-08	.10898E-03
100	30	.3	21.00	3.380	.43159E-08	.12712E-03
100	20	.2	24.00	3.375	.31851E-08	.14512E-03
100	10	.1	27.00	3.371	.24401E-08	.16306E-03
100	0	.0	30.00	3.366	.19272E-08	.18083E-03
100	-10	-.1	33.00	3.361	.15602E-08	.19843E-03
90	36	.4	16.20	3.393	.60384E-08	.76691E-04
90	27	.3	18.90	3.390	.42201E-08	.89581E-04
90	18	.2	21.60	3.386	.31016E-08	.10244E-03
90	9	.1	24.30	3.383	.23663E-08	.11524E-03
90	0	.0	27.00	3.380	.18594E-08	.12802E-03
90	-9	-.1	29.70	3.376	.14990E-08	.14063E-03
80	32	.4	14.40	3.399	.59570E-08	.51611E-04
80	24	.3	16.80	3.397	.41537E-08	.60358E-04
80	16	.2	19.20	3.395	.30391E-08	.69100E-04
80	8	.1	21.60	3.393	.23105E-08	.77835E-04
80	0	.0	24.00	3.390	.18103E-08	.86557E-04
80	-8	-.1	26.40	3.388	.14522E-08	.95205E-04

TABLE 25. SENSITIVITY OF λ, C, $\overline{(\Delta\sigma^b)}^{1/b}$, $C\overline{(\Delta\sigma^b)}^{\lambda/b}$ TO DIFFERENT CONSTANT AMPLITUDE LOADINGS (b=2, R_{cut}^{-} = -0.15, R_{cut}^{+} = 0.45, σ_{LIM} = 30 KSI) (CONT)

σ_{max} %	σ_{min} %	R	$\overline{(\Delta\sigma^b)}^{1/b}$	λ	C	$C\overline{(\Delta\sigma^b)}^{\lambda/b}$
70	28	.4	12.60	3.407	.58691E-08	.32943E-04
70	21	.3	14.70	3.404	.40826E-08	.38432E-04
70	14	.2	16.80	3.402	.29914E-08	.44058E-04
70	7	.1	18.90	3.400	.22718E-08	.49686E-04
70	0	.0	21.00	3.399	.17739E-08	.55287E-04
70	-7	-.1	23.10	3.397	.14201E-08	.60882E-04
60	24	.4	10.80	3.412	.58046E-08	.19508E-04
60	18	.3	12.60	3.411	.40299E-08	.22860E-04
60	12	.2	14.40	3.410	.29376E-08	.26206E-04
60	6	.1	16.20	3.410	.22171E-08	.29543E-04
60	0	.0	18.00	3.408	.17347E-08	.32920E-04
60	-6	-.1	19.80	3.403	.13979E-08	.36173E-04
50	20	.4	9.00	3.423	.56470E-08	.10427E-04
50	15	.3	10.50	3.418	.39589E-08	.12258E-04
50	10	.2	12.00	3.414	.29112E-08	.14072E-04
50	5	.1	13.50	3.417	.21787E-08	.15865E-04
50	0	.0	15.00	3.416	.16970E-08	.17690E-04
50	-5	-.1	16.50	3.413	.13656E-08	.19520E-04
40	16	.4	7.20	3.440	.54254E-08	.48248E-05
40	12	.3	8.40	3.423	.39091E-08	.57054E-05
40	8	.2	9.60	3.427	.28138E-08	.65324E-05
40	4	.1	10.80	3.432	.20882E-08	.73603E-05
40	0	.0	12.00	3.416	.17015E-08	.82561E-05
40	-4	-.1	13.20	3.417	.13484E-08	.90954E-05
30	12	.4	5.40	3.587	.39566E-08	.16756E-05
30	9	.3	6.30	3.446	.36778E-08	.20913E-05
30	6	.2	7.20	3.473	.24877E-08	.23611E-05
30	3	.1	8.10	3.445	.20113E-08	.27131E-05
30	0	.0	9.00	3.429	.16374E-08	.30656E-05
30	-3	-.1	9.90	3.427	.13095E-08	.33835E-05

TABLE 25. SENSITIVITY OF λ, C, $\overline{(\Delta\sigma^b)}^{1/b}$, $C\overline{(\Delta\sigma^b)}^{\lambda/b}$ TO DIFFERENT CONSTANT AMPLITUDE LOADINGS (b=2, $R^-_{cut} = -0.15$, $R^+_{cut} = 0.45$, $\sigma_{LIM} = 30$ KSI) (CONCL)

	$\overline{(\Delta\sigma^b)}^{1/b}$ (ksi)	λ	C	$C\overline{(\Delta\sigma^b)}^{\lambda/b}$
Air-to-Air (A-A)	11.100	3.405	8.171×10^{-8}	2.964×10^{-4}
Air-to-Ground (A-G)	10.310	3.436	4.652×10^{-8}	1.408×10^{-4}
Instrumentation and Navigation (I-N)	7.008	3.558	1.485×10^{-8}	1.513×10^{-5}
Composite	10.760	3.451	5.850×10^{-8}	2.129×10^{-4}

Note: Parameter Values Listed in the Categories A-A, A-G, I-N and Composite for Stress Intensity Factor Range

$K_{TH} < \overline{K} < K_{IC}$ are Taken from Table 4-IV.

TABLE 26. SENSITIVITY OF λ, C, $\overline{(\Delta\sigma^b)}^{1/b}$, $C\overline{(\Delta\sigma^b)}^{\lambda/b}$ TO DIFFERENT CONSTANT AMPLITUDE LOADINGS (b=2, R^-_{cut} = -0.15, R^+_{cut} = 0.45, σ_{LIM} = 40 KSI)

σ_{max} %	σ_{min} %	R	$\overline{(\Delta\sigma^b)}^{1/b}$ (ksi)	λ	C	$C\overline{(\Delta\sigma^b)}^{\lambda/b}$
120	48	.4	28.80	3.340	.68188E-08	.51004E-03
120	36	.3	33.60	3.326	.49289E-08	.58776E-03
120	24	.2	38.40	3.312	.37540E-08	.66305E-03
120	12	.1	43.20	3.297	.29787E-08	.73561E-03
120	0	.0	48.00	3.280	.24575E-08	.80374E-03
120	-12	-.1	52.80	3.274	.20099E-08	.87769E-03
110	44	.4	26.40	3.360	.65010E-08	.38841E-03
110	33	.3	30.80	3.350	.46391E-08	.44967E-03
110	22	.2	35.20	3.340	.34849E-08	.50958E-03
110	11	.1	39.60	3.330	.27218E-08	.56814E-03
110	0	.0	44.00	3.319	.21946E-08	.62516E-03
110	-11	-.1	48.40	3.308	.18141E-08	.68042E-03
100	40	.4	24.00	3.376	.62724E-08	.28608E-03
100	30	.3	28.00	3.369	.44321E-08	.33234E-03
100	20	.2	32.00	3.361	.32957E-08	.37798E-03
100	10	.1	36.00	3.354	.25473E-08	.42290E-03
100	0	.0	40.00	3.347	.20292E-08	.46718E-03
100	-10	-.1	44.00	3.340	.16570E-08	.51046E-03
90	36	.4	21.60	3.388	.61059E-08	.20265E-03
90	27	.3	25.20	3.383	.42857E-08	.23609E-03
90	18	.2	28.80	3.378	.31632E-08	.26924E-03
90	9	.1	32.40	3.373	.24252E-08	.30214E-03
90	0	.0	36.00	3.368	.19166E-08	.33461E-03
90	-9	-.1	39.60	3.363	.15515E-08	.36666E-03
80	32	.4	19.20	3.397	.59891E-08	.13709E-03
80	24	.3	22.40	3.394	.41829E-08	.16005E-03
80	16	.2	25.60	3.391	.30711E-08	.18291E-03
80	8	.1	28.80	3.387	.23412E-08	.20564E-03
80	0	.0	32.00	3.384	.18396E-08	.22824E-03
80	-8	-.1	35.20	3.381	.14805E-08	.25069E-03

249

TABLE 26. SENSITIVITY OF λ, C, $\overline{(\Delta\sigma^b)}^{1/b}$, $C\overline{(\Delta\sigma^b)}^{\lambda/b}$ TO DIFFERENT CONSTANT AMPLITUDE LOADINGS (b=2, R_{cut}^- = -0.15, R_{cut}^+ = 0.45, σ_{LIM} = 40 KSI) (CONT)

σ_{max} %	σ_{min} %	R	$\overline{(\Delta\sigma^b)}^{1/b}$ (ksi)	λ	C	$C\overline{(\Delta\sigma^b)}^{\lambda/b}$
70	28	.4	16.80	3.404	.59051E-08	.87617E-04
70	21	.3	19.60	3.402	.41106E-08	.10244E-03
70	14	.2	22.40	3.400	.30073E-08	.11724E-03
70	7	.1	25.20	3.398	.22831E-08	.13202E-03
70	0	.0	28.00	3.396	.17874E-08	.14677E-03
70	-7	-.1	30.80	3.394	.14323E-08	.16141E-03
60	24	.4	14.40	3.409	.58473E-08	.52044E-04
60	18	.3	16.80	3.408	.40632E-08	.60911E-04
60	12	.2	19.20	3.407	.29617E-08	.69795E-04
60	6	.1	21.60	3.406	.22438E-08	.78676E-04
60	0	.0	24.00	3.405	.17517E-08	.87573E-04
60	-6	-.1	26.40	3.403	.14004E-08	.96414E-04
50	20	.4	12.00	3.415	.57840E-08	.28033E-04
50	15	.3	14.00	3.413	.40205E-08	.32814E-04
50	10	.2	16.00	3.411	.29374E-08	.37604E-04
50	5	.1	18.00	3.413	.22073E-08	.42430E-04
50	0	.0	20.00	3.411	.17261E-08	.47280E-04
50	-5	-.1	22.00	3.410	.13785E-08	.52091E-04
40	16	.4	9.60	3.415	.57756E-08	.13062E-04
40	12	.3	11.20	3.413	.40129E-08	.15308E-04
40	8	.2	12.80	3.418	.28859E-08	.17583E-04
40	4	.1	14.40	3.418	.21810E-08	.19869E-04
40	0	.0	16.00	3.417	.16984E-08	.22115E-04
40	-4	-.1	17.60	3.417	.13530E-08	.24390E-04
30	12	.4	7.20	3.447	.53748E-08	.48444E-05
30	9	.3	8.40	3.425	.38982E-08	.57126E-05
30	6	.2	9.60	3.430	.27975E-08	.65504E-05
30	3	.1	10.80	3.438	.20714E-08	.73921E-05
30	0	.0	12.00	3.414	.17051E-08	.82449E-05
30	-3	-.1	13.20	3.416	.13515E-08	.90852E-05

TABLE 26. SENSITIVITY OF λ, C, $\overline{(\Delta\sigma^b)}^{1/b}$, $C\overline{(\Delta\sigma^b)}^{\lambda/b}$ TO DIFFERENT CONSTANT AMPLITUDE LOADINGS (b=2, R^-_{cut} = -0.15, R^+_{cut} = 0.45, σ_{LIM} = 40 KSI) (CONCL)

	$\overline{(\Delta\sigma^b)}^{1/b}$ (ksi)	λ	C	$C\overline{(\Delta\sigma^b)}^{\lambda/b}$
Air-to-Air (A-A)	14.800	3.320	9.691×10^{-8}	7.454×10^{-4}
Air-to-Ground (A-G)	13.750	3.390	5.161×10^{-8}	3.726×10^{-4}
Instrumentation and Navigation (I-N)	9.344	3.545	1.564×10^{-8}	4.312×10^{-5}
Composite	14.350	3.363	6.935×10^{-8}	5.396×10^{-4}

Note: Paramter Values Listed in the Categories A-A, A-G, I-N and Composite for Stress Intensity Factor Range $K_{TH} < \overline{K} < K_{IC}$ are taken from Table 4-V.

TABLE 27. SIMPLIFIED FLIGHT SPECTRA (FIGURE 129)

Test No. Rockwell Inter.	Case Number	σ_{max} (ksi)	σ_{min} (ksi)	σ'_{min} (ksi)	n_1 Cycles	Remarks
M - 61	I	20	-2	4	25	Air-to-Air
	II	15	-2	4	25	
	III	10	-2	4	25	
M - 62	I	18	-4	4	20	Air-to-Ground
	II	14	-4	4	20	
	III	10	-4	4	20	
M - 63	I	14	-2	4	10	Instrumentation & Navigation
	II	12	-2	4	10	
	III	10	-2	4	10	
	IV	9	-2	4	10	
	V	8	-2	3	6	
M - 64	I	20	-3	4	22	Composite
	II	15	-3	4	22	
	III	10	-3	4	22	

TABLE 28. SIMPLIFIED FLIGHT SPECTRA (FIGURE 130)

Test No. Rockwell Inter.	Case Number	σ_{max} (ksi)	σ_{min} (ksi)	σ'_{min} (ksi)	σ''_{min} (ksi)	n_1 Cycles	n_2 Cycles	Remarks
M – 69	I	20	-2	6	8	20	40	Air-to-Air
	II	15	-2	4	6	20	40	
	III	10	-2	3	4	20	40	
	IV	8	-2	2	3	20	40	
M – 70	I	18	-4	6	8	15	30	Air-to-Ground
	II	14	-4	4	6	15	30	
	III	10	-4	3	4	15	30	
	IV	8	-4	2	3	15	30	
	V	8	-4	2	3	10	20	
M – 71	I	14	-2	6	8	10	20	Instrumentation & Navigation
	II	12	-2	4	5	10	20	
	III	10	-2	3	4	10	20	
	IV	7	-2	2	3	10	20	
	V	7	-2	2	3	5	7	
M – 72	I	19	-3	6	8	15	35	Composite
	II	14	-3	4	6	15	35	
	III	9	-3	3	4	15	35	
	IV	8	-3	2	3	15	35	

TABLE 29.   SIMPLIFIED FLIGHT SPECTRA (FIGURE 131)

Test No. Rockwell Inter.	Case Number	σ_{max} (ksi)	σ'_{max} (ksi)	σ_{min} (ksi)	σ'_{min} (ksi)	σ''_{min} (ksi)	σ'''_{min} (ksi)	n_1 Cycles	n_2 Cycles	n_3 Cycles	n_4 Cycles
M – 77*	I	20	2	-3	-1	6	8	2	4	15	35
	II	15	2	-3	-1	4	6	2	4	15	35
	III	10	2	-3	-1	3	4	2	4	15	35
	IV	10	2	-3	-1	3	4	2	4	10	20
M – 78*	I	18	2	-6	-1	4	8	4	8	20	40
	II	14	2	-6	-1	4	6	4	8	20	40
	III	9	2	-6	-1	3	4	4	8	20	40
	IV	8	2	-6	-1	2	3	4	8	20	40

TABLE 30. PARAMETERS λ, C, $\overline{(\Delta\sigma^b)}^{1/b}$ AND $C\overline{(\Delta\sigma^b)}^{\lambda/b}$ (σ_{LIM} = 20 KSI, LOAD SPECTRA FROM TABLE 27)

Test No. Rockwell Inter.	Case Number	Stress Intensity Factor Range	λ	C	$\overline{(\Delta\sigma^b)}^{1/b}$ b = 2 ksi	$\overline{C(\Delta\sigma^b)}^{\lambda/b}$ b = 2 $in^{\frac{\lambda}{2}}\sqrt{in}$ / Flight
M – 61	I	(1) $\overline{K} \leq K_{TH}$			16.28	
		(2) $K_{TH} < \overline{K} < K_{IC}$	3.129	1.171×10^{-7}		7.247×10^{-4}
		(3) $\overline{K} < K_{IC}$	3.129	1.171×10^{-7}		7.247×10^{-4}
	II	(1)			11.30	
		(2)	3.264	1.052×10^{-7}		2.877×10^{-4}
		(3)	3.264	1.052×10^{-7}		2.877×10^{-4}
	III	(1)	3.469	8.808×10^{-9}	6.350	5.369×10^{-6}
		(2)	3.988	2.893×10^{-8}		4.600×10^{-5}
		(3)	4.517	8.269×10^{-9}		3.493×10^{-5}
M – 62	I	(1)			14.51	
		(2)	3.200	8.276×10^{-8}		4.312×10^{-4}
		(3)	3.200	8.276×10^{-8}		4.312×10^{-4}
	II	(1)			10.55	
		(2)	3.314	7.611×10^{-8}		1.869×10^{-4}
		(3)	3.314	7.611×10^{-8}		1.869×10^{-4}
	III	(1)	3.469	7.571×10^{-9}	6.633	5.365×10^{-6}
		(2)	3.952	2.178×10^{-8}		3.851×10^{-5}
		(3)	4.437	6.787×10^{-9}		3.001×10^{-5}

TABLE 30. PARAMETERS λ, C, $\overline{(\Delta\sigma^b)}^{1/b}$ AND $C\overline{(\Delta\sigma^b)}^{\lambda/b}$ (σ_{LIM} = 20 KSI, LOAD SPECTRA FROM TABLE 27) (CONT)

Test No. Rockwell Inter.	Case Number	Stress Intensity Factor Range	λ	C	$\overline{(\Delta\sigma^b)}^{1/b}$ b = 2 ksi	$C\overline{(\Delta\sigma^b)}^{\lambda/b}$ b_λ = 2 in $\sqrt{in}$ / Flight
	II	(1) $\overline{K} \leqq K_{TH}$	3.271	8.933×10^{-8}	11.41	2.565×10^{-4}
		(2) $K_{TH} < \overline{K} < K_{IC}$	3.271	8.933×10^{-8}		2.565×10^{-4}
		(3) $\overline{K} < K_{IC}$				
M – 64	III	(1)	3.469	8.192×10^{-9}		5.370×10^{-6}
		(2)	3.968	2.496×10^{-8}	6.484	4.154×10^{-5}
		(3)	4.471	7.509×10^{-9}		3.203×10^{-5}
Air-to-Air (A-A)		(1)	5.139	1.483×10^{-8}		4.354×10^{-4}
		(2)	3.446	7.449×10^{-8}	7.402	7.384×10^{-5}
		(3)	3.547	5.814×10^{-8}		7.050×10^{-5}
Air-to-Ground (A-G)		(1)	4.964	1.083×10^{-8}		1.548×10^{-4}
		(2)	3.467	4.352×10^{-8}	6.873	3.473×10^{-5}
		(3)	3.583	3.310×10^{-8}		3.298×10^{-5}
Instrumentation & Navigation (I-N)		(1)	5.191	2.814×10^{-9}		8.412×10^{-6}
		(2)	3.633	1.265×10^{-8}	4.672	3.423×10^{-6}
		(3)	4.048	5.400×10^{-9}		2.771×10^{-6}
Composite		(1)	4.980	1.375×10^{-8}		2.514×10^{-4}
		(2)	3.466	5.562×10^{-8}	7.176	5.145×10^{-5}
		(3)	3.557	4.459×10^{-8}		4.938×10^{-5}

TABLE 30. PARAMETERS λ, C, $(\overline{\Delta\sigma^b})^{1/b}$ AND $\overline{C(\Delta\sigma^b)}^{\lambda/b}$ (σ_{LIM} = 20 KSI, LOAD SPECTRA FROM TABLE 27) (CONCL)

Test No. Rockwell Inter.	Case Number	Stress Intensity Factor Range	λ	C	$(\overline{\Delta\sigma^b})^{1/b}$ b = 2 ksi	$\overline{C(\Delta\sigma^b)}^{\lambda/b}$ b = 2 $in \sqrt{in}$ / Flight
M – 63	I	(1) $\overline{K} \leq K_{TH}$				
		(2) $K_{TH} < \overline{K} < K_{IC}$	3.361	3.425×10^{-8}	10.75	1.003×10^{-4}
		(3) $\overline{K} < K_{IC}$	3.361	3.425×10^{-8}		1.003×10^{-4}
	II	(1)				
		(2)	3.674	1.682×10^{-8}	8.786	4.936×10^{-5}
		(3)	3.849	1.069×10^{-8}		4.583×10^{-5}
	III	(1)	3.469	6.802×10^{-9}		5.365×10^{-6}
		(2)	3.822	1.434×10^{-8}	6.841	2.229×10^{-5}
		(3)	4.174	6.102×10^{-9}		1.868×10^{-5}
	IV	(1)	3.566	7.485×10^{-9}		4.150×10^{-6}
		(2)	3.483	3.696×10^{-8}	5.882	1.769×10^{-5}
		(3)	4.169	7.595×10^{-9}		1.227×10^{-5}
	V	(1)	3.666	3.895×10^{-9}		2.989×10^{-6}
		(2)	3.439	1.674×10^{-8}	6.124	8.521×10^{-6}
		(3)	4.023	4.275×10^{-9}		6.267×10^{-6}
M – 64	I	(1)				
		(2)	3.144	9.925×10^{-8}	16.38	6.529×10^{-4}
		(3)	3.144	9.925×10^{-8}		6.529×10^{-4}

TABLE 31. PARAMETERS λ, C, $(\overline{\Delta\sigma^b})^{1/b}$ AND $\overline{C(\Delta\sigma^b)}^{\lambda/b}$ (σ_{LIM} = 20 KSI, LOAD SPECTRA FROM TABLE 28)

Test No. Rockwell Inter.	Case Number	Stress Intensity Factor Range	λ	C	$(\overline{\Delta\sigma^b})^{1/b}$ $b=2$ ksi	$\overline{C(\Delta\sigma^b)}^{\lambda/b}$ $b=2$ $in^{-\lambda}\sqrt{in}$ / Flight
M – 69	I	(1) $\overline{K} \leq K_{TH}$			12.89	
		(2) $K_{TH} < \overline{K} < K_{IC}$	3.066	4.853×10^{-7}		1.229×10^{-3}
		(3) $\overline{K} < K_{IC}$	3.066	4.853×10^{-7}		1.229×10^{-3}
	II	(1)			9.856	
		(2)	3.168	3.933×10^{-7}		5.534×10^{-4}
		(3)	3.246	2.716×10^{-7}		5.115×10^{-4}
	III	(1)	3.469	8.236×10^{-9}	6.474	5.365×10^{-6}
		(2)	3.529	1.864×10^{-7}		1.359×10^{-4}
		(3)	4.584	1.427×10^{-8}		7.466×10^{-5}
	IV	(1)	3.666	7.489×10^{-9}	5.123	2.991×10^{-6}
		(2)	3.363	3.069×10^{-7}		7.464×10^{-5}
		(3)	4.910	1.027×10^{-8}		3.130×10^{-5}
M – 70	I	(1)			11.060	
		(2)	3.135	3.615×10^{-7}		6.752×10^{-4}
		(3)	3.135	3.615×10^{-7}		6.752×10^{-4}
	II	(1)			8.999	
		(2)	3.365	1.924×10^{-7}		3.123×10^{-4}
		(3)	3.460	1.481×10^{-7}		2.963×10^{-4}

TABLE 31. PARAMETERS λ, C, $\overline{(\Delta\sigma b)}^{1/b}$ AND $C\overline{(\Delta\sigma b)}^{\lambda/b}$ σ_{LIM} = 20 KSI, LOAD SPECTRA FROM TABLE 28) (CONT)

Test No. Rockwell Inter.	Case Number	Stress Intensity Factor Range	λ	C	$\overline{(\Delta\sigma^b)}^{1/b}$ $b = 2$ ksi	$C\overline{(\Delta\sigma^b)}^{\lambda/b}$ $b = 2$ in $\sqrt{in}$ / Flight
M – 70	III	(1) $\overline{K} \leq K_{TH}$	3.469	7.691×10^{-9}		5.365×10^{-6}
		(2) $K_{TH} < \overline{K} < K_{IC}$	3.554	1.268×10^{-7}	6.603	1.039×10^{-4}
		(3) $\overline{K} < K_{IC}$	4.521	1.198×10^{-8}		6.091×10^{-5}
	IV	(1)	3.666	5.501×10^{-9}		2.990×10^{-6}
		(2)	3.411	1.675×10^{-7}	5.574	5.874×10^{-5}
		(3)	4.840	6.520×10^{-9}		2.663×10^{-5}
	V	(1)	3.666	5.130×10^{-9}		2.991×10^{-6}
		(2)	3.428	1.030×10^{-7}	5.680	3.969×10^{-5}
		(3)	4.688	5.826×10^{-9}		2.002×10^{-5}
M – 71	I	(1)	3.482	1.801×10^{-8}		1.734×10^{-5}
		(2)	3.513	1.234×10^{-7}	7.193	1.265×10^{-4}
		(3)	3.980	3.856×10^{-8}		9.925×10^{-5}
	II	(1)	3.418	9.207×10^{-9}		9.613×10^{-6}
		(2)	3.494	1.060×10^{-7}	7.642	1.291×10^{-4}
		(3)	4.094	2.292×10^{-8}		9.455×10^{-5}
	III	(1)	3.469	7.723×10^{-9}		5.365×10^{-6}
		(2)	3.599	8.010×10^{-8}	6.595	7.118×10^{-5}
		(3)	4.438	1.058×10^{-8}		4.575×10^{-5}

TABLE 31. PARAMETERS λ, C, $\overline{(\Delta\sigma^b)}^{1/b}$ AND $C\overline{(\Delta\sigma^b)}^{\lambda/b}$ (σ_{LIM} = 20 KSI, LOAD SPECTRA FROM TABLE 28) (CONT)

Test No. Rockwell Inter.	Case Number	Stress Intensity Factor Range	λ	C	$\overline{(\Delta\sigma^b)}^{1/b}$ $b = 2$ ksi	$C\overline{(\Delta\sigma^b)}^{\lambda/b}$ $b = 2$ in$\sqrt{\text{in}}$ / Flight
M – 71	IV	(1) $\overline{K} \le K_{TH}$	6.667	1.909×10^{-9}		4.773×10^{-5}
		(2) $K_{TH} < \overline{K} < K_{IC}$	3.851	5.143×10^{-8}	4.568	1.787×10^{-5}
		(3) $\overline{K} < K_{IC}$	4.764	7.671×10^{-9}		1.066×10^{-5}
	V	(1)	5.405	2.184×10^{-9}		1.229×10^{-5}
		(2)	3.765	1.970×10^{-8}	4.941	8.069×10^{-6}
		(3)	4.377	5.249×10^{-9}		5.717×10^{-6}
M – 72	I	(1)				
		(2)	3.114	3.985×10^{-7}	11.90	8.919×10^{-4}
		(3)	3.114	3.985×10^{-7}		8.919×10^{-4}
	II	(1)				
		(2)	3.366	2.178×10^{-7}	8.865	3.370×10^{-4}
		(3)	3.469	1.640×10^{-7}		3.180×10^{-4}
	III	(1)	3.566	9.394×10^{-9}		4.150×10^{-6}
		(2)	3.418	2.443×10^{-7}	5.519	8.385×10^{-5}
		(3)	4.787	1.080×10^{-8}		3.843×10^{-5}
	IV	(1)	3.666	5.863×10^{-9}		2.991×10^{-6}
		(2)	3.402	1.992×10^{-7}	5.477	6.479×10^{-5}
		(3)	4.874	7.172×10^{-9}		2.854×10^{-5}

TABLE 31. PARAMETERS λ, C, $(\overline{\Delta\sigma^b})^{1/b}$ AND $C(\overline{\Delta\sigma^b})^{\lambda/b}$ $\sigma_{LII} = 20$ KSI, LOAD SPECTRA FROM TABLE 28) (CONCL)

Type of Maneuver	Stress Intensity Factor Range	λ	C	$(\overline{\Delta\sigma^b})^{1/b}$ $b=2$ ksi	$C(\overline{\Delta\sigma^b})^{\lambda/b}$ $b=2$ $in^{-\lambda}\sqrt{in}$ / Flight
Air-to-Air (A-A)	(1) $\overline{K} \leqq K_{TH}$	5.139	1.483×10^{-8}		4.354×10^{-4}
	(2) $K_{TH} < \overline{K} < K_{IC}$	3.446	7.449×10^{-8}	7.402	7.384×10^{-5}
	(3) $\overline{K} < K_{IC}$	3.547	5.814×10^{-8}		7.050×10^{-5}
Air-to-Ground (A-G)	(1)	4.964	1.083×10^{-8}		1.548×10^{-4}
	(2)	3.467	4.352×10^{-8}	6.873	3.473×10^{-5}
	(3)	3.583	3.310×10^{-8}		3.298×10^{-5}
Instrumentation & Navigation (I-N)	(1)	5.191	2.814×10^{-9}		8.412×10^{-6}
	(2)	3.633	1.265×10^{-8}	4.672	3.423×10^{-6}
	(3)	4.048	5.400×10^{-9}		2.771×10^{-6}
Composite	(1)	4.980	1.375×10^{-8}		2.514×10^{-4}
	(2)	3.466	5.562×10^{-8}	7.176	5.145×10^{-5}
	(3)	3.557	4.459×10^{-8}		4.938×10^{-5}

TABLE 32. PARAMETERS λ, C, $(\overline{\Delta\sigma^b})^{1/b}$ AND $C(\overline{\Delta\sigma^b})^{\lambda/b}$ (σ_{LIM} = 20 KSI, LOAD SPECTRA FROM TABLE 29)

Test No. Rockwell Inter.	Case Number	Stress Intensity Factor Range	λ	C	$(\overline{\Delta\sigma^b})^{1/b}$ $b=2$ ksi	$C(\overline{\Delta\sigma^b})^{\lambda/b}$ $b=2$ λ in$\sqrt{\text{in}}$ / Flight
		(1) $\overline{K} \leqq K_{TH}$				
		(2) $K_{TH} < \overline{K} < K_{IC}$				
		(3) $\overline{K} < K_{IC}$				
M – 77	I	(1)			12.32	
		(2)	3.066	5.026×10^{-7}		1.109×10^{-3}
		(3)	3.066	5.026×10^{-7}		1.109×10^{-3}
	II	(1)			9.466	
		(2)	3.177	3.938×10^{-7}		4.975×10^{-4}
		(3)	3.303	2.751×10^{-7}		4.610×10^{-4}
	III	(1)	3.504	2.485×10^{-8}	6.384	1.645×10^{-5}
		(2)	3.532	1.754×10^{-7}		1.223×10^{-4}
		(3)	4.193	3.547×10^{-8}		8.433×10^{-5}
	IV	(1)	6.867	1.952×10^{-9}	5.884	3.777×10^{-4}
		(2)	3.382	2.020×10^{-7}		8.092×10^{-5}
		(3)	4.460	1.667×10^{-8}		4.514×10^{-5}
M – 78	I	(1)			10.200	
		(2)	3.113	6.582×10^{-7}		9.080×10^{-4}
		(3)	3.113	6.582×10^{-7}		9.080×10^{-4}
	II	(1)	3.422	1.676×10^{-7}	7.974	2.040×10^{-4}
		(2)	3.175	5.980×10^{-7}		4.358×10^{-4}
		(3)	3.412	3.144×10^{-7}		3.746×10^{-4}

TABLE 32. PARAMETERS λ, C, $\overline{(\Delta\sigma^b)}^{1/b}$ AND $C\overline{(\Delta\sigma^b)}^{\lambda/b}$ (σ_{LIM} = 20 KSI, LOAD SPECTRA FROM TABLE 29) (CONCL)

Test No. Rockwell Inter.	Case Number	Stress Intensity Factor Range	λ	C	$\overline{(\Delta\sigma^b)}^{1/b}$ $b = 2$ ksi	$C\overline{(\Delta\sigma^b)}^{\lambda/b}$ $b = 2$ $in \sqrt{in}$ / Flight
M – 78	III	(1) $\overline{K} \le K_{TH}$	7.463	3.611×10^{-9}	4.780	4.244×10^{-4}
		(2) $K_{TH} < \overline{K} < K_{IC}$	3.312	5.663×10^{-7}		1.007×10^{-4}
		(3) $\overline{K} < K_{IC}$	4.840	2.124×10^{-8}		4.124×10^{-5}
	IV	(1)	3.510	7.006×10^{-9}	5.369	2.553×10^{-6}
		(2)	3.393	2.593×10^{-7}		7.761×10^{-5}
		(3)	4.824	1.027×10^{-8}		3.409×10^{-5}
Air-to-Air (A-A)		(1)	5.139	1.483×10^{-8}	7.402	4.354×10^{-4}
		(2)	3.446	7.449×10^{-8}		7.384×10^{-5}
		(3)	3.547	5.814×10^{-8}		7.050×10^{-5}
Air-to-Ground (A-G)		(1)	4.964	1.083×10^{-8}	6.873	1.548×10^{-4}
		(2)	3.467	4.352×10^{-8}		3.473×10^{-5}
		(3)	3.583	3.310×10^{-8}		3.298×10^{-5}
Instrumentation & Navigation (I-N)		(1)	5.191	2.814×10^{-9}	4.672	8.412×10^{-6}
		(2)	3.633	1.265×10^{-8}		3.423×10^{-6}
		(3)	4.048	5.400×10^{-9}		2.771×10^{-6}
Composite		(1)	4.980	1.375×10^{-8}	7.176	2.514×10^{-4}
		(2)	3.466	5.562×10^{-8}		5.145×10^{-5}
		(3)	3.557	4.459×10^{-8}		4.938×10^{-5}

TABLE 33. SIMPLIFIED FLIGHT SPECTRA (NEW VALUES OF MATERIAL CONSTANTS)

TEST NO. ROCKWELL INTER.	σ_{LIM}	σ_{max} ksi	σ'_{max} ksi	σ_{min} ksi	σ'_{min} ksi	σ''_{min} ksi	σ'''_{min} ksi	n_1 Cycles	n_2 Cycles	n_3 Cycles	n_4 Cycles
M – 61	30	15	-	-2	4	-	-	25	-	-	-
	40	20	-	-2	4	-	-	25	-	-	-
M – 62	30	14	-	-4	4	-	-	20	-	-	-
	40	18	-	-4	4	-	-	20	-	-	-
M – 63	30	10	-	-2	4	-	-	10	-	-	-
	20	10	-	-3	4	-	-	22	-	-	-
M – 64	30	15	-	-3	4	-	-	22	-	-	-
	40	20	-	-3	4	-	-	22	-	-	-
M – 69	30	12	-	-2	3	4	-	20	40	-	-
M – 70	30	10	-	-4	3	4	-	15	30	-	-
M – 72	20	8	-	-3	2	3	-	15	35	-	-
	30	14	-	-3	4	6	-	15	35	-	-
	40	19	-	-3	6	8	-	15	35	-	-
M – 77	30	14	2	-6	-1	4	6	4	8	20	40

TABLE 34. PARAMETERS λ, C, $\overline{(\Delta\sigma^b)}^{1/b}$, AND $\overline{C(\Delta\sigma^b)}^{\lambda/b}$ ESTIMATED PER FLIGHT FOR SIMPLIFIED LOAD SPECTRA

TEST NO. ROCKWELL INTER.	σ_{LIM} KSI	STRESS INTENSITY FACTOR RANGE	λ	C	$\overline{(\Delta\sigma^b)}^{1/b}$ b = 2 (KSI)	$\overline{C(\Delta\sigma^b)}^{\lambda/b}$ b = 2 $in^{-\lambda}\sqrt{in}$/Flight
M – 61	30	(2) $K_{TH} < \overline{K} < K_{IC}$	3.605	3.247×10^{-8}	11.30	2.030×10^{-4}
	40	(2)	3.529	3.364×10^{-8}	16.28	6.347×10^{-4}
M – 62	30	(2)	3.626	2.451×10^{-8}	10.55	1.257×10^{-4}
	40	(2)	3.590	2.409×10^{-8}	14.51	3.560×10^{-4}
M – 63	30	(2)	3.686	1.217×10^{-8}	6.841	1.457×10^{-5}
	20	(2)	3.676	2.914×10^{-8}	6.484	2.811×10^{-5}
M – 64	30	(2)	3.610	2.774×10^{-8}	11.41	1.819×10^{-4}
	40	(2)	3.543	2.851×10^{-8}	16.38	5.723×10^{-4}
M – 69	30	(2)	3.623	8.177×10^{-8}	8.461	1.872×10^{-4}
M – 70	30	(2)	3.687	5.759×10^{-8}	6.603	6.068×10^{-5}
	20	(2)	3.752	5.073×10^{-8}	5.477	2.993×10^{-5}
M – 72	20	(3) $\overline{K} < K_{fc}$	3.877	3.896×10^{-8}	5.477	2.843×10^{-5}
	30	(2)	3.614	8.064×10^{-8}	8.865	2.146×10^{-4}
	40	(2)	3.539	9.323×10^{-8}	11.90	5.982×10^{-4}
M – 77	30	(2)	3.604	1.438×10^{-7}	7.974	2.552×10^{-4}

TABLE 35. SIMPLIFIED FLIGHT SPECTRA (TRANSPORT AIRCRAFT)

Stress Magnification Factor	Test No. Rockwell Inter.	Case Number	σ_{max} (ksi)	σ'_{max} (ksi)	σ_{min} (ksi)	σ'_{min} (ksi)	σ''_{min} (ksi)	σ'''_{min} (ksi)	n_1 Cycles	n_2 Cycles	n_3 Cycles	n_4 Cycles
	M-65	I	12.0		-7.5	8.0			133			
		II	12.0		-7.5	9.0			133			
		III	12.0		-7.5	10.0			133			
		IV	12.0		-7.5	11.5			133			
		V	12.0		-7.5	11.6			133			
		VI	12.0		-7.5	11.9			133			
$\eta = 1.0$	M-73	I	12.0		-7.5	7.0	9.0		25	108		
		II	12.0		-7.5	8.0	10.0		25	108		
		III	12.0		-7.5	9.0	11.0		25	108		
		IV	12.0		-7.5	10.0	11.0		25	108		
		V	12.0		-7.5	10.5	11.5		25	108		
		VI	12.0		-7.5	11.0	11.5		25	108		
	M-79	I	12.0	3.2	-7.5	-3.0	7.0	9.0	2	4	25	108
		II	12.0	3.2	-7.5	-3.0	8.0	10.0	2	4	25	108
		III	12.0	3.2	-7.5	-3.0	9.0	11.0	2	4	25	108
		IV	12.0	3.2	-7.5	-3.0	10.0	11.0	2	4	25	108
		V	12.0	3.2	-7.5	-3.0	10.0	11.5	2	4	25	108
		VI	12.0	3.2	-7.5	-3.0	10.5	11.5	2	4	25	108

TABLE 35. SIMPLIFIED FLIGHT SPECTRA (TRANSPORT AIRCRAFT) (CONCL)

Stress Magnification Factor	Test No. Rockwell Inter.	Case Number	σ_{max} (ksi)	σ'_{max} (ksi)	σ_{min} (ksi)	σ'_{min} (ksi)	σ''_{min} (ksi)	σ'''_{min} (ksi)	n_1 Cycles	n_2 Cycles	n_3 Cycles	n_4 Cycles
$\eta = 1.2$	M-65	I	14.4		-9.0	13.8			133			
		II	14.4		-9.0	14.16			133			
	M-73	I	14.4		-9.0	13.2	13.8		25	108		
		II	14.4	3.84	-9.0	13.2	14.16		25	108		
	M-79	I	14.4	3.84	-9.0	-3.6	12.0	13.8	2	4	25	108
		II	14.4		-9.0	-3.6	12.0	13.2	2	4	25	108
$\eta = 1.4$	M-65	I	16.8		-10.5	16.1			133			
		II	16.8		-10.5	16.52			133			
	M-73	I	16.8	4.48	-10.5	15.4	16.1		25	108		
		II	16.8	4.48	-10.5	15.4	16.52		25	108		
	M-79	I	16.8	4.48	-10.5	-4.2	14.0	16.1	2	4	25	108
		II	16.8	4.48	-10.5	-4.2	14.0	15.4	2	4	25	108
		III	16.8	4.48	-10.5	-4.2	14.7	16.1	2	4	25	108

TABLE 36. PARAMETERS λ, C, $(\overline{\Delta\sigma^b})^{1/b}$, AND $C(\overline{\Delta\sigma^b})^{\lambda/b}$ (σ_{LIM} = 20 KSI)

Stress Magnification Factor η	Test No. Rockwell Inter.	Case Number	Stress Intensity Factor Range	λ	C	$(\overline{\Delta\sigma^b})^{1/b}$ b = 2 (ksi)	$C(\overline{\Delta\sigma^b})^{\lambda/b}$ b = 2 $in^{-\lambda}\sqrt{in}$/Flight
		I	(1) $\overline{K} \leq K_{TH}$	3.647	5.806×10^{-8}		1.216×10^{-5}
			(2) $K_{TH} < \overline{K} < K_{IC}$	4.202	1.245×10^{-7}	4.329	5.880×10^{-5}
			(3) $\overline{K} < K_{IC}$	4.412	8.250×10^{-8}		5.294×10^{-5}
		II	(1)	3.647	1.350×10^{-7}		1.214×10^{-5}
			(2)	4.457	1.226×10^{-7}	3.434	2.993×10^{-5}
			(3)	4.440	1.254×10^{-7}		3.000×10^{-5}
		III	(1)	3.603	3.618×10^{-7}		1.152×10^{-5}
$\eta = 1.0$	M - 65		(2)	3.693	7.552×10^{-7}	2.613	2.622×10^{-5}
			(3)	4.096	3.908×10^{-7}		1.999×10^{-5}
		IV	(1)	3.603	1.495×10^{-6}		1.152×10^{-5}
			(2)	3.629	1.551×10^{-6}	1.763	1.213×10^{-5}
			(3)	3.642	1.524×10^{-6}		1.201×10^{-5}
		V	(1)	3.603	1.575×10^{-6}		1.152×10^{-5}
			(2)	3.629	1.635×10^{-6}	1.737	1.213×10^{-5}
			(3)	3.642	1.607×10^{-6}		1.201×10^{-5}
		VI	(1)	3.603	1.726×10^{-6}		1.152×10^{-5}
			(2)	3.629	1.792×10^{-6}	1.694	1.213×10^{-5}
			(3)	3.642	1.762×10^{-6}		1.201×10^{-5}

TABLE 36. PARAMETERS λ, C, $\overline{(\Delta\sigma^b)}^{1/b}$, AND $C\overline{(\Delta\sigma^b)}^{\lambda/b}$ (σ_{LIM} = 20 KSI) (CONT)

Stress Magnification Factor η	Test No. Rockwell Inter.	Case Number	Stress Intensity Factor Range	λ	C	$\overline{(\Delta\sigma^b)}^{1/b}$ b = 2 (ksi)	$C\overline{(\Delta\sigma^b)}^{\lambda/b}$ b = 2 $in^{-\lambda}\sqrt{in}$/Flight
η = 1.0	M – 73	I	(1) $\overline{K} \leq K_{TH}$	6.856	1.132×10^{-7}	3.831	1.131×10^{-9}
			(2) $K_{TH} < \overline{K} < K_{IC}$	4.026	2.300×10^{-7}		5.131×10^{-5}
			(3) $\overline{K} < K_{IC}$	4.149	1.849×10^{-7}		4.865×10^{-5}
		II	(1)	5.097	2.854×10^{-7}	2.999	7.705×10^{-5}
			(2)	4.125	3.042×10^{-7}		2.822×10^{-5}
			(3)	4.179	2.804×10^{-7}		2.762×10^{-5}
		III	(1)	3.603	5.722×10^{-7}	2.301	1.152×10^{-5}
			(2)	3.694	9.026×10^{-7}		1.961×10^{-5}
			(3)	3.937	6.264×10^{-7}		1.666×10^{-5}
		IV	(1)	3.603	8.011×10^{-7}	2.096	1.152×10^{-5}
			(2)	3.714	9.484×10^{-7}		1.481×10^{-5}
			(3)	3.788	8.509×10^{-7}		1.404×10^{-5}
		V	(1)	3.603	1.226×10^{-6}	1.862	1.152×10^{-5}
			(2)	3.683	1.314×10^{-6}		1.297×10^{-5}
			(3)	3.702	1.278×10^{-6}		1.277×10^{-5}
		VI	(r)	3.603	1.384×10^{-6}	1.801	1.152×10^{-5}
			(2)	3.648	1.422×10^{-6}		1.215×10^{-5}
			(3)	3.651	1.414×10^{-6}		1.211×10^{-5}

TABLE 36. PARAMETERS λ, C, $\overline{(\Delta\sigma^b)}^{1/b}$, AND $\overline{C(\Delta\sigma^b)}^{\lambda/b}$ $((\sigma_{LIM} = 20.\ KSI)$ (CONT)

Stress Magnification Factor η	Test No. Rockwell Inter.	Case Number	Stress Intensity Factor Range	λ	C	$\overline{(\Delta\sigma^b)}^{1/b}$ b = 2 (ksi)	$\overline{C(\Delta\sigma^b)}^{\lambda/b}$ b = 2 in$^{-\lambda}\sqrt{in}$/Flight
$\eta = 1.0$	M – 79	I (1)	$\overline{K} \leq K_{TH}$	7.603	4.221×10^{-8}	4.204	2.327×10^{-3}
		I (2)	$K_{TH} < \overline{K} < K_{IC}$	4.059	1.442×10^{-7}		4.903×10^{-5}
		I (3)	$\overline{K} < K_{IC}$	4.216	1.072×10^{-7}		4.576×10^{-5}
		II (1)		5.601	9.150×10^{-8}	3.530	1.070×10^{-4}
		II (2)		4.225	1.231×10^{-7}		2.537×10^{-5}
		II (3)		4.294	1.099×10^{-7}		2.471×10^{-5}
		III (1)		3.993	1.692×10^{-7}	3.011	1.380×10^{-5}
		III (2)		4.088	1.541×10^{-7}		1.396×10^{-5}
		III (3)		4.044	1.654×10^{-7}		1.428×10^{-5}
		IV (1)		3.728	1.972×10^{-7}	2.870	1.005×10^{-5}
		IV (2)		3.889	1.952×10^{-7}		1.179×10^{-5}
		IV (3)		3.880	1.974×10^{-7}		1.181×10^{-5}
		V (1)		3.728	2.247×10^{-7}	2.771	1.005×10^{-5}
		V (2)		3.833	2.329×10^{-7}		1.159×10^{-5}
		V (3)		3.847	2.273×10^{-7}		1.147×10^{-5}
		VI (1)		3.728	2.414×10^{-7}	2.718	1.005×10^{-5}
		VI (2)		3.797	2.362×10^{-7}		1.053×10^{-5}
		VI (3)		3.782	2.414×10^{-7}		1.061×10^{-5}

TABLE 36. PARAMETERS λ, C, $(\overline{\Delta\sigma^b})^{1/b}$, AND $C(\overline{\Delta\sigma^b})^{\lambda/b}$ (σ_{LIM} = 20 KSI) (CONT)

Stress Magnification Factor η	Test No. Rockwell Inter.	Case Number	Stress Intensity Factor Range	λ	C	$(\overline{\Delta\sigma^b})^{1/b}$ $b=2$ (ksi)	$\overline{C(\Delta\sigma^b)}^{\lambda/b}$ $b=2$ $in^{-\lambda}\sqrt{in}/Flight$
$\eta = 1.2$	M - 65	I	(1) $\overline{K} \leq K_{TH}$	3.635	1.535×10^{-6}	2.115	2.339×10^{-5}
			(2) $K_{TH} < \overline{K} < K_{IC}$	3.608	1.583×10^{-6}		2.362×10^{-5}
			(3) $\overline{K} < K_{IC}$	3.629	1.537×10^{-6}		2.331×10^{-5}
		II	(1)	3.635	1.742×10^{-6}	2.043	2.339×10^{-5}
			(2)	3.608	1.795×10^{-6}		2.362×10^{-5}
			(3)	3.629	1.744×10^{-6}		2.331×10^{-5}
	M - 73	I	(1)	3.635	1.421×10^{-6}	2.161	2.339×10^{-5}
			(2)	3.642	1.443×10^{-6}		2.389×10^{-5}
			(3)	3.650	1.427×10^{-6}		2.376×10^{-5}
		II	(1)	3.635	1.568×10^{-6}	2.103	2.339×10^{-5}
			(2)	3.642	1.593×10^{-6}		2.389×10^{-5}
			(3)	3.650	1.575×10^{-6}		2.376×10^{-5}
	M - 79	I	(1)	4.030	2.283×10^{-7}	3.325	2.893×10^{-5}
			(2)	3.850	2.219×10^{-7}		2.265×10^{-5}
			(3)	3.834	2.284×10^{-7}		2.288×10^{-5}
		II	(1)	4.030	1.982×10^{-7}	3.444	2.893×10^{-5}
			(2)	3.955	1.800×10^{-7}		2.395×10^{-5}
			(3)	3.910	1.951×10^{-7}		2.455×10^{-5}

TABLE 36. PARAMETERS λ, C, $(\overline{\Delta\sigma^b})^{1/b}$, AND $C(\overline{\Delta\sigma^b})^{\lambda/b}$ (σ_{LIM} = 20 KSI) (CONCL.)

Stress Magnification Factor η	Test No. Rockwell Inter.	Case Number	Stress Intensity Factor Range	λ	C	$(\overline{\Delta\sigma^b})^{1/b}$ b = 2 (ksi)	$C(\overline{\Delta\sigma^b})^{\lambda/b}$ b = 2 $in^{-\lambda}\sqrt{in}$/Flight
$\eta = 1.4$	M - 65	I	(1) $\overline{K} \leq K_{TH}$	3.629	1.536×10^{-6}		4.072×10^{-5}
			(2) $K_{TH} < \overline{K} < K_{IC}$	3.599	1.598×10^{-6}	2.468	4.125×10^{-5}
			(3) $\overline{K} < K_{IC}$	3.624	1.539×10^{-6}		4.063×10^{-5}
		II	(1)	3.629	1.742×10^{-6}		4.072×10^{-5}
			(2)	3.575	1.862×10^{-6}	2.384	4.153×10^{-5}
			(3)	3.617	1.748×10^{-6}		4.045×10^{-5}
	M - 73	I	(1)	3.629	1.421×10^{-6}		4.072×10^{-5}
			(2)	3.619	1.497×10^{-6}	2.521	4.250×10^{-5}
			(3)	3.648	1.429×10^{-6}		4.168×10^{-5}
		II	(1)	3.629	1.568×10^{-6}		4.072×10^{-5}
			(2)	3.600	1.688×10^{-6}	2.454	4.272×10^{-5}
			(3)	3.643	1.579×10^{-6}		4.154×10^{-5}
	M - 79	I	(1)	3.993	2.266×10^{-7}		5.083×10^{-5}
			(2)	3.826	2.225×10^{-7}	3.880	3.982×10^{-5}
			(3)	3.812	2.287×10^{-7}		4.014×10^{-5}
		II	(1)	3.993	1.969×10^{-7}		5.083×10^{-5}
			(2)	3.929	1.840×10^{-7}	4.018	4.346×10^{-5}
			(3)	3.902	1.939×10^{-7}		4.409×10^{-5}
		III	(1)	3.993	2.447×10^{-7}		5.083×10^{-5}
			(2)	3.761	2.418×10^{-7}	3.806	3.684×10^{-5}
			(3)	3.747	2.482×10^{-7}		3.713×10^{-5}

TABLE 37. EQUIVALENT SIMPLIFIED FLIGHT SPECTRA FOR TRANSPORT AIRCRAFT (σ_{LIM} = 20 KSI)

Test No. Rockwell Inter.	η	σ_{max} ksi	σ'_{max} ksi	σ_{min} ksi	σ'_{min} ksi	σ''_{min} ksi	σ'''_{min} ksi	n_1 Cycles	n_2 Cycles	n_3 Cycles	n_4 Cycles
M – 65	1.0	12.0	–	-7.5	11.5	–	–	133	–	–	–
	1.2	14.4	–	-9.0	13.8	–	–	133	–	–	–
	1.4	16.8	–	-10.5	16.1	–	–	133	–	–	–
M – 73	1.0	12.0	–	-7.5	11.0	11.5	–	25	108	–	–
	1.2	14.4	–	-9.0	13.2	13.8	–	25	108	–	–
	1.4	16.8	–	-10.5	15.4	16.1	–	25	108	–	–
M – 79	1.0	12.0	3.2	-7.5	-3.0	10.0	11.5	2	4	25	108
	1.2	14.4	3.84	-9.0	-3.6	12.0	13.8	2	4	25	108
	1.4	16.8	4.48	-10.5	-4.2	14.0	16.1	2	4	25	108

TABLE 38. PARAMETERS λ, C, $(\overline{\Delta\sigma^b})^{1/b}$, AND $C(\overline{\Delta\sigma^b})^{\lambda/b}$ ESTIMATED PER CYCLE FOR DIFFERENT MISSION SEGMENTS (σ_{LIM} = 20 KSI)

Type of Loading	Stress Intensity Factor Range		λ	C	$(\overline{\Delta\sigma^b})^{1/b}$ b = 2 ksi	$C(\overline{\Delta\sigma^b})^{\lambda/b}$ $\frac{b}{2}$ = 2 $\sqrt{in}$ / cycle in
Case (I) Random (I-N)	(1)	$\overline{K} \leq K_{TH}$	5.628	3.321×10^{-10}		1.212×10^{-6}
	(2)	$K_{TH} < \overline{K} < K_{IC}$	3.465	2.480×10^{-9}	4.295	3.869×10^{-7}
	(3)	$\overline{K} < K_{IC}$	4.101	7.046×10^{-10}		2.775×10^{-7}
Case (II) Random (A-G)	(1)		5.412	3.773×10^{-10}		9.654×10^{-6}
	(2)		3.484	2.121×10^{-9}	6.523	1.463×10^{-6}
	(3)		3.646	1.458×10^{-9}		1.359×10^{-6}
Case (III) Random	(1)		8.343	9.257×10^{-11}		1.399×10^{-7}
	(2)		3.421	4.203×10^{-9}	2.405	8.459×10^{-8}
	(3)		5.349	2.334×10^{-10}		2.550×10^{-8}
Case (IV) Random Composite	(1)		5.399	6.558×10^{-10}		4.848×10^{-6}
	(2)		3.510	2.657×10^{-9}	5.208	8.704×10^{-7}
	(3)		3.718	1.713×10^{-9}		7.908×10^{-7}

TABLE 39. MEAN STRESS RATIO $\bar{R}_4$ AND NUMBER OF CYCLES N_{TH} CONTRIBUTED TO CRACK GROWTH PER UNITBLOCK FOR DIFFERENT INITIAL CRACK SIZE c_0

Initial Crack Size c_0 (inch)	Case (I) Unitblock = 500 cycles		Case (II) Unitblock = 1000 cycles		Case (III) Unitblock = 1000 cycles	
	Mean Stress Ratio $\bar{R}_4$	Number of Cycles Contributed to Crack Growth N_{TH}	Mean Stress Ratio $\bar{R}_4$	Number of Cycles Contributed to Crack Growth N_{TH}	Mean Stress Ratio $\bar{R}_4$	Number of Cycles Contributed to Crack Growth N_{TH}
0.02	0.032	3	0.057	66	0.0	0
0.03	0.075	9	0.071	160	0.0	0
0.04	0.106	19	0.094	243	0.0	0
0.05	0.146	30	0.108	315	-0.028	1
0.08	0.202	68	0.123	433	0.035	16
0.10	0.229	87	0.134	491	0.061	34
0.25	0.267	179	0.159	671	0.279	202
0.40	0.289	233	0.172	745	0.324	310
0.60	0.301	269	0.183	802	0.352	407
0.80	0.310	291	0.189	828	0.362	464
1.00	0.317	310	0.192	851	0.371	517
1.20	0.320	322	0.196	869	0.377	556
1.40	0.324	334	0.198	876	0.384	614
1.60	0.325	339	0.200	888	0.387	643
Mean $\bar{R}_4$	0.232		0.148		0.211	

TABLE 40. ESTIMATED VALUES OF μ, λ, C, $(\overline{\Delta\sigma^b})^{1/b}$, AND $C(\overline{\Delta\sigma^b})^{\lambda/b}$ FOR AVERAGE STRESS RATIO $\bar{R}$ CALCULATED BY SEVERAL DIFFERENT METHODS

Stress Ratio $\bar{R}$	Value	Type of Loading	Mean Stress μ (ksi)	$(\overline{\Delta\sigma^b})^{1/b}$ $b=2$ ksi	λ	C	$C(\overline{\Delta\sigma^b})^{\lambda/b}$ $b=2$ in·$\sqrt{\text{in}}$/cycle
$\bar{R}_0$	0.0	Case I	4.637	4.295	3.465	2.480×10^{-9}	3.869×10^{-7}
	0.0	Case II	4.727	6.523	3.484	2.127×10^{-9}	1.463×10^{-6}
	0.0	Case III	3.748	2.405	3.421	4.203×10^{-9}	8.459×10^{-8}
	0.0	Case IV	4.444	5.208	3.510	2.657×10^{-9}	8.704×10^{-7}
$\bar{R}_1$	0.430	Case I	4.637	4.295	3.744	3.201×10^{-10}	7.495×10^{-8}
	0.233	Case II	4.727	6.523	3.509	1.043×10^{-9}	7.527×10^{-7}
	0.583	Case III	3.748	2.405	3.600	3.494×10^{-10}	8.226×10^{-8}
	0.366	Case IV	4.444	5.208	3.563	7.600×10^{-10}	2.720×10^{-7}
$\bar{R}_2$	0.364	Case I	4.637	4.295	3.656	5.244×10^{-10}	1.077×10^{-7}
	0.217	Case II	4.727	6.523	3.509	1.099×10^{-9}	7.928×10^{-7}
	0.411	Case III	3.748	2.405	3.600	8.332×10^{-10}	1.961×10^{-8}
	0.303	Case IV	4.444	5.208	3.531	1.042×10^{-9}	3.532×10^{-7}
$\bar{R}_3$	0.367	Case I	4.637	4.295	3.656	5.170×10^{-10}	1.066×10^{-7}
	0.183	Case II	4.727	6.523	3.509	1.217×10^{-9}	8.779×10^{-7}
	0.514	Case III	3.748	2.405	3.600	5.133×10^{-10}	1.208×10^{-8}
	0.261	Case IV	4.444	5.208	3.531	1.202×10^{-9}	4.078×10^{-7}
$\bar{R}_4$	0.232	Case I	4.637	4.295	3.427	1.095×10^{-9}	1.617×10^{-7}
	0.148	Case II	4.727	6.523	3.351	1.813×10^{-9}	9.722×10^{-7}
	0.211	Case III	3.748	2.405	3.288	1.781×10^{-9}	3.189×10^{-8}
	0.174	Case IV	4.444	5.208	3.301	2.249×10^{-9}	5.221×10^{-7}

TABLE 41. PARAMETERS λ, C, $\overline{(\Delta\sigma^b)}^{1/b}$, AND $C\overline{(\Delta\sigma^b)}^{\lambda/b}$ ESTIMATED PER CYCLE FOR DIFFERENT MISSION SEGMENTS (σ_{LIM} = 20 KSI, WITH NEW CONSTANTS)

Type of Loading	Stress Intensity Factor Range		λ	C	$\overline{(\Delta\sigma^b)}^{1/b}$ $b = 2$ ksi	$C\overline{(\Delta\sigma^b)}^{\lambda/b}$ $b = 2$ $in^{-\lambda}\sqrt{in}$ / cycle
Case (I) Random (I-N)	(1)	$\overline{K} \leqq K_{TH}$	4.929	5.781×10^{-10}		7.615×10^{-7}
	(2)	$K_{TH} < \overline{K} < K_{IC}$	3.806	7.901×10^{-10}	4.295	2.026×10^{-7}
	(3)	$\overline{K} < K_{IC}$	3.838	7.452×10^{-10}		2.001×10^{-7}
Case (II) Random (A-G)	(1)		-	-		-
	(2)		3.690	1.019×10^{-9}	6.523	1.032×10^{-6}
	(3)		3.690	1.019×10^{-9}		1.032×10^{-6}
Case (III) Random	(1)		4.296	1.509×10^{-10}		6.544×10^{-9}
	(2)		3.777	1.150×10^{-9}	2.405	3.163×10^{-8}
	(3)		4.967	1.903×10^{-10}		1.486×10^{-8}
Case (IV) Random Composite	(1)		-	-		-
	(2)		3.702	1.312×10^{-9}	5.208	5.899×10^{-7}
	(3)		3.716	1.274×10^{-9}		5.865×10^{-7}

TABLE 42. MEAN STRESS RATIO $\bar{R}_4$ AND NUMBER OF CYCLES N_{TH} CONTRIBUTED TO CRACK GROWTH PER UNITBLOCK FOR DIFFERENT INITIAL CRACK SIZE c_0 (WITH NEW CONSTANTS)

Initial Crack Size c_0 (inch)	Case (I) Unitblock = 500 cycles		Case (II) Unitblock = 1000 cycles		Case (III) Unitblock = 1000 cycles	
	Mean Stress Ratio R_4	Number of Cycles Contributed to Crack Growth N_{TH}	Mean Stress Ratio R_4	Number of Cycles Contributed to Crack Growth N_{TH}	Mean Stress Ratio R_4	Number of Cycles Contributed to Crack Growth N_{TH}
0.02	0.167	39	0.111	347	-0.033	3
0.03	0.201	72	0.128	445	0.029	17
0.04	0.230	93	0.137	511	0.084	41
0.05	0.242	115	0.144	559	0.158	68
0.08	0.261	164	0.155	643	0.259	171
0.10	0.273	189	0.160	677	0.291	222
0.25	0.304	274	0.185	811	0.354	422
0.40	0.315	306	0.192	847	0.370	509
0.60	0.322	327	0.197	871	0.381	588
0.80	0.325	337	0.200	886	0.387	643
1.00	0.326	343	0.201	890	0.389	665
1.20	0.330	353	0.202	896	0.391	683
1.40	0.331	358	0.203	903	0.392	699
1.60	0.333	363	0.205	910	0.394	720
Mean $\bar{R}_4$	0.283		0.173		0.275	

TABLE 43. ESTIMATED VALUES OF μ, λ, C, $(\overline{\Delta\sigma^b})^{1/b}$ AND $C(\overline{\Delta\sigma^b})^{\lambda/b}$ FOR AVERAGE STRESS RATIO $\overline{R}$ CALCULATED BY SEVERAL DIFFERENT METHODS (WITH NEW CONSTANTS)

Stress Ratio $\overline{R}$	Value	Type of Loading	Mean Stress μ (ksi)	$(\overline{\Delta\sigma^b})^{1/b}$ $b=2$ ksi	λ	C	$C(\overline{\Delta\sigma^b})^{\lambda/b}$ $b=2$ $\lambda=2$ in$\sqrt{\text{in}}$/cycle
$\overline{R}$	0.0	Case I	4.637	4.295	3.806	7.901×10^{-10}	2.027×10^{-7}
	0.0	Case II	4.727	6.523	3.690	1.019×10^{-9}	1.032×10^{-6}
	0.0	Case III	3.748	2.405	3.777	1.150×10^{-9}	3.163×10^{-8}
	0.0	Case IV	4.444	5.208	3.702	1.312×10^{-9}	5.899×10^{-7}
$\overline{R}_0$	0.430	Case I	4.637	4.295	3.806	3.357×10^{-10}	8.607×10^{-8}
	0.233	Case II	4.727	6.523	3.690	6.886×10^{-10}	6.975×10^{-7}
	0.583	Case III	3.748	2.405	5.423	1.437×10^{-11}	1.675×10^{-9}
		Case IV	4.444	5.208	3.716	6.472×10^{-10}	2.980×10^{-7}
$\overline{R}_1$	0.364	Case I	4.637	4.295	3.806	3.964×10^{-10}	1.017×10^{-7}
	0.217	Case II	4.727	6.523	3.690	7.104×10^{-10}	7.196×10^{-7}
	0.411	Case III	3.748	2.405	4.652	1.135×10^{-10}	6.725×10^{-9}
		Case IV	4.444	5.208	3.716	7.452×10^{-10}	3.431×10^{-7}
$\overline{R}_2$	0.367	Case I	4.637	4.295	3.806	3.940×10^{-10}	1.010×10^{-7}
	0.183	Case II	4.727	6.523	3.690	7.555×10^{-10}	7.652×10^{-7}
	0.514	Case III	3.748	2.405	5.423	2.002×10^{-11}	2.333×10^{-9}
		Case IV	4.444	5.208	3.702	8.383×10^{-10}	3.769×10^{-7}
$\overline{R}_3$	0.283	Case I	4.637	4.295	3.703	5.458×10^{-10}	1.205×10^{-7}
	0.173	Case .II	4.727	6.523	3.625	8.681×10^{-10}	7.776×10^{-7}
	0.275	Case III	3.748	2.405	4.501	1.591×10^{-10}	8.258×10^{-9}
$\overline{R}_4$	0.216	Case IV	4.444	5.208	3.597	1.078×10^{-9}	4.079×10^{-7}

TABLE 44. SENSITIVITY OF TRANSITION PARAMETERS α AND n' ON ESTIMATION OF λ, C AND $C(\overline{\Delta\sigma^b})^{\lambda/b}$ (b=2)

Number of Transition Cycles n'	Modification Factors for Transition Cycles		$(\overline{\Delta\sigma^b})^{1/b}$ b = 2	λ	C	$C(\overline{\Delta\sigma^b})^{\lambda/b}$ $in^{-\lambda}\sqrt{in}$/Flight
	Rise α_1	Fall α_2				
1	1.2	0.8	5.143	3.798	4.716×10^{-8}	2.369×10^{-5}
	1.6	0.8		3.793	4.868×10^{-8}	2.425×10^{-5}
	2.0	0.8		3.794	4.942×10^{-8}	2.469×10^{-5}
3	1.2	0.8	5.143	3.798	4.797×10^{-8}	2.412×10^{-5}
	1.6	0.8		3.784	5.256×10^{-8}	2.579×10^{-5}
	2.0	0.8		3.789	5.478×10^{-8}	2.711×10^{-5}
5	1.2	0.8	5.143	3.799	4.878×10^{-8}	2.454×10^{-5}
	1.6	0.8		3.776	5.641×10^{-8}	2.733×10^{-5}
	2.0	0.8		3.784	6.014×10^{-8}	2.952×10^{-5}

TABLE 45. METHODOLOGY DEVELOPMENT TESTING PROGRAM GROUP I - CONSTANT AMPLITUDE LOAD
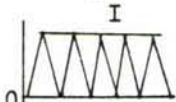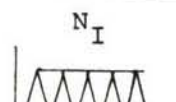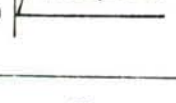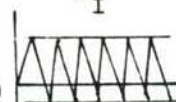
Test No.	Applied Base Load			Comments
	Loading Profile	σ_{max} Ksi	σ_{min} Ksi	
M-5		40	0	da/dn at high ΔK range, R = 0
M-6		40	12	da/dn at high ΔK range, R = 0.3
M-7		40	28	da/dn at high ΔK range, R = 0.7
M-8		40	-4	da/dn of negative stress ratio at high ΔK range
M-10		40	-12	da/dn of negative stress ratio at high ΔK range, R = -0.3

279

TABLE 46. PARAMETERS λ, C, $\overline{(\Delta\sigma^b)}^{1/b}$ AND $C\overline{(\Delta\sigma^b)}^{\lambda/b}$ ESTIMATED PER FLIGHT FOR CONSTANT AMPLITUDE LOAD SPECTRA $\sigma_{LIM} = 40$ KSI

TEST NO. ROCKWELL INTER.	STRESS INTENSITY FACTOR RANGE	λ	C	$\overline{(\Delta\sigma^b)}^{1/b}$ b = 2 (KSI)	$C\overline{(\Delta\sigma^b)}^{\lambda/b}$ b = 2 $in^{-\lambda}\sqrt{in}/Flight$
M - 5	(2) $K_{TH} < \overline{K} < K_{IC}$	3.550	1.056×10^{-9}	40.00	5.149×10^{-4}
M - 6	(2)	3.601	1.542×10^{-9}	28.00	2.506×10^{-4}
M - 7	(2)	3.636	4.879×10^{-9}	12.00	4.094×10^{-5}
M - 8	(2)	3.540	8.593×10^{-10}	44.00	5.645×10^{-4}
M - 10	(2)	3.518	6.077×10^{-10}	52.00	6.604×10^{-4}

TABLE 47. RATIO OF FLIGHTS PREDICTED BY THEORY AND
EXPERIMENT AT THE LARGEST CRACK SIZE
MEASURED (CONSTANT AMPLITUDE SPECTRA)

Test No. Rockwell International	N_{thr}/N_{exp} $\sigma_{LIM} = 40$ KSI
M − 5	0.662
M − 6	0.979
M − 7	0.841
M − 8	1.864
M − 10	2.908

TABLE 48. RATIO OF FLIGHTS TO FAILURE PREDICTED BY
THEORY AND EXPERIMENT (RANDOM LOAD SPECTRA)

TEST NO. ROCKWELL INTERNATIONAL	DESIGN LIMIT STRESS, σ_{LIM} KSI	N_{thr}/N_{exp}
AIR-TO-AIR		
M − 82	30	1.10
M − 83	40	1.31
AIR-TO-GROUND		
M − 85	30	0.99
M − 86	40	0.92
INSTRUMENTATION AND NAVIGATION		
M − 88	30	1.01
M − 89	40	0.80
COMPOSITE		
M − 90	20	1.70
M − 91	30	1.34
M − 92	40	1.44

TABLE 49. RATIO OF FLIGHTS TO FAILURE PREDICTED BY THEORY
AND EXPERIMENT (SIMPLIFIED LOAD SPECTRA)

TEST NO. ROCKWELL INTERNATIONAL	DESIGN LIMIT STRESS, σ_{LIM} KSI	N_{thr}/N_{exp}
M - 61a	30	1.33
M - 61	40	1.23
M - 62a	30	1.19
M - 62	40	1.34
M - 63a	30	1.26
M - 64b	20	1.40
M - 64a	30	1.39
M - 64	40	1.27
M - 69a	30	1.44
M - 70a	30	1.44
M - 72b	20	1.57
M - 72a	30	1.61
M - 72	40	1.39
M - 77a	30	1.21

TABLE 50. CRACK LIFE PREDICTION ANALYSIS AND TEST RESULTS
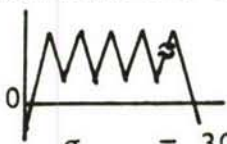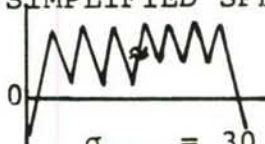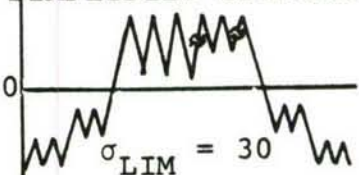
TEST NO. ROCKWELL INTER.	CRACK LIFE (FLIGHTS)		REMARKS
	TEST	ANALYSIS	
M - 82	2259	2490	RANDOM SPECTRA AIR-TO-AIR σ_{LIM} = 30 KSI
M - 6	1693 (1815)	2245 (2486)	CONSTANT AMPLITUDE σ_{LIM} = 30 KSI
M - 61a	2083 (1876)	2770 (2495)	SIMPLIFIED SPECTRA σ_{LIM} = 30 KSI
M - 69a	2090 (1727)	3001 (2480)	SIMPLIFIED SPECTRA σ_{LIM} = 30 KSI
M - 77a	1820 (2045)	2203 (2475)	SIMPLIFIED SPECTRA σ_{LIM} = 30 KSI
M - 83	717	939	RANDOM SPECTRA AIR-TO-AIR σ_{LIM} = 40 KSI

TABLE 50. CRACK LIFE PREDICTION ANALYSIS AND TEST RESULTS (CONT)
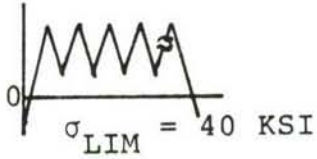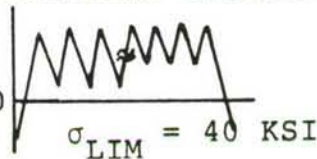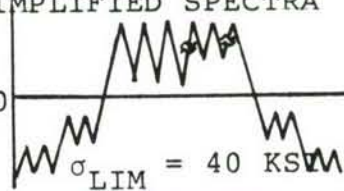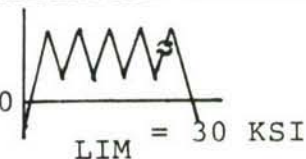
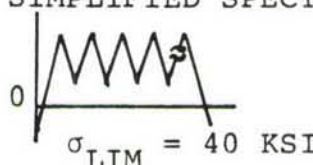| TEST NO. ROCKWELL INTER.	CRACK LIFE (FLIGHTS)		REMARKS
	TEST	ANALYSIS	
M - 8	469 (439)	1001 (937)	CONSTANT AMPLITUDE σ_{LIM} = 40 KSI
M - 61	727 (765)	891 (938)	SIMPLIFIED SPECTRA σ_{LIM} = 40 KSI
M*-69	489 (992)	-	SIMPLIFIED SPECTRA σ_{LIM} = 40 KSI
M*-77	561 (1033)	-	SIMPLIFIED SPECTRA σ_{LIM} = 40 KSI
M - 85	3288	3259	RANDOM SPECTRA AIR-TO-GROUND σ_{LIM} = 30 KSI
M - 62a	2481 (2726)	2462 (3255)	SIMPLIFIED SPECTRA $_{LIM}$ = 30 KSI

TABLE 50. CRACK LIFE PREDICTION ANALYSIS AND TEST RESULTS (CONT)
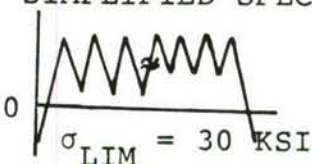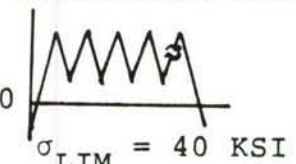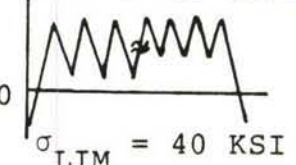
TEST NO. ROCKWELL INTER.	CRACK LIFE (FLIGHTS)		REMARKS
	TEST	ANALYSIS	
M - 70a	4287 (2598)	6179 (3745)	SIMPLIFIED SPECTRA σ_{LIM} = 30 KSI
M - 86	1920	1769	RANDOM SPECTRA AIR-TO-GROUND σ_{LIM} = 40 KSI
M - 6	1693 (1330)	2245 (1768)	CONSTANT AMPLITUDE σ_{LIM} = 40 KSI
M - 62	1183 (1329)	1580 (1775)	SIMPLIFIED SPECTRA σ_{LIM} = 40 KSI
M*-70	1141 (2420)	-	SIMPLIFIED SPECTRA σ_{LIM} = 40 KSI
M - 88	63,497	63,825	RANDOM SPECTRA INSTRUMENTATION AND NAVIGATION σ_{LIM} = 30 KSI

TABLE 50. CRACK LIFE PREDICTION ANALYSIS AND TEST RESULTS (CONT)
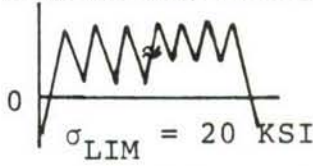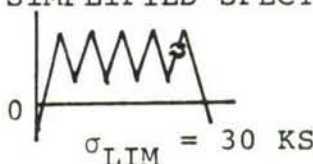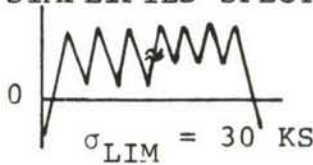
| TEST NO. ROCKWELL INTER. | CRACK LIFE (FLIGHTS) | | REMARKS |
	TEST	ANALYSIS	
M - 72b	11,888 (9,587)	18,650 (15,040)	SIMPLIFIED SPECTRA σ_{LIM} = 20 KSI
M - 91	2518	3369	RANDOM SPECTRA COMPOSITE σ_{LIM} = 30 KSI
M - 6	1693 (2542)	2245 (3370)	CONSTANT AMPLITUDE σ_{LIM} = 30 KSI
M - 64a	2223 (2416)	3092 (3361)	SIMPLIFIED SPECTRA σ_{LIM} = 30 KSI
M - 72a	1668 (2138)	2687 (3445)	SIMPLIFIED SPECTRA σ_{LIM} = 30 KSI
M - 92	875	1256	RANDOM SPECTRA COMPOSITE σ_{LIM} = 40 KSI

TABLE 50. CRACK LIFE PREDICTION ANALYSIS AND TEST RESULTS (CONT)
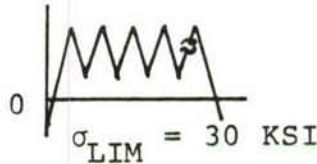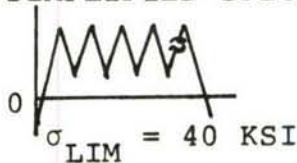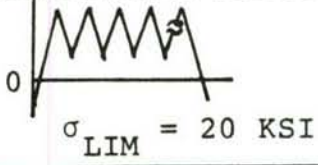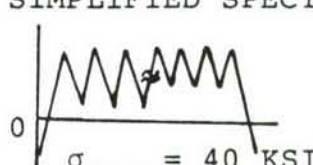
TEST NO. ROCKWELL INTER.	CRACK LIFE (FLIGHTS)		REMARKS
	TEST	ANALYSIS	
M − 63a	30,520 (50,816)	38,441 (64,004)	SIMPLIFIED SPECTRA σ_{LIM} = 30 KSI
M − 89	26,750	21,519	RANDOM SPECTRA INSTRUMENTATION AND NAVIGATION σ_{LIM} = 40 KSI
M*−63	6,563 (25,279)	−	SIMPLIFIED SPECTRA σ_{LIM} = 40 KSI
M − 90	8886	15,150	RANDOM SPECTRA COMPOSITE σ_{LIM} = 20 KSI
M − 7	14,870 (16,449)	13,935 (15,414)	CONSTANT AMPLITUDE σ_{LIM} = 20 KSI
M − 64b	14,240 (10,789)	19,941 (15,107)	SIMPLIFIED SPECTRA σ_{LIM} = 20 KSI

TABLE 50.   CRACK LIFE PREDICTION ANALYSIS AND TEST RESULTS (CONCL)

TEST NO. ROCKWELL INTER.	CRACK LIFE (FLIGHTS)		REMARKS
	TEST	ANALYSIS	
M - 5	846 (972)	784 (901)	CONSTANT AMPLITUDE σ_{LIM} = 40 KSI
M - 64	775 (994)	988 (1267)	SIMPLIFIED SPECTRA σ_{LIM} = 40 KSI
M - 72	679 (905)	947 (1263)	SIMPLIFIED SPECTRA σ_{LIM} = 40 KSI

APPENDIX A

BASELINE CRACK GROWTH TEST
DATA SOURCE DESCRIPTIONS

BOEING 2219-T851 ALUMINUM ALLOY BASELINE CRACK GROWTH RATE DATA GENERATION TESTING

DATA SOURCE NUMBER

B-2219-BOEING-1

GENERAL DESCRIPTION

1. Report number: AFFDL-TR-74-47[3]

2. Title: "Fracture and Fatigue Crack Growth Behavior of Surface Flaw and Flaws Originating at Fastener Holes"

3. Authors: Hall, L. R., Shah, R. C., and Enstrom, W. L.

4. Performing organization: Boeing Aerospace Company, Seattle, Washington

5. Sponsoring agency: USAF Flight Dynamics Laboratory, Wright-Patterson Air Force Base, Dayton, Ohio 45433

TEST DESCRIPTION

1. Type of test - Fatigue crack growth tests, conducted to develop baseline crack growth rate data for use in evaluating other test results

2. Test machine - Not given

3. Loading condition - Constant-amplitude cyclic loading, uniaxial tension

4. Stress ratios - R = 0.1, 0.3, 0.5

5. Test environment - Room temperature, desiccated air

6. Test frequency - 1 Hz

SPECIMEN DESCRIPTION

1. Material - 2219-T851 aluminum alloy.

2. Specimen dimensions: 27.0 inches long, 9.0 inches wide, 0.45 inch thick at test section, 1 inch thick at gripping area.

3. Tensile properties:

Grain properties	TYS (ksi)	TUS (ksi)	Elong (%)	RA (%)	E (ksi)
Long	52.6	66.1	16	28	
Trans	51.3	66.3	15	25	

4. Flaw preparation - Crack starters were introduced using an electric discharge machine, kerosene dialectric, and 0.06-inch-thick circular electrodes.

5. Precracking - Peak cyclic stresses, 10 ksi; stress ratio, 0.06; cyclic frequency, 30 Hz.

GRUMMAN 2219-T851 ALUMINUM ALLOY BASELINE CRACK GROWTH RATE DATA GENERATION
TESTING

DATA SOURCE NUMBER

    B-2219-GRUMMAN-1

GENERAL DESCRIPTION

1.   Report number: AFFDL-TR-74-129[4]

2.   Title: "Crack Growth Analysis for Arbitrary Spectrum Loading,"
     Vol I and II

3.   Authors: Bell, P. D., and Creager, M.

4.   Performing organization: Grumman Aerospace Corporation, Bethpage,
     New York 11714

5.   Sponsoring agency: USAF Flight Dynamic Laboratory, Wright-Patterson
     Air Force Base, Dayton, Ohio 45433

TEST DESCRIPTION

1.   Type of test - Fatigue crack growth test to characterize the steady-
     state crack growth behavior

2.   Test apparatus - Closed-loop servo-hydraulic testing machines

3.   Loading condition - Constant-amplitude cyclic loading, uniaxial
     tension

4.   Stress ratios - R = 0.05, 0.1, 0.3, 0.5, 0.7, -0.3, -1

5.   Test environment - Room temperature, laboratory air

6.   Test frequency - Exceed 1 Hz

SPECIMEN DESCRIPTION

1.   Material - 2219-T851 aluminum alloy

2. Tensile properties:

Grain direction	TYS (ksi)	TUS (ksi)	Elong (%)	RA (%)	E (ksi)
	54.7	66.9	10.3		

3. Specimen configuration and dimensions:

a. Center-cracked panel: 36.0 inches long, 6.0 inches wide, and 0.25 inch thick at test section

b. Compact tension specimens

    (1) ASTM configuration

$$W = 2.5 \text{ or } 2.2 \text{ inches}$$

$$H/W = 0.6$$

$$d/W = 0.25$$

    (2) Grumman configuration

$$W = 2.5 \text{ inches}$$

$$H/W = 0.95$$

$$d/W = 0.6$$

c. Flaw preparation - Not given

d. Precracking - All specimens were precracked

BOEING Ti-6AL-4VβA TITANIUM ALLOY BASELINE CRACK-GROWTH RATE DATA GENERATION
TESTING

DATA SOURCE NUMBER

    B-Ti-6-4βA-BOEING-1

GENERAL DESCRIPTION

1. Report number: AFFDL-TR-74-47[3]

2. Title: "Fracture and Fatigue Crack Growth Behavior of Surface
Flaws and Flaws Originating at Fastener Holes," Vol I and II.

3. Authors: Hall, L.R., Shah, R.C., and Engstrom, W.L.

4. Performing organization: The Boeing Aerospace Company, Seattle,
Washington

5. Sponsoring agency: USAF Flight Dynamics Laboratory., Wright-
Patterson Air Force Base, Dayton, Ohio 45433

TEST DESCRIPTION

1. Type of test - Fatigue crack-growth tests, conducted to develop
baseline crack-growth rate data for use in evaluating other
test results

2. Test machine - Not given

3. Loading condition - Constant-amplitude cyclic loading, uniaxial
tension

4. Stress ratios - R = 0.1, 0.3, 0.5

5. Test environment - Room temperature, desiccated air

6. Test frequency - 1 Hz

SPECIMEN DESCRIPTION

1. Material - Ti-6Al-4V beta-annealed titanium alloy

2. Specimen dimensions: 27.0 inches long, 6.0 or 4.25 inches wide, 0.60 inch thick.

3. Tensile properties:

Grain direction	TYS (ksi)	TUS (ksi)	Elong (%)	RA (%)	E (ksi)
Long	125.3	138.4	16	26	
Trans	128.0	138.6	16	25	

4. Flaw preparation - Crack starters were introduced using an electric discharge machine, kerosene dielectric, and 0.06-inch-thick circular electrodes

5. Precracking - Peak cyclic stresses, 10 ksi; stress ratio, 0.06; cyclic frequency, 30 Hz

GRUMMAN Ti-6Al-4V MILL-ANNEALED TITANIUM ALLOY BASELINE CRACK GROWTH RATE DATA GENERATION TESTING

DATA SOURCE NUMBER

B-Ti-6-4-MA-GRUMMAN-1

GENERAL DESCRIPTION

1. Report number: AFFDL-TR-74-129[4]

2. Title: "Crack Growth Analysis for Arbitrary Spectrum Loading," Vol. I and Vol. II.

3. Authors: Bell, P.D., and Creager, M.

4. Performing organization: Grumman Aerospace Corporation, Bethpage, New York 11714

5. Sponsoring agency: USAF Flight Dynamic Laboratory, Wright-Patterson Air Force Base, Dayton, Ohio 45433

TEST DESCRIPTION

1. Type of test - Fatigue crack growth test to characterize the steady-state crack growth behavior

2. Test apparatus - Closed-loop servo-hydraulic testing machines

3. Loading condition - Constant-amplitude cyclic loading, uniaxial tension

4. Stress ratios - R = 0.01, 0.05, 0.3, 0.5, 0.7, -1.0

5. Test environment - Room temperature, laboratory air

6. Test frequency - Exceed 1 Hz

SPECIMEN DESCRIPTION

1. Material - Ti-6Al-4V mill-annealed titanium alloy

2. Tensile properties:

Thickness (in.)	TYS (ksi)	TUS (ksi)	Elong (%)	RA (%)	E (ksi)
1/4	130.0	132.6	17.8		
3/4	135.3	137.6	12.6		

3. Specimen configuration and dimensions:

    a. Center-cracked panel: 36.0 inches long, 6.0 inches wide, and 0.29 inch thick at test section

    b. Compact tension specimens

        1. ASTM configuration

$$W = 2.5 \text{ or } 2.2 \text{ inches}$$
$$H/W = 0.6$$
$$d/W = 0.25$$

        2. Grumman configuration

$$W = 2.5 \text{ inches}$$
$$H/W = 0.95$$
$$d/W = 0.6$$

4. Flaw preparation - not given

5. Precracking - all specimens were precracked

BOEING 9Ni-4co-0.2C STEEL ALLOY BASELINE CRACK GROWTH RATE DATA GENERATION
TESTING

DATA SOURCE NUMBER

   B-HP9-4-20-BOEING-1

GENRAL DESCRIPTION

   1. Report number: AFFDL-TR-74-47[3]

   2. Title: "Fracture and Fatigue Crack Growth Behavior of Surface Flaws
       and Flaws Originating at Fastener Holes," Vol I and II

   3. Authors: Hall, L.R., Shah, R.C., and Engstrom, W.L.

   4. Performing organization: The Boeing Aerospace Company, Seattle,
       Washington

   5. Sponsoring agency: USAF Flight Dynamics Laboratory, Wright-
       Patterson Air Force Base, Dayton, Ohio 45433

TEST DESCRIPTION

   1. Type of test - Fatigue crack-growth tests, conducted to develop base-
       line crack-growth rate data for use in evaluating other test results

   2. Test machine - Not given

   3. Loading condition - Constant-amplitude cyclic loading, uniaxial
       tension

   4. Stress ratios - R = 0.1, 0.3, 0.5

   5. Test environment - Room temperature, desiccated air

   6. Test frequency - 1 Hz

SPECIMEN DESCRIPTION

   1. Material - HP 9Ni-4Co-0.2C steel alloy

   2. Specimen dimensions: 27.0 inches long, 5.5, 4.25, 4.0 inches wide,
       0.5 inch thick

3. Tensile properties:

Grain Direction	TYS (ksi)	TUS (ksi)	Elong (%)	RA (%)	E (ksi)
Long	185.3	203.2	23	56	
Trans	186.6	203.5	23	55	

4. Flaw preparation - Crack starters were introduced using an electric discharge machine, kerosene dielectric, and 0.06-inch-thick circular electrodes

5. Precracking - Peak cyclic stresses, 25-30 ksi; stress ratio, 0.06; cyclic frequency, 30 Hz

APPENDIX B

VARIABLE LOADING CRACK GROWTH TEST
DATA SOURCE DESCRIPTIONS

GRUMMAN 2219-T851 ALUMINUM ALLOY VARIABLE-AMPLITUDE LOAD TESTING

DATA SOURCE NUMBER

V-2219-GRUMMAN

GENERAL DESCRIPTION

1. Report: AFFDL-TR-74-129

2. Title: "Crack Growth Analysis for Arbitrary Spectrum Loading," Vol I and II

3. Authors: Bell, P.D., and Creager, M.

4. Performing organization: Grumman Aerospace Corporation, Bethpage, New York 11714

5. Sponsoring agency: USAF Flight Dynamic Laboratory, Wright-Patterson Air Force Base, Dayton, Ohio 45433

TEST DESCRIPTION

1. Type of test: Fatigue crack growth test to study the load interaction effects

2. Test apparatus: Closed-loop servo hydraulic testing machines

3. Loading condition: Variable-amplitude cyclic loading, uniaxial tension

4. Test environment: Room temperature, laboratory air

5. Test frequency: Exceed 1 Hz

SPECIMEN DESCRIPTION

1. Material: 2219-T851 aluminum alloy

2. Tensile properties:

Grain direction	TYS (ksi)	TUS (ksi)	Elong (%)	RA (%)	E (ksi)
	54.7	66.9	10.3		

3. Specimen configuration and dimensions:

   a. Center-cracked panel: 36 inches long, 6 inches wide, and 0.25 inch thick at test section

b. Compact tension specimens

    (1) ASTM configuration

        $W = 2.5$ or 2.2 inches
      $H/W = 0.6$
      $d/W = 0.25$

    (2) Grumman configuration

        $W = 2.5$ inches
      $H/W = 0.95$
      $d/W = 0.6$

4. Flaw preparation: Not given

5. Precracking: All specimens were precracked

DATA SOURCE NUMBER

V-Ti-6-4-MA-GRUMMAN

GENERAL DESCRIPTION

1. Report: AFFDL-TR-74-129

2. Title: "Crack Growth Analysis for Arbitrary Spectrum Loading,"
Vol I and II

3. Authors: Bell, P.D., and Creager, M.

4. Performing organization: Grumman Aerospace Corporation, Bethpage,
New York 11714

5. Sponsoring agency: USAF Flight Dynamic Laboratory, Wright-Patterson
Air Force Base, Dayton, Ohio 45433

TEST DESCRIPTION

1. Type of test: Fatigue crack growth test to study the load interaction
effects

2. Test apparatus: Closed-loop servo hydraulic testing machines

3. Loading condition: Variable-amplitude cyclic loading, uniaxial
tension

4. Test environment: Room temperature, laboratory air

5. Test frequency: Exceed 1 Hz

SPECIMEN DESCRIPTION

1. Material: Ti-6Al-4V mill-annealed titanium alloy

2. Tensile properties:

Thickness (in.)	TYS (ksi)	TUS (ksi)	Elong %	RA (%)	E (ksi)
1/4	130.0	132.6	17.8		
3/4	135.3	137.6	12.6		

3. Specimen configuration and dimensions:

   a. Center-cracked panel: 36 inches long, 6 inches wide, and 0.29 inch thick at test section

   b. Compact tension specimens

      (1) ASTM configuration

          W = 2.5 or 2.2 inches
          H/W = 0.6
          d/W - 0.25

      (2) Grumman configuration

          W - 2.5 inches
          H/W - 0.95
          d/W = 0.06

4. Flaw preparation: Not given

5. Precracking: All specimens were precracked

ROCKWELL HP 9Ni-4Co-0.2C STEEL ALLOY VARIABLE-AMPLITUDE LOAD TESTING

DATA SOURCE NUMBER

V-HP-9-4-20-ROCKWELL

GENERAL DESCRIPTION

1. Report: NA-75-675

2. Title: "Summary Report of the B-1 Fracture Mechanics Analysis Verification Test Program"

3. Author: Stolpestad, J.H.

4. Performing organization: Rockwell International Corporation, B-1 Division, Los Angeles, California 90009

5. Sponsoring agency: USAF Aeronautical System Division

TEST DESCRIPTION

1. Type of test: Fatigue crack growth test to develop analytical prediction methodology

2. Test apparatus: Closed-loop servo hydraulic testing machines

3. Loading condition: Flight-by-flight spectrum loading, uniaxial tension

4. Test environment: Room temperature, laboratory air or sump tank water

5. Test frequency: 0.1 to 5 Hz

SPECIMEN DESCRIPTION

1. Material: HP 9Ni-4Co-0.2C steel alloy

2. Tensile properties:

TYS (ksi)	TUS (ksi)	Elong (%)	RA (%)	E (ksi)
180	190	15	65	29×10^3

3. Specimen configuration and dimensions:

   a. Part-through-crack specimen: 36 inches long, 4 inches wide, and 0.5 inch thick at test section

4. Flap preparation: Electrical discharge machining

5. Precracking: All specimens were precracked by bending

APPENDIX C

PHASE I METHODOLOGY DEVELOPMENT
TESTING PROGRAM
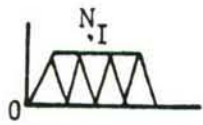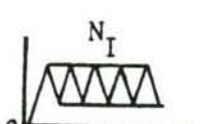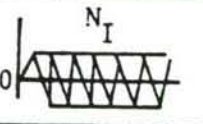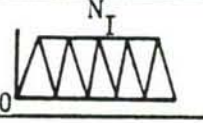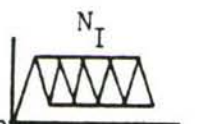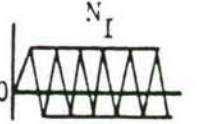
| Test No. | Applied Base Load | | | Over-/Under-load | | N_I Cycle | N_{II} Cycle | Comments |
	Loading Profile	σ_{Max} Ksi	σ_{Min} Ksi	σ_{Max} Ksi	σ_{Min} Ksi			
M-1		8	0					da/dn at low ΔK range, R = 0
M-2		8	2.4					da/dn at low ΔK range, R = 0.3
M-3		8	-8					da/dn at R = -1
M-4		8	-2.4					da/dn of negative stress ratio at low ΔK range
M-5		40	0					da/dn at high ΔK range, R = 0
M-6		40	12					da/dn at high ΔK range, R = 0.3
M-7		40	28					da/dn at high ΔK range, R = 0.7
M-8		40	-4					da/dn of negative stress ratio at high ΔK range
M-9		8	-0.8					da/dn of negative stress ratio at low ΔK range, R = -0.1
M-10		20	-6					da/dn of negative stress ratio at high ΔK range, R = -0.3

TABLE C-2. METHODOLOGY DEVELOPMENT TESTING PROGRAM GROUP II - SINGLE OR PERIODICAL OVERLOAD/COMP LOAD
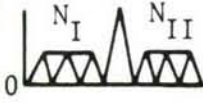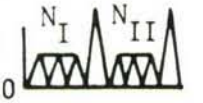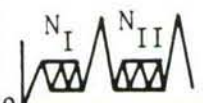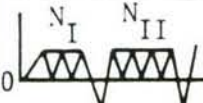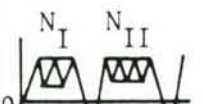
Test No.	Applied Base Load			Overload/ Underload		N_I Cycle	N_{II} Cycle	Comments
	Loading Profile	σ_{Max} Ksi	σ_{Min} Ksi	σ_{Max} Ksi	σ_{Min} Ksi			
M-11		20	0	30	0	2,500	To failure	Single over-load effect
M-12		20	0	30	0	2,500	2,500	Periodically applied single load effect, $R_I = 0$, $R_{OL} = 1.5$
M-13		20	0	45	0	2,500	2,500	Periodically applied single load effect, $R_I = 0$, $R_{OL} = 2.25$
M-14		20	6	40	6	2,500	2,500	Periodically applied single load effect, $R_I = 0.3$, $R_{OL} = 2$
M-15		30	21	40	21	2,500	2,500	Periodically applied single load effect, $R_I = 0.7$, $R_{OL} = 1.33$
M-16		20	0	20	-6.0	2,500	2,500	Periodically applied comp load effect $R_I = 0$
M-17		20	6	20	-6.0	2,500	2,500	Periodically applied comp load effect $R_I = 0.3$
M-18		40	28	40	-12	2,500	2,500	Periodically applied comp load effect $R_I = 0.7$
M-19		20	0	30	-6.0	2,500	To failure	Single overload/ comp load effect $R_I = 0$, $R_{OL} = 1.5$

TABLE C-2. METHODOLOGY DEVELOPMENT TESTING PROGRAM GROUP II -
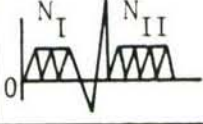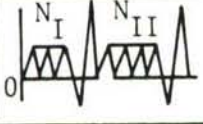SINGLE OR PERIODICAL OVERLOAD/COMP LOAD (CONT)
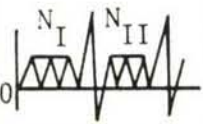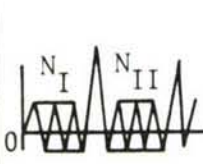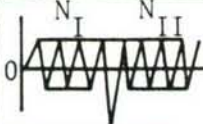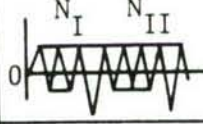
Test No.	Applied Base Load			Overload/Underload		N_I Cycle	N_{II} Cycle	Comments
	Loading Profile	σ_{Max} Ksi	σ_{Min} Ksi	σ_{Max} Ksi	σ_{Min} Ksi			
M-20		20	0	30	-6.0	2,500	2,500	Periodically applied overload-comp load effect
M-21		20	0	40	-12	2,500	2,500	Periodically applied overload-comp load effect
M-22		20	0	30	-6.0	2,500	To failure	Single comp load-overload effect
M-23		20	0	30	-6.0	2,500	2,500	Periodically applied comp load-overload effect
M-24		20	-6	30	-6	2,500	2,500	Periodically applied overload effect, $R<0$
M-25		20	-6	40	-6	2,500	2,500	Periodically applied overload effect, $R<0$, higher stress
M-26		8	-2.4	8	-16	2,500	To failure	Single comp-overload effect $R<0$
M-27		8	-2.4	8	-16	2,500	2,500	Periodically applied comp-overload effect
M-28		20	-6	30	-15	2,500	2,500	Periodically applied tension-comp overload effect

313
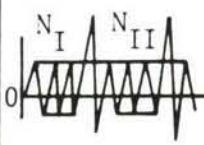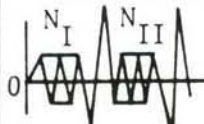
Test No.	Applied Base Load			Overload/ Underload		N_I Cycle	N_{II} Cycle	Comments
	Loading Profile	σ_{Max} Ksi	σ_{Min} Ksi	σ_{Max} Ksi	σ_{Min} Ksi			
M-29		20	-6	40	-15	2,500	2,500	Periodically applied tension-comp overload effect, higher stress
M-30		20	-6	40	-15	2,500	2,500	Periodically applied comp-tension overload effect

TABLE C-3. METHODOLOGY DEVELOPMENT TESTING PROGRAM GROUP III -
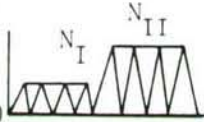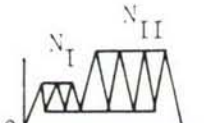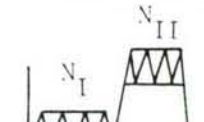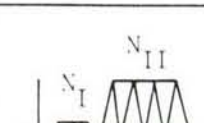MULTIPLE OVERLOAD/UNDERLOAD
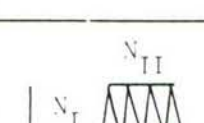
Test No.	Loading Profile	STEP I		STEP II		N_I Cycle	N_{II} Cycle	Comments
		Max Ksi	Min Ksi	Max Ksi	Min Ksi			
M-31	N_I N_{II}	8	0	20	0	10,000	To failure	Underload effect, low stress level
M-32		20	0	40	0	5,000	To failure	Underload effect, high stress level
M-33	N_I N_{II}	8	2.4	20	2.4	10,000	To failure	Underload effect, low stress level
M-34		20	6	40	12	5,000	To failure	Underload effect, high stress level
M-35	N_{II} N_I	8	0	20	14	10,000	To failure	Underload effect, two-level stress ratios, low stress
M-36		20	0	40	28	5,000	To failure	Underload effect, high stress level
M-37	N_{II} N_I	8	-2.4	20	0	10,000	To failure	Comp/tension load effect, low stress level
M-38		20	-6	40	0	5,000	To failure	Underload effect, high stress level
M-39	N_{II} N_I	0	-6	20	0	5,000	To failure	Comp - comp-load effect, low stress level
M-40		0	-12	40	0	5,000	To failure	Comp-comp load effect, high stress level

315

TABLE C-3. METHODOLOGY DEVELOPMENT TESTING PROGRAM GROUP III MULTIPLE OVERLOAD/UNDERLOAD (CONT)
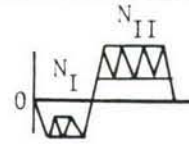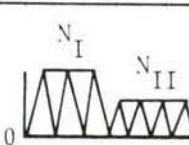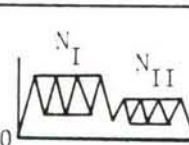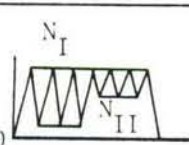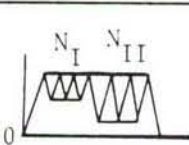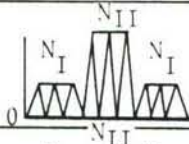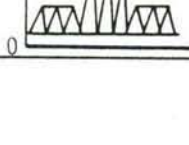
Test No.	Loading Profile	STEP I Max Ksi	STEP I Min Ksi	STEP II Max Ksi	STEP II Min Ksi	N_I Cycle	N_{II} Cycle	Comments
M-41		-3	-6	20	10	500	To failure	Comp-comp load effect
M-42		-3	-12	20	10	5,000	To failure	Comp-comp load effect
M-43		30	0	20	0	500	To failure	Multiple load retardation, R = 0
M-44		40	0	20	0	500	To failure	Multiple load retardation, R = 0
M-45		30	9	20	6	3,370	To failure	Multiple load retardation, R = 0.3
M-46		40	12	20	6	500	To failure	Multiple load retardation, R = 0.3
M-47		20	6	20	14	500	To failure	Stress ratio effect
M-48		40	12	40	28	500	To failure	Stress ratio effect
M-49		20	14	20	6	500	To failure	Stress ratio effect
M-50		40	28	40	12	500	To failure	Stress ratio effect
M-51		8	0	20	0	2,500	500	Repeat steps 1 & 2
M-52		20	0	40	0	500	50	Repeat steps 1 & 2
M-53		8	2.4	20	2.4	2,500	500	Repeat steps 1 & 2
M-54		20	6	40	6	500	50	Repeat steps 1 & 2

316

TABLE C-3. METHODOLOGY DEVELOPMENT TESTING PROGRAM GROUP III -
MULTIPLE OVERLOAD/UNDERLOAD (CONCL)

Test No.	Loading Profile	STEP I		STEP II		N_I Cycle	N_{II} Cycle	Comments
		Max Ksi	Min Ksi	Max Ksi	Min Ksi			
M-55	N_{II}, N_I, N_I	8	0	20	0	2,500	50	Repeat steps 1 & 2
				0	-6		50	
M-56		20	0	40	0	2,500	50	Repeat steps 1 & 2
				0	-12		50	
M-57	N_I - N_{II}, N_I	20	0	0	-12	2,500	50	Repeat steps 1 & 2
				40	0		50	
M-58	N_I, N_I, N_{II}	20	-6	40	-6	2,500	500	Repeat steps 1 & 2
M-59		8	-2.4	50	-2.4	5,000	2,500	Repeat steps 1 & 2
M-60	N_{II}, N_I, N_I	8	-2.4	8	-16	2,500	2,500	Repeat steps 1 & 2

317

TABLE C-4. METHODOLOGY DEVELOPMENT TESTING PROGRAM GROUP V - SIMPLIFIED FLIGHT SPECTRUM
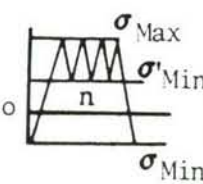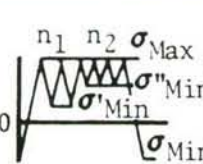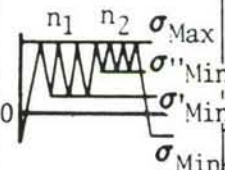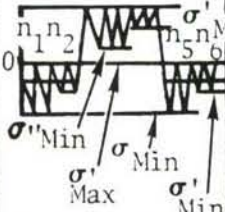
Test No.	Loading Profile	G-A-G Step σ_{Max} Ksi	σ_{Min} Ksi	Flight Step σ'_{Min} Ksi	σ''_{Min} Ksi	n_1 Cycle	n_2 Cycle	Comments
M-61		20	-2	4		25		Typical fighter, air-to-air σ Lim = 40 Ksi & 30 Ksi
M-61a		15	-2	4		25		
M-62		18	-4	4		20		Typical fighter, air-to-ground σ Lim = 40 Ksi & 30 Ksi
M-62a		14	-4	4		20		
M-63		14	-2	4		10		Typical fighter, instrumentation and navigation σ Lim = 40 Ksi & 30 Ksi
M-63a		10	-2	4		10		
M-64		20	-3	4		22		Typical fighter, composite mission σ Lim = 40, 30 & 20 Ksi
M-64a		15	-3	4		22		
M-64b		10	-3	4		22		
M-65		12	-7.5	11.5		133		Typical transport
M-66		16.8	-10.5	16.1		133		Typical transport
M-69		20	-2	6	8	20	40	Typical fighter, air-to-air σ Lim = 40 Ksi & 30 Ksi
M-69a		12	-2	3	4	20	40	
M-70		18	-4	6	8	15	30	Typical fighter, air-to-ground σ Lim = 40 Ksi & 30 Ksi
M-70a		10	-4	3	4	15	30	

318

TABLE C-4. METHODOLOGY DEVELOPMENT TESTING PROGRAM GROUP V SIMPLIFIED FLIGHT SPECTRUM (CONCL)

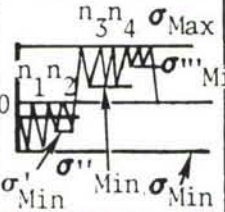| Test No.	Loading Profile	G-A-G Step σ_{Max} Ksi	σ_{Min} Ksi	Flight Steps σ'_{Min} Ksi	σ''_{Min} Ksi	σ'''_{Min} Ksi	n_1 Cyc	n_2 Cyc	n_3 Cyc	n_4 Cyc	Comments
M-71		14	-2	6	8		10	20			Typical fighter, instrumentation and navigation
M-72		19	-3	6	8		15	35			Typical fighter, composite mission σ_{Lim} = 40,30,& 20 Ksi
M-72a		14	-3	4	6		15	35			
M-72b		8	-3	2	3		15	35			
M-74		16.8	-10.5	15.4	16.1		25	108			Typical transport
M-77		20	-3	-1	6	8	2	4	15	35	Typical fighter σ_{Lim} = 40 Ksi & 30 Ksi
M-77a		14	-6	1	4	6	4	8	20	40	
M-78		18	-6	-1	4	8	4	8	20	40	Typical fighter

Test No.	Loading Profile	σ_{Max} Ksi	σ_{Min} Ksi	σ'_{Min} Ksi	σ''_{Min} Ksi	σ'''_{Min}	σ'_{Max}	n_1 n_5	n_2 n_6	n_3	n_4	Comments
M-79		12	-7.5	-3.0	10	11.5	3.2	2	4	25	108	Typical transport
M-80		16.8	-10.5	-4.2	14	16.1	4.48	2	4	25	108	Typical transport